Modelling and simulation of a multi-valve heat pump integrating a heat storage for flexible operating modes

Thesis by

Miryam Essadik

Submitted in fulfilment of the requirements for
the Degree of Doctor of Philosophy (PhD)

James Watt School of Engineering
College of Science and Engineering
University of Glasgow

December 2024

Abstract

To address the urgent need to reduce global warming, it is essential to transition to low-emission technologies in the heating sector. In this context, heat pumps are expected to play a major role. The UK government has set ambitious targets for heat pump adoption, with air-source heat pumps seen as a promising alternative to gas boilers for individual households due to their affordability and flexibility. However, research shows two main challenges with air-source heat pumps that can significantly affect performance in a UK setting: lack of flexibility and high operating costs when supplying hot water at high temperatures; frosting issues in cold and humid conditions. These challenges could reduce the economic appeal of heat pumps compared to gas boilers. This raises the question: What modifications or improvements could be made to the heat pump cycle to address both the need for cost-efficient operation at a 60 °C supply temperature and effective defrosting in the UK climate, without making the system overly complex or costly, while still allowing for flexible operation?

This thesis addresses this question by establishing a theoretical foundation through a benchmark numerical study of a multi-valve heat pump concept with integrated heat storage for flexible operation. The study analyses this system's potential to address these challenges and deliver efficient, cost-competitive performance in the UK. The flexible heat pump's four operating modes and thermodynamic benefits are evaluated relative to a conventional heat pump cycle in different scenarios. Economic and environmental impacts are also assessed against an A-rated gas boiler and a conventional air-source heat pump water heater, forming a basis for future experimental validation, model improvements, and commercial applications.

The defrosting process is examined under ideal conditions, comparing the thermodynamic behaviour and performance of the flexible heat pump to that of a standard reverse cycle defrosting system. By using latent heat storage as the evaporating unit during defrosting, the flexible heat pump can effectively defrost the evaporator while maintaining continuous heating capacity, saving power, and achieving a COP increase from 8.9 % to 13.2 % at maximum improvement storage temperature, depending on refrigerant choice. Key parameters, including storage temperature and defrost duration, are examined in detail. An exergy analysis highlights the main sources of losses in the cycle, identifying the compressor and heat exchangers as major contributors due to the deviation from isentropic compression and temperature differentials. The latent heat storage also affects these losses during

discharging/defrosting, especially if the temperature difference between the storage and the refrigerant is not minimised. System exergy efficiency is notably higher in discharging/defrosting mode than in heating/charging mode due to the lower compression ratio.

In addition to thermodynamic performance, the economic and environmental assessments highlight the flexible heat pump's potential as a viable UK alternative to gas boilers and conventional air-source heat pumps. The system's power-saving mode demonstrated a lower total annual cost rate than a conventional air-source heat pump water heater, with an average payback period of about four years. Additionally, it showed potential operating cost savings compared to an A-rated gas boiler. The Total Equivalent Warming Impact of the flexible heat pump was also lower than that of a conventional air-source heat pump, supporting its environmental benefits. With rising energy costs and the UK's commitment to Net Zero Emissions, these findings suggest that the flexible heat pump system could be an economically attractive option for sustainable heating.

The thesis also explores a dedicated charging mode to store heat during periods when heating is not required, which could take advantage of off-peak electricity rates. Both latent and sensible heat storage configurations are evaluated, and results indicate that this mode still improves performance compared to a conventional heat pump cycle. Analyses of extended parameters, such as thermal storage losses and temperature variations in the water storage tank, provide further insights into how to increase cycle efficiency. A roadmap for selecting the best refrigerants across the flexible heat pump's operating modes is also provided.

Overall, this thesis shows that the flexible heat pump with integrated heat storage has strong potential for residential applications in the UK and could play an important role in reducing carbon emissions in the heating sector. Further research is encouraged to support the development and deployment of practical flexible heat pump systems.

Table of Contents

Abstract .... **ii**

List of Tables .... **vii**

List of Figures .... **viii**

Preface .... **xiii**

Acknowledgement .... **xv**

Author's Declaration .... **xvi**

Nomenclature .... **xvii**

Chapter 1 Introduction **1**

1.1 Background 1

1.2 Fundamentals of heat pump thermodynamic cycle 3

1.2.1 Principles of reverse Carnot and Lorenz cycles 5

1.2.2 Non-ideal reverse Rankine cycle (vapour-compression cycle) 8

1.3 Aim and objectives of the Thesis 9

1.4 Thesis structure 10

Chapter 2 Literature review **13**

2.1 Heat pumps in the UK: status, fundamentals and challenges 13

2.1.1 UK market and policy overview for heat pumps 13

2.1.2 Types of domestic heat pumps 15

2.1.3 Deployment challenges for domestic heat pumps in the UK 18

2.2 Enhancing flexibility and performance in domestic heat pump systems 20

2.2.1 Improvement in single-stage vapour compression system 21

2.2.2 Performance improvement through flexible heat pump operation 31

2.3 Developments in defrosting technologies for air-source heat pumps 40

2.3.1 Mechanisms and impacts of frost formation 41

2.3.2 Frost mitigation strategies 41

2.3.3 Overview of defrosting methods 44

2.3.4 Recent innovations in defrosting techniques 48

2.4 Identified research gaps and questions 54

Chapter 3 Multi-valve flexible heat pump with integrated storage: concept and modelling **57**

3.1 Introduction 57

3.2 System concept and operating principles 58

3.2.1 Mode 1: Heating and charging of heat storage 60

3.2.2 Mode 2: Discharging of heat storage and power-saving....60
3.2.3 Mode 3: Discharging of heat storage, power-saving and defrosting....61
3.2.4 Mode 4: Charging heat storage at lower temperature....64
3.3 Modelling approach and development....65
3.3.1 Theoretical thermodynamic model: Equations and assumptions....66
3.3.2 Exergy model development....76
3.3.3 Economic and environmental model development....81
3.4 Validation of model results....86
3.4.1 Validation against compressor power data....87
3.4.2 Validation against COP data....89
3.5 Criteria for refrigerant selection....90
3.6 Summary....93
Chapter 4 Defrosting operation with latent heat storage....94
4.1 Introduction....94
4.2 Methodology....95
4.2.1 Assumptions adopted in this chapter....96
4.2.2 Description of case study....97
4.3 Results and discussions....98
4.3.1 Fixed defrost duration with varying storage temperature....98
4.3.2 Fixed storage temperature with varying defrost duration....105
4.4 Summary....108
Chapter 5 Exergy analysis of defrosting with latent heat storage....110
5.1 Introduction....110
5.2 Methodology....112
5.2.1 Assumptions adopted in this chapter....112
5.2.2 Description of case study....113
5.3 Results and discussion....114
5.3.1 Impact of storage integration on exergy destruction....115
5.3.2 Influence of compressor efficiency....123
5.3.3 Combined effect of compressor efficiency and storage-refrigerant temperature differential....125
5.3.4 Exergy analysis at 2.5 K storage-refrigerant temperature differential and 75 % compressor efficiency....130
5.3.5 Design implications based on exergy results....134
5.4 Summary....135
Chapter 6 Energy, economic and environmental analysis of power-saving mode...138

6.1 Introduction 138
6.2 Methodology 139
6.2.1 Assumptions adopted in this chapter 139
6.2.2 Description of case study 140
6.3 Results and discussion 144
6.3.1 Energy and performance analysis 144
6.3.2 Economic and environmental analysis 164
6.4 Summary 173
Chapter 7 Energy analysis of storage charging at lower temperature during off-heating periods 176
7.1 Introduction 176
7.2 Methodology 177
7.2.1 Assumptions adopted in this chapter 178
7.2.2 Description of case study 178
7.3 Results and discussion 179
7.3.1 Results for latent heat storage system 179
7.3.2 Results for sensible heat storage system 195
7.4 Summary 200
Chapter 8 Conclusions and outlook 203
8.1 Summary of thesis findings 203
8.2 Directions for future research 206
References 209

List of Tables

Table 2-1: Retrofit field trials[11] 17

Table 2-2: Properties of common used refrigerants[38] 26

Table 2-3: ASHRAE Standard 34 Safety group classification[73] 27

Table 3-1: Four operating modes of the flexible heat pump 59

Table 3-2: Exergy equations for each component and whole system for Mode 1 78

Table 3-3: Exergy equations for each component and whole system for Mode 3 79

Table 3-4: List of sources of experimental data for compressor power validation 89

Table 3-5: List of sources of experimental data for COP validation 90

Table 3-6: Thermophysical properties of the tested refrigerants 92

Table 4-1: Input parameters 97

Table 5-1: Input parameters 113

Table 6-1: Chapter main parameters 141

Table 6-2: Economic and environmental analysis parameters 143

Table 6-3: PCM properties 144

Table 6-4: Scenarios 156

Table 6-5: Additional components of the flexible heat pump 165

Table 6-6: CapEx and annual capital and maintenance cost rate for a gas boiler, a conventional ASHPWH and the flexible heat pump 165

Table 6-7: Economic and environmental analysis scenarios 166

Table 6-8: Total annual cost rate for the conventional ASHPWH and flexible heat pump across various scenarios 170

Table 6-9: Payback period based on a conventional ASHPWH depending on scenario 170

Table 7-1: Chapter main parameters 179

Table 7-2: Refrigerants enthalpy of vaporisation and $T_{max,\alpha}$ depending on ΔT_{HS} 183

List of Figures

Fig. 1-1: Schematic of a heat pump[14] 3

Fig. 1-2: T-S diagrams for: (a) Carnot cycle (b) Lorenz cycle[16] 5

Fig. 1-3: Ideal vapour-compression cycle or reverse Rankine cycle (dash) and real cycle (solid) 8

Fig. 2-1: Households heating system and fuel type[7] 14

Fig. 2-2: Annual sales (grey bars) and market growth (red dots) of air-source heat pumps in 2021[5] 14

Fig. 2-3: Illustration of air, water and ground source heat pumps....16

Fig. 2-4: Number of accreditations under Domestic RHI grant by type of technology from April 2014 to September 2022 in the UK[22,30] 17

Fig. 2-5: Comparative operating cost of heat pumps and gas boilers[24] 18

Fig. 2-6: Distribution of oversizing homes in a sample of UK households[6] 19

Fig. 2-7: P-H diagrams of: (a) subcritical cycle; (b) transcritical cycle 28

Fig. 2-8: Ejector geometry[46] 29

Fig. 2-9: Schematic and P-H diagrams of an ejector-expansion system[46]....30

Fig. 2-10: Refrigerant injection system with (a) subcooler; (b) flash tank[46] 32

Fig. 2-11: Schematic and P-H diagram of a refrigerant injection system with a thermoelectric heat exchanger[46]....33

Fig. 2-12: Recuperative heat pump system[111] 34

Fig. 2-13: Schematic of an air-source heat pump water heater[130] 36

Fig. 2-14: PCMs considered in the literature for heat pump applications[132] 37

Fig. 2-15: Schematic of the solar-assisted heat pump with an integrated PCM storage in the condenser[136]....38

Fig. 2-16: Schematic of the hot gas bypass defrosting method[180] 45

Fig. 2-17: Schematic of the reverse cycle defrosting 47

Fig. 2-18: Schematic of the novel defrosting method using heat dissipated by compressor's casing[217] 53

Fig. 2-19: Schematic of the novel frost-free air-source heat pump water heater[220] 54

Fig. 3-1: The multi-valve flexible heat pump (a) Schematic; (b) P-H diagram 58

Fig. 3-2: Mode 1: heating and charging of heat storage; (a) Schematic; (b) P-H diagram 60

Fig. 3-3: Mode 2: discharging of heat storage and power-saving; (a) Schematic; (b) P-H diagram.......61

Fig. 3-4: Mode 3: discharging of heat storage, power-saving and defrosting; (a) Schematic; (b) P-H diagram.......62

Fig. 3-5: Recovery phase (a) Schematic; (b) P-H diagram.......63

Fig. 3-6: Mode 4: charging the heat storage at lower temperature; (a) Schematic; (b) P-H diagram.......65

Fig. 3-7: Experimental data of ice mass buildup with time (Reichl et al.[224]**)** and linear fitting.......73

Fig. 3-8: Schematic of the flexible heat pump including the external loops in (a) Mode 1; (b) Mode 3.......80

Fig. 3-9: Photographs of the flexible heat pump prototype taken from Yu et al.[223] (a) Overview of the prototype; (b) Evaporator.......87

Fig. 3-10: Validation of predicted compressor power against experimental data.......88

Fig. 3-11: Validation of predicted COP against experimental data.......90

Fig. 3-12: Saturation curves of the selected refrigerants.......91

Fig. 4-1: Simulation flowchart of a run of the flexible heat pump.......96

Fig. 4-2: Theoretical average COP depending on heat storage temperature for R134a and R410a and their potential low GWP replacements.......99

Fig. 4-3: Theoretical COP improvement depending on heat storage temperature for R134a and R410a and their potential low GWP replacements.......99

Fig. 4-4: P-H diagrams with isotherms (red) and isentropic (yellow) lines for (a) R410a; (b) R32; (c) R134a; (d) R1234yf.......101

Fig. 4-5: Percentage of stored energy in the heat storage used to defrost for R134a and R410a.......103

Fig. 4-6: Part of the mass flow rate used to defrost the evaporator ($\dot{m}_{defrost}$) as a ratio of the discharging mass flow rate ($\dot{m}_d$) for R134a and R410a.......104

Fig. 4-7: Impact of the chosen defrosting time on COP improvement, storage discharging time after defrosting (Mode 2) and total discharging time.......105

Fig. 4-8: Evolution of $\dot{m}_d$, $\dot{m}_d + \dot{m}_{defrost}$ and σ with defrosting time.......106

Fig. 4-9: Defrosting heat rate in the evaporator and discharging rate of the heat storage during defrosting.......107

Fig. 5-1: Relative irreversibilities of heat storage and evaporator when storage-refrigerant temperature differential varies in Modes 1 and 3 116

Fig. 5-2: Relative irreversibility of the heat storage depending on storage-refrigerant temperature differential and condensing temperature in Mode 1 118

Fig. 5-3: Relative irreversibility of the heat storage depending on storage-refrigerant temperature differential and condensing temperature in Mode 3 118

Fig. 5-4: Exergy destruction when storage temperature varies in Mode 1 ($\Delta T_{HS} = 2.5$ K) 121

Fig. 5-5: Exergy destruction when storage temperature varies in Mode 3 ($\Delta T_{HS} = 2.5$ K) 121

Fig. 5-6: Exergy destruction when compressor efficiency varies in Mode 1 ($\Delta T_{HS} = 2.5$ K) 124

Fig. 5-7: Exergy destruction when compressor efficiency varies in Mode 3 ($\Delta T_{HS} = 2.5$ K) 124

Fig. 5-8: Exergy destruction per component and system in Modes 1 and 3, at $\Delta T_{HS} = 0$ K, $\eta_{comp} = 100$ % 126

Fig. 5-9: Exergy destruction per component and system in both modes, at $\Delta T_{HS} = 0$ K, $\eta_{comp} = 75$ % 126

Fig. 5-10: Exergy destruction per component and system in both modes, at $\Delta T_{HS} = 2.5$ K, $\eta_{comp} = 100$ % 127

Fig. 5-11: Exergy destruction per component and system in both modes, at $\Delta T_{HS} = 2.5$ K, $\eta_{comp} = 75$ % 127

Fig. 5-12: Exergy destruction per component and system in both modes, at $\Delta T_{HS} = 5$ K, $\eta_{comp} = 100$ % 128

Fig. 5-13: Exergy destruction per component and system in both modes, at $\Delta T_{HS} = 5$ K, $\eta_{comp} = 75$ % 128

Fig. 5-14: Relative irreversibility per component in Mode 1 131

Fig. 5-15: Relative irreversibility per component in Mode 3 131

Fig. 5-16: System exergy destruction in Modes 1 and 3, for various refrigerants ($\Delta T_{HS} = 2.5$ K and $\eta_{comp} = 75$ %) 133

Fig. 5-17: Exergy efficiency in Modes 1 and 3, for various refrigerants ($\Delta T_{HS} = 2.5$ K and $\eta_{comp} = 75$ %) 133

Fig. 6-1: Maximum improvement storage temperature as a function of condensing and evaporating temperatures ($\Delta T_{HS} = 0$; $T_{sb} = 0$; $T_{sh} = 0$) 145

Fig. 6-2: Average COP and improvement depending on storage temperature ($\Delta T_{HS} = 0$; $T_{sb} = 0$; $T_{sh} = 0$)..147

Fig. 6-3: Impact of the storage temperature on: heat rate in the evaporator and compressor power in Mode 1 ($\Delta T_{HS} = 0$; $T_{sb} = 0$; $T_{sh} = 0$) 148

Fig. 6-4: Impact of the storage temperature on: discharging rate of the heat storage and compressor power in Mode 2 ($\Delta T_{HS} = 0$; $T_{sb} = 0$; $T_{sh} = 0$).......................................148

Fig. 6-5: $T_{max,\alpha}$ and corresponding average COP and improvement depending on ΔT_{HS} 151

Fig. 6-6: $T_{max,\alpha}$ and corresponding average COP and improvement depending on the superheating degree T_{sh} 153

Fig. 6-7: $T_{max,\alpha}$ and corresponding average COP and improvement depending on the subcooling degree T_{sb} 154

Fig. 6-8: Impact of different scenarios on evaporating rate in Mode 1 and discharging rate of heat storage in Mode 2...157

Fig. 6-9: Impact of different scenarios on compressor power in Modes 1 and 2 157

Fig. 6-10: Impact of different scenarios on average COP and improvement, and $T_{max,\alpha}$ 158

Fig. 6-11: Scenarios impact on average COP and improvement, and $T_{max,\alpha}$ for propane 161

Fig. 6-12: Scenarios impact on the average COP and improvement, and $T_{max,\alpha}$ for R32 161

Fig. 6-13: Scenarios impact on average COP and improvement, and $T_{max,\alpha}$ for R134a .162

Fig. 6-14: Scenarios impact on average COP and improvement, and $T_{max,\alpha}$ for: R410a 162

Fig. 6-15: Scenarios impact on average COP and improvement, and $T_{max,\alpha}$ for R1234ze(E) 163

Fig. 6-16: Operational cost per year of a gas boiler, conventional ASHPWH and flexible heat pump with and without CO_2e cost...168

Fig. 6-17: Scenarios impact on annual energy consumption in kWh/year.......................168

Fig. 6-18: Annual CO_2e emissions of gas boiler, conventional ASHPWH and flexible heat pump across different scenarios..171

Fig. 6-19: TEWI of a conventional ASHPWH and flexible heat pump across different scenarios..172

Fig. 7-1: Average COP depending on T_{HS} and ΔT_{HS} 180

Fig. 7-2: Variation of $T_{max,\alpha}$ with ΔT_{HS} for R1234yf, R134a, R410a and R32 182

Fig. 7-3: Variation with ΔT_{HS} in both modes of pressure ratio 184

Fig. 7-4: Variation with ΔT_{HS} in both modes of refrigerant charging and discharging temperatures 184

Fig. 7-5: Variation with ΔT_{HS} in both modes of compressor power 185

Fig. 7-6: Variation with ΔT_{HS} of evaporator heat transfer rate in Mode 4 186

Fig. 7-7: Variation with ΔT_{HS} of discharging rate of storage in Mode 2 187

Fig. 7-8: Variation with ΔT_{HS} of discharging time in Mode 2 187

Fig. 7-9: Variation of the average COP and improvement depending on storage-refrigerant temperature differential 190

Fig. 7-10: Variation of the average COP and improvement depending on thermal storage losses 190

Fig. 7-11: Variation of the average COP and improvement depending on compressor efficiency 191

Fig. 7-12: COP improvement depending on T_{cond} and ΔT_{HS} at $T_{max,\alpha}$ 192

Fig. 7-13: Average COP and improvement for various refrigerants at $\Delta T_{HS} = 2.5$ K 194

Fig. 7-14: Variation with ΔT_w of charging and discharging times 196

Fig. 7-15: Variation with ΔT_w of average COP and improvement 197

Fig. 7-16: Variation with thermal storage losses of charging and discharging times, and time ratio at $\Delta T_w = 2$ K 198

Fig. 7-17: Variation with thermal storage losses of charging and discharging times, and time ratio at $\Delta T_w = 10$ K 199

Fig. 7-18: Variation with thermal storage losses of average COP and improvement 200

Preface

Papers included in this thesis:

Journal papers

1. **Essadik M.**, Hajabdollahi O. Z. and Yu Z., "Combined exergy-pinch point analysis of a multi-valve flexible heat pump with integrated latent thermal energy storage for defrosting operation". International Journal of Refrigeration, 176 (2025)

2. **Essadik M.**, Hajabdollahi O. Z., McKeown A., Lu Y. and Yu Z., "A multi-valve flexible heat pump system with latent thermal energy storage for defrosting operation". Energy and Buildings, 321 (2024)
   - → Featured in major renewable energy magazine's article: "New defrosting tech may increase coefficient of performance of air-source heat pumps by up to 11.2%", *PV Magazine Global*

3. Yu Z., McKeown A., Hajabdollahi O. Z. and **Essadik M.**, "A flexible heat pump cycle for heat recovery". Nature Communications Engineering, 1 (2022)

Conference papers

1. **Essadik M.**, Hajabdollahi O. Z. and Yu Z., "Exergy analysis of the defrosting operation of a flexible heat pump with an integrated latent heat storage". Paper presented at the 15th International Conference on Applied Energy (2023)

Papers related to but not included in this thesis:

Conference papers

1. **Essadik M.**, McKeown A., Hajabdollahi O. Z., Mokarram N. and Yu Z., "Study of the defrosting operation of the flexible heat pump cycle". Paper presented at the 26th IIR International Congress of Refrigeration (2023)
   - → Featured in IIR news article: "Heat pumps, the central theme of the recent IIR Congress", *IIR website;* and paper labelled as "*Recommended by the IIR*"

2. Hajabdollahi O. Z., McKeown A., **Essadik M.**, Mokarram N. and Yu Z., (2023). "A flexible heat pump for combined domestic hot water supply and space heating supply". Paper presented at the 26th IIR International Congress of Refrigeration (2023)

→ Paper labelled as "Recommended by the IIR"

3. **Essadik M.**, Hajabdollahi O. Z. and Yu Z., "Study of the defrosting operation of a flexible heat pump cycle with a sensible heat storage". Paper presented at the 15th International Green Energy Conference (2023)

Awards and honours

STEM for BRITAIN poster competition finalist, 2025

Best Presentation award at the ETP 11th Annual Conference, 2022

Acknowledgement

In the name of Allah, the Most Gracious, the Most Merciful.

The PhD journey is a tremendous and difficult one that takes one into the deepest reserves of oneself, uncovering new strength and wisdom and unlocking a new part of your being, like a butterfly undergoing its metamorphosis. This transformation will notably challenge your patience, endurance, and resilience. Allah (Glorified and Exalted is He) says: "**O you who have believed, seek help through patience and prayer. Indeed, Allah is with the patient**" (Qur'an 2:153). First and foremost, I would like to praise Allah for guiding me through this difficult journey, providing me with the strength to reach this culminant point, and for continuing to illuminate my path in the future, Ameen.

Secondly, I would like to dedicate this work and express my deepest gratitude to my family for always being by my side, notably to my beloved mother and sister, who always supported me, encouraged me, and lifted my mood when times were difficult. It wasn't always easy, but I knew I could count on them for anything. They are my rocks, my safe place. I wouldn't have been able to complete this journey without them, and words could never translate how much I love them and how deeply I am forever grateful to them. On a lighter note, I would also like to give a special mention to my cat; he is also part of the family, and his support in between naps has not gone unnoticed.

I would like to thank my supervisors, Pr. Zhibin Yu and Dr. Siming You, as well as my research fellows and friends whom I met along the way. Notably, I would like to give a special thanks to my brilliant fellow team member and friend, Dr. Zahra Hajabdollahi Ouderji, who was truly my mentor throughout this PhD journey and my early researcher's life. This journey would have been even more difficult without her guidance, support and advice. Talking to and laughing with her always lifted my spirits, and I am truly thankful to have met her. I sincerely wish her a well-deserved and very successful future career. Another special thanks to, as I like to call him, "my favourite colleague", Dr. Nan Zhang, a very talented researcher with whom I greatly enjoyed working and laughing. A shoutout to Andy, aka the expert in the lab, and a mention to our Saudi dream team, it was fun working with them. Final mention to all the other PhD students in my group or among my friends, I wish them the best of luck; there is, in fact, light at the end of the tunnel!

In closing, I dedicate this thesis to the people of Palestine, in recognition of their resilience and hope for a just and peaceful future, Ameen. They are an inspiration to all of us.

Author's Declaration

I certify that the thesis presented here for examination for a PhD degree of the University of Glasgow is solely my own work other than where I have clearly indicated that it is the work of others and that the thesis has not been edited by a third party beyond what is permitted by the University's PGR Code of Practice.

I declare that the thesis does not include work forming part of a thesis presented successfully for another degree.

I declare that this thesis has been produced in accordance with the University of Glasgow's Code of Good Practice in Research.

I acknowledge that if any issues are raised regarding good research practice based on review of the thesis, the examination may be postponed pending the outcome of any investigation of the issues.

Nomenclature

<u>*Symbols*</u>

$\emptyset$	Maintenance factor [-]
$\%\Delta Q_{loss}$	Percentage of heat loss to the environment [%]
A	Area [m^2]
c_{elec}	Unit cost of electricity [£ kWh^{-1}]
c_g	Unit cost of gas [£ kWh^{-1}]
c_p	Specific heat capacity [J kg^{-1} K^{-1}]
$CapEx$	Capital expenditure [£]
C_{CO_2e}	Penalty price of CO_2e emission [£ kg^{-1}]
$\overline{COP}$	Average COP [-]
ex	Exergy flow [J kg^{-1}]
$\dot{E}_X$	Exergy rate [kW]
E_{yearly}	Average annual energy consumption [kWh $year^{-1}$]
h	Specific enthalpy [J kg^{-1}]
H	Enthalpy [J]
ir	Interest rate [%]
L_{fus}	Latent heat of fusion [J kg^{-1}]
L_y	Yearly leakage of refrigerant [%]
$\dot{m}$	Mass flow rate [kg s^{-1}]
m_{CO_2e}	Annual CO_2e emissions [tons $year^{-1}$]
m_{ice}	Mass of ice [kg]
M_{ref}	Refrigerant charge [kg]
$M_{ref,evap}$	Mass of refrigerant in the evaporator [kg]
M_{PCM}	Mass of the PCM [kg]
n	Equipment lifetime [year]
P	Pressure [bar]
P_{dis}	Discharged pressure from compressor [bar]
P_{suc}	Suction pressure in compressor [bar]
q_{PCM}	Heat storage capacity of the PCM [kJ kg^{-1}]

$\dot{Q}$	Heat rate [kW]
Q	Heat [kJ]
$Q_{cond,hourly}$	Hourly heating capacity [kWh]
RI	Relative Irreversibility [%]
s	Specific entropy [J K^{-1} kg^{-1}]
s_{charge}	Daily standing charge for gas [£ day^{-1}]
S	Entropy [J K^{-1}]
t	Time [s]
T	Temperature [°C]
U	Overall heat transfer coefficient [W m^{-2} K^{-1}]
$\dot{W}$	Compressor power [kW]
W	Compressor work [kJ]
W_{ASHP}	Annual energy consumption of a conventional heat pump [kWh year^{-1}]
$W_{comp,conv}$	Hourly energy consumption of a conventional heat pump [kWh]
W_{FHP}	Annual energy consumption of the flexible heat pump [kWh year^{-1}]
Z	Capital cost function [£]
$\dot{Z}$	Annual capital and maintenance cost rate [£ year^{-1}]
$\dot{Z}_{op}$	Annual operational cost rate [£ year^{-1}]
$\dot{Z}_{tot}$	Total annual expense rate [£ year^{-1}]

Greek letters

α	COP improvement [%]
$\alpha_{recycling}$	Recycling factor [%]
δ	Time ratio between discharging and charging times [-]
Δt	Time difference [s]
ΔT_{HS}	Storage-refrigerant temperature differential [K]
ΔT_w	Water temperature differential [K]
η_b	Boiler efficiency [%]
η_{carnot}	Carnot efficiency [-]
η_{comp}	Compressor efficiency [%]
η_{ex}	Exergy efficiency [%]

η_{Lorenz}	Lorenz efficiency [-]
λ	Percentage of stored energy used for defrosting [%]
μ	CO_2e emission factor [kg kWh^{-1}]
σ	Ratio between defrosting and discharging mass flow rates [-]

<u>*Subscripts*</u>

0	Dead state parameter
1,2,3,4	Operating modes of the flexible heat pump
α	Improvement
a	Air
ASHP	Air-source heat pump
b	Gas boiler
c	Charge
comp	Compressor
cond	Condenser
conv	Conventional
C	Cold
d	Discharge
dest	Destruction
elec	Electricity
evap	Evaporator
ex	Exergy destruction
exp	Expansion valve
FHP	Flexible heat pump
g	Natural gas
H	Hot
HS	Heat storage
i	Heat pump component
j	Type of heat pump
max	Maximum
min	Minimum
out	Outlet

r	Real
ref	Refrigerant
s	Isentropic
sb	Subcooling
sh	Superheating
syst	System
tot	Total
w	Water
y	Yearly

Abbreviations

ASHPWH	Air-source heat pump water heater
BUS	Boiler upgrade scheme
CFCs	Chlorofluorocarbons
CO_2e	Carbon dioxide equivalents
COP	Coefficient of performance
CRF	Capital recovery factor
DHW	Domestic hot water
EEV	Electronic expansion valve
EHECSD	Extra heat exchanger coated with solid desiccant
ESD	Energy storage device
EU	European union
GWP	Global warming potential
HCs	Hydrocarbons
HCFCs	Hydrochlorofluorocarbons
HCFOs	Hydrochlorofluoroolefins
HFCs	Hydrofluorocarbons
HFOs	Hydrofluoroolefins
HS	Heat storage
IEA	International energy agency
IHX	Intermediate heat exchanger
LMTD	Logarithmic mean temperature difference

MPC	Model predictive control
NZE	Net zero emission
ODP	Ozone depletion potential
PCM	Phase change material
PP	Payback period
PV	Photovoltaic
PV/T	Photovoltaic/Thermal
RHI	Domestic renewable heat incentive
$SCOP_{net}$	Seasonal coefficient of performance
SPF	Seasonal performance factor
ST	Solar thermal
TES	Thermal energy storage
TEWI	Total equivalent warming impact
UK	United Kingdom

Chapter 1 Introduction

1.1 Background

Climate change is a critical and urgent global challenge for this generation and transitioning to more sustainable and low-emission technologies is essential to mitigating its harmful effects. As of June 2024, 107 countries worldwide have committed to Net Zero Emissions (NZE) pledges[1], aiming to reduce greenhouse gas emissions to limit global warming to no more than 1.5 °C, as stipulated by the Paris Agreement in 2015[2]. Achieving these targets requires reducing emissions across the most polluting sectors, including electricity production, transport, industry, and heating.

According to the International Energy Agency (IEA), energy demand for space and water heating was accounting for almost half of energy use in buildings and emitting 2.4 Gt of CO_2 directly, and 1.7 Gt of CO_2 indirectly, in 2022[3]. Fossil fuels still meet over 60 % of the global heating demand. In the European Union (EU), one third of the natural gas demand is for heating[4].

Although heat pump adoption has been growing, currently they only meet around 10 % of global heating demand in buildings. In 2021, global heat pump sales rose by 13 % compared to the previous year, with the fastest growth (35 %) in the EU[4]. However, sales dropped globally by about 3 % in 2023, with major European markets (France, Germany, and Italy) experiencing a 5 % decline. China was an exception, with a 12 % increase in sales. According to the IEA's NZE scenario, heat pumps must cover at least 24 % of global heating needs by 2030 and 52 % by 2050 to meet climate goals. This would require a rapid acceleration in adoption rates; at the current pace, only 253 million heat pumps would be installed worldwide by 2030, falling short of the NZE target of 600 million units, a projected shortfall of 58 %[5].

In Europe, the highest shares of heat pumps are found in northern countries, where policy support has been strong for years. In Norway, heat pumps meet 60 % of total heating demand, and in Sweden and Finland, they cover over 40 %. Finland, for example, converted 34 % of homes to heat pumps between 2000 and 2018 and is currently achieving a conversion rate of 3 % per year.

In the United Kingdom (UK), heating is a major source of carbon emissions, largely due to the widespread use of gas. On average, 73 % of UK households rely on gas central heating, making it one of the highest contributors to CO_2e emissions[6,7]. By 2022, heating in buildings accounted for 20 % of the UK's CO_2e emissions, with 15 % specifically from domestic heating[8]. The UK's Climate Change Act, passed in 2008, established a legally binding commitment to reduce greenhouse gas emissions by 100 % of 1990 levels by 2050[9]. Consequently, reducing reliance on gas for heating has become a critical focus in decarbonising the UK's heating sector and achieving NZE.

The UK government has set ambitious heat pump adoption targets: 600,000 installations per year by 2028, equivalent to roughly 2.5 % of homes annually. This target escalates to 900,000 installations per year by 2030 and 1.1 million by 2035, to transition away from gas heating systems and make heat pumps a mainstream, low-carbon heating solution[10]. Despite these targets, heat pump adoption in the UK remains low compared to other European countries. In 2022, only 72,000 heat pumps were installed in the UK, far below the government's target[11]. The UK also ranked among the lowest in air-source heat pump sales in Europe in 2021[5].

Heat pumps can be used for both heating and cooling applications and come in various types based on heat sources, including air-source, water-source, ground-source, waste heat, sorption heat pumps etc. For residential heating, air-source heat pumps and ground-source heat pumps are the most common, with air-source heat pumps being particularly popular for domestic use due to their lower cost and greater flexibility[12,13]. Heat pumps can also be used to heat different sink fluids, such as air or water, making them suitable for space heating or domestic hot water (DHW) production.

However, air-source heat pumps, while economical, are highly sensitive to ambient conditions, with performance decreasing when there is a high temperature lift between the source and sink. They are also susceptible to frosting on the outdoor heat exchanger in cold and humid environments, typical of a UK winter, further impacting efficiency and increasing running costs. These factors pose challenges for the UK market, where air-source heat pumps are competing against efficient and inexpensive gas boilers. These issues will be examined further in Chapter 2[11]. Therefore, improvements in air-source heat pump technology are essential to make them more suitable and economically attractive to a broader UK audience.

1.2 Fundamentals of heat pump thermodynamic cycle

A heat pump is a thermodynamic device with a vapour-compression cycle that extracts heat from a low temperature source and discharges it to a high temperature sink and is used to provide either heating or cooling. A schematic of a heat pump is presented in Fig. 1-1, with its four main components: compressor, condenser, expansion device and evaporator.

During the cycle, the refrigerant undergoes four transformations:

- Compression (1 to 2): At point 1, the refrigerant enters the compressor at a saturated or superheated vapour state. It is then compressed to reach point 2, as a high pressured and superheated gas.
- Condensation (2 to 3): From 2 to 3, it flows through the condenser where it releases heat to an external fluid (the sink). It first discharges its superheat and then condenses into a liquid by point 3.
- Expansion (3 to 4): From 3 to 4, the refrigerant is being expanded in an expansion device. Its pressure and temperature drop significantly, exiting as a two-phase mixture at point 4.
- Evaporation (4 to 1): Finally, from point 4 to 1, it enters the evaporator where it absorbs heat from another external fluid (the source). It is evaporated to reach the vapour state again and complete the cycle.

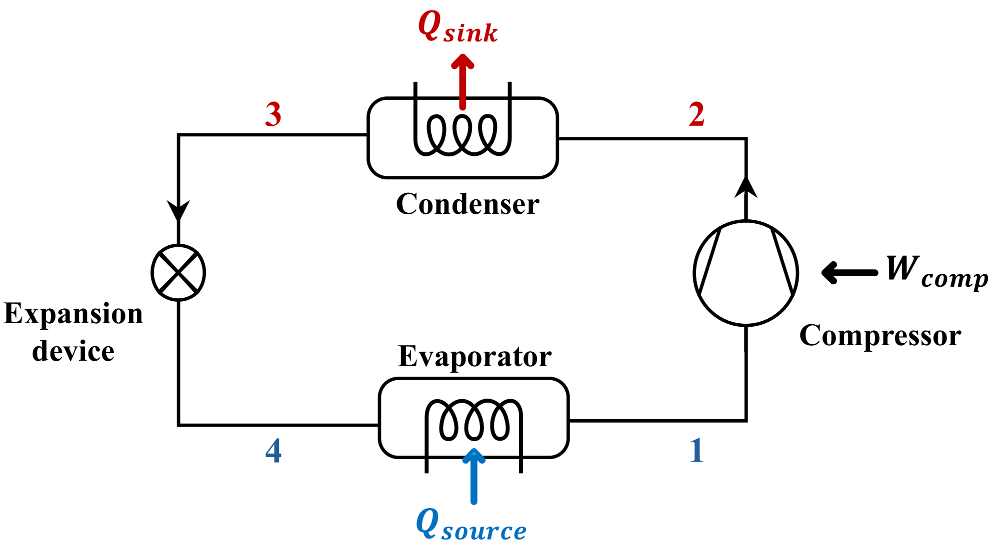

Fig. 1-1: Schematic of a heat pump[14]

The efficiency of a heat pump is commonly evaluated using the coefficient of performance (COP), which is defined as the ratio of useful heating output to the total electrical energy consumed by the heat pump. Based on the First Law of Thermodynamics and Fig. 1-1, it is expressed as follows[14]

$$COP = \frac{Desired\ output}{Required\ input} = \frac{|Q_{sink}|}{|W_{comp}|} \tag{1.1}$$

where Q_{sink} is the heat supplied to the high-temperature sink (such as a house) and W_{comp} is the net work input to the compressor. From a techno-economic perspective, only the work input to the cycle is considered in evaluating heat pump performance, since it is not free, while the heat extracted from the cold reservoir (Q_{source}) is considered neutral. Furthermore, because the heat pump cycle is closed and the final and initial thermodynamic states coincide, the change in internal energy over a cycle is zero (Eq. 1.2). Based on the energy balance for a practical heat pump, this can be expressed as

$$\Delta U_{cycle} = 0 \tag{1.2}$$

$$W_{comp} = Q_{sink} - Q_{source} \tag{1.3}$$

Therefore Eq. (1.1) can also be expressed as

$$COP = \frac{Q_{sink}}{Q_{sink} - Q_{source}} = \frac{1}{1 - \frac{Q_{source}}{Q_{sink}}} > 1 \tag{1.4}$$

Based on Eq. (1.3), the ratio in magnitude between Q_{source} and Q_{sink} always lies between 0 and 1 (excluded), and therefore the COP of a heat pump is theoretically always greater than 1.

This coefficient is widely used in engineering to assess heat pump performance under quasi-instantaneous operating conditions, over a representative working cycle. It will serve as the basis for evaluating performance throughout this thesis. The COP is greater than 1, meaning the heat pump delivers more heat than the electrical power it consumes, making it a highly efficient heating device, especially in comparison to an electric heater, which has a maximum efficiency of 1. In practical applications, the COP of a heat pump can occasionally drop below 1, although this is rare. Such situations can occur when there are significant losses in the heat supply process or when there is a large temperature difference between the source and sink[14]. The role of the source-sink temperature differential will be demonstrated in the following section.

To theorise the thermodynamic processes and efficiency of the heat pump cycle, particularly under varying source and sink conditions, engineers and physicists have developed and applied various ideal and non-ideal cycle models over time. These models serve as references for evaluating heat pump performance.

1.2.1 Principles of reverse Carnot and Lorenz cycles

Firstly, the well-known theoretical and ideal reference for a heat pump cycle operating between two heat reservoirs at constant temperatures is the reverse Carnot heat pump cycle (Fig. 1-2a). This cycle is fully reversible and comprises four transformations: two isothermal heat exchanges (where the refrigerant matches the temperature of both reservoirs, necessitating an infinite heat transfer area) and two adiabatic, isentropic work exchanges (compression and expansion). The calculated COP for the reversible Carnot heat pump cycle is the maximum achievable performance for a heat pump operating between two temperature limits. Based on Eq. (1.1) and as illustrated in Fig. 1-2a, the Carnot heat pump COP is expressed as[15]

$$COP_{carnot} = \frac{-Q_{23}}{W_{cycle}} \tag{1.5}$$

where Q_{23} is the amount of heat rejected to the high temperature medium, conventionally taken as negative because it is released by the system to the environment. W_{cycle} is the work applied by the environment to the system during a full cycle.

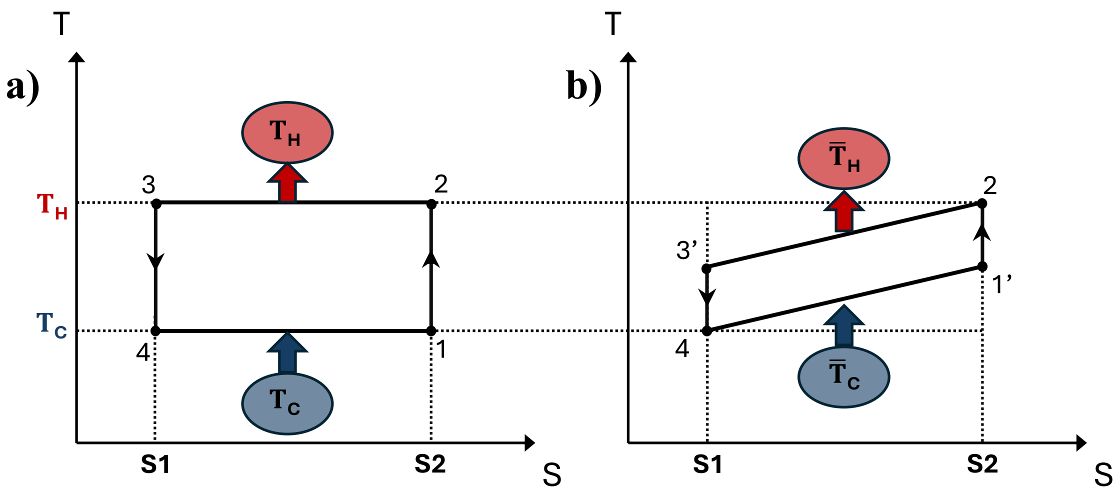

Fig. 1-2: T-S diagrams for: (a) Carnot cycle (b) Lorenz cycle[16]

Since the initial and final states are the same, the change in internal energy over a cycle is zero. According to the First Law of Thermodynamics, the work over a cycle can be expressed, based on the notation in Fig. 1-2a, as

$$W_{cycle} = -Q_{cycle} = -(Q_{23} + Q_{41}) \tag{1.6}$$

where Q_{cycle} is the total heat exchanged over the cycle and Q_{41} is the heat absorbed from the low-temperature medium. Eq. (1.6) shows that the total work done to the gas over a cycle is the opposite of the total heat exchanged. Therefore, Eq. (1.5) can be rewritten as

$$COP_{carnot} = \frac{Q_{23}}{Q_{23}+Q_{41}} \tag{1.7}$$

This expression can be further modified by replacing the heat transfer terms with the thermodynamic temperatures in the cycle. According to the Second Law of Thermodynamics, for a closed reversible cycle, the infinitesimal heat transfer at thermodynamic temperature T is given by

$$\delta Q = T\,dS \tag{1.8}$$

Applied, for instance, to the heat rejected to the high temperature reservoir at constant T_H in a Carnot cycle, this gives

$$Q_{23} = \int_2^3 T_H\,ds = T_H \Delta s_{21} = -T_H \Delta s_{12} \tag{1.9}$$

The same relationship applies to Q_{41}, and by substituting these expressions into Eq. (1.7), the Carnot COP becomes

$$COP_{carnot} = \frac{Q_{23}}{Q_{23}+Q_{41}} = \frac{-T_H\,\Delta s_{12}}{-(T_H-T_C)\Delta s_{12}} = \frac{T_H}{(T_H-T_C)} > 1 \tag{1.10}$$

where T_H and T_C are the temperatures of the sink and source, respectively. This equation highlights the critical influence of the sink-source temperature differential on heat pump efficiency.

When using the Carnot cycle as a reference, a Carnot efficiency can be defined as a simplified expression of the Second Law or exergetic efficiency, comparing actual performance to the ideal limit[17]

$$\eta_{carnot} = \frac{COP}{COP_{Carnot}} \tag{1.11}$$

However, when sensible heat is exchanged (such as when external fluids experience a gradual change in temperature during heat exchange, or in transcritical heat pump cycles), the Carnot COP is no longer the ideal reference. In this case, the Lorenz cycle becomes the most efficient model for evaluating maximum performance between the two sources. Shown in Fig. 1-2b, the Lorenz cycle is a reversible cycle with the same adiabatic, isentropic work exchanges as the Carnot cycle. However, the heat exchange processes between the refrigerant and reservoirs are non-isothermal and occur at the logarithmic mean temperatures of the reservoirs, which account for temperature gradients and minimise entropy generation.

With a similar derivation to the Carnot COP, the Lorenz heat pump cycle COP between two reservoirs, based on the notation in Fig. 1-2b, is written as[18]

$$COP_{Lorenz} = \frac{-Q_{23'}}{W_{cycle}} = \frac{\bar{T}_H}{(\bar{T}_H - \bar{T}_C)} > 1 \tag{1.12}$$

with $\bar{T}_H$ and $\bar{T}_C$ being the logarithmic mean temperatures of the sink and the source, respectively, and defined as

$$\bar{T}_H = \frac{T_2 - T_{3'}}{\ln\left(\frac{T_2}{T_{3'}}\right)} \tag{1.13}$$

$$\bar{T}_C = \frac{T_{1'} - T_4}{\ln\left(\frac{T_{1'}}{T_4}\right)} \tag{1.14}$$

It can be noted that, when there is no temperature variation, the Lorenz COP equals the Carnot COP.

Similarly to the Carnot cycle, when using the Lorenz cycle as a reference, a Lorenz efficiency can be defined as[17]

$$\eta_{Lorenz} = \frac{COP}{COP_{Lorenz}} \tag{1.15}$$

These theoretical tools are valuable for evaluating the maximum efficiency of the heat pump vapour-compression cycle. However, the real vapour-compression cycle is inherently irreversible, with efficiency dependent not only on reservoir temperatures but also on the performance of the heat pump components and the properties of the selected refrigerant. The gap between ideal and real performance is strongly influenced by these factors.

1.2.2 Non-ideal reverse Rankine cycle (vapour-compression cycle)

As compared to the two ideal cycles described previously, the real vapour-compression cycle is an irreversible process. It is typically characterised as a non-ideal reverse Rankine cycle, whose T-S diagram is shown in Fig. 1-3, alongside the ideal reverse Rankine cycle for comparison.

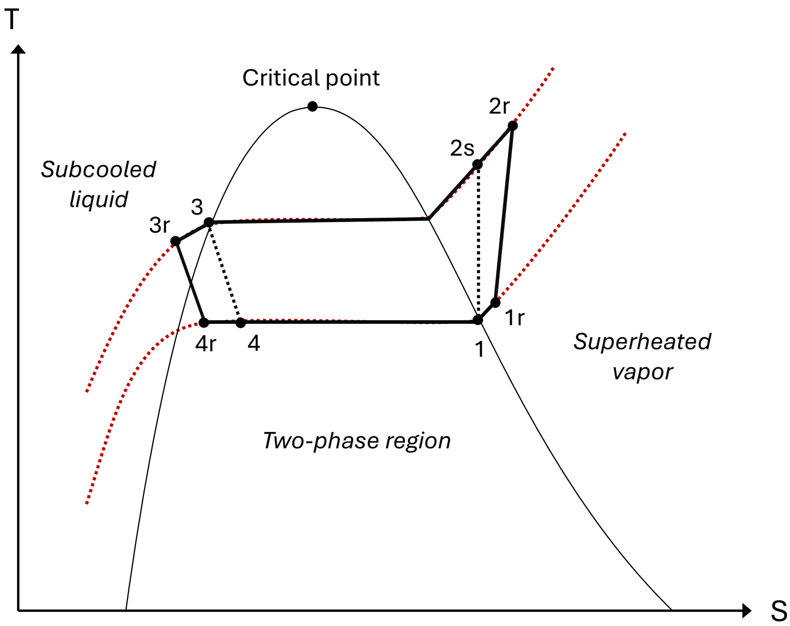

Fig. 1-3: Ideal vapour-compression cycle or reverse Rankine cycle (dash) and real cycle (solid)

All four transformations in the real vapour-compression cycle generate entropy, making them inherently irreversible. These transformations include irreversible compression, two isobaric heat exchanges, and one isenthalpic expansion. The main sources of losses in the cycle arise from five key areas:

- Compressor irreversibility: No compressor can achieve ideal isentropic compression due to factors like friction losses, heat dissipation to the surroundings, mechanical and electrical losses, etc., all of which contribute to entropy generation.

- Expansion process irreversibility: The expansion process is isenthalpic rather than isentropic. Unlike in ideal cycles, no work is extracted from the refrigerant during expansion; instead, the abrupt pressure drop (typically through an expansion valve) dissipates energy and increases entropy. Additionally, fluid friction in the valve further contributes to entropy generation and losses.

- Non-ideal heat transfer: In practice, a temperature difference is necessary between the sink/source and refrigerant to enable heat transfer, resulting in temperature differential within the heat exchangers. This difference introduces irreversibilities and leads to entropy generation.

- Subcooling and superheating: To protect components such as the compressor and expansion device, in practical heat pumps refrigerant is usually subcooled in the condenser and superheated in the evaporator. These stages increase entropy generation but are necessary for system stability.

- Pressure drops in pipes and heat exchangers: Small but inevitable pressure drops occur as the refrigerant flows through pipes and heat exchangers, which further contribute to system inefficiencies.

To mitigate these losses, improvements can be made within the vapour-compression cycle, including the use of advanced compressors, optimised expansion devices, and enhanced heat exchanger designs. Careful heat pump design, such as minimising temperature differentials in the heat exchangers, also reduces entropy generation and improves efficiency.

Therefore, the performance of a heat pump is heavily influenced not only by source and sink temperatures but also by the quality of its components and system design. Despite these practical losses, heat pumps remain highly efficient heating technologies. However, depending on the heat pump type and application environment, further improvements to the cycle may be necessary to ensure both efficiency and economic viability in certain regions.

1.3 Aim and objectives of the Thesis

The main aim of this thesis is to establish a baseline numerical study of a multi-valve heat pump concept, named the flexible heat pump, integrating a heat storage for flexible operation. This concept is designed to address challenges associated with air-source heat pumps in the UK, such as the need for cost-efficient and flexible heating supply, as well as the frequent defrosting cycles required. The goal is to assess the potential benefits of this system compared to a conventional air-source heat pump by examining both cycles, thereby establishing a foundation for future model improvements, experimental studies, and commercial designs. Additionally, the thesis evaluates the economic feasibility of this system relative to a conventional air-source heat pump and a gas boiler

The specific objectives of this thesis include:

- To investigate the thermodynamic performance and behaviour of the flexible heat pump defrosting cycle compared to reverse cycle defrosting. This includes evaluating its impact on overall system performance and identifying parameters that contribute to optimal efficiency.

- To determine the main sources of exergy losses in key components during two typical modes of operation of the flexible heat pump and to identify the influence of critical parameters on these losses. Additionally, to estimate the system exergy efficiency of these modes and explore the reasons for efficiency differences between them.

- To provide a comprehensive comparison of the performance, economic viability, and environmental impact of the power-saving mode of the flexible heat pump relative to a conventional air-source heat pump water heater in a UK application. This analysis also includes an evaluation of potential economic and environmental savings in comparison with both a conventional air-source heat pump water heater and an A-rated gas boiler.

- To conduct a thermodynamic analysis of a dedicated charging (non-heating) mode for the flexible heat pump, examining potential improvements over a conventional heat pump cycle. This objective includes assessing the impact of extended parameters, different heat storage types, and refrigerant options, leading to recommendations on the optimal refrigerant choice across all operating modes of the flexible heat pump.

1.4 Thesis structure

The thesis is structured into eight chapters. They proceed as follow.

Chapter 2 provides a comprehensive literature review on three major topics central to this thesis. First, it examines the current state of heat pumps in the UK, identifying the main barriers to widespread adoption, particularly for small capacity air-source heat pumps used in domestic heating. Second, it reviews advancements in the scientific literature that address the need for efficient high temperature lift and flexibility in single-stage air-source heat pumps. Finally, it explores enhancements to defrosting methods for air-source heat pumps. The chapter concludes by highlighting research gaps and presenting the research questions that form the basis of this thesis.

In Chapter 3, a detailed explanation of the multi-valve flexible heat pump concept is provided, developed to address the challenges identified in the literature. The modelling approach, including assumptions, is thoroughly explained. The steady-state models used for energy, exergy, economic, and environmental analyses are described in depth. Numerical results from compressor power and COP are validated against experimental data to ensure accuracy. The chapter also introduces the refrigerants selected for the study and their thermophysical properties.

Chapter 4 focuses on evaluating the defrosting operation of the flexible heat pump, which involves three of its four operating modes. Using an idealised model, this chapter simplifies the assessment of maximal thermodynamic performance, exploring the impact of key parameters such as storage temperature, and comparing performance with the conventional reverse cycle defrosting method. The study incorporates a latent heat storage system, with performance assessed over a complete charge/discharge cycle. Various refrigerants are analysed to understand their impact on the system. This chapter serves as a preliminary investigation of the multi-valve flexible heat pump under idealised condition.

Building on Chapter 4, Chapter 5 presents an exergy analysis using an updated model that incorporates non-ideal conditions, such as compressor efficiency and the temperature difference between storage and refrigerant. This chapter aims to identify the primary sources of losses and to evaluate the system's exergy efficiency during the heating/charging and defrosting/discharging modes with latent heat storage. The refrigerant with the best performance, identified in Chapter 4, is used here as a reference, with comparisons made to other refrigerants.

Chapter 6 shifts focus to the energy, economic, and environmental performance of the power-saving mode of the flexible heat pump system with integrated latent heat storage, for UK applications. Expanding on the model from Chapter 4, this chapter analyses the effects of non-ideal conditions and additional parameters on system performance. Economic and environmental comparisons are made against a conventional air-source heat pump water heater (ASHPWH) and a new A-rated gas boiler to assess the system's economic and environmental attractiveness.

In Chapter 7, the alternative charging mode of the flexible heat pump is introduced and evaluated. This chapter investigates the thermodynamic behaviour and performance of the system with both latent and sensible heat storage. The goal is to determine if using this mode to charge the heat storage without heating improves performance compared to a conventional heat pump cycle, and to evaluate how it impacts the system. Extended parameters and their effects are analysed, concluding with an assessment of refrigerant selection for the best efficiency across all operating modes.

Finally, Chapter 8 summarises the key findings of this thesis and offers recommendations for future research.

Chapter 2 Literature review

This chapter reviews existing literature to establish the foundation of the research presented in this thesis, identify research gaps, and outline associated research questions. First, it examines the current use of heat pumps in the UK and highlights the main challenges to their broader adoption, especially in individual dwellings compared to gas boilers. Next, it reviews studies that investigate performance improvement and the flexibility of domestic heat pumps for reducing operating costs, particularly under conditions of high temperature lift and variable ambient temperatures. Finally, it examines the issue of frost affecting the efficiency of air-source heat pumps and summarises the solutions proposed in the literature to address this problem.

2.1 Heat pumps in the UK: status, fundamentals and challenges

Heat pumps can be used for a wide range of applications, including domestic, industrial, cogeneration, etc.[19]. In this thesis, the focus is given to domestic use of heat pumps in the context of the UK transition to more sustainable heating solutions to replace fuel based heating systems. This is one of the UK government goals in reducing its emissions as it will be highlighted in the following sections.

2.1.1 UK market and policy overview for heat pumps

In the effort to reach Net Zero by 2050 and decarbonise the heating sector, the UK government has committed to a target of 600,000 heat pump installations per year by 2028, equivalent to covering 2.5 % of homes per year[20]. Heating in the UK is still mainly provided by gas, as illustrated in Fig. 2-1. On average, 73 % of households rely on gas central heating according to the 2021–2022 censuses, making heating one of the largest carbon-emitting sectors in the UK[7,8].

However, despite government intentions, only 72,000 heat pumps were installed in 2022[11]. In fact, the UK has seen limited adoption of heat pumps in recent years, ranking among the lowest in Europe for heat pump sales in both 2022 and 2021, as illustrated in Fig. 2-2[5,21].

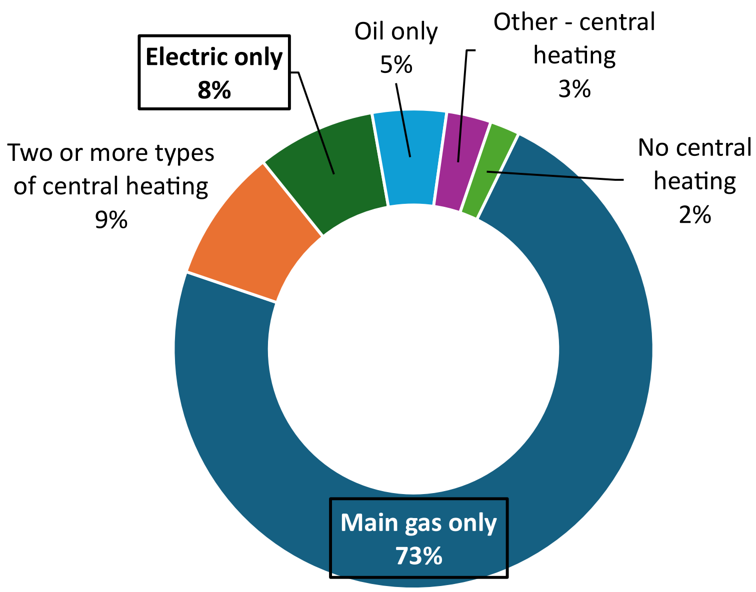

Fig. 2-1: Households heating system and fuel type[7]

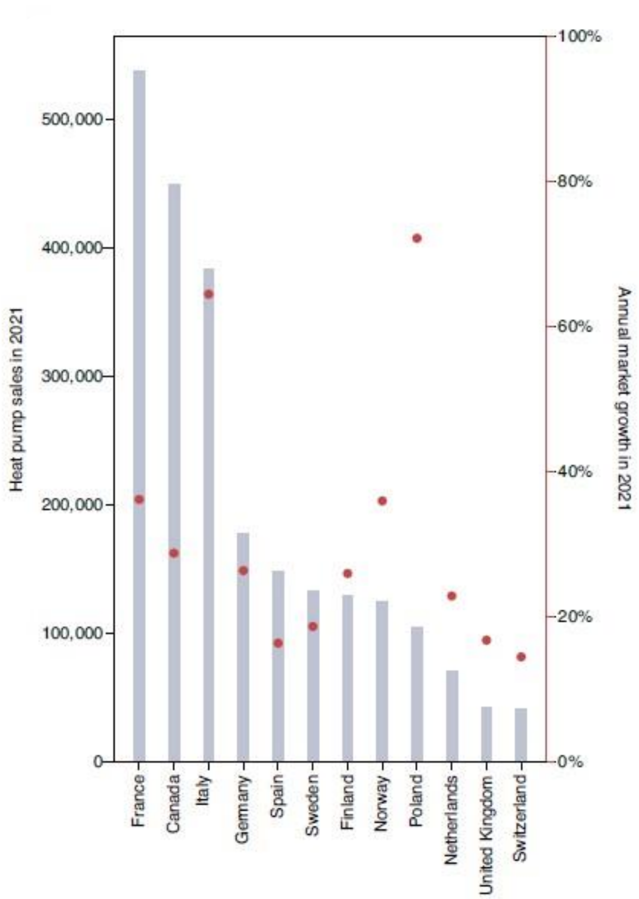

Fig. 2-2: Annual sales (grey bars) and market growth (red dots) of air-source heat pumps in 2021[5]

According to the UK government, three key actions would support greater deployment of heat pumps[11]:

- positioning heat pumps as the most cost-effective heating solution
- providing financial assistance for individuals unable to afford the transition
- implementing standards to guarantee installation quality and phase out fossil fuel systems

Underscoring the first point, a critical factor in the wide adoption of heat pumps is their economic viability, which depends on overall costs, including initial investment, installation and operating expenses. The first two may be reduced with government support schemes like the Boiler Upgrade Scheme (BUS)[22,23]. However, operating costs are directly related to the net active Seasonal Coefficient of Performance ($\mathrm{SCOP_{net}}$), also known as the Seasonal Performance Factor (SPF) of the heat pump, which is defined as follows[11,24]

$$SCOP_{net} = \frac{Total\ heat\ output\ per\ annum}{Total\ electricity\ consumed\ per\ annum} \tag{2.1}$$

Operating costs are also affected by electricity prices, another area that may require government attention[21].

2.1.2 Types of domestic heat pumps

When it comes to domestic heat pumps, three main types are available on the market, each distinguished by its heat source[12], as illustrated in Fig. 2-3:

- Air-source heat pumps: These extract heat from outdoor air. Only the outdoor heat exchanger needs to be located outside the dwelling, making air-source heat pumps the most cost-effective and easiest to install, and thus, attractive for residential use[22]. However, since the heat source is outdoor air, the temperature available for heat extraction will vary with weather conditions.
- Ground-source heat pumps: These systems use the stable temperature of the ground as their heat source. They require access to land and excavation work to install the ground heat exchanger. They are used for both individual residential heating and district heating networks, with particular emphasis on the latter[25].

- Water-source heat pumps: These extract thermal energy from large bodies of water such as rivers, lakes, or underground aquifers. While they also benefit from stable temperatures, their use in residential settings is limited due to the need for proximity to suitable water sources. Additionally, there is a risk of water pollution, for example from contaminants released by pipe corrosion[12,26] .

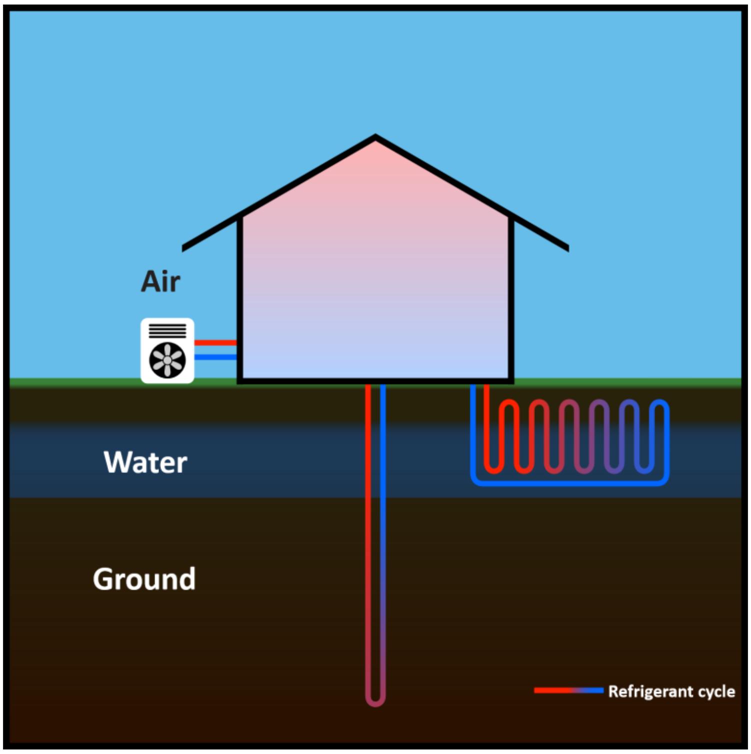

Fig. 2-3: Illustration of air, water and ground source heat pumps

With current government support, two types of heat pumps are eligible for grants: ground-source heat pumps and air-source heat pumps. While ground-source heat pumps tend to perform better due to the stable ground temperatures[11,27], they are significantly more expensive to install because of the groundwork involved (even when deducting the government grant) and are less flexible[23,28,29]. This makes air-source heat pumps more appealing, especially for individual homes, as shown in Fig. 2-4.

The Domestic Renewable Heat Incentive (RHI) mentioned in Fig. 2-4 is a government scheme that previously helped reduce costs to promote renewable heating and lower carbon emissions. This scheme operated from November 2011 until March 2022 and provided partial funding for adopting renewable heating systems (e.g., heat pumps and biomass boilers) as alternatives to fossil fuel-based systems (e.g., gas boilers).

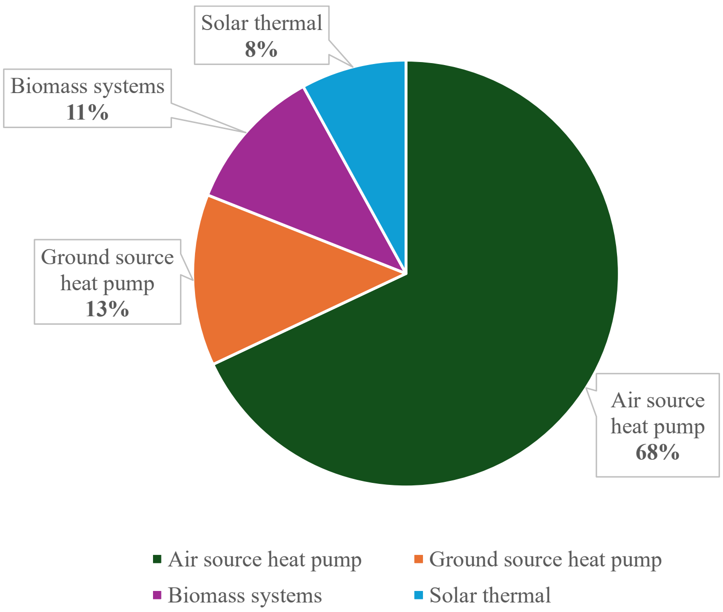

Fig. 2-4: Number of accreditations under Domestic RHI grant by type of technology from April 2014 to September 2022 in the UK[22,30]

Table 2-1: Retrofit field trials[11]

Trial	Average air-source heat pump SPF	Average ground-source heat pump SPF
UK trials		
Energy Saving Trust phase 1 (2009-2010)	1.9	2.5
Energy Saving Trust phase 2 (2011-2012)	2.45	2.82
Renewable Heat Premium Payment (2013-2015)	2.44	2.71
Electrification of Heat Demonstration Project (2020-2023)	2.80	Data not available
Selected European trials		
Superhomes (Ireland, 2017-2019)	3.35	No data
Fraunhofer (Germany, 2018-2019)	3.1	4.1

Air-source heat pumps have more flexible installation requirements, as they only use air as a heat source. This makes them among the most affordable and widely used heat pump types. However, their performance is highly impacted by seasonal variations, unlike ground-source heat pumps and gas boilers, and they generally perform less efficiently than ground-source heat pumps in year-round field trials, as shown in Table 2-1.

2.1.3 Deployment challenges for domestic heat pumps in the UK

As seen previously, air-source heat pumps are the most prevalent type for domestic applications due to their flexible installation options and lower cost. Although air-source heat pumps could be economically viable compared to gas boilers, this depends heavily on their seasonal performance, as illustrated in Fig. 2-5. It is seen that below a COP of 3.1 – 3.2, air-source heat pumps cannot economically compete with gas boilers, especially when compared to new A-rated gas boilers with over 90 % efficiency. The Energy Saving Trust's research further suggests that there would currently be no annual cost savings from installing a standard air-source heat pump in an average three-bedroom semi-detached home with radiators compared to a new A-rated gas boiler[29]. One of the reasons is the high cost of electricity as compared to gas in the UK.

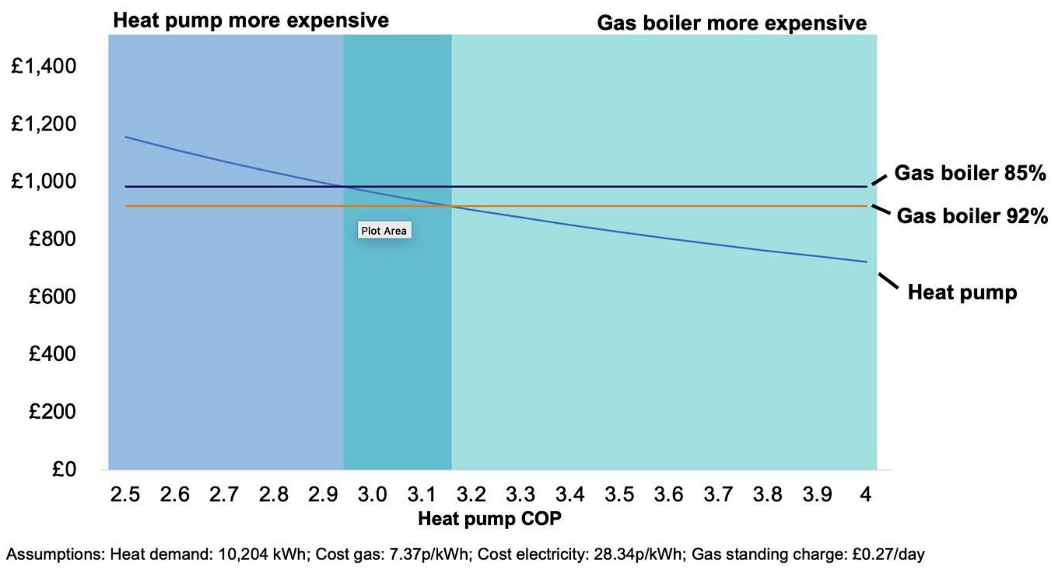

Fig. 2-5: Comparative operating cost of heat pumps and gas boilers[24]

Another reason is that air-source heat pump performance is dependent on weather, with reduced efficiency in winter as temperatures drop, increasing the temperature difference between the source and sink. Seasonal variations directly affect the COP of air-source heat pumps, making them less efficient during winter which is a critical period for heating.

This reduced performance is emphasised by the prevalence of oversized heating systems and inadequate insulation in existing UK homes, as shown in Fig. 2-6. In this figure, 515 domestic properties were surveyed by the UK government for the study on "Domestic Heat

Distribution Systems"[6]. The "oversizing factor" is defined as the ratio of the rated thermal output of the radiators in a dwelling to the peak steady-state demand for that dwelling. As seen, a majority of UK homes have an "oversizing factor" greater than 1, meaning the rated radiator output exceeds the peak steady-state thermal demand.

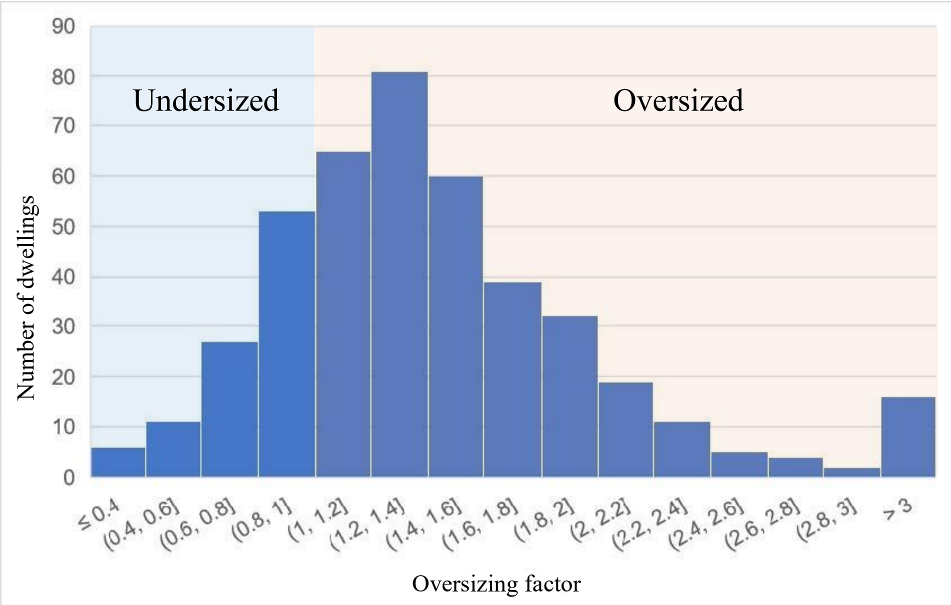

Fig. 2-6: Distribution of oversizing homes in a sample of UK households[6]

A study found that only 11 % of UK homes are fully "heat pump ready"[21]. When existing heating systems, typically designed for high temperature supply (60 °C or more[31]), are fitted with heat pumps, which supply heat at lower temperatures (usually around 45 °C), underperformance is a risk. Notably, 90 % of UK households have systems designed for higher temperatures, according to the UK housing survey[6]. Although some research suggests that certain buildings could operate at temperatures around 55 °C[21,32,33], for the majority of buildings, retrofitting heating systems and upgrading insulation would be required to achieve reduced supply temperatures[21,34–37]. These changes, while beneficial long-term, are often costly, posing a significant barrier to the widespread of heat pumps[21].

For homes where the existing radiators remain, a heat pump would be necessary to maintain temperatures of around 60 °C, even during winter[11,38,39]. Data from the Department for Business, Energy and & Industrial Strategy show that 53 % of homes could operate with a 55 °C flow temperature for most of the heating season without changes to heat emitters or flow rates; however, only 10 % would be suitable for this temperature on peak winter days[6]. Therefore, if the heat pump can meet the maximum flow temperature requirements during peak demand, the flow temperature could be reduced for most of the heating season, thereby increasing overall efficiency. This suggests that most UK homes would benefit from an air-source heat pump that can adjust to a flexible flow temperature.

Maintaining a high COP for air-source heat pumps with a large temperature difference between source and supply in winter is challenging, particularly due to frost accumulation, which also affects heat pump performance. This issue is particularly relevant in the UK, where cold and humid winter conditions lead to lower heating efficiency and higher energy consumption. Frequent defrost cycles are needed, consuming additional energy and affecting overall efficiency, which could compromise user comfort[27,28,40].

In summary, many UK homes would benefit from reliable, high-performance, and adaptable air-source heat pumps that are capable of operating at high temperature lifts during peak winter demand, and at variable temperature flow for most of the heating season, without costing significantly more than gas boilers. Consequently, extensive research has focused on addressing the challenges related to performance and flexibility in air-source heat pumps, as well as resolving frost issues to enhance their overall efficiency.

2.2 Enhancing flexibility and performance in domestic heat pump systems

As previously discussed, air-source heat pumps are the predominant type of domestic heat pump on the market, and their performance is sensitive to weather variations. At lower outdoor temperatures, the compression ratio and discharge temperatures increase significantly, causing the heat pump to reach peak electricity consumption[41]. At very low temperatures, depending on the design, an air-source heat pump may be unable to provide adequate heating without supplementary electrical heating[36], or may require a hybrid configuration, such as integration with a gas boiler for domestic hot water (DHW) production, for instance[42]. This can be particularly challenging in terms of performance and cost when aiming to achieve a supply temperature of 60 °C, as discussed earlier.

To palliate to this issue, extensive research has focused on expanding the operational range and improving the performance of air-source heat pumps to deliver heat effectively at sub-zero temperatures as low as - 15 °C[43–45]. In cases where a temperature lift greater than 50 K or very high condensing temperatures are required, two-stage compression cycles, or cascade heat pumps are typically the most effective configurations of heat pumps[46,47]. The two-stage compression cycle involves a dual-loop system using the same refrigerant, linked by an intermediate heat exchanger (IHX), as an intercooler, subcooler/economizer or flash tank, for instance[48]. The cascade heat pumps combine two independent cycles, each using a different refrigerant and joined by an IHX[49]. These advanced heat pump systems are common in industrial applications and climates with very low temperatures, as they can achieve very high temperature lift, and supply temperatures exceeding 100 °C[50,51].

However, for individual domestic applications, the smaller capacity of heat pumps and cost considerations often limit the feasibility of these complex designs. Particularly in moderate climates like the UK, the additional expenses and complexity involved in implementing features such as extra compressors and internal heat exchangers, solely to cost-effectively meet peak winter demand, make these solutions impractical[52]. Therefore, the literature reviewed here focuses on performance and flexibility improvements for single-stage vapour compression cycles to meet peak heat supply demands above 55 °C, even at low ambient temperatures, and flexibly switch to lower temperature flow to save power when required[6].

The improvements discussed in the literature are not limited to air-source heat pumps but are applicable to all types of domestic heat pumps, as they share the same main components and working principles, as mentioned in Chapter 1. However, these improvements are especially important for air-source heat pumps due to their operation with variable heat source temperatures.

2.2.1 Improvement in single-stage vapour compression system

Heat pumps incorporating a single-stage vapour compression cycle are widely used in domestic applications due to their relatively low cost. However, as previously mentioned, these systems are limited by having only a single compression stage and cannot maintain high compression ratios with high performance in a cost-effective manner. For example, most commercially available domestic air-source heat pumps are designed to operate at condensing temperatures up to approximately 55 °C[40].

2.2.1.1 Improvements in thermodynamic cycle

Firstly, research aimed at improving the thermodynamic cycle itself to enhance overall heat pump performance is reviewed in this section. A review of the available literature shows that these improvements are mainly focused on specific parameters that play a critical role in heat pump performance, namely compressor power consumption and heat transfer in the condenser for heating applications[53]. As shown by Eq. (1.1), the COP, and therefore the performance of the heat pump, is determined by the ratio of heat supplied to the indoor environment to the compressor power required to provide that supply. As a result, most research has naturally concentrated on improving these two key processes: the compression process and heat supply.

Therefore, the following sections focus on these two aspects of the heat pump.

Compressor efficiency and selection

A primary area for improvement within the cycle is the compressor, where optimising efficiency to reduce compression losses is essential for enhancing the COP of single-stage heat pumps designed to achieve high-temperature lifts in a cost-effective manner.

Scroll compressors have become a preferred choice due to their efficiency, approximately 10 % higher than that of reciprocating compressors[54,55]. This improvement results from the scroll's slow compression process over 540 degrees of rotation, which avoids the rapid compression and energy losses typically associated with reciprocating compressors operating on 180 degrees of rotation[19]. This design also eliminates suction and discharge valves, which are primary sources of pressure losses in reciprocating compressors, further enhancing efficiency and reliability in small-scale heat pump applications. Oquendo et al. notably concluded that, for pressure ratios below 7.5, a vapour injection cycle using a scroll compressor demonstrated higher efficiency and COP compared to a two-stage cycle using two reciprocating compressors in a two-stage air-source heat pump[56]. Conversely, for pressure ratios above 7.5, the two-stage system with reciprocating compressors performed better.

The variable-speed scroll compressor is another advancement that has proven beneficial, particularly in colder climates. Studies show that variable-speed compressors, which adjust their speed to match the ambient temperature, improve efficiency, flexibility and reduce the reliance on auxiliary heating, making them well-suited for domestic heat pumps with variable source temperatures such as air-source heat pumps[57,58].

Single-stage heat pumps operating under high temperature lift are frequently limited by high discharge temperatures, which can accelerate compressor wear, induce thermal stress on non-adapted components and chemical degradation of refrigerant mixtures, affecting the lifespan of the system[17]. This temperature should not generally exceed 150°C[38], necessitating safety mechanisms, either through the control unit or within the compressor's mechanical design. High discharge temperatures also lead to exergy losses, as entropy increases in the superheated section of the condenser when there is a large temperature differential between the compressor discharge and refrigerant saturation temperatures.

To address these losses, cooling mechanisms have been studied to manage discharge temperatures. For example, Wang et al. investigated external cooling of the compressor motor instead of suction gas preheating[59]. The results show that R22, R410A and R744 have larger potential benefits than R134a. They also proposed achieving combined isentropic and isothermal compression by transferring heat from the compression chamber, and found that this strategy can reduce the compression work up to 14% as compared to the solely isentropic compression process for the R22 refrigeration system.

Subcooling in condenser for enhanced efficiency

Performance of heat pump can also be improved by increasing the heat transfer within the condenser. This can be achieved by subcooling the refrigerant, which cools the refrigerant below its saturation temperature following condensation, notably for low temperature gradient heating systems[17]. By optimising subcooling, the heat transfer within the condenser can be significantly enhanced, allowing for an increase in the amount of thermal energy delivered by the refrigerant. Hervas-Blasco et al. investigated the optimal degree of subcooling in subcritical cycles with refrigerants R290, R134a, R1234yf and R32[60]. It was found that this optimal degree is significantly influenced by the temperature differential of the secondary fluid, and is found when two pinch points occur in the condenser: one at the condenser outlet and another within the condenser at the refrigerant dew point[16]. Furthermore, an increase in COP of up to 30 % was achievable under certain conditions with an appropriate control strategy.

Pinch minimisation

As highlighted in the previous section, pinch point temperature analysis within the heat exchanger is a valuable strategy to enhance heat supply to the secondary fluid loop. The pinch point in a heat exchanger refers to the location where the smallest thermal gradient between the hot and cold streams occurs, marking the most constrained and thermodynamically critical region of heat transfer[61,62]. Identifying this point is essential because the temperature gradient at the pinch point drives heat transfer and corresponds to the region of lowest exergy destruction, as it is where entropy generation is minimised. In practical systems with a finite heat transfer area, the pinch point temperature difference is always greater than zero[16].

Optimising heat exchanger design often involves careful consideration of pinch points, and minimising this temperature difference will improve heat-transfer effectiveness and energy efficiency, though it requires a larger heat transfer area and thus increased cost[63,64]. Typically, when using counterflow heat exchangers to reduce the temperature differential between the two fluids, and when using pure refrigerants or azeotropic mixtures (which behave like a single component), condensation and evaporation occur at a constant temperature. As a result, two pinch points are usually found in the condenser (at the refrigerant dew point and at a certain degree of subcooling, depending on the temperature profiles) and one in the evaporator (at the outlet of the source fluid). Both of these can be optimised for best efficiency[16,60,61,65].

However, as will be further discussed in the next section, zeotropic refrigerant blends (which behave like mixtures of components) have also been investigated in the literature because they condense and evaporate over a temperature range, which can help match the temperature profile of the secondary fluid in the heat exchanger[66]. For these types of refrigerants, Venkatarathnam et al.[67], as well as Liu et al.[68] and Gao and Zhao[69], found that there is a nonlinear relationship between temperature and enthalpy in the two-phase region. This can result in internal pinch points or maximum temperature differentials, which increase entropy generation and reduce efficiency. Therefore, when selecting zeotropic mixtures, it is important to consider the occurrence of pinch points within the condenser and evaporator in order to effectively match temperature profiles. Notably, Liu et al.[68] highlighted that a zeotropic mixture with a smaller maximum temperature difference in the condenser and a smaller minimum temperature difference in the evaporator can result in a higher COP.

2.2.1.2 Refrigerants selection

Significant efforts in chemical engineering have been made to identify suitable fluids for refrigeration and heating systems (in both subcritical and transcritical cycles), addressing safety, stability and performance concerns.

Subcritical cycle

In selecting refrigerants for heat pumps operating in subcritical cycles, refrigerant preferences have evolved multiple times in response to environmental and safety regulations. The introduction of hydrofluorocarbon refrigerants (HFCs) in the 1980s-1990s, following the phase-out of chlorofluorocarbon refrigerants (CFCs) and hydrochlorofluorocarbons (HCFCs) due to their ozone depletion potential (ODP), led to the adoption of refrigerants such as HFC-134a (R134a), HFC-410a (R410a) and HFC-407c (R407c)[17]. However, these

HFCs are also facing limitations due to their global warming potential (GWP), prompting renewed interest on refrigerants with lower GWP[38], such as hydrofluoroolefins (HFOs), hydrochlorofluoroolefins (HCFOs), hydrocarbons (HCs), and other natural refrigerants.

To ensure that a selected refrigerant remains in the subcritical cycle, the refrigerant's critical temperature serves as the upper temperature limit, ideally maintaining a temperature gap of about 10 to 15 K above the condensing temperature required for subcritical operation[38]. Moreover, the closer the critical temperature is to the condensing temperature, the lower is the refrigerant's latent heat of vaporisation, which reduces both the heating capacity and the COP[70,71]. Another criteria to consider is the refrigerant's boiling point at 1 atm, ideally maintaining a minimum temperature difference of at least 5 K between the outdoor air temperature and the refrigerant's boiling temperature[72]. In the UK, where temperatures rarely drop below -15 °C, a refrigerant with a boiling point of approximately -20 °C would be suitable.

In Table 2-2, common refrigerants used in the literature for heat pump and refrigeration applications are listed, with a focus on operating conditions relevant to the UK. Greyed cells are commonly used HFCs, such as R134a, R410a and R32, which have GWP values exceeding 150. Orange cells are refrigerants classified as flammable or toxic, based on varying levels of hazard, as defined in the updated ASHRAE standard 34 classification visible in Table 2-3[73]. Red cells indicate refrigerants that fall into both categories.

As seen in Table 2-2, all listed refrigerant fall within at least one category of restrictions. Under UK and EU F-Gas regulations (covering fluorinated gases including HFCs and HFOs), refrigerants with a GWP higher than 150 have been prohibited in new commercial refrigerators and freezers since 1st January 2022, and those exceeding 750 are banned in single split air-conditioning systems containing less than 3 kg of HFCs as of 1st January 2025[74,75]. Furthermore, according to the new EU F-Gas Regulation 2024/573, from 1st January 2027, new single split air-to-water heat pump systems with a rated capacity up to 12 kW that rely on F-gases with a GWP higher than 150 will be prohibited, except where needed to meet safety requirements[74].

For refrigerants with flammability properties, standards such as ISO 5149 and EN 378 specify regulations regarding the maximum allowable charge size and safety procedures. Manufacturers must apply these based on the system location, occupancy type, and refrigerant's safety class[76]. Flammable refrigerants are permitted for all refrigeration and heat pump applications as long as these safety regulations are followed. In contrast, refrigerants classified as toxic, such as R717 (ammonia), are prohibited in domestic application[77]. Further research is needed on low GWP, non toxic or flammable refrigerants, such as new HFO blends or safe natural mixtures, to achieve future efficiency and safety goals for heat pumps.

Table 2-2: Properties of common used refrigerants[38]

Type	**Refrig-erant**	**Chemical formula**	T_c **[°C]**	P_c **[bar]**	**ODP [-]**	**GWP [-]**	**Safety group**	**Boiling point at 1 atm [°C]**	**Molecul-ar weight [g/mol]**
HFC	R152a	CH_3CHF_2	113.3	45.2	0	138	A2	-24	66.1
	R134a	$C_2H_2F_4$	101.1	40.6	0	1430	A1	-26.1	102.03
	R32	CH_2F_2	78.11	57.8	0	675	A2L	-51.65	52.02
	R410a	CH_2F_2 (50%) CHF_2CF_3 (50%)	72.8	49	0	2088	A1	-48.5	72.6
HFO	R1234ze(E)	$C_3H_2F_4$	109.4	36.4	0	7	A2L	-18.95	114
	R1234yf	$C_3H_2F_4$	94.7	33.8	0	4	A2L	-29.49	114.04
HC	R290	C_3H_8	96.7	42.5	0	3	A3	-42.12	44.1
	R1270	$CH_3CH=CH_2$	91.1	45.6	0	2	A3	-47.6	42.1
Natural	R717	NH_3	132.3	113.3	0	0	B2L	-33.3	17

Legend:

- Orange: Refrigerants classified as *Flammable* or *Toxic* according to ASHRAE classification
- Grey: Refrigerants with a GWP exceeding 150
- Red: Refrigerants that fall into both categories

Table 2-3: ASHRAE Standard 34 Safety group classification[73]

Flammability	**Lower Toxicity**	**Higher Toxicity**
Higher Flammability	A3	B3
Lower Flammability	A2 A2L*	B2 B2L*
No Flame Propagation	A1	B1

*A2L and B2L are referring to lower flammability refrigerants with a maximum burning velocity of $\leq 10\ \mathrm{cm/s}$.

To address the issues associated with the refrigerants listed in Table 2.2 and to improve their performance, research has examined blended mixtures[78]. Zeotropic refrigerant mixtures, in particular, change phase over a temperature range known as the temperature glide. This property can allow a more efficient match with the temperature profile of the external fluid loop in heat exchangers, increasing system efficiency. However, careful consideration is needed to avoid internal pinch points or excessive temperature differences, as highlighted in the previous section[46].

Hakkaki-Fard et al. investigated the use of zeotropic refrigerant mixtures, as compared to pure refrigerants, to increase the performance of residential air-source heat pumps in cold climates. They notably concluded that a R32/CO_2 mixture (80/20) could increase the heating capacity by 30 % relative to R410a, while lowering GWP by 25 % and reducing R32's flammability and CO_2's high pressure. However, a major drawback of zeotropic refrigerant mixtures is the preferential leakage of more volatile components, which can alter the mixture's composition over time[78].

The use of azeotropic or near azeotropic blends has also been investigated. They allow adjustments to component properties while conserving a constant boiling point. For instance, Sun et al. studied a R134a/RE170/R152a mixture (35/35/30) as a replacement for R134a, concluding that it could directly replace R134a while ensuring a lower cost, a 61.79 % reduction in GWP, and enhanced heating capacity and COP[79].

Transcritical cycle

Among natural refrigerants CO_2 is an attractive alternative to HFCs due to its favourable physical properties, including non-toxicity, non-flammability, high volumetric heat capacity, high vapour pressure, and high density, which facilitate compact equipment, easy availability, and recycling[78]. However, because of its low critical temperature and high critical pressure, 31.1 °C and 73 bar, respectively, the heat pump needs to operate in transcritical conditions, as depicted in Fig. 2-7b. This mode of operation means that heating is provided through sensible heat transfer, and the condenser is replaced by a gas cooler. This approach is particularly suitable for hot water heating, especially when there is an important temperature difference at the sink, as transcritical CO_2 high temperature differential enhances heat transfer efficiency[80,81].

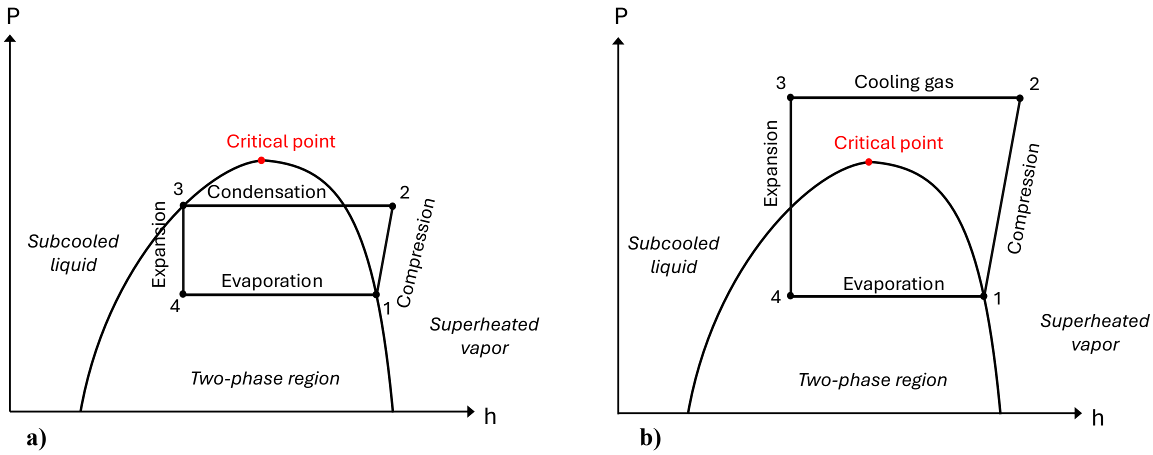

Fig. 2-7: P-H diagrams of: (a) subcritical cycle; (b) transcritical cycle

Since Lorentzen's pioneering work in the 90's, there has been a resurgence of interest in transcritical CO_2 cycles for refrigeration, air conditioning, and heat pump systems[82–84]. Fernandez et al. found that overall COP was maximised at higher ambient temperatures and lower hot water temperatures, with a 30 % higher COP observed when heating a full tank of cold water compared to reheating a warm tank after standby losses[85]. Hu et al. investigated an extremum-seeking, self-optimising control scheme to maximise the COP of an air-source CO_2 water heater, achieving promising results for maintaining peak COP under variable operating conditions, while satisfying the hot water outlet temperature setpoint[86].

However, transcritical CO_2 cycles suffer significant losses, particularly exergy losses in the gas cooler due to large temperature differentials and throttling losses from substantial pressure drops during expansion[87]. To address these, studies have investigated the incorporation of IHX between the gas cooler outlet and the compressor inlet, as well as ejectors to recover energy from the expansion process[88,89]. For instance, Boewe et al. concluded that an IHX could increase system efficiency by up to 25 % as compared to a classic CO_2 transcritical cycle[90].

Other techniques include combined systems, such as a CO_2 cycle paired with a subcooling cycle. Song and Cao investigated a CO_2-R134a combined cycle that performed more efficiently than a traditional transcritical CO_2 cycle, achieving a COP of 2.015 compared to 1.525 at an ambient temperature of 0 °C with a return/supply water temperature of 50/70 °C[91]. Dai et al. reported a COP of 2.13 for a CO_2 heat pump system incorporating vapour injection and dedicated mechanical subcooling when heating water at 65 °C with an ambient temperature of -20 °C[92].

However, due to the high-pressure operating conditions, significant losses, and complex design, the CO_2 transcritical cycle for heating applications, although widely researched and applied in Japan, particularly for CO_2 heat pump water heaters[93,94], has not yet gained widespread adoption among European researchers, who primarily focus on CO_2 refrigeration applications. In domestic heating applications, subcritical cycles remain the preferred approach[87].

2.2.1.3 Ejector technology

As discussed previously, the integration of ejector technology into heat pump systems has also been a focus for improving energy efficiency, particularly in refrigeration applications[95].

As explained in Chapter 1, unlike the Carnot heat pump cycle, the expansion process in real heat pumps does not provide work to the surroundings and is irreversible. This results in major losses, as energy is dissipated due to the significant pressure drop without producing useful output. To address these losses, research has been carried out to recover some of the unused energy. Ejectors are one of the most widely studied solutions for this purpose.

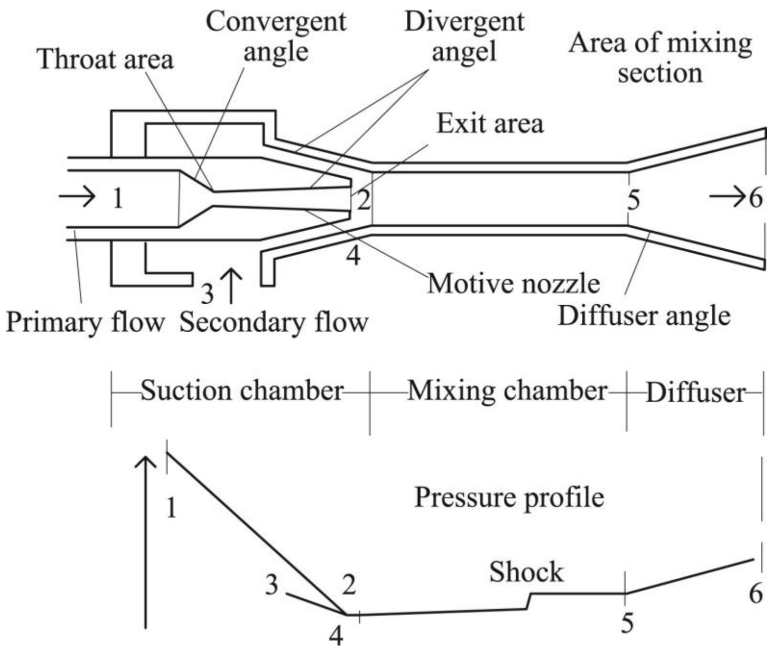

Fig. 2-8: Ejector geometry[46]

Ejectors consist of four main sections: the motive nozzle (also known as the primary nozzle), a suction chamber, a mixing chamber, and a diffuser. A schematic of the geometry is illustrated in Fig. 2-8. The ejector uses pressure differentials in the primary flow to drive the secondary flow.

Ejectors can serve as throttling and compression enhancement devices, known as ejector-expansion systems, using the expansion energy from throttling to raise compressor suction pressure above that of the evaporator, thus reducing the compressor's power input, as shown in Fig. 2-9. Chen et al. also explored the use of ejectors as jetting devices between the compressor and the condenser, with an added subcooler[96]. This setup was applied to enhance heating performance for air-source heat pump water heaters, particularly with non-azeotropic refrigerant mixtures in the evaporating temperature range of −15 to 10 °C and condensing temperature range of 55 – 60 °C. The results indicated that the maximum COP and volumetric heating capacity could be improved by up to 6.92 % and 37.32 %, respectively, depending on the operating conditions, compared to a conventional heat pump cycle.

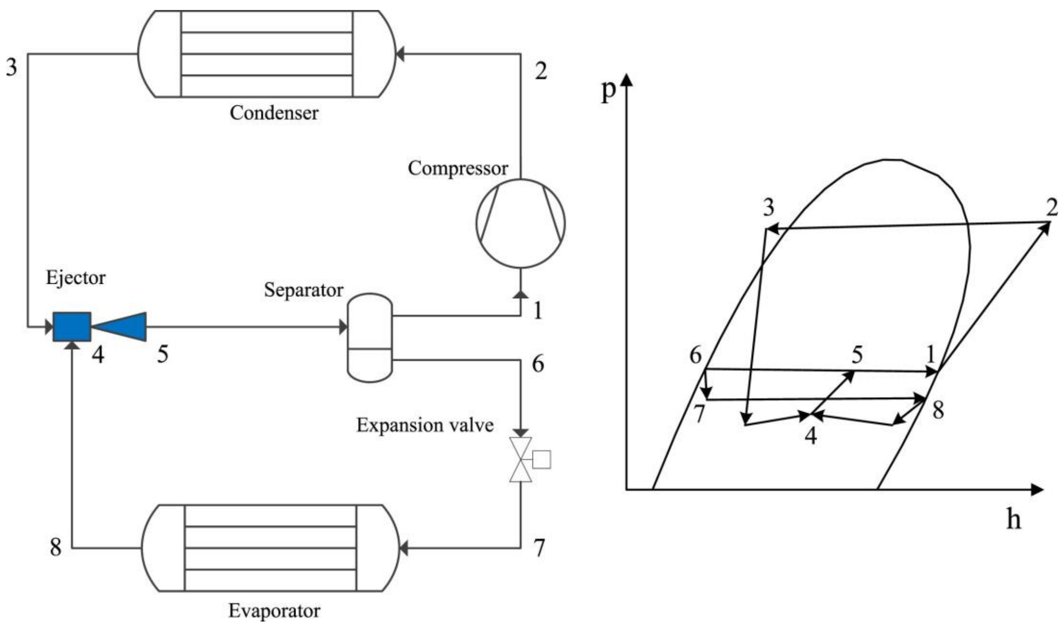

Fig. 2-9: Schematic and P-H diagrams of an ejector-expansion system[46]

While research shows that ejector-expansion systems enhance performance, especially at higher pressure ratios, most studies focus on improving cooling performance for refrigeration applications under low temperature conditions rather than in heating applications[97–99]. Therefore, additional research is recommended to investigate the potential of these systems for heating applications, optimising ejector design and system integration to maximise performance across variable operating conditions.

2.2.2 Performance improvement through flexible heat pump operation

In addition to the use of variable scroll compressors, which adapt to ambient conditions and allow for adjustment of the flow temperature in heat pumps, other investigations have focused on increasing the adaptability, flexibility, and performance of single-stage heat pumps operating under variable conditions.

2.2.2.1 Quasi two-stage operation

Quasi two-stage operation is intended to achieve higher sink temperatures more effectively without requiring two compressors, as in conventional two-stage heat pumps, or subjecting a single compressor to high compression ratios. Two primary strategies have been explored to accomplish this: refrigerant injection compressors and recuperative heat pump systems.

Refrigerant injection's compressor

Recent developments in compressor technology have made it possible to implement two-stage cycle with a single compressor by allowing direct refrigerant injection into the compression chamber via an auxiliary suction port[100]. This lowers the compression ratio and increases the refrigerant mass flow rate in the condenser by injecting refrigerant into the compressor, resulting in enhanced system performance, particularly under low ambient temperatures[101]. Modified compressors are central to this improved cycle, and it has been found that scroll compressors with multiple independent compression chambers are most suited to these systems[102].

Besides the compressor, the system can be built similarly to classic two-stage cycles, with the addition of a subcooler or flash tank, as seen in Fig. 2-10a and Fig. 2-10b. Studies indicate that these designs can achieve higher heating capacities, better COP, and lower discharge temperatures, especially in deep-frozen ambient conditions[55,103–105]. For instance, Guoyuan et al. investigated the performance of a vapour injection air-source heat pump with a subcooler heat exchanger over an entire winter in Beijing[43]. Results showed that the heat pump could operate efficiently at ambient temperatures as low as -15 °C, outperforming conventional air-source heat pumps.

When comparing both systems, it is usually concluded that the flash tank configuration is simpler, more cost-effective, and offers greater heating efficiency at low ambient temperatures, as it uses saturated vapour for injection[101,106]. The subcooler configuration, on the other hand, is using superheated vapour for injection making the controlling easier through adjustments of the degree of superheat, however the COP of this design is usually 10.5 % lower than that of the flash tank[40,54].

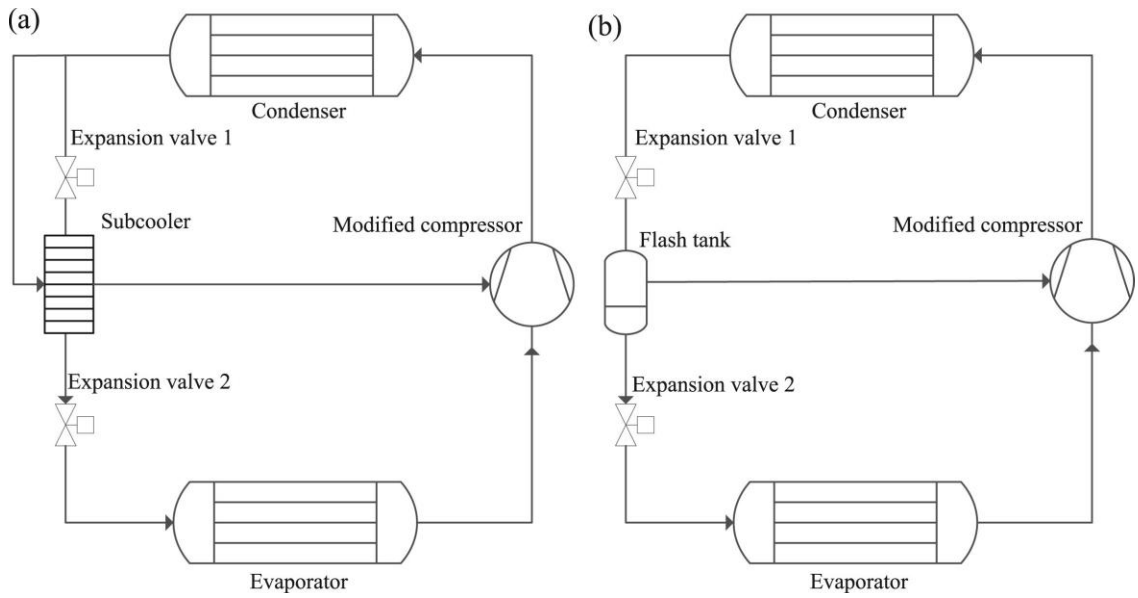

Fig. 2-10: Refrigerant injection system with (a) subcooler; (b) flash tank[46]

Further advancements in refrigerant injection systems have investigated advanced intermediate configurations, such as thermoelectric heat exchangers, as illustrated in Fig. 2-11. For example, Okuma et al. studied a system coupled with a thermoelectric heat exchanger with R410a for residential application, comparing it to vapour injection system with a flash tank[107]. Their findings showed an increase in heating capacity of nearly 20 % at -17.8 °C of ambient temperature compared to a vapour injection system, and 48 % increase compared to a conventional heat pump.

However, refrigerant injection systems come with increased costs due to the modified compressor and additional components. Moreover, advanced control strategies are required to manage oil return and refrigerant charge to ensure optimal efficiency making it difficult to maintain optimal injection ratio across a wide range of compressor speeds and load demands[108–110].

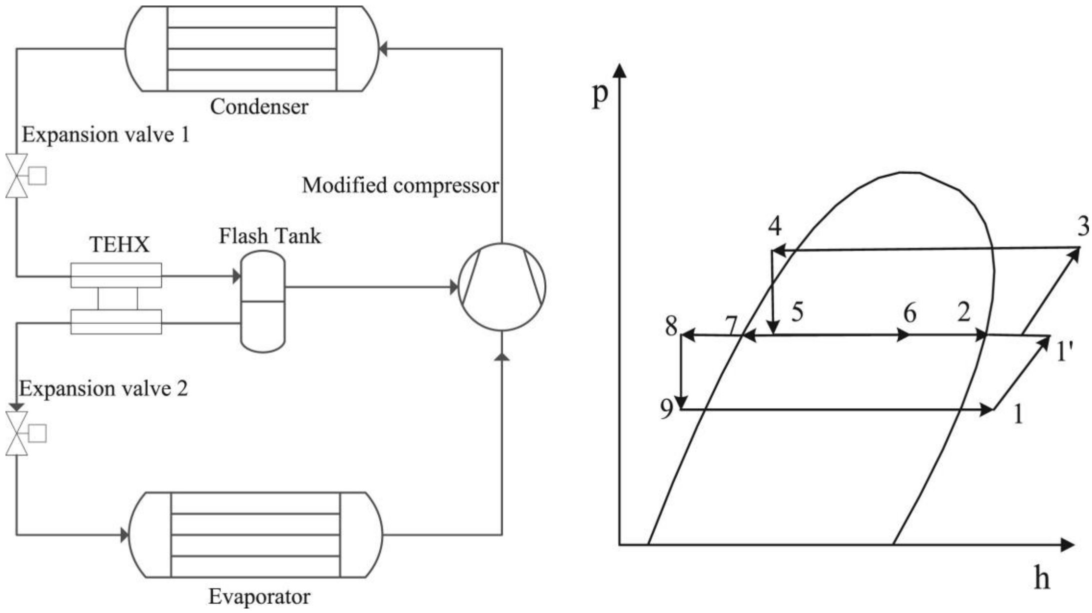

Fig. 2-11: Schematic and P-H diagram of a refrigerant injection system with a thermoelectric heat exchanger[46]

Recuperative heat pump systems

For water heating applications that require a large temperature differential, studies have investigated the use of recuperative heat pump systems to achieve significant temperature lift more efficiently with a single-stage compression cycle.

For example, Sun et al. conducted studies on a novel recuperative cycle, comparing the performance of high temperature lift applications in a single-stage heat pump with zeotropic refrigerant mixtures[111,112]. This study evaluated three distinct systems: non-recuperative, single-phase recuperative, and two-phase recuperative, depending on the refrigerant's phase in S1, as shown in Fig. 2-12. Water is heated progressively, with an important temperature differential in the condenser and the recuperative heat exchanger. Heat is also recovered through heat exchange between the refrigerant exiting the condenser and that exiting the evaporator (from S1 to S2), making the recuperative heat exchanger a three-stream heat exchanger. Simulation results show that a large temperature glide of the refrigerant mixture is necessary to minimise irreversible losses during condensation and heat recuperation. The two-phase recuperative system demonstrates a higher COP when the supply temperature exceeds 72 °C, and even at - 20 °C ambient temperature, a COP of 2.1 was achieved, whereas the non-recuperative system was unable to operate below 0 °C. The experimental investigation with a n-hexane and propylene refrigerant mixture showed optimal performance when heating water from approximately 24 °C to nearly 92 °C, achieving a COP of 2.83 and an exergy efficiency of 27.97 %.

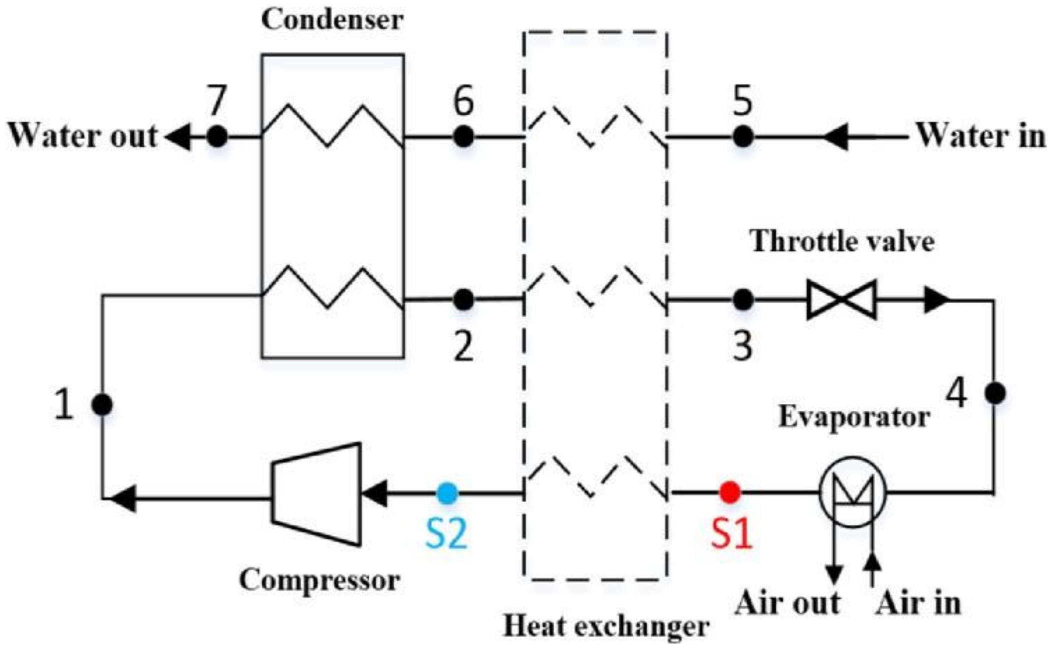

Fig. 2-12: Recuperative heat pump system[111]

However, this system requires an additional three-stream heat exchanger, which can be costly and challenging to manage, particularly under varying ambient conditions. Such system also requires sophisticated control, especially regarding water flow rate, which has a significant impact on its efficiency. Additionally, potential shifts in the composition ratio of refrigerant mixtures necessitate careful monitoring and possibly regular adjustments.

Based on the available literature, incorporating quasi two-stage operation into single-stage compression heat pumps offers clear benefits for performance enhancement when achieving higher temperature lifts, but it is limited by cost and design complexity. These enhancements are generally intended for industrial or large-capacity residential heat pumps, whereas small-capacity domestic heat pumps are typically designed with minimal components and complexity to maximise cost efficiency[17]. Additionally, the need for advanced control strategies presents a major drawback to their potential flexible use. As a result, hybrid systems have also been explored in the literature to improve the flexible performance of small-capacity heat pumps.

2.2.2.2 Hybrid heat pump systems

To improve the flexibility and performance of single-stage heat pump systems, hybrid configurations have been investigated. These systems integrate a conventional heat pump with external components to improve efficiency under variable operating conditions. This section focuses on hybrid systems that combine solar energy and/or thermal energy storage, as these are the most commonly used types of hybrid systems for domestic applications[25,113–115].

Combination with solar energy systems

The integration of solar technology with heat pumps has been studied as a solution to enhance performance by leveraging solar energy as an auxiliary heat or power source for the heat pump. Solar-assisted heat pumps combine heat pump technology with solar thermal (ST), photovoltaic (PV), or hybrid photovoltaic/thermal (PV/T) systems. These configurations use renewable energy sources, which enhance the COP throughout the year compared to conventional heat pumps used for domestic hot water[116,117].

The ST-heat pump setup benefits from additional thermal input provided by solar collectors, which can either increase the efficiency of the heat pump or directly supply heat to the user, allowing for flexible operation depending on weather conditions. Parallel and series configurations have been widely investigated, with parallel designs proving effective in high solar radiation areas, while series configurations are more suitable in low-radiation environments where additional temperature boosting is required. This approach has achieved water temperatures up to 55 °C, with Du et al. reporting that parallel configurations deliver superior COP compared to series arrangements[118,119].

In PV-heat pump setups, the PV panels generate electricity to be used by the heat pump. Hybrid PV/T-heat pump systems provide both thermal and electrical energy outputs, increasing system resilience under varying operational conditions. Experimental study by Wang et al. show COP values ranging from 2.74 to 5.98, with an average of 4.08 when supplying hot water up to 50 °C, and achieving electrical gains of approximately 278 W and heat gains of 664 W[120]. PV/T-heat pump configurations have also successfully reached water temperatures above 50 °C. In another study by Pei et al., part of the collected solar energy was converted into heat for the refrigerant, while the remainder generated electricity to increase overall power output[121]. They concluded that this configuration had superior performance than a conventional heat pump. Additionally, Cai et al. conducted a dynamic simulation to evaluate the behaviour of a hybrid PV/T-air-source heat pump, showing that the system maintained an average COP above 2 at an ambient temperature of 10 °C and solar irradiation of 100 W/m², while providing hot water at 50 °C[122].

However, the broader adoption of solar-assisted heat pumps faces challenges, such as the high cost of collector-evaporators, long payback periods of up to 14 years, lack of standardisation in manufacturing efficient solar-assisted heat pumps, lack of control strategies development for these systems, and limited field test applications[116].

Solar-assisted heat pumps have also been studied in combination with phase change materials (PCMs) as thermal energy storage to store and release heat as needed to meet heating demand[123–125].

In addition to their use in solar-assisted systems, PCMs and other thermal energy storage methods have been widely researched as integrated elements in standalone heat pumps, with the aim of increasing flexible load response and reducing operating costs.

Combination with thermal energy storage

The integration of thermal energy storage (TES) or heat storage (HS) systems with heat pumps has been increasingly considered as a method to improve heating performance and reduce power consumption, especially under fluctuating heating demands[126,127]. TES enables the storage of thermal energy for later use and is generally categorised into three types: sensible heat storage, latent heat storage, and thermochemical heat storage[128].

Sensible heat storage, a well-known approach, has been commonly applied in heating systems, particularly with water tanks for domestic hot water[129]. For an air-source heat pump water heater, heat is typically extracted from ambient air and stored in an insulated water tank, as illustrated in Fig. 2-13. Hot water is then available on demand. These tanks are often combined with an electric heater backup for when the air-source heat pump cannot operate, especially at low ambient temperatures or during defrosting cycles[53,129]. Studies have shown that heat pump water heater configurations are at least twice more efficient than conventional electric water heaters[53].

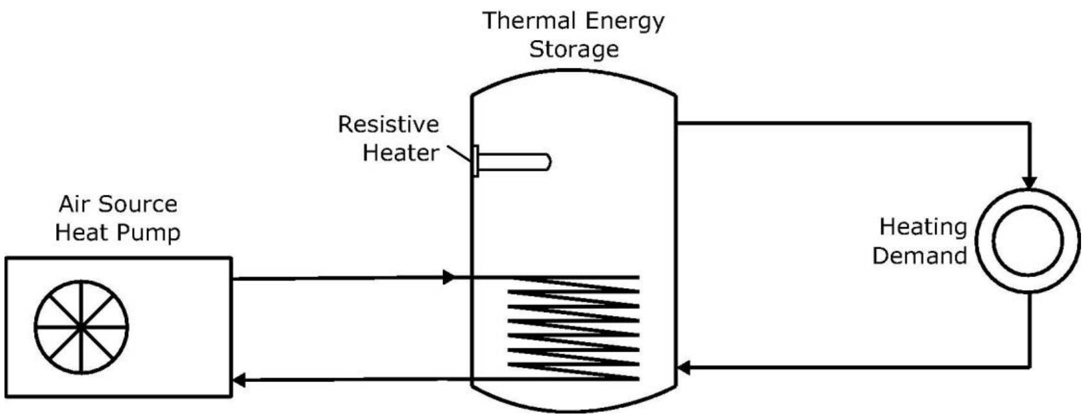

Fig. 2-13: Schematic of an air-source heat pump water heater[130]

For UK applications, Renaldi et al. investigated a combined air-source heat pump water heater with a water tank[130]. Through design and optimisation analysis, they found that a system with an 8.5 kW heating capacity and a 300 L water tank, operating on the Economy 10 electricity tariff, had the lowest operating cost, even lower than that of a gas boiler.

Recent advancements in combining heat pumps with TES have introduced PCMs as an innovative storage method. PCMs can store and release significant amount of latent heat with minimal temperature fluctuations and offer higher storage density than water. Consequently, they have attracted extensive research interest over the past several years[53,131]. Fig. 2-14 shows the types of PCMs reported in the literature for use with heat pumps.

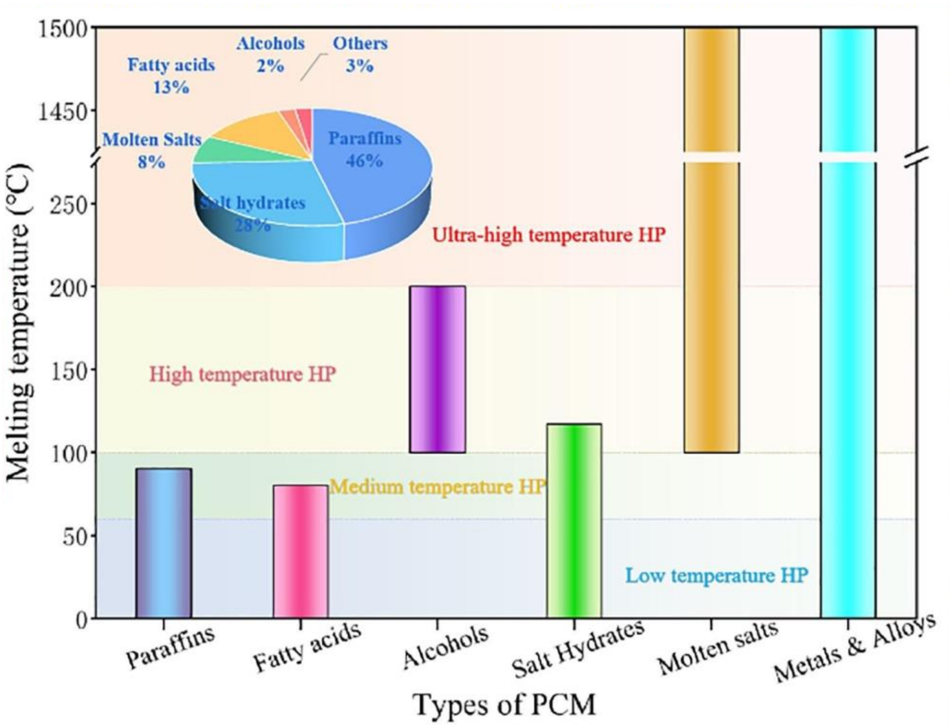

Fig. 2-14: PCMs considered in the literature for heat pump applications[132]

These materials have been considered as TES in various applications both within and outside the heat pump cycle. For instance, Zou et al. investigated an air-source heat pump water heater with a PCM layer featuring fins within a water tank to increase storage capacity without reducing water volume[133]. They achieved a 14 % increase in heat storage capacity while consistently delivering hot water at 55 °C. Gado and Hassan simulated PCM integration within a conditioned space heated and cooled by a heat pump, aiming to reduce the cooling and heating loads over the year, and thereby reduce electricity consumption by moderating room temperature fluctuations[134]. Results showed that, in summer, forced convection systems consumed 4.6 % less electricity than conventional heat pumps, and 1.4 % less in winter under natural convection.

Besides increasing storage capacity and reducing heating load, research has also investigated the integration of PCMs directly within the vapour compression cycle. Due to their high storage density, PCMs can store substantial heat in relatively small volumes, enabling improved heating load management within the heat pump system[132]. Lin et al. conducted experimental studies on an air-source heat pump with a condenser-integrated PCM storage unit to improve performance in cold regions[135]. In this setup, heat is directly transferred from the condenser to the PCM, reducing heat loss. The PCM stores heat during the charging cycle while the heat pump is active and later releases it to heat a water circuit during the discharge phase, with the heat pump turned off. This setup demonstrated a COP improvement of up to 4.01 % and an overall exergy efficiency increase of 4.65 %. A similar process was explored by Koşan and Aktaş in a solar-assisted air-source heat pump shown in Fig. 2-15, resulting in a performance increase of up to 15.67 %[136].

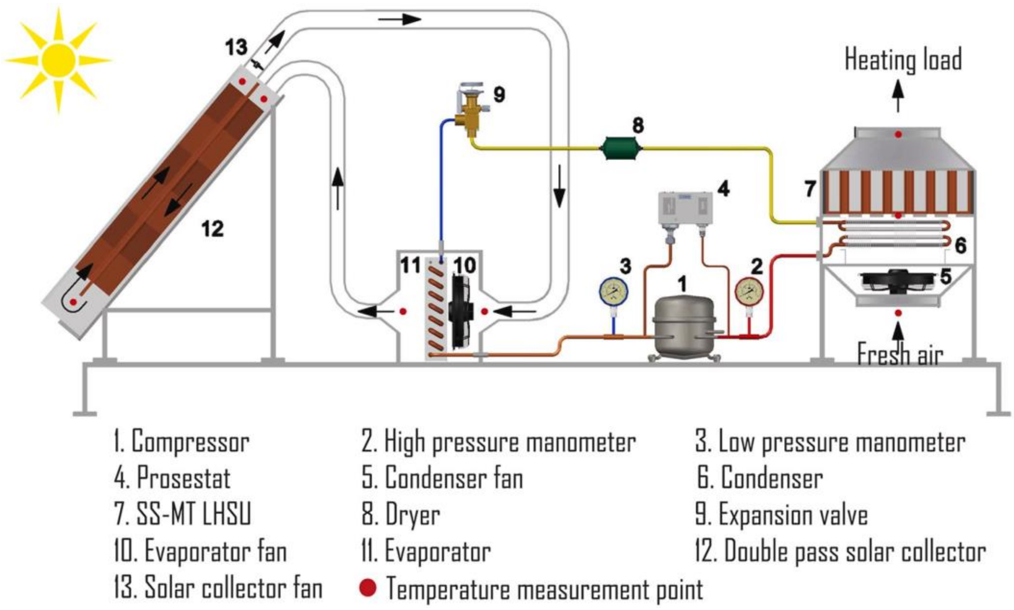

Fig. 2-15: Schematic of the solar-assisted heat pump with an integrated PCM storage in the condenser[136]

Long and Zhu conducted both numerical and experimental studies on a PCM water heater, storing heat during off-peak electricity hours and discharging it to heat water to 35 – 50 °C during peak hours, achieving an average COP of over 3.08 with this technique[137].

Although these studies demonstrate the potential of TES in improving heating load management, stabilising supply temperatures, and enhancing flexibility and heating performance, they have not directly addressed improvements to the heat pump cycle itself. For example, they have not considered reducing compressor power consumption by lowering the temperature lift and discharge temperature, which would also reduce operating costs and compressor wear over time. Additionally, Le et al. investigated a domestic high temperature air-source heat pump with a TES water tank in Northern Ireland[138]. They found that the continuous coupling of the heat pump and storage for household heating led to poorer performance and higher running costs compared to direct heating from the heat pump alone, and neither configuration could compete with gas boilers in terms of running cost.

2.2.2.3 Control strategies

Regardless of the type of heat pump or the operating conditions, adapted control strategies are essential for improving the performance of heat pump systems. These strategies allow for optimal operation of the device and adaptability to environmental conditions and demand loads. Effective control involves determining when to operate or shut down the system, when to reduce or increase its output, and when to store or extract heat from TES, all based on the current demand.

Recent studies on residential heat pump controls have explored advanced strategies to improve efficiency and flexibility during part-load operation. Two main categories of control strategies have been studied and implemented: rule-based controls and model predictive control (MPC)[139]. Rule-based controls use simple heuristic methods, such as "if-then" logic and set points, to adapt the operation of the heat pump according to a defined strategy. These methods rely on sensors to monitor trigger parameters, such as compressor power or room temperature. MPC are more complex and use optimisation algorithms based on accurate models of the system or, more recently, digital twins[140]. These models predict future behaviour and find the optimal management of heat pump operation over time[141].

Rule-based controls are commonly used in commercial heat pumps because they are simple, robust, and inexpensive[142]. These strategies can provide some flexibility by advancing the control objectives beyond simply maintaining a set point temperature for user comfort[139]. For example, Péan et al.[139] identified objectives such as load shifting according to a fixed schedule[143], peak shaving[144], or increased use of renewable energy[145], often in hybrid systems as described earlier. TES can play a key role in shifting the load, and solar power can help reduce electricity costs. However, rule-based controls have limitations, including poor dynamic response due to fixed threshold values and an inability to predict optimal heat pump operation over time.

To overcome the limitations of rule-based control, recent research has increasingly explored the use of MPC, particularly in hybrid heat pump systems, to improve flexibility and responsiveness under variable conditions. MPC strategies rely on real-time optimisation algorithms, where the controller seeks to minimise objectives such as energy cost, temperature deviation, or equipment wear over a defined prediction horizon[146]. The controller uses a mathematical model of the heat pump system to forecast future behaviour and determine the optimal sequence of control actions, taking into account operational constraints such as temperature set points and actuator limits. Initially, applications of model predictive control focused primarily on increasing energy efficiency and reducing operating costs[139–141,147]. For instance, Kuboth et al.[148] reported a 9 % reduction in energy cost by applying MPC to an air-source heat pump combined with photovoltaic panels and a storage tank, compared to a traditional controller. More recently, these control methods have also been used within smart grid contexts to explore the grid support potential of heat pump systems. By leveraging weather forecasts and electricity prices, MPC can shift heat pump operation to off-peak times, optimising energy consumption and reducing stress on the grid[149,150].

In summary, while advanced control strategies have improved the flexibility and part-load efficiency of heat pumps, as well as reduced operating costs, these improvements remain limited during periods of high temperature lift in the heating season. During prolonged cold weather, the heat pump will eventually need to operate at full capacity to maintain heating or charge a storage tank, which results in peak electricity consumption due to the high temperature lift required.

Furthermore, for air-source heat pumps, operating during winter will eventually lead to frosting of the outdoor coil, and no control strategy alone can fully resolve this operational challenge, which continues to impact the efficiency of air-source heat pumps. The next section discusses recent advancements in defrosting technology to address this issue.

2.3 Developments in defrosting technologies for air-source heat pumps

In addition to requiring improvements for high-temperature supply performance under varying weather conditions, air-source heat pumps used for heating applications are also susceptible to frosting on their outdoor heat exchanger, which negatively affects their efficiency. Consequently, this phenomenon has been extensively studied in the scientific literature, with researchers actively investigating methods to mitigate its impact, making it a major focus within the research associated with air-source heat pumps[151].

2.3.1 Mechanisms and impacts of frost formation

In cold and humid environments, frost tends to form on the outdoor heat exchanger of an air-source heat pump, making it highly vulnerable to weather conditions. More specifically, frost generally occurs when the air temperature drops below 6 °C and relative humidity is higher than 50 %[152,153]. Studies indicate that increased relative humidity is, in fact, the most critical factor in frost formation. Yao et al. developed a mathematical model for the outdoor unit of an air-source heat pump water heater/chiller, concluding that, at constant temperatures, frost formation becomes more pronounced with higher air relative humidity[154]. While at fixed humidity levels, frost formation is more significant at higher temperatures, but only below the frosting temperature. Other environment conditions, such as air velocity affect frost formation. The study notably highlighted a correlation between the increase of air velocity and the decrease of frost formation.

Frosting drastically reduces the efficiency of air-source heat pumps. The frost layer acts as an insulator, increasing the thermal resistance of the evaporator and obstructing airflow. Together, these factors diminish heat transfer efficiency in the evaporator, ultimately decreasing the heat pump's overall performance[155,156]. Observations indicate that frost initially has a negligible impact on the heat pump performance, but, as ice buildup progresses, performance deteriorates rapidly[153,157]. For example, Wang et al. observed a 29 % reduction in heating capacity after 55 minutes of frost accumulation on an air-source heat pump[158].

When the evaporator becomes frosted, an auxiliary backup heating device, typically an electric heater, is often used to sustain adequate indoor heat output. Votsis et al. found that this auxiliary device accounted for nearly 70 % of the overall performance degradation during defrosting periods, with the steady-state COP dropping between 10 % and 27 %, depending on ambient conditions[159].

Consequently, numerous studies have explored solutions to delay, prevent, and remove frost from the outdoor heat exchanger.

2.3.2 Frost mitigation strategies

Frost formation is caused by specific weather conditions leading researchers to explore methods to prevent or delay ice buildup on the evaporator. This is achieved either by mitigating these conditions or by addressing frost formation in its early stages.

2.3.2.1 Frost-free heat pumps

Humidity has been identified as the most important factor in frost formation. Consequently, removing humidity from the inlet air of the evaporator has been investigated as a solution to prevent frost formation on outdoor heat exchangers. Wang and Liu studied the integration of a solid adsorbent bed to dehumidify incoming air, resulting in improved heat pump performance and successful prevention of frost formation[152]. The pressure loss in the bed was minimal, avoiding any negative impact on the evaporator fan. However, the bed requires periodic desorption when its adsorptive capacity is low, which consumes additional energy and temporarily stops air dehumidification.

A liquid desiccant, specifically a lithium chloride solution, has also been investigated to maintain a frost-free operation by reducing the dew point of the inlet air by 8 °C[160,161]. The water removed from the evaporator inlet air was used to humidify a room, leading to a COP improvement of 30 – 40 % compared to a heat pump with an electric heater for humidification. However, the additional cost and complexity of installing dehumidifier and regenerator systems might restrain practical applications.

2.3.2.2 Frost delay strategies

Heating ambient air

The second most critical factor in frost formation is ambient air temperature. Increasing the temperature of the outdoor air can delay frost formation. Kwak et al. investigated a method using an electric heater to warm the inlet air entering the evaporator for a small-capacity heat pump[162]. They concluded that this method effectively delayed frost on the outdoor heat exchanger while maintaining stable heating capacity and efficiency at outdoor temperatures of 2 °C and 4 °C. However, this approach results in additional energy consumption from the electric heater, especially in winter when outdoor temperatures are low.

Increasing evaporator coil temperature

Frosting can also be delayed by raising the temperature of the evaporator coil surface. This can be achieved by stopping refrigerant flow through specific circuits with an actively distributing valve while continuously blowing air over the evaporator[163]. As a result, frosting period is prolongated. When the ambient temperature is above 0 °C, frost on closed tubes melts; at temperatures below 0 °C, the frost becomes compact, improving heat transfer and partially recovering the heating capacity. Thus, this method allows for a longer frost delay and reduces the frequency of defrost cycles, though defrosting will eventually still be needed.

Heating refrigerant

Heating the refrigerant within the cycle can delay frost formation by raising the temperature of the refrigerant entering the evaporator, which in turn increases the coil temperature. Mei et al. investigated this approach, using an electric heater to heat the refrigerant in the accumulator[164]. This method raised the coil temperature by several degrees, delayed frost formation, and increased the supply air temperature by increasing the compressor suction pressure. However, it was noted that this approach is inefficient when outdoor temperatures fall below 0 °C.

Ultrasonic vibration

Ultrasonic vibration as a frost removing technique uses ultrasonic mechanical vibrations to fracture frost crystals and layers, making them fall off due to gravity[165]. Frost removal through ultrasonic vibration is a complex mix of mechanical and acoustical effects[166]. Wang et al. showed that high frequency ultrasonic vibrations effectively delayed frost growth on a finned-tube evaporator with a hydrophilic coating, leaving two thirds of the evaporator fin gaps unblocked after 92 minutes of operation, compared to nearly complete blockage after 32 minutes without ultrasonic suppression[165]. Tan et al. further explored ultrasonic defrosting in a fin-and-tube evaporator, using an ultrasonic transducer at 28 kHz and 60 W with intermittent resonance[167]. They found that intermittent 4 minutes followed by 1 minute vibration, was more effective than continuous operation, reducing frost buildup and extending operational efficiency. However, high frequency ultrasonic vibrations are less effective on the initial frost layer, which adheres strongly to the coil surface and thickens over time. Moreover, further research is needed to assess real world applications and to minimise ultrasonic system power consumption[168].

Hot gas bypass method

Byun et al. investigated using the hot gas bypass method to delay frost formation while the heat pump remains in heating mode[169]. Although initially developed as a defrosting technique, it was applied here to delay frost formation. It consists in bypassing high temperature, high pressure gas discharged by the compressor into the evaporator, and in this study, without mixing it with the expanded refrigerant as it is usually the case. It was concluded that an optimal refrigerant flow rate bypass of 20 % could extend the defrost cycle to 170 minutes in heating mode, compared to 60 minutes without the bypass. During 210 minutes of operation, this method achieved a COP increase of 8.5 %, compared to a conventional system without defrosting measures. However, this method also led to temporary fluctuations in heat pump operation.

2.3.3 Overview of defrosting methods

The literature provides various approaches to achieve frost-free operation or delay frost formation in air-source heat pumps. While these methods can effectively prevent or postpone frost accumulation, they often involve significant costs, complexity, or increased energy consumption, eventually requiring a defrosting cycle to remove frost buildup. This section reviews the primary defrosting techniques explored in the literature, including: compressor shutdown[170], electric heating[171], hot water spray[172], hot gas bypass[173] and reverse cycle[174].

2.3.3.1 Compressor shutdown

The compressor shutdown method consists of allowing ambient air to melt the frost on the outdoor coil. This approach has been studied by Ameen et al., who highlighted the importance of air velocity in enhancing the melting process[170]. Higher air velocity results in faster defrosting times. A numerical study indicated that, with an ambient temperature of 2 °C and a dew point of 0 °C, this method achieved a defrosting capacity comparable to the hot gas bypass method while reducing power consumption by a factor of 10[175]. However, compressor shutdown is only effective when ambient temperatures are above 0 °C and requires long defrosting duration, limiting its practical application.

2.3.3.2 Electric heating

Electric heating is a widely used technique for defrosting and involves placing an electric heater in the outdoor unit to melt frost on the tubes. Melo et al. experimentally compared different types of electric heaters for defrosting the evaporator of a household refrigerator and found similar defrost efficiency across the tested heaters, although, the glass tube heater demonstrated the highest average efficiency at 48 %[176]. The main drawback of this technique is the significant power consumption, as Bansal et al. found that a freezer with 500 g of frost and normal defrosting cycle consumed 17.7 % more energy than under normal operation[171].

2.3.3.3 Hot water spray

The hot water spray method involves spraying hot water onto the outdoor tubes to melt frost. Although there is limited research on this technique, Abdel-Wahed et al. observed that defrosting time is relatively short[172]. However, repeated water spraying may enhance future frost formation on the outdoor coils.

2.3.3.4 Hot gas bypass

The hot gas bypass cycle, described earlier and illustrated in Fig. 2-16, is a commonly studied and applied defrosting method[168]. It requires minimal modifications to the heat pump and is more efficient when frosting is in its early stages, as it generally takes longer to melt frost compared to the reverse cycle method[177].

A portion of the hot gas is directed to the evaporator to carry out the defrosting process. The hot gas refrigerant is typically mixed with the expanded refrigerant before entering the evaporator, and in this case, the higher temperature of the flowing refrigerant gradually melts the frost. However, the significant pressure drop that occurs when mixing both fluids causes rapid condensation of the discharged gas. As a result, liquid refrigerant accumulates in the evaporator coil and in an accumulator or protected suction line, which is necessary to prevent liquid slugging in the compressor[177–179]. This presents a challenge with the hot gas bypass technique: over time, less gas returns to the compressor as more liquid refrigerant accumulates in the coils and accumulator, leading to a reduced supply of hot gas[180,181].

Other drawbacks of this defrosting method, as reported in the literature, include the long defrosting time due to the sole reliance on compressor power as the energy source for defrosting, and the potential for mechanical shock when hot, high-pressure gas is released abruptly into a cold, low-pressure evaporator[177,178].

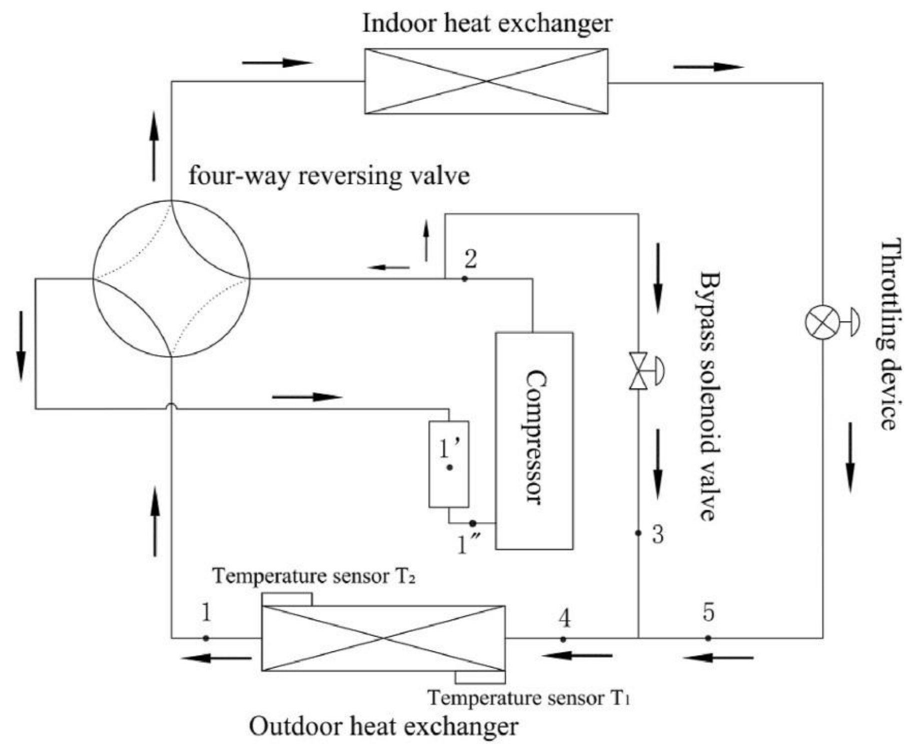

Fig. 2-16: Schematic of the hot gas bypass defrosting method[180]

To improve the defrosting efficiency of this technique, Choi et al. investigated a modified hot gas bypass cycle, incorporating a dual hot bypass setup with two lines connected to the inlet and outlet of the evaporator[181]. This configuration shortened defrosting time compared to a conventional hot gas bypass but remained slower than reverse cycle defrosting, while also achieving faster recovery and preserving up to 50 % of heating capacity during defrosting. Another study explored a continuous heating approach with a hot gas bypass in a multi-evaporator system[182]. While one evaporator was being defrosted using the hot gas bypass method, the others continued providing heat to the cycle, resulting in a 17.5 % increase in defrost energy efficiency compared to the reverse cycle method and a smaller drop in supplied hot water temperature. This method, however, requires an extra evaporator and remains slower in defrosting than the reverse cycle.

2.3.3.5 Hot liquid defrosting

Hot liquid defrosting uses high temperature liquid refrigerant exiting the condenser to defrost the evaporator through subcooling. For example, Niu et al. developed a hot liquid defrosting system with multiple evaporators for refrigeration[183]. When one or more evaporators required defrosting, all hot liquid refrigerant from the condenser was directed to these evaporators acting as subcoolers, while other evaporators maintained cooling capacity without additional power input. Similarly, Ma et al. experimentally studied an air-source heat pump with four parallel evaporators defrosting in rotation, allowing continuous indoor heating[184]. When compared to hot gas bypass defrosting, the heating capacity and COP are increased by 10 – 20 %.

However, in both cases, each evaporator must be alternately defrosted, requiring precise timing and control. Moreover, to achieve continuous heating or cooling, these systems require multiple evaporators and control mechanisms, which increase system complexity and cost.

2.3.3.6 Reverse cycle defrosting

Reverse cycle defrosting, is a widely adopted, efficient method requiring only a four-way valve as an additional component to operate[157]. A schematic of this method is shown in Fig. 2-17. When frost has been accumulated on the outdoor heat exchanger, the defrosting cycle is initiated by reversing the valve, causing hot refrigerant to flow through the evaporator to melt the frost. During defrosting, the condenser becomes the evaporator, drawing heat from the indoor heat exchanger to defrost the outdoor coil. In air-to-air heat pumps, the indoor fan is typically turned off to prevent cold air from being blown indoors[185].

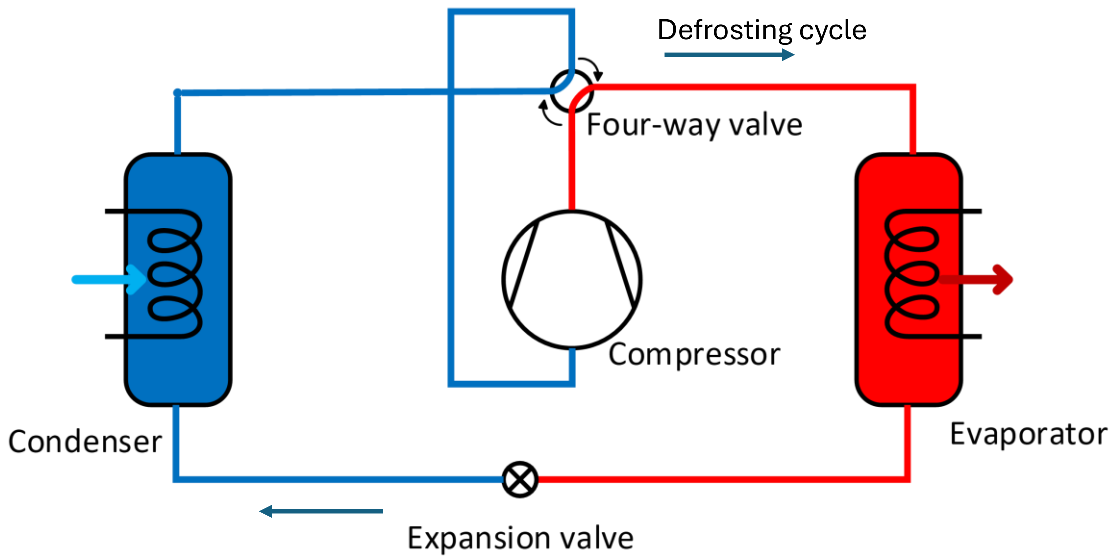

Fig. 2-17: Schematic of the reverse cycle defrosting

Comparative studies indicate that reverse cycle defrosting is nearly three times faster than the hot gas bypass method[177]. This is mainly due to the multiple energy sources available to melt the frost during reverse cycle defrosting, including compressor power, condenser coil heat, and heated air or water, whereas hot gas bypass defrosting relies solely on high pressure gas heat[186]. However, reverse cycle defrosting interrupts heating and, by extracting heat from the indoor environment, leads to temperature fluctuations. Dong et al. found that, for an air-to-air heat pump, when the condenser fan is kept on during reverse cycle defrosting, the heat supplied by indoor air accounted for 71.8 % of the defrosting energy, reducing defrosting time[186]. However, this can negatively impact indoor comfort.

Experimental and numerical studies of reverse cycle defrosting have highlighted that the system incurs important mechanical shocks when switching between defrosting and heating modes[180,187,188]. Upon switching, suction pressure rises while discharge pressure falls abruptly until the refrigerant stabilises, potentially delaying heating recovery. Additionally, Qu et al. noted that downward flowing of melted frost along the coil surface during defrosting reduces defrosting efficiency[185,189].

Among the various defrosting techniques studied, the reverse cycle and hot gas bypass methods are the most widely used in air-source heat pumps because they offer a balance between effectiveness and practicality[177,190,191]. Therefore, the next section focuses on recent advancements aimed at improving the efficiency and reliability of these two common defrosting strategies.

2.3.4 Recent innovations in defrosting techniques

Given the limitations of common defrosting methods, particularly reverse cycle and hot gas bypass, various studies have examined optimisation strategies for defrosting processes by addressing different aspects of the system such as: the components, control strategies and the use of TES[192].

2.3.4.1 Components optimisation

Expansion Valves

Expansion devices have also been shown to impact defrosting efficiency. O'Neal et al. studied different expansion devices in a reverse cycle defrost system, testing five different orifice sizes and one open line[193]. Results indicated that larger orifices enhanced defrosting performance. Huang et al. investigated an air-source heat pump with a thermostatic expansion valve in frosting and defrosting conditions, and noted an unstable refrigerant flow due to valve "hunting" during frosting periods[155]. Ding et al. tested the addition of a bypass solenoid valve in a system using a thermal expansion valve, which successfully smoothed the reverse cycle defrosting operation and allowed quicker resumption of the heating cycle after defrost[194]. Finally, Qu et al. used an electronic expansion valve (EEV), regulated by superheat, and concluded that this improved the defrosting efficiency through better refrigerant flow regulation and minimised wasted heat[195].

Optimisation of the evaporator structure

During the frosting and defrosting process, ice does not form and melt evenly on the evaporator's upper and lower circuits, with the lower circuits usually taking longer to become frost-free[185]. This uneven melting wastes defrosting energy on warming the upper circuits and ambient air. Dong et al. reported that a quarter of the total energy in reverse cycle defrosting goes towards vaporising melted frost and heating the ambient air[186]. Therefore, removing melted frost quickly can significantly shorten defrosting time and improve efficiency. To optimise the defrosting process, research has focused on adjusting the evaporator structure to address issues like downward flow of melted frost and poor heat management, thereby improving defrosting time and efficiency.

For example, Song et al. studied a heat pump with a horizontally installed multi-circuit evaporator, which improved defrosting efficiency by 9.8 % and limited the downward flow of melted frost compared to a vertically installed evaporator[196]. Additionally, turning the outdoor fan on to blow melted frost away was investigated, which reduced retained water but decreased defrost efficiency due to increased heat transfer. A circular shaped evaporator coil has been studied by Newitt and Huang for hot gas bypass defrosting[173]. This design, with increased fin spacing by curving the evaporator's tubes, prevents frost from blocking the airflow path and lowers the noise level of air passing through. Furthermore, Yu et al. studied a bowl-shaped finned tube evaporator as an anti-frosting option[197]. This design reduces frost driving force and improves the evaporator's frost resistance using fan vortex wind and gravity. This resulted in a partially frost-free area, extended heating time, and an increase in COP by up to 17.3 % compared to a conventional evaporator. However, some parts of the evaporator still require eventual defrosting.

Fan pre-start

Fan pre-start involves starting the evaporator fan before the end of the defrosting cycle. This method, typically used during reverse cycle defrosting, helps to lower refrigerant pressure in the evaporator before defrosting completes, which in turn reduces refrigerant discharge pressure[198,199]. This lowers the pressure transient at the end of defrosting and prevents compressor shutdown.

Hydrophobic/hydrophilic treatment

Surface treatments have been investigated to enhance anti-frosting effect, notably by modifying surface wettability to give the surface specific wetting characteristics in contact with liquid[157]. Wang et al. studied the effect of superhydrophobic fin treatment combined with high-speed hot air blowing on the evaporator coils during the early stages of frost formation[200]. The coating on the tubes reduces frost adhesion, enabling most frost embryos to be removed, with remaining frost evaporating within 3.5 seconds. To further reduce defrosting time, the surface of the evaporator fins should have a large contact angle with minimal contact angle hysteresis. However, this method requires continuous operation to prevent frost from forming and additional equipment to blow and heat air, which increases power usage.

Jhee et al. explored the effects of both hydrophobic and hydrophilic coatings on the outdoor heat exchanger[201]. Results showed that hydrophilic treatments affect frosting behaviour, while hydrophobic treatments impact defrosting behaviour. Defrosting efficiency improved by 3.5 % with hydrophilic treatment and by 10.8 % with hydrophobic treatment compared to untreated surfaces. However, hydrophobic surfaces had a faster blockage ratio from frost buildup than the other surfaces.

2.3.4.2 Control strategies

While various component improvements have been investigated to optimise the defrosting process and enhance system efficiency, effective control of the system remains essential. Particularly in terms of when to initiate and terminate the defrosting cycle when periodic defrosting is necessary. Proper control is critical to minimise energy waste during defrosting and reduce negative impacts on the sink environment[168]. Song et al. identified two main types of control strategies for initiating defrosting: time-based and on-demand[192].

The time-based approach relies on pre-set timing to start the defrosting cycle and is the most widely used due to its easier implementation. However, it can often lead to "mal-defrost", such as defrosting starting too late, when frost has already significantly built up, or too early, when frost has not yet formed on the outdoor heat exchanger. Wang et al. has observed a mal-defrost issue under moderate climate conditions[202]. After five days of operation, frost covered over 60 % of the evaporator, reducing the COP and heating capacity by 40.4 % and 43.4 %, respectively.

The second strategy, on-demand control, initiates defrosting based on real-time measurements of ice buildup, providing more accurate timing but with a more complex implementation. Various studies have explored different on-demand defrosting methods, such as: temperature-based control, temperature difference-based control, neural network control, refrigerant flow instability control, frost layer thickness detection, temperature and humidity coupled control, artificial intelligence control, optimal defrosting duration control, fan power sensors, fibre optic sensors, etc.[157,168,192,203–207].

Hewitt and Huang compared three control methods: time-based control, discharge temperature control, and temperature difference control between the inner and outer sides of the evaporator coil[173]. The aim was to find the defrost initiation method that provided the highest heating capacity with the fewest defrost cycles. Although the temperature difference control achieved the highest COP, it led to frequent defrosting cycles, which could deteriorate heat pump performance in prolonged sub-zero conditions. Consequently, a 30 minutes interval with 2 minutes defrost duration was chosen with the time-based control.

Wang et al. used photoelectric sensors to monitor frost levels and initiate defrosting, extending the defrost interval from 28.8 minutes to 52 minutes and reducing the number of cycles from 9 to 5[208]. Tassou and Marquand studied an air-to-water heat pump under varying ambient conditions[153]. They suggested that an evaporator pressure differential control method would be an efficient defrost initiation strategy, as it accounts for both ambient temperature and humidity effects. They concluded that selecting an appropriate pressure drop threshold could limit the negative impact of frost buildup to under 10 %.

2.3.4.3 Combination with thermal energy storage

Although research has focused on optimising defrosting cycles through improved components, energy management, control strategies, and various defrosting techniques, a common issue remains the lack of sufficient energy for defrosting in the main methods: hot gas bypass and reverse cycle. In hot gas bypass, the defrost relies solely on the heat from the pressurised refrigerant gas, leading to a slower process. Reverse cycle defrosting extracts enough energy for quick defrosting, but a substantial portion of this energy comes from the sink environment (e.g., hot water or indoor air), which disrupts the heating process and may lead to indoor discomfort, such as cold air blow. Additionally, the continuous heating while defrosting has not been investigated without multiple evaporators, which can be problematic when numerous or prolonged defrost cycles are needed, particularly during heavy winter usage and in the night.

The standard solution to maintain heating during defrosting is to add an electric heater to the heat pump, but this increases power consumption and may require costly modifications. Jang et al. tested dual-spray hot gas defrosting for continuous heating, but only achieved 50% of the normal heating capacity[209]. In an experimental study on reverse cycle defrost energy consumption, Dong et al. highlighted the potential of TES, specifically PCMs storage, as an alternative energy source to address the energy shortage during defrosting[186]. This approach has been explored in various configurations[157,192].

Shen et al. reviewed defrosting methods using PCM storage as a heat exchanger, finding that many of these configurations could address the energy shortage for melting frost in reverse cycle defrosting, or hot gas bypass, by storing heat during the heating cycle and using it for defrosting[191,210–212]. They successfully reduced defrosting time and enhanced overall system performance. Minglu et al. compared conventional reverse cycle defrosting with a novel reverse cycle defrosting that used a PCM heat exchanger, noting improvements in thermal comfort, defrosting time, and recovery, since heat was drawn from the PCM storage rather than the indoor environment[213]. Moreover, Dong et al. investigated the impact on system performance of different types of energy accumulators during the heating/storage cycle in a multi-split air-source heat pump[214]. They concluded that the fin-tube energy accumulator with serial energy storage achieved the longest heating period. Therefore, TES show good potential for increasing the defrosting performance. However, in these studies, heating is still discontinued during defrosting.

Qu et al. investigated using a water tank as a TES in a cascade air-source heat pump to improve defrosting efficiency compared to hot gas bypass[215]. The storage was used as a heat source to defrost the low-temperature cycle section and as an evaporator for the high-temperature section, providing continuous heat to the sink. However, the stored heat was insufficient to supply for both cycles, causing a drop in suction pressure. In a follow-up study, water was replaced with a PCM heat exchanger, but the PCM supplied more heat to the low-temperature cycle than the high-temperature cycle (62.3 % compared to 37.7 %), resulting in only partial heating recovery[216]. Therefore, further investigation is needed.

An air-source heat pump incorporating a TES, and shown in Fig. 2-18, was designed by Long et al. to recover the dissipated heat from the compressor's casing, achieve continuous heating while defrosting and, reduce the recovery time[217]. A PCM storage was used to store the heat dissipated by the compressor and was later used as heat source during defrosting mode. Continuous heating is provided by dividing the refrigerant in two flows at the outlet of the compressor, one part to defrost and the other to heat indoors. After what, the refrigerant flows are mixed after being expanded and are evaporated in the PCM heat exchanger. As compared to a conventional reverse cycle defrosting, they observed higher suction and discharge pressures during defrosting, avoiding system shutdown. The defrosting time was reduced by 65 %, total defrost and recovery energy consumption reduced by 27.9 %, and COP increased by 1.4 %. However, compressor power use was higher, and only part of the heating capacity could be recovered during defrosting due to the split refrigerant flow.

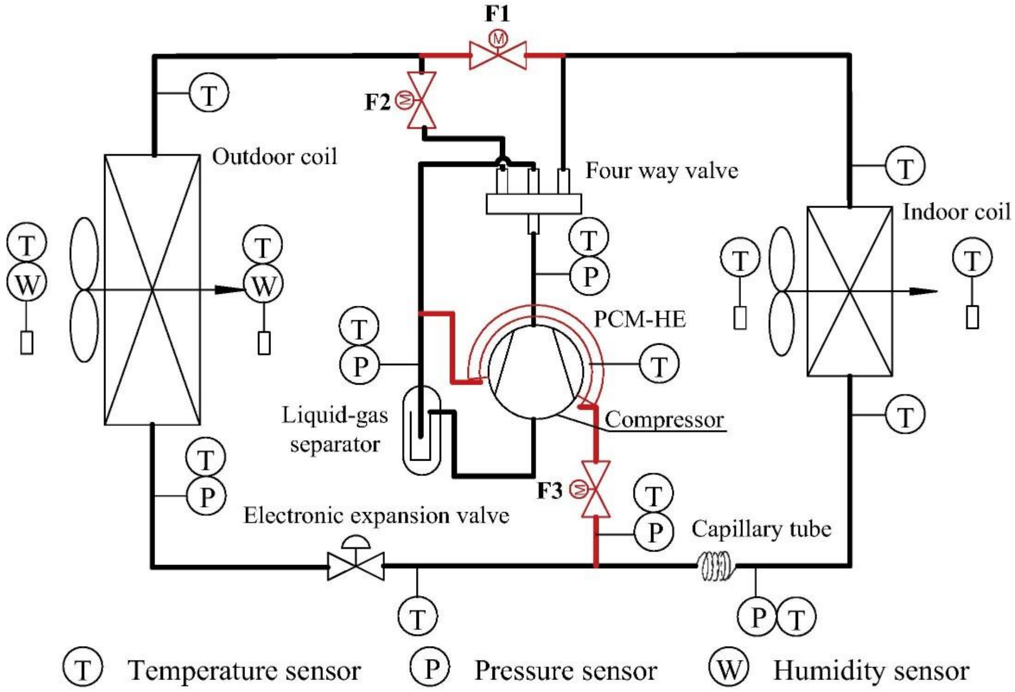

Fig. 2-18: Schematic of the novel defrosting method using heat dissipated by compressor's casing[217]

TES has also been applied to an air-source heat pump water heater to achieve frost-free operation and continuous heating by Wang et al.[218]. The system is presented in Fig. 2-19. It uses an extra heat exchanger coated by a solid desiccant (EHECSD) and an energy storge device (ESD) to achieve frost-free operation. The heat pump can operate in two modes: heating mode and regeneration mode. During heating, the EHECSD prevents frost formation by dehumidifying incoming air, and the ESD stores subcooled heat from the refrigerant exiting the condenser. Regeneration occurs by heating the solid desiccant with subcooled refrigerant from the condenser, and the ESD is used to evaporate refrigerant before it enters the compressor. Experimental and numerical studies analysed the effects of different atmospheric conditions, EEV settings, desiccant materials, and PCM storage[218–222]. This heat pump demonstrated COP improvement of 17.9 % compared to a reverse cycle defrosting, and frost-free operation during 32 minutes at -3 °C and 85 % relative humidity[219]. At 3 °C, the improvement is 3.4 % for 36 minutes of frost-free operation. The dehumidification efficiency decreased with higher temperature. However, this system presents the same issues as frost-free systems described in section 2.3.2.1. Moreover, it is more effective at lower ambient temperatures and may not be as suitable in milder climates. It has also only been tested in laboratories, so real-life performance data are not yet available.

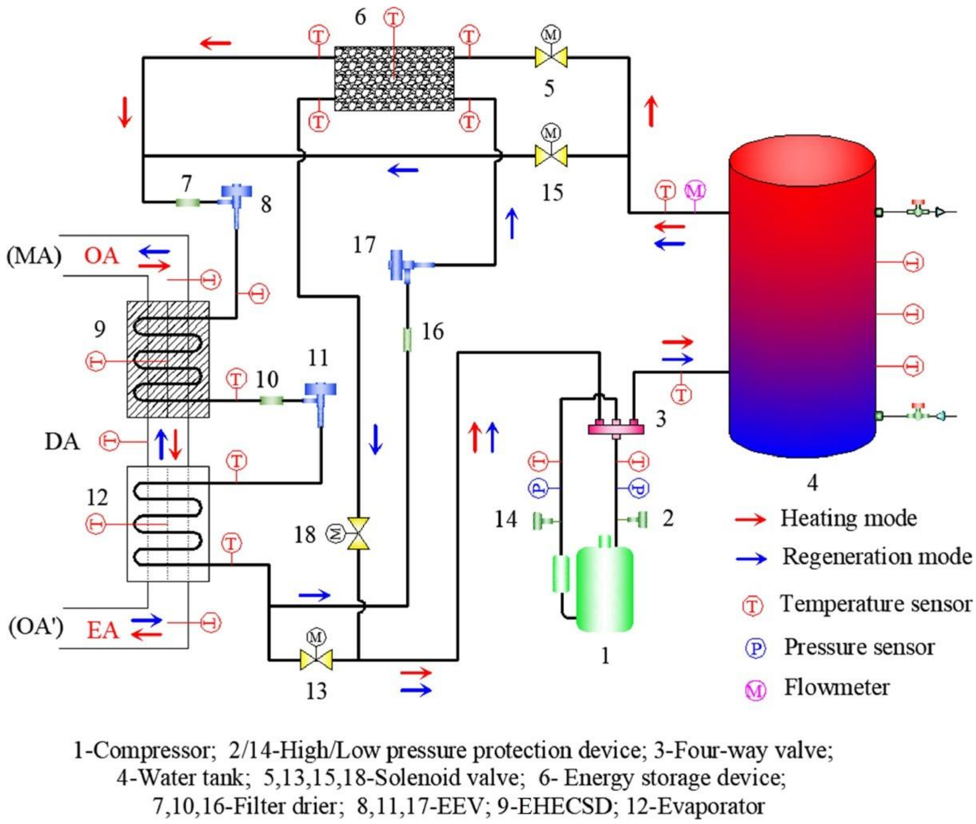

Fig. 2-19: Schematic of the novel frost-free air-source heat pump water heater[220]

2.4 Identified research gaps and questions

Heat pumps are a crucial element in efforts to decarbonise the heating sector in the UK, as highlighted by various government and academic reports. One of the main action plans to encourage widespread adoption of heat pumps is to make them the most cost-effective heating option compared to gas boilers. In the UK's climate, achieving this goal will require improvements to the current heat pump technology available on the market. For individual households, which generally require small capacity heat pumps, air-source heat pumps are the most economical choice. However, this type of heat pump is highly sensitive to fluctuations in ambient conditions. Therefore, this literature review has focused on investigating improvements that could make air-source heat pumps more suitable for typical UK applications, ensuring they are cost-effective, efficient, and flexible. Based on the review, two main research gaps have been identified, and corresponding research questions are posed to guide the research conducted in this thesis:

1. The UK's oceanic climate, characterised by high humidity and mild winter temperatures, presents ideal conditions for frosting on the outdoor heat exchanger of air-source heat pumps. Frost accumulation is a common issue in air-source heat pumps, as it gradually reduces the heating capacity until the system potentially shuts

down entirely. Consequently, effective defrosting is essential and has been widely examined in both refrigeration and heating applications. While various defrosting methods have been considered in the literature, hot gas bypass defrosting and reverse cycle defrosting are the mainly used approaches in practical applications. However, these methods come with drawbacks, including interrupted heating during the defrosting process, lack of energy available in the vapour compression cycle leading to user discomfort, and sometimes increased power consumption. Although the literature discusses improvements in defrosting cycles, through components optimisation, control strategies, and the use of TES, these solutions only partially address the issues and often involve complex systems unsuitable for small capacity heat pumps. Continuous heating during defrosting has generally only been achievable with either partial heating capacity recovery or by adding an extra evaporator, which affects user comfort or significantly raises costs.

→ **<u>This raises the question:</u>** How can air-source heat pumps be improved to be efficient in the UK climate, provide uninterrupted heating, avoid performance declines, limit increased operating costs to compete with gas boilers, and remain cost-effective, with the potential for frequent defrosting cycles during winter?

2. Most UK homes have heating systems that are oversized and designed to receive water at 60 °C. Without insulation upgrades or modifications to the existing heating system, an air-source heat pump would need to match the temperature provided by gas boilers, especially on peak winter days, and later operate at a lower temperature flow for the rest of the heating season to maintain cost efficiency. Achieving this supply temperature under variable ambient conditions can be costly if the required temperature lift is high, and it is important for the heat pump to remain cost-effective while adapting to changing weather. Various solutions have been explored in the literature, including improvements to system components, careful refrigerant selection, quasi two-stage operations with a single compressor (such as vapour injection systems and recuperative heat pumps), hybrid heat pump systems and various control strategies. While these approaches have increased heating capacity, achievable temperature lift, and operational flexibility, they do not always result in significant power savings. Furthermore, these solutions are often complex, expensive, require advanced control strategies, and likely increase maintenance needs, making them less suitable for small-capacity heat pumps in the UK market when competing with gas boilers.

→ **<u>This raises the following question:</u>** How can a small-capacity, single-stage air-source heat pump be improved with minimal additional components and complexity to efficiently operate at a 60 °C supply temperature on peak winter days, avoid significantly higher operating costs, and remain cost-effective under variable ambient conditions?

<u>Finally, considering both challenges, a central question arises:</u>

→ What modifications or improvements could be made to the air-source heat pump cycle to address both the need for cost-efficient operation at a 60 °C supply temperature and effective defrosting in the UK climate, without making the system overly complex or costly, while still allowing for flexible operation?

To address these questions, this thesis introduces a novel concept of a heat pump integrated with heat storage. The following chapter presents the concept and explains how it can effectively address both challenges, along with detailing the methodology used for the analysis. Chapters 4 and 5 specifically focus on the defrosting issue and provide an overview of the benefits of this heat pump layout compared to conventional systems. Subsequently, Chapters 6 and 7 explore the advantages of the new concept when achieving high-temperature supplies while remaining flexible and cost-effective. Finally, Chapter 8 summarises the findings.

Chapter 3 Multi-valve flexible heat pump with integrated storage: concept and modelling

To address the research questions outlined in the previous chapter, this chapter presents the fundamentals of the multi-valve flexible heat pump with integrated heat storage, including its working principles and various operational modes. The modelling approach, along with its underlying assumptions, is thoroughly explained. The steady-state models used to analyse the energy performance of the flexible heat pump in different modes are detailed. Additionally, the chapter presents the exergy, economic, and environmental models that provide a comprehensive evaluation of the system's performance as compared to a conventional single-stage heat pump. To ensure model accuracy, the predicted compressor power and COP are validated against experimental data. Furthermore, an overview of the refrigerants selected for this study is provided along with their thermophysical properties.

3.1 Introduction

In Chapter 2, a comprehensive literature review was conducted on the state-of-the-art in heat pump technology, focusing on efficiency and flexibility enhancements in air-source heat pumps for high temperature supply applications. The review also examined advancements in defrosting methods for air-source heat pumps. Research gaps were identified, along with associated research questions that form the foundation of this thesis. As discussed, heat pumps are crucial to decarbonising the heating sector, making it essential to improve their accessibility and performance across a wider range of applications. This is notably the case in the UK, where they must compete with traditional fossil fuel heating systems like gas boilers. These improvements must be cost-effective to ensure that the already high cost of heat pumps does not increase significantly.

This chapter introduces the concept of the multi-valve flexible heat pump, explaining its working principles and potential to enhance efficiency with minimal modifications. The differences between this flexible heat pump and a conventional single-stage heat pump are thoroughly explained, along with the functions and operations of each mode. The chapter also details the fundamentals of the energy model, including the assumptions and modelling approach, as well as the exergy, economic, and environmental models. The modelling methodology is validated with experimental results, which are presented alongside the simulation outcomes. Finally, the refrigerants considered for this study are introduced, along with their thermophysical properties.

3.2 System concept and operating principles

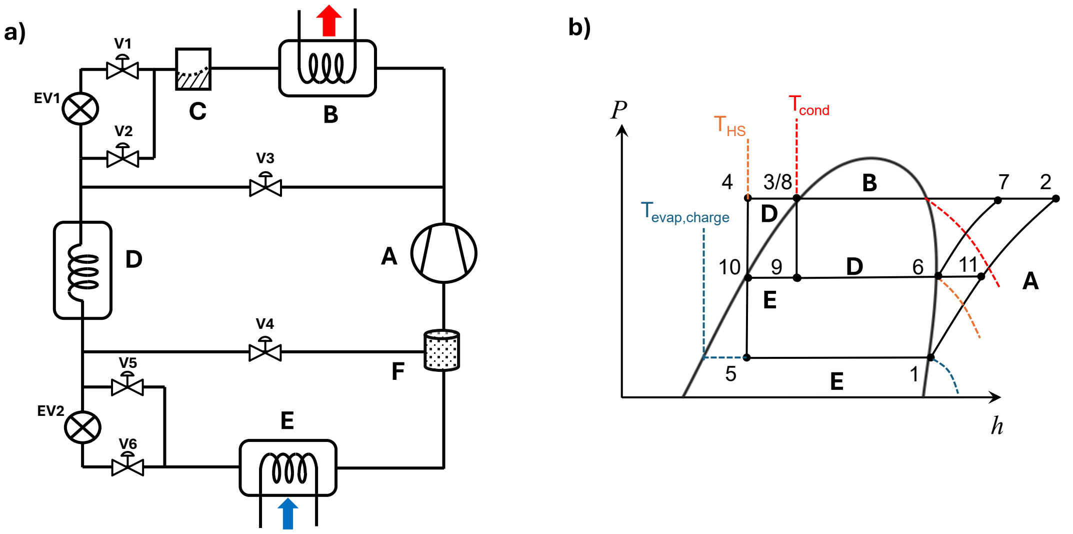

A	B	C	D	E	F	V1, V2, V3, V4, V5, V6	EV1, EV2
Compressor	Condenser	Refrigerant storage	Heat storage	Evaporator	Accumulator	Ball valves	Expansion devices

Fig. 3-1: The multi-valve flexible heat pump (a) Schematic; (b) P-H diagram

A schematic and related P-H diagram of the multi-valve flexible heat pump are illustrated in Fig. 3-1. This design is an alternative one to the flexible heat pump presented in a previous paper by our group[223]. The differences with the previous design are listed below:

- There is no four-way valve in this design. It has been replaced by 6 ball valves allowing for a flexible switch between the different modes;

- The defrosting mode of this system is not made by subcooling refrigerant in the evaporator but by condensing hot gas after its evaporation in the heat storage;

- The system allows a new charging mode for heat storage.

The design of this setup consists of a compressor (A), a condenser (B), a refrigerant storage tank (C), a heat storage (D), an evaporator (E), an accumulator (F), two expansion devices (EV1, EV2) and six ball valves (V1, V2, V3, V4, V5, V6).

The flexible heat pump concept differs from a regular heat pump in that it modifies the classic vapour compression cycle to enable heat recovery from the subcooled refrigerant at the exit of the condenser. This recovered heat is stored in an additional heat storage unit (latent or sensible heat storage) while the system continues to provide heat as usual, corresponding to the transformation from point 3 to point 4 on the P-H diagram shown in Fig. 3-1b. The stored heat can later be utilised for two main purposes: power-saving and defrosting. Additionally, the system offers a mode where heat is directly recovered into the storage unit by condensing the refrigerant at a lower temperature when heating is not required. Ultimately, this system can operate in four distinct modes, as outlined in Table 3-1.

Table 3-1: Four operating modes of the flexible heat pump

Mode	Operating modes	P-H cycle	Valves open
1	Heating and charging of heat storage	1-2-3-4-5-1	V2, V6
2	Discharging of heat storage and power-saving	6-7-8-9-6	V1, V4
3	Discharging of heat storage, power-saving and defrosting	6-7-8-9-6 and 6-10	V1, V4, V5
4	Charging heat storage at lower temperature	1-11-10-5-1	V3, V6

Switching between modes should be operated automatically via an accurate control strategy (e.g., PID controller, micro controller, etc.), which opens the relevant valves according to the real-time requirements for flexible operation. The flexible heat pump should be combined with different monitoring strategies to initiate and terminate the modes at the right times. For instance, a time-based control method is suitable for Mode 4, as it can operate during off-peak hours to reduce electricity costs. A temperature-based control method is beneficial for Mode 2, where a set-point temperature for the heat storage is determined during Mode 1, triggering the transition to Mode 2 and vice versa. Finally, a temperature difference-based method is appropriate for Mode 3, with a specific set point defined by the temperature difference between the evaporator coils and the inlet air. The detailed control strategy is out the scope of this thesis which focuses on the fundamental working principles, and potential benefits of the new concept.

To provide a clearer understanding, the modes mentioned in Table 3-1 are described comprehensively below.

3.2.1 Mode 1: Heating and charging of heat storage

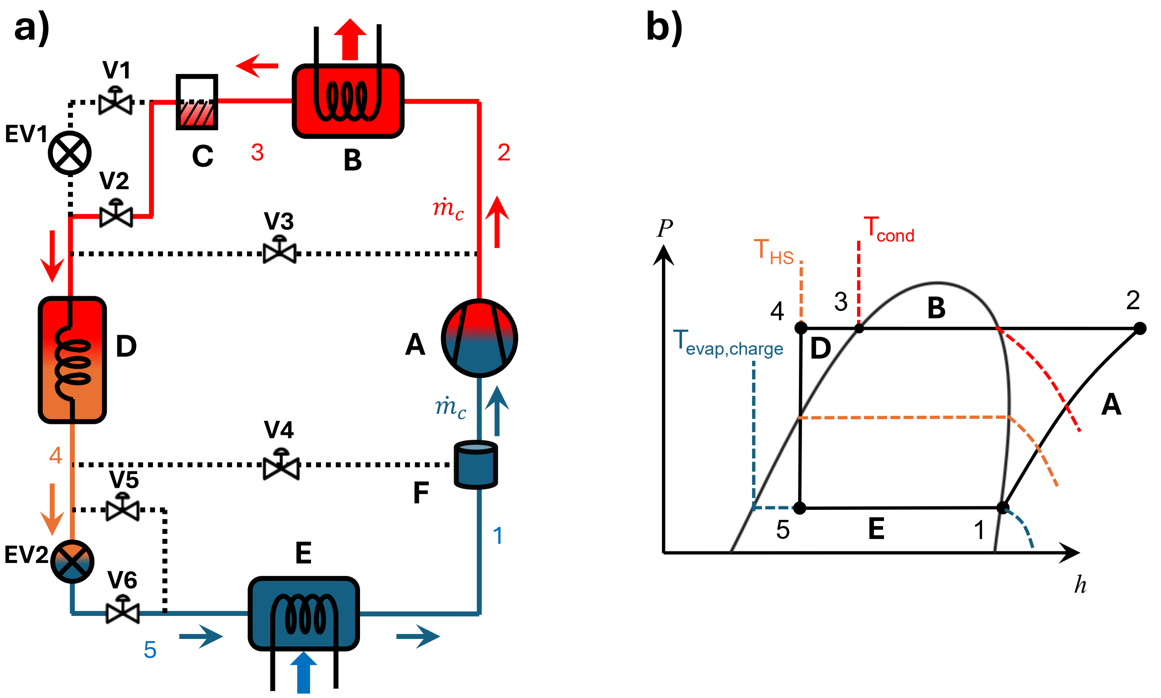

Fig. 3-2: Mode 1: heating and charging of heat storage; (a) Schematic; (b) P-H diagram

The heating and charging mode is shown in Fig. 3-2. The discharged refrigerant from the compressor flows through the condenser and then through valve V2. Afterwards, it is subcooled in the heat storage to store heat. The refrigerant is throttled by the expansion valve EV2 and flows through the valve V6 to the evaporator where it is evaporated. The refrigerant returns to the compressor to complete the cycle. This mode allows the heat pump to recover subcooled heat and charge it into the heat storage for later use. This mode also functions as the standard heating mode of a vapour compression cycle, providing heat to a sink while extracting heat from a source. In the case of an air-source heat pump, under certain outdoor conditions, this mode can lead to the formation of ice on the evaporator after operating for an extended period of time.

3.2.2 Mode 2: Discharging of heat storage and power-saving

Fig. 3-3 illustrates Mode 2 of the flexible heat pump. The evaporator is bypassed, and the heat storage becomes the heat source for the cycle. The refrigerant flows from the compressor to the condenser keeping the same heating capacity. It then goes through valve V1 and the expansion valve EV1. Next, it flows to the heat storage to be evaporated at a higher temperature than in Mode 1. The refrigerant goes through valve V4 and finally returns to the compressor. In this mode, compressor power is being saved by increasing the evaporating temperature which reduces electrical consumption by decreasing the source-sink temperature gradient. Additionally, thermal energy is extracted from the heat storage to provide heat to the refrigerant's cycle.

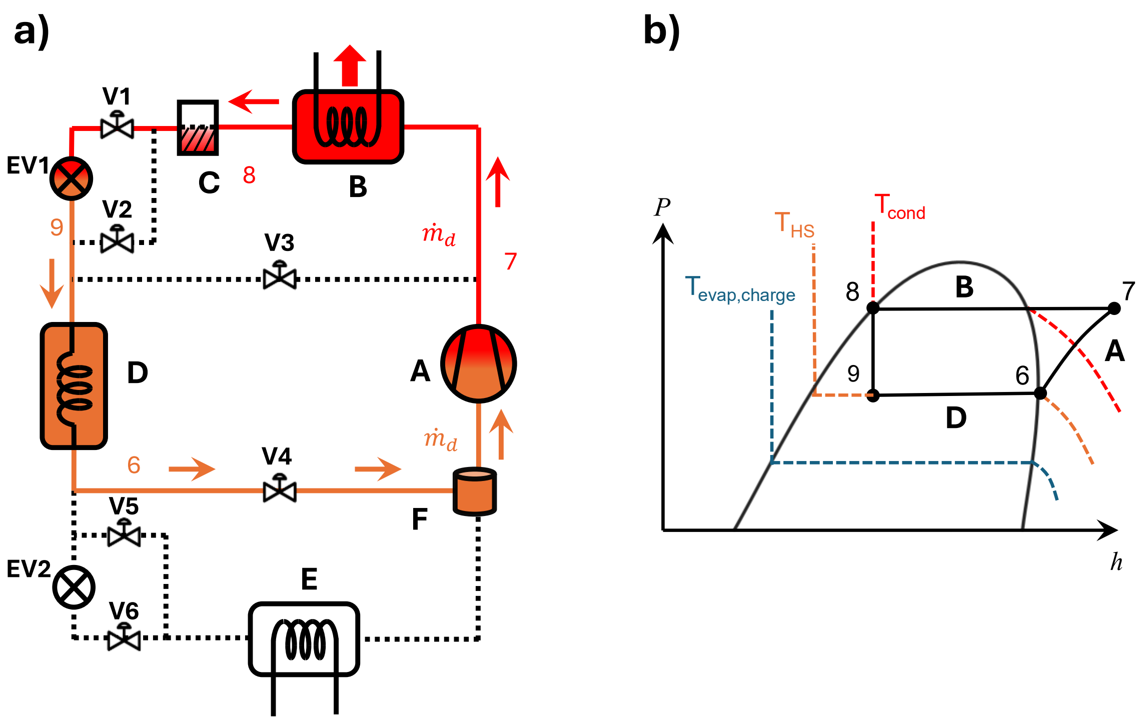

Fig. 3-3: Mode 2: discharging of heat storage and power-saving; (a) Schematic; (b) P-H diagram

3.2.3 Mode 3: Discharging of heat storage, power-saving and defrosting

For air-source heat pump application, this flexible heat pump layout provides a defrosting mode represented in Fig. 3-4. The refrigerant flows from the compressor to the condenser and keeps the same heating capacity during the defrosting operation. The refrigerant is then expanded by the expansion device EV1 and evaporated in the heat storage. Afterwards, it is split into two flows, one part is going back to the compressor through valve V4. A smaller percentage of the mass flow rate flows through valve V5 and to the evaporator to defrost it. The refrigerant is condensed during the process to melt the frost, and the resulting liquid refrigerant is collected in an accumulator in the suction line to prevent liquid slugging in the compressor. Refrigerant storage C is used to compensate for the amount of refrigerant retained in the system during the cycle. Similar than in Mode 2, the heat storage is utilised as the heat source, however its discharging rate is more important due to the increased mass flow rate flowing through it. The flexible heat pump can therefore maintain the same heating capacity indoors and save compressor power while defrosting.

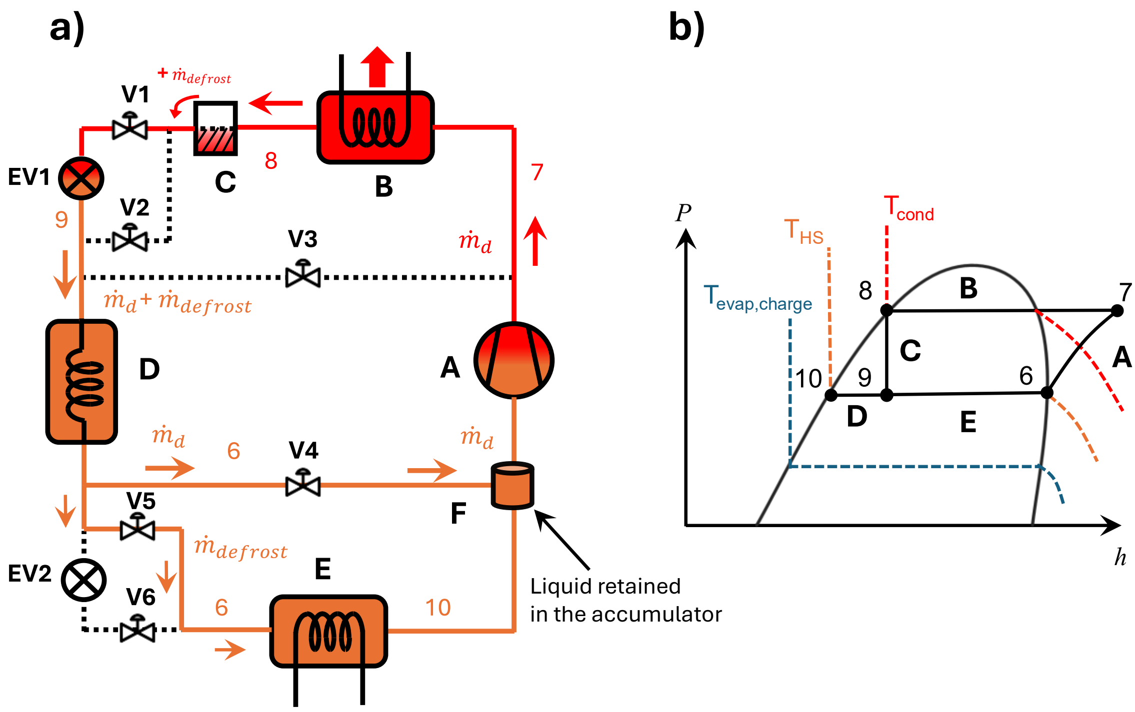

Fig. 3-4: Mode 3: discharging of heat storage, power-saving and defrosting;
(a) Schematic; (b) P-H diagram

Essentially, this defrosting technique is similar to the hot gas bypass defrosting, but with corrections addressing its shortcomings reported in the literature review, notably:

1. The issue of insufficient energy available in the cycle, which can result in a long defrosting time, is resolved by the use of heat storage that supplies additional heat alongside the compressor, enabling more efficient defrosting.

2. The heating output does not need to be partially reduced, as the refrigerant storage compensates for the refrigerant retained in the evaporator and accumulator, thus maintaining the indoor heating level.

3. After expansion and evaporation, the hot gas is directed at an intermediate pressure to prevent a sudden rise in evaporator pressure and to avoid mechanical shock.

4. The gas refrigerant is not mixed with low-temperature refrigerant, preventing heat loss due to unnecessary heating of the refrigerant flow.

Storing liquid refrigerant during defrosting in the evaporator coils and the accumulator is also widely reported in the technical literature for hot gas bypass defrosting. The accumulator is essential to prevent liquid flooding of the compressor, as significant refrigerant movements occur at the beginning and end of the defrost cycle[177,178,180]. It should be sized to accommodate the maximum expected liquid floodback.

When switching the heat pump back to Mode 1, as with hot gas defrosting, the pressure in the suction line drops, allowing some of the liquid refrigerant to flash and re-enter the cycle. The literature reports that this process occurs over a short, transient period, and that excess liquid refrigerant in the accumulator vaporises mainly through the pumping action of the compressor, without the need for additional heating[177,181].

Similarly, in this case, it can be assumed that the excess liquid in the accumulator returns to the cycle at a controlled rate and vaporizes to saturated gas (state 1 in Fig. 3-5b) by both compressor action and heat absorbed from the environment or the suction gas. This interval is referred to as the '*recovery phase*', and the P-H diagram illustrating this return of refrigerant to the cycle for model development is shown in Fig. 3-5. Although only the path of excess liquid refrigerant is shown in the figure, all valves as in Mode 1 remain open and the cycle continues uninterrupted.

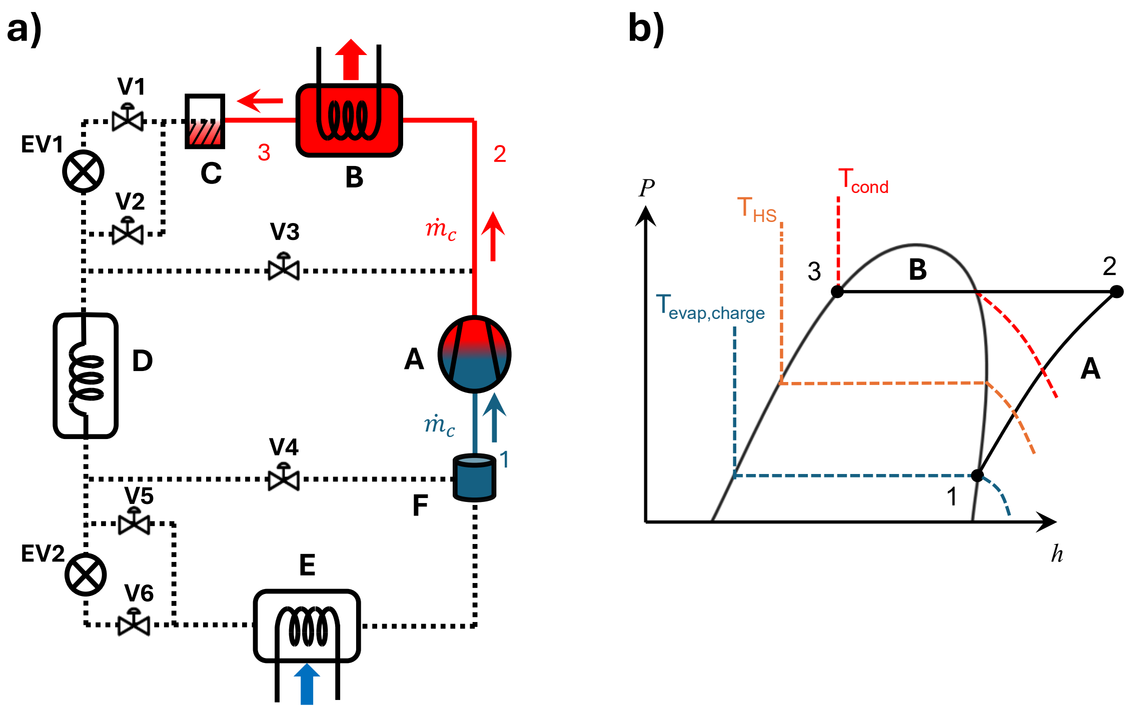

Fig. 3-5: Recovery phase (a) Schematic; (b) P-H diagram

While the recovery phase is typically a transient phenomenon as described in the literature, it is evaluated here as a steady-state process for the purpose of calculating the total compressor work required to return the refrigerant to storage C. Although some defrosting energy is supplied by the heat storage through the evaporation of a larger quantity of refrigerant, this alone is not sufficient to achieve energy balance. Additional energy input is therefore provided by the compressor, which contributes to the defrosting process by converting the additional refrigerant used for defrosting back into high-temperature gas. This is what the recovery phase accounts for.

In the model, the strategy for evaluating the defrosting mode total performance is to isolate the flow of excess liquid refrigerant (as depicted in Fig. 3-5) and calculate the additional compressor work required during the '*recovery time*' to transform this refrigerant from low-pressure, low-temperature gas to high-pressure, high-temperature gas. In practice, however, the excess liquid is cycled back as the heat pump transitions back to heating mode. Notably, the heating capacity is not reduced, as the heat pump is never shut off, but instead switches directly back to Mode 1 with the appropriate operating conditions.

3.2.4 Mode 4: Charging heat storage at lower temperature

This process is shown in Fig. 3-6. The refrigerant flows from the compressor directly to the heat storage through valve V3 to be condensed and store heat in it. The refrigerant is then expanded by the expansion device EV2 and flows to the evaporator through valve V6. Afterwards, it goes back to the compressor. The condenser is bypassed. When heating indoors is not required, this mode allows to charge heat faster inside the heat storage by directly condensing the refrigerant inside. No heat is provided to the indoor environment when this mode is operated.

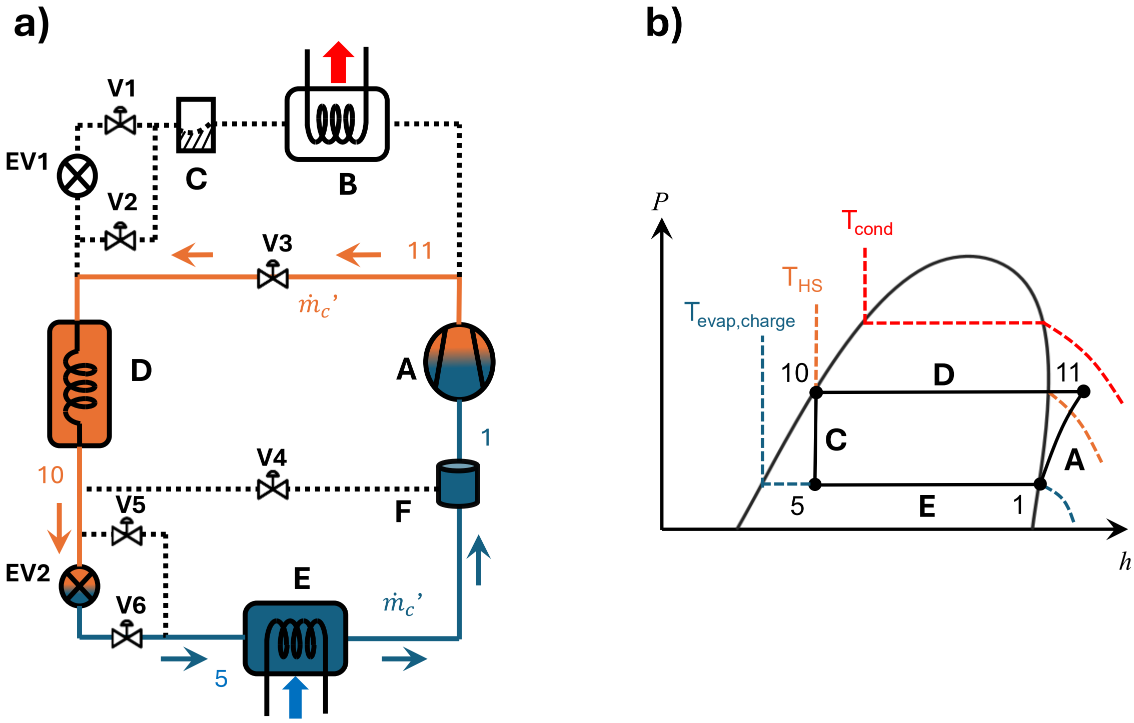

Fig. 3-6: Mode 4: charging the heat storage at lower temperature; (a) Schematic; (b) P-H diagram

3.3 Modelling approach and development

A thermodynamic model for the various modes of the flexible heat pump has been developed, with a primary focus on the internal refrigerant cycle. This modelling approach builds upon previously validated experimental results[223]. It has been adapted and modified for the current application. Given the novelty of the concept, it was essential to establish a baseline and develop a modelling strategy to gain a clear understanding of the operating principles and assess the potential benefits of the flexible heat pump. As no models for these modes exist in the literature, the development of simplified models was undertaken to enhance understanding of the thermodynamic processes and performance of the flexible heat pump, particularly concerning the COP improvement compared to conventional single-stage heat pumps. The average COP of the flexible heat pump is evaluated over a complete charge and discharge cycle of the heat storage and is compared to the COP of a conventional heat pump to assess potential power savings.

The objective is to demonstrate the benefits of this flexible heat pump and establish a foundation for future improvements, including but not limited to dynamic modelling and experimental analysis of the flexible heat pump. To facilitate a fair comparison with conventional heat pumps, the models used are simplified and assume steady-state conditions.

As a result, aspects such as design specifications, heat transfers, pressure losses or external loops have not been considered. Exceptions are made for exergy, economic, and environmental analyses. In these cases, specific assumptions and parameter choices are outlined in the respective chapters.

The heat storage model is simplified to focus only on potential heat recovery from the refrigerants, rather than providing a detailed representation of the storage system. Various types of TES could be utilised to demonstrate energy saving potential. Initially, a latent TES model with a fixed storage temperature is considered, though a sensible heat storage model is also included for comparison. In the case of latent heat storage, a PCM is considered, with its melting temperature defined as the storage temperature. These appellations are used indiscriminately in the study.

The models were developed from scratch in MATLAB and are coupled with the REFPROP database to calculate refrigerant properties.

3.3.1 Theoretical thermodynamic model: Equations and assumptions

In the energy model, the equations governing the system differ based on the type of TES used. When latent heat storage is employed, the equations are independent of time. However, with sensible heat storage, the equations become time-dependent and are incorporated into the general model described below.

3.3.1.1 Assumptions

The following assumptions are applied to all the models:

1) Negligible heat and pressure losses: Heat and pressure losses through pipes and heat exchangers are disregarded, as these losses are highly dependent on specific heat pump design parameters, such as pipe diameter and types of heat exchangers, which are not within the scope of this study.

2) Constant heating capacity: As commercial heat pumps are typically sold with a set nominal heating capacity, the model assumes that the condenser heating capacity remains constant throughout operation, with any minor variations considered negligible.

3) Evaporator fan work not considered: The contribution of the evaporator fan's work has been ignored, as it is highly dependent on the evaporator’s design and outdoor conditions.

4) Isenthalpic expansion process: The refrigerant expands at constant enthalpy, causing a drop in pressure and temperature without energy exchange with the surroundings.

5) Sensible heat exchange in the latent heat storage is disregarded: The charging and discharging processes of the PCM heat storage are simplified to consider only the latent heat absorbed and released during the melting and solidification processes, maintaining a constant storage temperature.

6) Recovery phase is simulated as a steady process: As discussed in section 3.2.3, the literature describes the recovery phase as a transient phenomenon. However, for the purpose of evaluating defrosting performance, it can be reasonably simplified as a steady-state process when the goal is to calculate the total compressor work required to return excess refrigerant to the cycle, rather than to analyse the transient flow behaviour of the refrigerant.

Additionally, the defrosting model is simplified to consider only the energy required for melting the frost, therefore the following assumptions are made:

7) Homogeneous frost distribution: Frost thickness and density are assumed to be homogeneously distributed on each tube pass, as the study does not focus on the ice formation process.

8) Negligible sensible heat exchange in the evaporator: Sensible heat exchange in the evaporator during defrosting is neglected compared to the required latent heat to melt the ice[174,196].

Comprehensive models for all modes are presented below and are obtained from Fig. 3-2 to Fig. 3-6.

3.3.1.2 Heating and charging mode (Mode 1)

The following equations are obtained from Fig. 3-2.

The power consumed by the compressor is calculated as

$$\dot{W}_{comp,charge,1} = \dot{m}_c(h_{2,r} - h_1) \tag{3.1}$$

with h_{2r} being the real discharged enthalpy, calculated as

$$h_{2,r} = h_1 + \frac{(h_{2,s} - h_1)}{\eta_{comp}} \quad (3.2)$$

where $h_{2,s}$ is the isentropic enthalpy and η_{comp} is the compressor efficiency. It should be noted that, from a theoretical thermodynamic perspective, and without considering experimental factors or specific compressor design, the compressor efficiency can be taken as the compressor isentropic efficiency η_s[14]. This assumption will be used in the results chapters.

According to assumption (2), the heating capacity of the condenser is kept constant and can be written as

$$\dot{Q}_{cond,charge} = \dot{m}_c(h_{2,r} - h_3) \quad (3.3)$$

with $\dot{m}_c$ being the mass flow rate of refrigerant during Mode 1. The charging rate of the heat storage is expressed as,

$$\dot{Q}_{HS,1} = \dot{m}_c(h_3 - h_4) \quad (3.4)$$

The total heat charged during Mode 1 is then expressed as

$$Q_{HS,1} = \int_0^{\Delta t_{charge,1}} \dot{Q}_{HS,1}\, dt \quad (3.5)$$

The heat rate in the evaporator is given as

$$\dot{Q}_{evap,1} = \dot{m}_c(h_1 - h_5) \quad (3.6)$$

3.3.1.3 Charging at lower temperature (Mode 4)

The following equations are obtained from Fig. 3-6.

The power consumed by the compressor in this mode is given by

$$\dot{W}_{comp,charge,4} = \dot{m}_c'(h_{11,r} - h_1) \quad (3.7)$$

with h_{11r} being the real discharged enthalpy and $\dot{m}_c'$ the mass flow rate of refrigerant during Mode 4.

In this mode, the heat storage is charged by condensing refrigerant directly within the storage unit. Here, the charging rate is kept constant at the same value as the heating capacity to respect assumption (2), and therefore is written as,

$$\dot{Q}_{HS,4} = \dot{m}_c'(h_{11,r} - h_{10}) = \dot{Q}_{cond,charge} \tag{3.8}$$

The total heat charged during Mode 4 is therefore

$$Q_{HS,4} = \dot{Q}_{HS,4}\, \Delta t_{charge,4} \tag{3.9}$$

The heat rate in the evaporator during Mode 4 is

$$\dot{Q}_{evap,4} = \dot{m}_c{}'(h_1 - h_5) \tag{3.10}$$

3.3.1.4 Compressor power and heating capacity in Modes 2 and 3

The following equations are obtained from Fig. 3-3 and Fig. 3-4.

During discharging in Modes 2 and 3 the heat storage replaces the evaporator providing a temporary heat source. The key difference between these two modes lies in the evaporator's defrosting operation, which affects the heat storage's discharge rate. Therefore, the compressor power and heating capacity are the same for both modes and can respectively be written as,

$$\dot{W}_{comp,discharge} = \dot{m}_d(h_{7,r} - h_6) \tag{3.11}$$

with h_{7r} being the real discharged enthalpy and $\dot{m}_d$ the discharge mass flow rate of refrigerant in Modes 2 and 3.

$$\dot{Q}_{cond,discharge} = \dot{m}_d(h_{7,r} - h_8) \tag{3.12}$$

According to assumption (2),

$$\dot{Q}_{cond,charge} = \dot{Q}_{cond,discharge} \tag{3.13}$$

3.3.1.5 Heat storage model in Mode 2

The following equations are obtained from Fig. 3-3.

In Mode 2, defrosting is not required. The discharging rate of the heat storage is expressed as,

$$\dot{Q}_{HS,2} = \dot{m}_d(h_6 - h_9) \tag{3.14}$$

The total energy discharged by the heat storage in Mode 2 can then be expressed as,

$$Q_{HS,2} = \int_0^{\Delta t_{discharge,2}} \dot{Q}_{HS,2}\, dt \tag{3.15}$$

3.3.1.6 COP improvement when operating Modes 1 and 2

When only Modes 1 and 2 are operated, the energy balance equation requires that the total heat discharged by the heat storage equals the heat charged during Mode 1, minus any heat losses occurring between the modes. Consequently, the balance equation is expressed as

$$\int_0^{\Delta t_{discharge,2}} \dot{Q}_{HS,2}\, dt = \int_0^{\Delta t_{charge,1}} \dot{Q}_{HS,1}\, dt \times (1 - \%\Delta Q_{loss}) \tag{3.16}$$

with $\%\Delta Q_{loss}$ being the percentage of heat losses to the environment through a charge/discharge cycle of the heat storage.

From assumption (2), the heating capacity is independent of time, therefore, the total heat provided through a full charge/discharge cycle of the heat storage in Modes 1 and 2 is given by

$$Q_{cond,total} = \dot{Q}_{cond,charge}(\Delta t_{charge,1} + \Delta t_{discharge,2}) \tag{3.17}$$

During Mode 1, the compressor power is not affected by the charging of the heat storage and is therefore independent of time. Consequently, the total compressor work is expressed as

$$W_{comp,total} = \dot{W}_{comp,charge,1}\Delta t_{charge,1} + \int_0^{\Delta t_{discharge,2}} \dot{W}_{comp,discharge} dt \tag{3.18}$$

The average COP of the flexible heat pump in that case is calculated by

$$\overline{COP} = \frac{Q_{cond,total}}{W_{comp,total}} \tag{3.19}$$

The conventional single-stage heat pump is simulated to provide the same heating capacity as the flexible heat pump. Consequently, its COP is

$$COP_{conv} = \frac{\dot{Q}_{cond,charge}}{\dot{W}_{comp,charge,1}} \tag{3.20}$$

Finally, the COP improvement is introduced and given as,

$$\alpha = \frac{\overline{COP} - COP_{conv}}{COP_{conv}} \times 100\% \tag{3.21}$$

To evaluate the efficiency of the heat storage system, the time ratio $\delta_{1,2}$ is calculated as the ratio between the discharging and charging times

$$\delta_{1,2} = \frac{\Delta t_{discharge,2}}{\Delta t_{charge,1}} \tag{3.22}$$

3.3.1.7 COP improvement when operating Modes 4 and 2

When only Modes 4 and 2 are operated, the heat storage balance is written as,

$$\int_0^{\Delta t_{discharge,2}} \dot{Q}_{HS,2}\, dt = \dot{Q}_{HS,4}\, \Delta t_{charge,4} \times (1 - \%\Delta Q_{loss}) \tag{3.23}$$

As explained in section 3.2.4, no heat is provided indoors when charging is operated in Mode 4. Therefore, when Modes 4 and 2 are run sequentially, the total heat production is modified to be expressed as

$$Q_{cond,total} = \dot{Q}_{cond,discharge} \Delta t_{discharge,2} \tag{3.24}$$

In Mode 4, the compressor work is affected by the storage temperature, therefore, the total compressor work is given by

$$W_{comp,total} = \int_0^{\Delta t_{charge,4}} \dot{W}_{comp,charge,4} dt + \int_0^{\Delta t_{discharge,2}} \dot{W}_{comp,discharge} dt \tag{3.25}$$

The corresponding average COP is,

$$\overline{COP} = \frac{Q_{cond,total}}{W_{comp,total}} \tag{3.26}$$

The conventional single-stage heat pump is modelled to deliver the same heating capacity and is therefore the same as in Eq. (3.20).

Finally, the COP improvement is given by

$$\alpha = \frac{\overline{COP} - COP_{conv}}{COP_{conv}} \times 100\% \tag{3.27}$$

The same time ratio as Eq. (3.22) is introduced, taking into consideration the charging time during Mode 4 and is,

$$\delta_{4,2} = \frac{\Delta t_{discharge,2}}{\Delta t_{charge,4}} \tag{3.28}$$

3.3.1.8 Heat storage and defrosted evaporator in Mode 3

The following equations are obtained from Fig. 3-4.

When defrosting is required, a part of the mass flow rate is used for the defrosting operation and is retained in the accumulator during the defrosting process. The refrigerant storage then compensates by releasing refrigerant into the cycle after the condenser. This added mass flow rate is named $\dot{m}_{defrost}$ in the following equations and is the mass flow rate used to defrost the evaporator.

The discharging rate of the heat storage during defrosting is then,

$$\dot{Q}_{HS,3} = \left(\dot{m}_d + \dot{m}_{defrost}\right)(h_6 - h_9) \tag{3.29}$$

Therefore, the total energy discharged throughout the defrosting operation is

$$Q_{HS,3} = \int_0^{\Delta t_{defrost}} \dot{Q}_{HS,3}\, dt \tag{3.30}$$

According to assumption (8), the energy required for defrosting the evaporator can be approximated using the latent heat of fusion of ice L_{fus}. Therefore, the heat rate in the evaporator is,

$$\dot{Q}_{defrost} = \frac{L_{\text{fus}}\, m_{ice}}{\Delta t_{defrost}} \tag{3.31}$$

where m_{ice} is the mass of frost on the surface of the evaporator. The assumption of m_{ice} is based on a study by Reichl et al., who investigated frosting on the evaporator of an air-source heat pump under specific outdoor conditions using R410a as the refrigerant[224]. Data from one of their experiments, which used an uncoated conventional evaporator with condensing and evaporating temperatures of 35 °C and -8 °C respectively, and a heating capacity of approximately 3.6 kW, has been used in this work. Fig. 3-7 shows the ice buildup over time extracted from their experimental data. Fitting the data produces a correlation, shown in Fig. 3-7, with an error margin of less than 5 %, and expressed as

$$m_{ice} = -0.16 + 3.9 \times 10^{-4} t. \tag{3.32}$$

where t is the time.

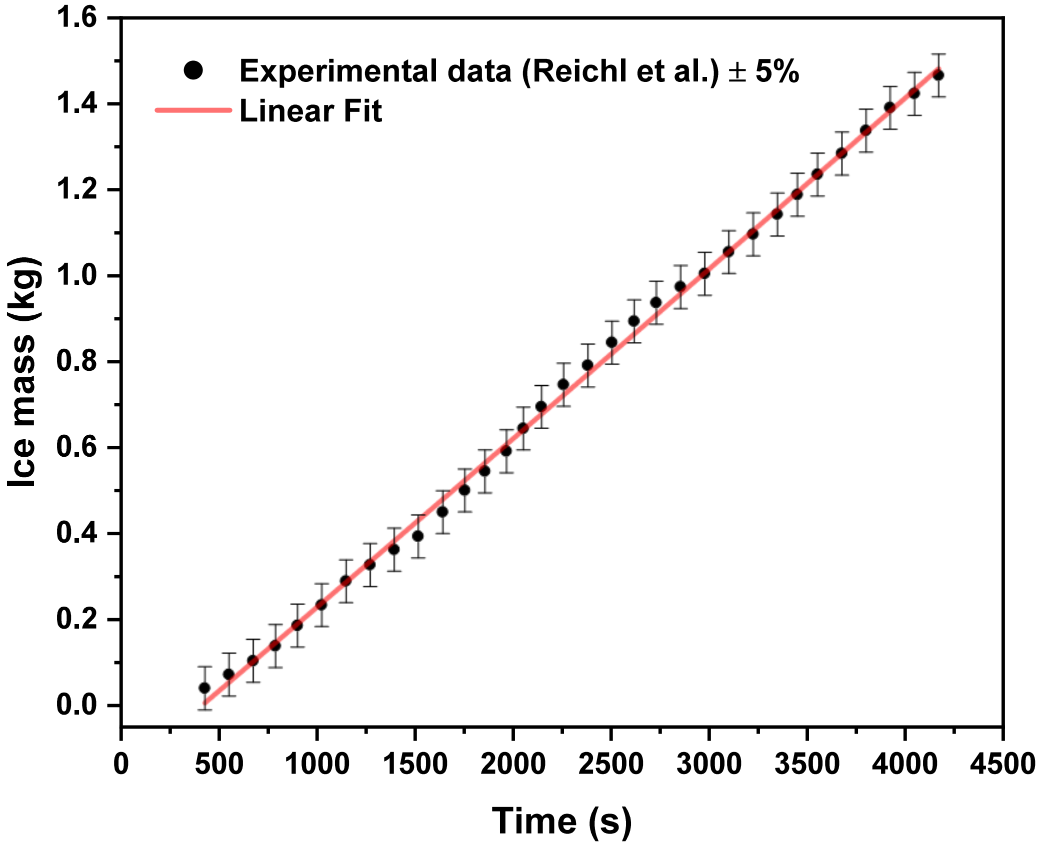

Fig. 3-7: Experimental data of ice mass buildup with time (Reichl et al.[224]) and linear fitting

The heat rate in the evaporator can also be defined as,

$$\dot{Q}_{defrost} = \dot{m}_{defrost}(h_6 - h_{10}) \tag{3.33}$$

The mass flow rate required to defrost the evaporator $\dot{m}_{defrost}$ is therefore written as,

$$\dot{m}_{defrost} = \frac{\dot{Q}_{defrost}}{(h_6 - h_{10})} \tag{3.34}$$

A ratio σ is defined as the ratio of the defrosting mass flow rate $\dot{m}_{defrost}$ and the discharging mass flow rate $\dot{m}_d$

$$\sigma = \frac{\dot{m}_{defrost}}{\dot{m}_d} \tag{3.35}$$

The total mass of refrigerant retained in the accumulator can be evaluated as

$$M_{ref,evap} = \int_0^{\Delta t_{defrost}} \dot{m}_{defrost}\, dt \tag{3.36}$$

To estimate the impact of defrosting on heat storage, the ratio of the energy used for defrosting relative to the energy stored in the heat storage is expressed as

$$\lambda = \frac{Q_{HS,3}}{Q_{HS,1}} \times 100\% \tag{3.37}$$

3.3.1.9 Recovery phase

The following equations are obtained from Fig. 3-5.

After a defrosting operation and completion of the heat storage discharge, the flexible heat pump will switch back to Mode 1. Liquid refrigerant that remains in the accumulator after defrosting must be returned to the refrigerant storage. This results in a short period during which the refrigerant is cycled back into the system. As discussed in assumption (6), this process is modelled here in order to estimate the compressor's contribution to defrosting by treating the process as steady-state.

According to assumption (2) and Fig. 3-5, the compressor power and heating capacity equations are the same as in Mode 1 and are given by Eqs. (3.1) and (3.3), respectively.

The recovery phase ends when all the remaining refrigerant in the accumulator has been moved to the refrigerant storage, therefore $\Delta t_{recovery}$ can be estimated with

$$\Delta t_{recovery} = \frac{M_{ref,evap}}{\dot{m}_c} \tag{3.38}$$

The total compressor work during the recovery phase is expressed as

$$W_{comp,recovery} = \dot{W}_{comp,charge,1} \Delta t_{recovery} \tag{3.39}$$

It should be noted that, although $\dot{W}_{comp,charge,1}$ is taken as the same value as in Mode 1, this assumption does not affect the total compressor work during the recovery process. The total compressor work is determined by the mass of liquid refrigerant remaining after defrosting and the enthalpy change during compression. If a higher mass flow rate is assumed, it would increase the compressor power but would also reduce the recovery time proportionally, ultimately resulting in the same total compressor work for the process. Furthermore, the enthalpy change during compression is determined by the compressor's operating conditions, and the mass of remaining liquid refrigerant is determined by the required defrosting energy. Heating is never interrupted because switching between operating modes does not involve stopping the compressor.

In practice, the mass flow rate may fluctuate slightly over time, as the accumulator releases vaporised liquid refrigerant at a controlled rate, which can lead to temporary increases in compressor power. However, the total additional compressor work required for this process can be estimated by applying a constant compressor power over the recovery duration, determined by the mass of refrigerant. This is the approach used in the present model.

3.3.1.10 COP improvement when operating Modes 1,3 and 2

Once defrosting is completed and Mode 3 is terminated, the evaporator is bypassed and the heat pump switches to Mode 2. Consequently, the total discharging time of the heat storage is

$$\Delta t_{discharge,total} = \Delta t_{discharge,2} + \Delta t_{defrost} \quad (3.40)$$

Because Mode 3 has been operated, Eq. (3.16) is adjusted to account for Mode 3 to ensure a consistent thermal balance in the storage. The updated energy balance of the heat storage is now

$$\int_0^{\Delta t_{discharge,2}} \dot{Q}_{HS,2}\, dt + \int_0^{\Delta t_{defrost}} \dot{Q}_{HS,3}\, dt = \int_0^{\Delta t_{charge,1}} \dot{Q}_{HS,1}\, dt \times (1 - \%\Delta Q_{loss}) \quad (3.41)$$

The total heat production for a full charging/discharging/recovery cycle is therefore calculated as

$$Q_{cond,total} = \dot{Q}_{cond,charge}\left(\Delta t_{charge,1} + \Delta t_{discharge,total} + \Delta t_{recovery}\right) \quad (3.42)$$

The total compressor work is expressed as

$$W_{comp,total} = \dot{W}_{comp,charge,1}\left(\Delta t_{charge,1} + \Delta t_{recovery}\right) + \int_0^{\Delta t_{discharge,total}} \dot{W}_{comp,discharge}\, dt \quad (3.43)$$

Therefore, the average COP of the flexible heat pump during one charging/discharging/recovery cycle when defrosting has been operated can be calculated as

$$\overline{COP} = \frac{Q_{cond,total}}{W_{comp,total}} \quad (3.44)$$

In this specific case, to compare the COP of the flexible heat pump to a conventional single-stage heat pump, a full heating/defrosting run with the same parameters is defined. The conventional heat pump is operated during the same amount of time as the flexible heat pump. The operation of Mode 1 corresponds to the frosting time on the conventional system to ensure a consistent comparison with the same amount of ice on the evaporator. The reverse cycle defrosting method is used as the benchmark. The frost is melted by condensing refrigerant in the evaporator and extracting heat from the indoor environment. During defrosting, no heating is provided indoors therefore the total heat production of the conventional heat pump is

$$Q_{cond,total,conv} = \dot{Q}_{cond,charge}(\Delta t_{charge,1} + \Delta t_{discharge,total} - \Delta t_{defrost,conv} + \Delta t_{recovery}) \tag{3.45}$$

The total defrosting time for the reverse cycle method is calculated as

$$\Delta t_{defrost,conv} = \frac{L_{fus}\, m_{ice}}{\dot{Q}_{defrost,conv}} \tag{3.46}$$

with $\dot{Q}_{defrost,conv}$ defined as

$$\dot{Q}_{defrost,conv} = \dot{m}_c(h_{2,r} - h_3) \tag{3.47}$$

The total compressor work for a conventional heat pump is

$$W_{comp,total,conv} = \dot{W}_{comp,charge,1}(\,\Delta t_{charge,1} + \Delta t_{discharge,total} + \Delta t_{recovery}) \tag{3.48}$$

The average COP for the conventional heat pump during a full frosting/defrosting cycle can be defined as

$$\overline{COP}_{conv} = \frac{Q_{cond,total,conv}}{W_{comp,total,conv}} \tag{3.49}$$

Hence, this averaged COP can be used as a comparison and the COP improvement of the flexible heat pump when defrosting is operated can be calculated as

$$\alpha = \frac{\overline{COP} - \overline{COP}_{conv}}{\overline{COP}_{conv}} \times 100\% \tag{3.50}$$

3.3.2 Exergy model development

A reversible thermodynamic process is one that can be reversed without leaving any visible impact on its surroundings. In other words, both the system and the surroundings revert to their initial states by the end of the reversing process. However, all real processes exhibit irreversibility. Various factors contribute to this irreversibility in a heat pump cycle, including fluid friction, finite temperature difference across all components, pressure drops etc. The irreversibility or exergy destruction is a crucial parameter to evaluate and manage the system losses. The lower the irreversibility, the higher is the efficiency of the studied system in an equilibrium environment.

The general exergy flow is given as

$$ex = h - h_0 - T_0(s - s_0) \tag{3.51}$$

with *h* being the enthalpy, *s* the entropy and T_0 the dead state temperature.

The exergy rate is written as

$$\dot{E}x = \dot{m}\, ex \tag{3.52}$$

The exergy destruction rate is defined by[225–228]

$$\dot{E}x_{dest} = \dot{E}x_{input} - \dot{E}x_{output} \tag{3.53}$$

The exergy efficiency can be expressed as a ratio of the useful exergy on the input exergy, which gives[229]

$$\eta_{ex} = \frac{\dot{E}x_{output}}{\dot{E}x_{input}} = 1 - \frac{\dot{E}x_{dest}}{\dot{E}x_{input}} \tag{3.54}$$

A relative irreversibility (RI) defined as the contribution of each component on the total system exergy destruction is expressed as[230]

$$RI_i = \frac{\dot{E}x_{dest,i}}{\dot{E}x_{dest,syst}} \times 100\% \tag{3.55}$$

with the subscript *i* corresponding to the specified component.

The specific exergy equations for each component and the system, in Modes 1 and 3 are listed in Table 3-2 and Table 3-3, respectively.

Table 3-2: Exergy equations for each component and whole system for Mode 1

<table>
<tr><th>Components</th><th></th><th>Mode1: Heating/charging</th><th></th></tr>
<tr><td rowspan="2">Compressor</td><td>*Exergy destruction [kW]*</td><td>$\dot{E}x_{dest,comp,c} = \dot{E}x_1 - \dot{E}x_2 + \dot{W}_{comp,charge}$
$= \dot{m}_c\left[\left(h_1 - h_{2,r}\right) - T_0\left(s_1 - s_{2,r}\right)\right]$
$+ \dot{W}_{comp,charge}$</td><td>(3.56)</td></tr>
<tr><td>*RI [%]*</td><td>$RI_{comp,c} = \frac{\dot{E}x_{dest,comp,c}}{\dot{E}x_{dest,syst,c}} \times 100\%$</td><td>(3.57)</td></tr>
<tr><td rowspan="2">Condenser</td><td>*Exergy destruction [kW]*</td><td>$\dot{E}x_{dest,cond,c} = \dot{E}x_2 - \dot{E}x_3 + \dot{E}x_{1w} - \dot{E}x_{2w}$
$= \dot{m}_c\left[\left(h_{2,r} - h_3\right) - T_0\left(s_{2,r} - s_3\right)\right]$
$+ \dot{m}_w[(h_{1w} - h_{2w}) - T_0(s_{1w} - s_{2w})]$</td><td>(3.58)</td></tr>
<tr><td>*RI [%]*</td><td>$RI_{cond,c} = \frac{\dot{E}x_{dest,cond,c}}{\dot{E}x_{dest,syst,c}} \times 100\%$</td><td>(3.59)</td></tr>
<tr><td rowspan="2">Expansion valve</td><td>*Exergy destruction [kW]*</td><td>$\dot{E}x_{dest,exp,c} = \dot{E}x_4 - \dot{E}x_5 = \dot{m}_c[(h_4 - h_5) - T_0(s_4 - s_5)]$</td><td>(3.60)</td></tr>
<tr><td>*RI [%]*</td><td>$RI_{exp,c} = \frac{\dot{E}x_{dest,exp,c}}{\dot{E}x_{dest,syst,c}} \times 100\%$</td><td>(3.61)</td></tr>
<tr><td rowspan="2">Evaporator</td><td>*Exergy destruction [kW]*</td><td>$\dot{E}x_{dest,evap,c} = \dot{E}x_5 - \dot{E}x_1 + \dot{E}x_{1a} - \dot{E}x_{2a}$
$= \dot{m}_c[(h_5 - h_1) - T_0(s_5 - s_1)]$
$+ \dot{m}_a[(h_{1a} - h_{2a}) - T_0(s_{1a} - s_{2a})]$</td><td>(3.62)</td></tr>
<tr><td>*RI [%]*</td><td>$RI_{evap,c} = \frac{\dot{E}x_{dest,evap,c}}{\dot{E}x_{dest,syst,c}} \times 100\%$</td><td>(3.63)</td></tr>
<tr><td rowspan="2">Heat storage</td><td>*Exergy destruction [kW]*[226,231–233]</td><td>$\dot{E}x_{dest,HS,c} = \dot{E}x_3 - \dot{E}x_4 - \dot{Q}_{HS,1}\left(1 - \frac{T_0}{T_{HS}}\right)$
$= \dot{m}_c[(h_3 - h_4) - T_0(s_3 - s_4)]$
$- \dot{Q}_{HS,1}\left(1 - \frac{T_0}{T_{HS}}\right)$</td><td>(3.64)</td></tr>
<tr><td>*RI [%]*</td><td>$RI_{HS,c} = \frac{\dot{E}x_{dest,HS,c}}{\dot{E}x_{dest,syst,c}} \times 100\%$</td><td>(3.65)</td></tr>
<tr><td rowspan="2">System</td><td>*Exergy destruction [kW]*</td><td>$\dot{E}x_{dest,syst,c} = \dot{E}x_{dest,comp,c} + \dot{E}x_{dest,cond,c} + \dot{E}x_{dest,exp,c}$
$+ \dot{E}x_{dest,evap,c} + \dot{E}x_{dest,HS,c}$</td><td>(3.66)</td></tr>
<tr><td>*Exergy efficiency [%]*[230,234–236]</td><td>$\eta_{ex,syst,c} = \frac{\left|\dot{E}x_{1w} - \dot{E}x_{2w}\right|}{\dot{W}_{comp,charge}} \times 100\%$</td><td>(3.67)</td></tr>
</table>

Table 3-3: Exergy equations for each component and whole system for Mode 3

Components		**Mode 3: Defrosting mode**	
Compressor	*Exergy destruction [kW]*	$\dot{E}x_{dest,comp,d} = \dot{E}x_6 - \dot{E}x_7 + \dot{W}_{comp,discharge} = \dot{m}_d\left[\left(h_6 - h_{7,r}\right) - T_0\left(s_6 - s_{7,r}\right)\right] + \dot{W}_{comp,discharge}$	(3.68)
	RI [%]	$RI_{comp,d} = \dfrac{\dot{E}x_{dest,comp,d}}{\dot{E}x_{dest,syst,d}} \times 100\%$	(3.69)
Condenser	*Exergy destruction [kW]*	$\dot{E}x_{dest,cond,d} = \dot{E}x_7 - \dot{E}x_8 + \dot{E}x_{1w} - \dot{E}x_{2w} = \dot{m}_d\left[\left(h_{7,r} - h_8\right) - T_0\left(s_{7,r} - s_8\right)\right] + \dot{m}_w[(h_{1w} - h_{2w}) - T_0(s_{1w} - s_{2w})]$	(3.70)
	RI [%]	$RI_{cond,d} = \dfrac{\dot{E}x_{dest,cond,d}}{\dot{E}x_{dest,syst,d}} \times 100\%$	(3.71)
Expansion valve	*Exergy destruction [kW]*	$\dot{E}x_{dest,exp,d} = \dot{E}x_8 - \dot{E}x_9 = \left(\dot{m}_d + \dot{m}_{defrost}\right)[(h_8 - h_9) - T_0(s_8 - s_9)]$	(3.72)
	RI [%]	$RI_{exp,d} = \dfrac{\dot{E}x_{dest,exp,d}}{\dot{E}x_{dest,syst,d}} \times 100\%$	(3.73)
Evaporator	*Exergy destruction [kW]*	$\dot{E}x_{dest,evap,d} = \dot{E}x_6 - \dot{E}x_{10} - \dot{Q}_{defrost}\left(1 - \dfrac{T_0}{T_{ice}}\right) = \dot{m}_{defrost}[(h_6 - h_{10}) - T_0(s_6 - s_{10})] - \dot{Q}_{defrost}\left(1 - \dfrac{T_0}{T_{ice}}\right)$	(3.74)
	RI [%]	$RI_{evap,d} = \dfrac{\dot{E}x_{dest,evap,d}}{\dot{E}x_{dest,syst,d}} \times 100\%$	(3.75)
Heat storage	*Exergy destruction [kW]*[231,237]	$\dot{E}x_{dest,HS,d} = \dot{E}x_6 - \dot{E}x_9 + \dot{Q}_{HS,3}\left(1 - \dfrac{T_0}{T_{HS}}\right) = \left(\dot{m}_d + \dot{m}_{defrost}\right)[(h_6 - h_9) - T_0(s_6 - s_9)] + \dot{Q}_{HS,3}\left(1 - \dfrac{T_0}{T_{HS}}\right)$	(3.76)
	RI [%]	$RI_{HS,d} = \dfrac{\dot{E}x_{dest,HS,d}}{\dot{E}x_{dest,syst,d}} \times 100\%$	(3.77)
System	*Exergy destruction [kW]*	$\dot{E}x_{dest,syst,d} = \dot{E}x_{dest,comp,d} + \dot{E}x_{dest,cond,d} + \dot{E}x_{dest,exp,d} + \dot{E}x_{dest,evap,d} + \dot{E}x_{dest,HS,d}$	(3.78)
	Exergy efficiency [%][230,234–236]	$\eta_{ex,syst,d} = \dfrac{\left\lvert\dot{E}x_{1w} - \dot{E}x_{2w}\right\rvert}{\dot{W}_{comp,discharge}} \times 100\%$	(3.79)

In Table 3-2 and Table 3-3, $\dot{m}_w$ is the mass flow rate of water and $\dot{m}_a$ the mass flow rate of air, as illustrated in Fig. 3-8. T_{HS} corresponds to the storage temperature and T_{ice} to the temperature of ice 0 °C.

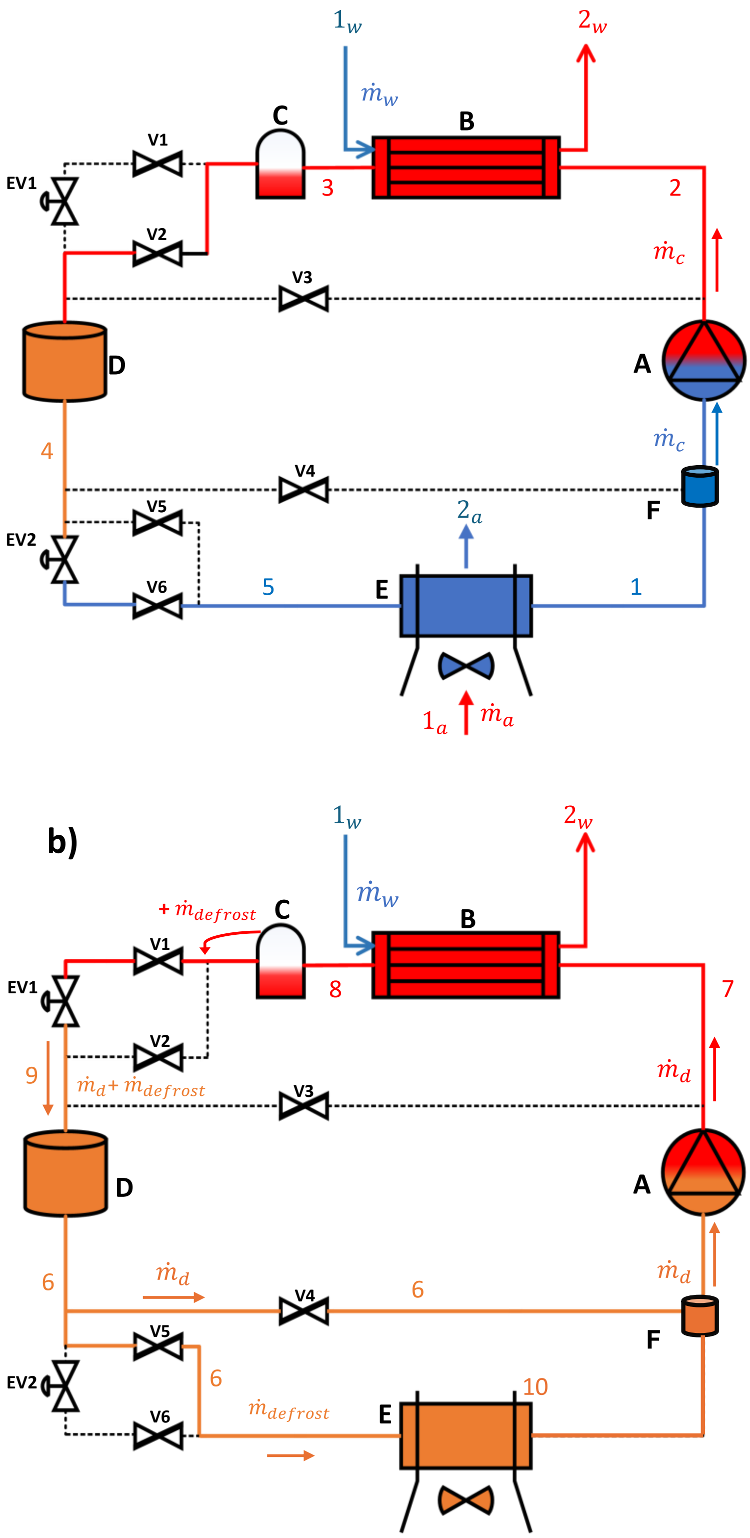

Fig. 3-8: Schematic of the flexible heat pump including the external loops in (a) Mode 1; (b) Mode 3

3.3.3 Economic and environmental model development

An economic model has been developed to evaluate and compare the economic performance of three systems: the flexible heat pump operating in power-saving mode, the conventional single-stage air-source heat pump, and the gas boiler. The primary objective is to assess the cost-efficiency of the flexible heat pump's power-saving mode.

The economic analysis is divided into two key components: (1) the upfront equipment costs, along with the annual capital costs and maintenance for each system, and (2) the operational costs associated with both heat pumps and the gas boiler. Additionally, the analysis considers the social cost of CO_2e emissions, providing a more comprehensive evaluation of each system's economic and environmental impact.

The mode selected for calculating the cost of the flexible heat pump is Mode 1, since this mode places the highest load on the main components. This is particularly important for determining the required storage capacity of the heat storage and for assessing the increased load on the evaporator during the charging process. To evaluate the economic impact of the heat storage on the flexible heat pump system, in addition to considering the storage's own cost, the analysis focuses on increasing the heat transfer area of the evaporator. This enables the flexible heat pump to recover more heat from the ambient air, thereby compensating for the subcooled refrigerant in the storage and the resulting increased evaporator load in Mode 1, as shown in the P-H diagram in Fig. 3-2b.

It should be noted that other strategies could have been considered to compensate for the increased load, such as increasing the fan speed or the external loop temperature gradient across the evaporator. However, energy consumption related to fan speed was not included in this study, and a significant temperature differential can worsen frosting issues[238]. Additionally, because the maximum evaporator load is mainly determined by its design[239], this study chose to focus on increasing the heat transfer area in order to provide a fair comparison.

Finally, to assess the environmental impact of the heat pump systems, the Total Equivalent Warming Impact (TEWI) metric is applied, capturing both direct emissions from refrigerants and indirect emissions resulting from energy consumption.

3.3.3.1 Economic analysis

For the gas boiler, the initial equipment cost is computed from the following equation[240]

$$Z_{boiler} = 30\,\dot{Q}_{boiler} \tag{3.80}$$

with $\dot{Q}_{boiler}$ being the heating capacity of the gas boiler.

For both heat pumps the following capital cost functions per components are used and listed below[241,242]:

$$Z_{comp} = \frac{39.5 * \dot{m}_c}{0.9 - \eta_{comp}} \frac{P_{dis}}{P_{suc}} \ln\left(\frac{P_{dis}}{P_{suc}}\right) \tag{3.81}$$

$$Z_{cond} = 516.62\,A_{cond} + 268.45 \tag{3.82}$$

$$Z_{evap} = 45\,A_{evap} \tag{3.83}$$

$$Z_{exp} = 114.5\,\dot{m}_c \tag{3.84}$$

It should be noted that Eqs (3.81), (3.82) and (3.84) are in dollars and should be multiplied by 0.77 to be converted to pounds sterling. Eq. (3.83) is in euros and should be multiplied by 0.84 to be converted to pounds sterling. P_{dis} and P_{suc} are the discharge and suction pressures respectively. A_{cond} and A_{evap} are the condenser and evaporator areas respectively, and calculated as

$$A_{cond} = \frac{\dot{Q}_{cond,charge}}{U_{cond} \times LMTD} \tag{3.85}$$

$$A_{evap} = \frac{\dot{Q}_{evap,1}}{U_{evap} \times LMTD} \tag{3.86}$$

with U_{cond} and U_{evap} corresponding to the overall heat transfer coefficient in the condenser and evaporator, respectively. LMTD is the logarithmic mean temperature difference for counter-flow heat exchangers, given by

$$LMTD = \frac{\Delta T_2 - \Delta T_1}{ln\left(\frac{\Delta T_2}{\Delta T_1}\right)} \tag{3.87}$$

For the flexible heat pump, the heat storage is included as an additional component. Specifically, a latent heat storage unit was considered for the economic analysis. Based on the results, the *PCM RT35 HC* was selected. The cost of this equipment, calculated using the manufacturer's pricing data, is provided as[243]

$$Z_{PCM} = 18.48\,M_{PCM} \tag{3.88}$$

with M_{PCM} being the mass of the PCM in kg expressed as

$$M_{PCM} = \frac{Q_{HS,1}}{q_{PCM}} \tag{3.89}$$

with q_{PCM} corresponding to the estimated heat storage capacity of the PCM, as a combination of latent and sensible heat in a temperature range of 27 °C to 42 °C, based on the manufacturer's data.

To convert the initial component costs into a capital cost rate that includes maintenance, the following formula is applied[244]

$$\dot{Z}_i = \emptyset \times CRF \times Z_i \tag{3.90}$$

where *i* is the component index, $\emptyset$ is the maintenance factor, and *CRF* is the capital recovery factor defined by[245]

$$CRF = \frac{ir(1+ir)^n}{(1+ir)^n - 1} \tag{3.91}$$

with *ir* being the interest rate and *n* the equipment lifetime.

The total initial cost for both the conventional air-source heat pump and the flexible heat pump are calculated as follows

$$CapEx_{ASHP} = \sum Z_{comp} + Z_{cond} + Z_{evap} + Z_{exp} \tag{3.92}$$

$$CapEx_{FHP} = \sum Z_{comp} + Z_{cond} + Z_{evap} + Z_{exp} + Z_{PCM} \tag{3.93}$$

Their annual capital and maintenance cost rate are formulated as

$$\dot{Z}_{ASHP} = \sum \dot{Z}_{comp} + \dot{Z}_{cond} + \dot{Z}_{evap} + \dot{Z}_{exp} \tag{3.94}$$

$$\dot{Z}_{FHP} = \sum \dot{Z}_{comp} + \dot{Z}_{cond} + \dot{Z}_{evap} + \dot{Z}_{exp} + \dot{Z}_{PCM} \tag{3.95}$$

After determining the upfront capital costs, another important metric in the economic analysis of an energy system is its operational cost. The annual operational cost rate of the gas boiler is calculated using the following formula

$$\dot{Z}_{op,boiler} = \frac{E_{yearly}\, c_g}{\eta_b} + s_{charge} \times 365 \tag{3.96}$$

where E_{yearly} is the average annual energy consumption in kWh/year, c_g is the unit cost of gas in £/kWh, η_b is the gas boiler efficiency, and s_{charge} is the daily standing charge for gas. As highlighted by a report from the Regulatory Assistance Project[24], the standing charge for gas is included in the operating costs of natural gas heating systems, but this cost does not apply to homes with heat pumps, as these dwellings rely solely on electricity for heating and hot water and therefore do not receive a gas supply.

Concerning the conventional air-source heat pump and the flexible heat pump the annual operational cost rate is obtained using

$$\dot{Z}_{op,ASHP} = W_{ASHP}\, c_{elec} \tag{3.97}$$

$$\dot{Z}_{op,FHP} = W_{FHP}\, c_{elec} \tag{3.98}$$

with c_{elec} being the unit cost of electricity in £/kWh, and W_{ASHP} and W_{FHP} corresponding to the annual energy consumption of the conventional heat pump and the flexible heat pump, respectively, in kWh/year. These values are calculated based on the average yearly energy consumption as follows

$$W_{ASHP} = \frac{E_{yearly} \times W_{comp,conv}}{Q_{cond,hourly}} \tag{3.99}$$

$$W_{FHP} = \frac{E_{yearly}\,(\dot{W}_{comp,charge,1}\,\Delta t_{charge} + \dot{W}_{comp,discharge}\,\Delta t_{discharge,2})}{Q_{cond,hourly}} \tag{3.100}$$

where $W_{comp,conv}$ is the hourly energy consumption of the conventional heat pump, and $Q_{cond,hourly}$ is the hourly heating capacity in kWh.

Therefore, the payback period of the flexible heat pump compared to the conventional heat pump can be calculated as the ratio of the difference in initial investments to the annual operating cost savings, as follows[246,247]

$$PP = \frac{CapEx_{FHP} - CapEx_{ASHP}}{\dot{Z}_{op,ASHP} - \dot{Z}_{op,FHP}} \tag{3.101}$$

The social cost of CO_2e is an important parameter to be considered when evaluating the environmental impact of different heating systems. It estimates the economic damages associated with the emission of an additional ton of CO_2e into the atmosphere. For energy systems, this cost is determined based on their CO_2e emissions resulting from their energy consumption. The yearly CO_2e emissions produced by the use of a gas boiler are calculated as follows

$$m_{CO_2e,boiler} = \frac{E_{yearly} \times \mu_g}{\eta_b} \tag{3.102}$$

where μ_g is the CO_2e emission factor of natural gas use in kg/kWh.

The CO_2e emissions from both conventional and flexible heat pumps primarily result from electricity production, which varies by country/region. These emissions can be estimated using

$$m_{CO_2e,ASHP} = W_{ASHP} \times \mu_{elec} \quad (3.103)$$

$$m_{CO_2e,FHP} = W_{FHP} \times \mu_{elec} \quad (3.104)$$

with μ_{elec} being the CO_2e emission factor for producing electricity in kg/kWh.

To incorporate the social cost associated with CO_2e emissions, Eqs. (3.96), (3.97) and (3.98) are modified to become

$$\dot{Z}_{op,boiler,tot} = \dot{Z}_{op,boiler} + m_{CO_2e,boiler} \times C_{CO_2e} \quad (3.105)$$

$$\dot{Z}_{op,ASHP,tot} = \dot{Z}_{op,ASHP} + m_{CO_2e,ASHP} \times C_{CO_2e} \quad (3.106)$$

$$\dot{Z}_{op,FHP,tot} = \dot{Z}_{op,FHP} + m_{CO_2e,FHP} \times C_{CO_2e} \quad (3.107)$$

with C_{CO_2e} being the penalty price for CO_2e emissions in £/kg.

Therefore, the total annual expense rate, which includes the capital cost rate, maintenance cost rate, operational cost rate, and the social cost of CO_2e emissions for both the conventional heat pump and the flexible heat pump, can be expressed as

$$\dot{Z}_{tot,ASHP} = \dot{Z}_{ASHP} + \dot{Z}_{op,ASHP,tot} \quad (3.108)$$

$$\dot{Z}_{tot,FHP} = \dot{Z}_{FHP} + \dot{Z}_{op,FHP,tot} \quad (3.109)$$

3.3.3.2 Environmental analysis

To evaluate the environmental impact of heat pump applications, the TEWI is a more precise and widely used metric. TEWI is used to calculate the total CO_2e emissions over the lifetime of a heat pump system and is divided into two components: direct and indirect emissions. Direct emissions result from refrigerant leakage and losses during recycling and are directly related to the refrigerant's GWP. Indirect emissions are caused by the system's energy consumption, specifically the emissions associated with electricity production. TEWI is expressed as follows[248,249]

$$TEWI = TEWI_{direct} + TEWI_{indirect} \tag{3.110}$$

$$TEWI_{direct} = GWP \times M_{ref} \times L_y \times n + GWP \times M_{ref} \times (1 - \alpha_{recycling}) \tag{3.111}$$

$$TEWI_{indirect} = m_{CO_2e,j} \times n \tag{3.112}$$

where L_y is the yearly leakage of refrigerant in percentage, $\alpha_{recycling}$ is the recycling factor in percentage, j is the index for *ASHP* or *FHP*, and M_{ref} is the refrigerant charge in kg defined as[250]

$$M_{ref} = 0.4 \times \dot{Q}_{cond} \tag{3.113}$$

3.4 Validation of model results

This section presents the validation of the models developed for calculating the performance of the flexible heat pump, with a particular focus on compressor power and COP. The models are tested against experimental data, and the comparison allows for evaluating their accuracy in replicating the system's behaviour.

As mentioned in the introduction of section 3.3, the modelling approach used in this thesis aims to explore the thermodynamic principles of the flexible heat pump and to assess its performance improvement compared to a conventional heat pump. This approach has been previously used and validated by our research group in a publication by Yu et al.[223], which used R134a as the refrigerant. A prototype was built from off-the-shelf parts as a proof of concept and is shown in Fig. 3-9. The heat storage system consisted of a small water tank weighing approximately 25 kg, installed after the condenser outlet. Mode switching was carried out manually by operating a four-way valve, which limited the overall performance of the setup. In addition, this flexible heat pump configuration was only able to operate in two modes: Mode 1 and an alternative defrosting mode. This alternative mode is different from the one discussed in this chapter, as defrosting was achieved by subcooling the refrigerant in the frosted evaporator.

The results from our tested prototype are used to validate some of the predicted results. However, since the prototype was unoptimized and could only run under a few different setup conditions due to compressor limitations, the model validation was completed with experimental data from the literature. This allowed validation over a wider range of parameters and for various refrigerants.

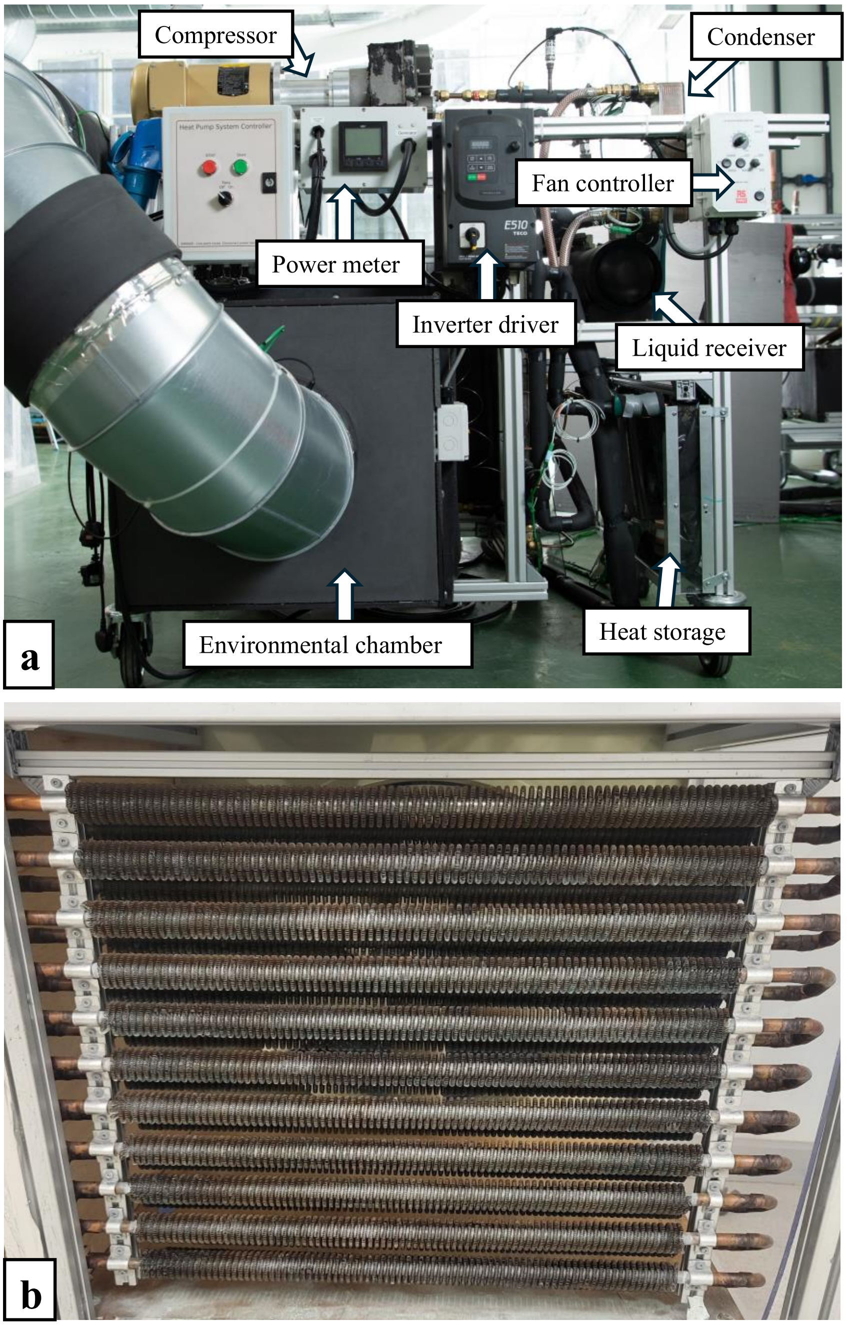

Fig. 3-9: Photographs of the flexible heat pump prototype taken from Yu et al.[223] (a) Overview of the prototype; (b) Evaporator

In this thesis, model validation is carried out by comparing the main parameter used to assess the performance of the heat pump which is the compressor power, considering that the heating capacity is assumed constant. The COP is also validated against experimental data.

3.4.1 Validation against compressor power data

Fig. 3-10 presents both the experimental data from our conducted experiments and from the literature (Cuevas and Lebrun[58]; Sánchez et al.[251]) as well as the simulation results from the compressor models. The experimental data and the relevant parameters for each dataset are summarized in Table 3-4, and these parameters are used to set the simulation conditions. The model has been tested over a wide range of compressor power, with various pressure ratios and refrigerants. As shown in Fig. 3-10, the model provides results with good accuracy, within 5 % error, for both low and high power consumption.

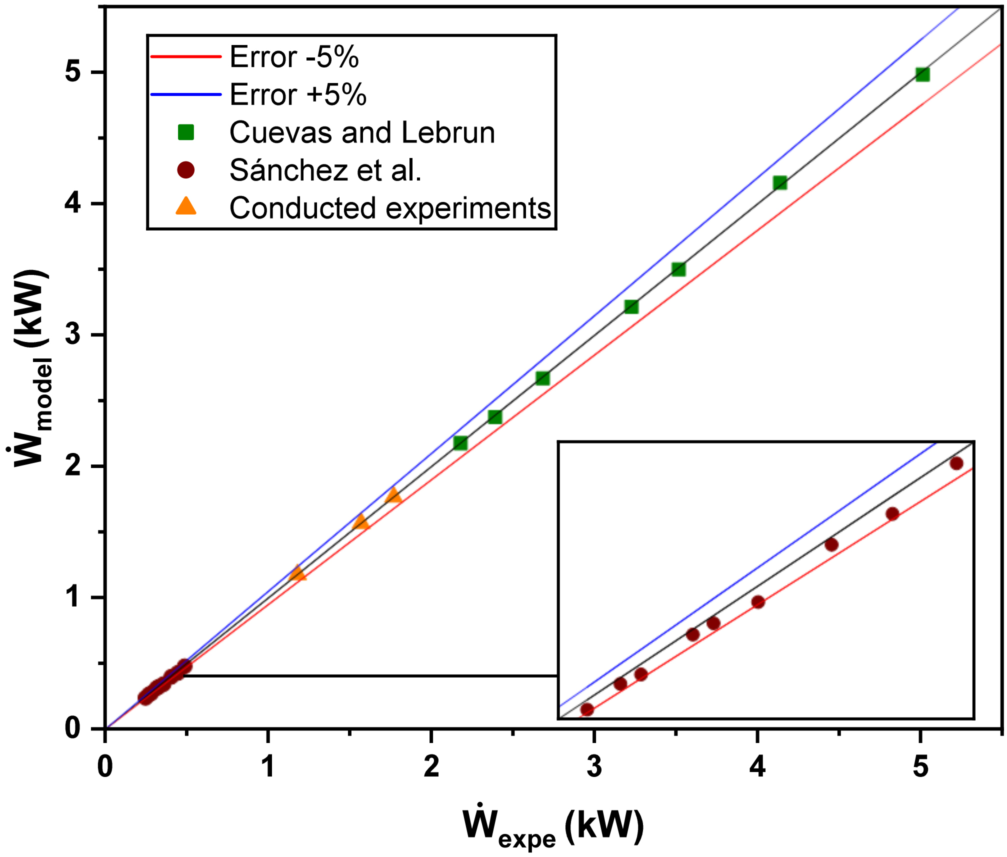

Fig. 3-10: Validation of predicted compressor power against experimental data

For our conducted experiments, the compressor power was validated at a constant evaporating temperature of 0 °C during the charging mode under steady conditions, using R134a. The mass flow rate was calculated using Eq. (3.3), with an approximate heating capacity of 2.5 kW, at three different condensing temperatures: 30 °C, 35 °C, and 40 °C. The compressor used is a 1 kW oil-free scroll compressor (Air Squared Ltd, Model: P15H022A-A01), which is controlled with an inverter drive. Both the inverter and compressor power were measured with a power meter, as illustrated in Fig. 3-9, so the measured power includes the power losses from the inverter as well as the power consumption of the compressor[223].

Therefore, to account for experimental constraints and practical global losses of the compressor, a global compressor efficiency is defined as follows[134,252,253]

$$\eta_{comp,expe} = \eta_s \times \eta_{mech} \times \eta_{elec} \quad (3.114)$$

$$\eta_{comp,expe} = \frac{\dot{W}_s}{\dot{W}_{actual}} \tag{3.115}$$

where η_{mech} is the mechanical efficiency and η_{elec} is the electrical efficiency, both of which depend on the selected compressor and the experimental setup. $\dot{W}_s$ is the isentropic compressor power, and $\dot{W}_{actual}$ is the measured compressor power.

Table 3-4: List of sources of experimental data for compressor power validation

Dataset	**Refrigerant**	**Type**	P_{dis} **[bar]**	P_{suc} **[bar]**
Conducted experiments (partially available in Yu et al.[223])	R134a	Scroll	9.09 – 10.0	1.87 – 1.91
Cuevas and Lebrun[58]	R134a	Scroll	15.6 – 30.4	8.1 – 12.0
Sánchez et al.[251]	R1234yf, R1234ze(E), Propane	Reciprocating	4.97 – 15.35	1.38 – 3.43

3.4.2 Validation against COP data

Fig. 3-11 presents the validation of steady-state performance calculations in heating mode, compared with experimental data and simulated using Eq. (3.20), with the setup conditions for each experiment summarised in Table 3-5. The compressor power is determined using the approach described in the previous section. The COP is validated for the same three condensing temperatures and a heating capacity of 2.5 kW in our experiments. For the study by Shuxue et al.[254], the COP is calculated at different evaporating temperatures and heating capacities.

As shown in Fig. 3-11, the results demonstrate good accuracy, with errors within 10 %. In the case of Shuxue et al.[254], the main source of error arises from the limited data available in the study, which required estimation of the suction temperatures, mass flow rates, and the inlet and outlet temperatures of the condenser for each point, thereby increasing the calculation error. These findings demonstrate that this approach is sufficiently accurate for assessing the heat pump's performance under steady-state conditions.

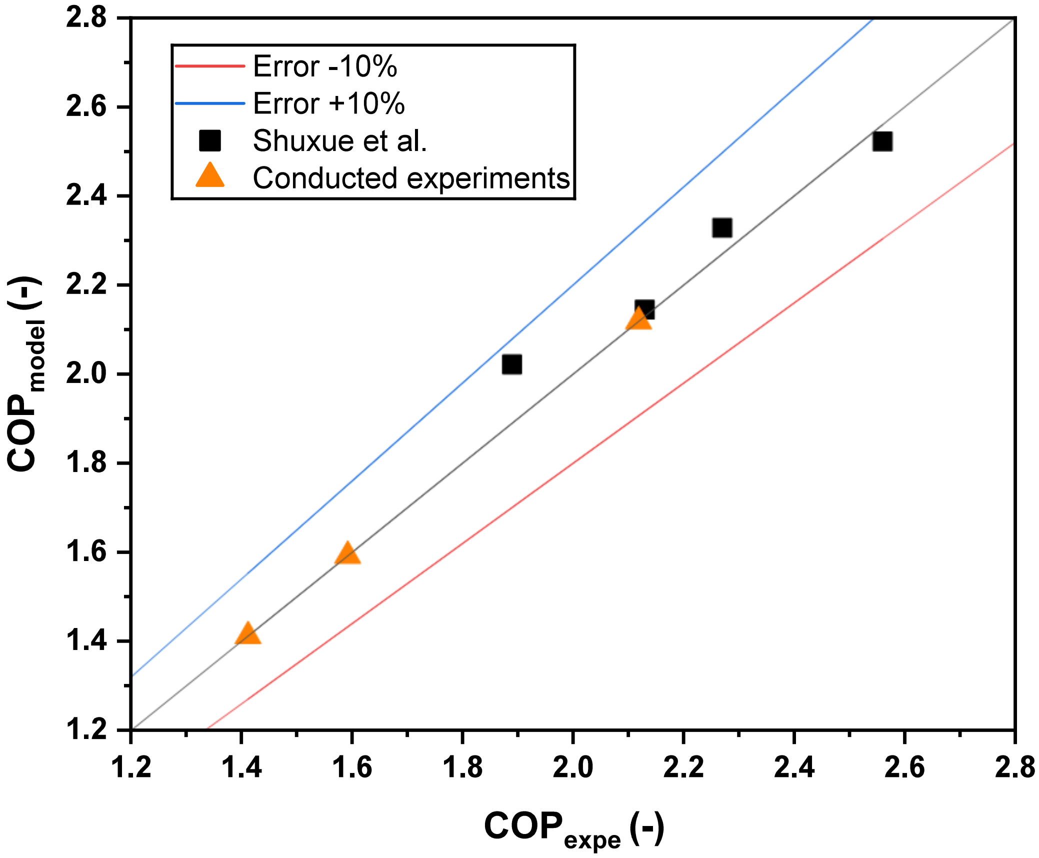

Fig. 3-11: Validation of predicted COP against experimental data

Table 3-5: List of sources of experimental data for COP validation

Dataset	Refrigerant	Discharge temperature [°C]	Suction temperature [°C]	Heating capacity [kW]
Conducted experiments (partially available in Yu et al.[223])	R134a	66.2 – 86.1	6.9 – 7.6	~ 2.5
Shuxue et al.[254]	R32	92.8 – 107.6	~ (-2) – 3	3.6 – 4.1

3.5 Criteria for refrigerant selection

This study evaluates the performance of various refrigerants with the flexible heat pump system, including R134a, R1234yf, R1234ze(E), propane, R410a, and R32. R410a and R134a, as mainstream used refrigerants in heat pumps, are included in this thesis. However, due to their high GWP and evolution of regulations, they are being phased out for certain heating and refrigeration applications[255]. As a result, their low-GWP alternatives have also been considered: R1234yf and R1234ze(E) as replacements for R134a, and R32 as a substitute for R410a, although R32 still has a GWP higher than 150. Additionally, propane has been examined as a potential low-GWP and natural hydrocarbon alternative to R134a. These refrigerants were selected based on their suitability for the required operating conditions in the studied applications, and their performance in the system has been evaluated. They are listed in Table 3-6 along with their thermophysical properties, which were obtained from REFPROP V9.0[256]. Their respective saturation curves are presented on a P-H diagram in Fig. 3-12.

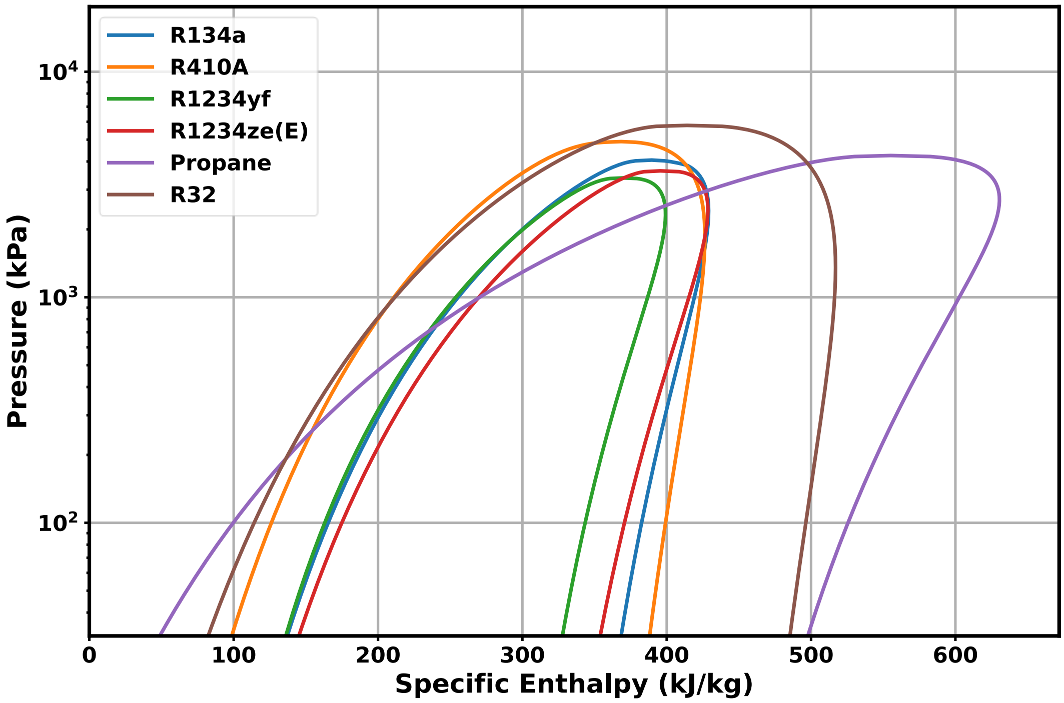

Fig. 3-12: Saturation curves of the selected refrigerants

Table 3-6: Thermophysical properties of the tested refrigerants

Refrigerant	R1234yf	R1234ze(E)	Propane	R134a	R410a	R32
Formula	$C_3H_2F_4$	$C_3H_2F_4$	C_3H_8	$C_2H_2F_4$	CH_2F_2 (50%) CHF_2CF_3 (50%)	CH_2F_2
Molecular weight [g/mol]	114.04	114	44.1	102.03	72.6	52.02
Boiling point at 1 atm [°C]	-29.49	-18.95	-42.12	-26.1	-48.5	-51.65
Critical temperature [°C]	94.7	109.4	96.7	101.06	72.8	78.11
Critical pressure [MPa]	3.38	3.64	4.25	4.06	4.9	5.78
Liquid specific heat capacity at 35 °C [kJ/kg K]	1.44	1.42	2.84	1.47	1.84	2.07
Enthalpy of vaporisation at 35 °C [kJ/kg]	137	159.1	317.5	168.3	169.3	249.5
Liquid specific heat capacity at 65 °C [kJ/kg K]	1.73	1.6	3.5	1.72	4.7	3.56
Enthalpy of vaporisation at 65 °C [kJ/kg]	104	130	245.1	132.3	84	155
ODP	0	0	0	0	0	0
GWP	4	7	3	1430	2088	675
ASHRAE safety group	A2L	A2L	A3	A1	A1	A2L

3.6 Summary

In this chapter, the concept of the multi-valve flexible heat pump with integrated heat storage has been presented, along with its thermodynamic working principles and the steady-state models used in the thesis. Key points covered include:

- The multi-valve flexible heat pump concept and its distinctions from a conventional heat pump.
- The operating modes of the system were thoroughly described and explained.
- The modelling approach was detailed, including the main assumptions and the equations used to conduct the energy, exergy, economic, and environmental analyses.
- The compressor power and COP models were validated using both our experimental data and data from the literature, and they demonstrated high accuracy.
- Finally, the refrigerants studied in this thesis were introduced, along with their thermophysical properties.

Chapter 4 Defrosting operation with latent heat storage

This chapter assesses the thermodynamic performance of the multi-valve flexible heat pump, with a latent heat storage, when the defrosting operation is run. A theoretical model has been established to study the heat pump performances during a full charge/discharge cycle of the storage. This analysis serves as a preliminary investigation focusing on the performance of the multi-valve flexible heat pump under idealised conditions and contributes to addressing research question 1. Results have been obtained here with R410a, R134a, R1234yf and R32. This chapter contains material from a published paper[257].

4.1 Introduction

In the previous chapter, the concept of the multi-valve flexible heat pump was introduced. This system integrates heat storage within the conventional vapour compression cycle to recover and store some of the sensible heat carried by the hot liquid refrigerant exiting the condenser. The different operation modes have been comprehensively characterised, and the underlying principles clarified. Given the novelty of the concept, it is essential to first elucidate the theoretical functioning and performance of the system under ideal conditions. As a starting point for this thesis, the methodology outlined in the previous chapter for the thermodynamic energy model is applied under ideal conditions.

In this chapter, the focus is on the defrosting operation of the multi-valve flexible heat pump. As explained previously, the novelty of this mode, compared to traditional defrosting methods, is that it could allow the heat pump to maintain consistent heating capacity throughout the process. By leveraging the heat storage, the system can increase the evaporating temperature, resulting in reduced electrical consumption and enhanced efficiency. Since no prior studies have examined this specific operation, an ideal theoretical model has been developed to analyse the operation when latent heat storage is used. This type of storage theoretically enables the heat pump to maintain a steady temperature throughout the process, ensuring the best operating conditions. However, as previously explained, the heat pump can also utilise a sensible heat storage tank, which will be explored in Chapter 7.

The chapter begins by briefly revisiting the defrosting operation process and detailing the execution of the model. The assumptions for this chapter, along with the case study, are then presented. The system's performance was evaluated using the COP improvement parameter, varying both the storage temperature and defrosting duration. The impact of these parameters on heat storage, mass flow rates, and discharging times of the heat storage was analysed. Results were presented for the mainstream refrigerants R134a and R410a, as well as for their low-GWP alternatives, R1234yf and R32. The objective was to determine the maximum theoretical improvement of the flexible heat pump compared to a conventional reverse cycle defrosting operation, to gain a deeper thermodynamic understanding of the system's internal processes, and to address research question 1.

4.2 Methodology

The defrosting operational principles are explained in Chapter 3, and the equations for the simulations conducted here are provided. A description of the simulation process for this operation is presented. References are made to Modes 1, 2, and 3, as outlined in Chapter 3 (Table 3-1).

As it was previously outlined, before initiating the defrosting mode, the system operates in Mode 1 (heating/charging mode) for a duration Δt_{charge}. During this period, ice will form on the evaporator, which requires initiating the defrosting mode to remove it. This process is simplified by assuming a constant heating capacity throughout the operation of Mode 1. It should be noted that the focus is not on the frost formation process, but rather on the impact of the defrosting operation on overall heat pump performance to address research question 1. It should also be noted that the model is not time-based, and the duration Δt_{charge} is only required to make an assumption on the ice buildup. However, this parameter has no impact on the simulation results.

Once Mode 1 is completed, the defrosting operation is initiated (Mode 3). Given that the defrosting operation takes up only a brief period of the total discharge process, Mode 2 is subsequently run until no heat remains in the storage. During this stage, the evaporator is bypassed, and no refrigerant is condensed inside. Finally, the flexible heat pump enters in its '*recovery phase*' when switching back to Mode1.

Therefore, the simulation progresses as follows: Mode 1 is maintained at steady state for $\Delta t_{charge} = 1$ h. The system then switches to Mode 3 for $\Delta t_{defrost}$, followed by Mode 2 for $\Delta t_{discharge,2}$. Finally, it enters the recovery phase for $\Delta t_{recovery}$ until all liquid refrigerant within the accumulator is cycled back, at which point the simulation stops. A simplified flowchart of this procedure is shown in Fig. 4-1.

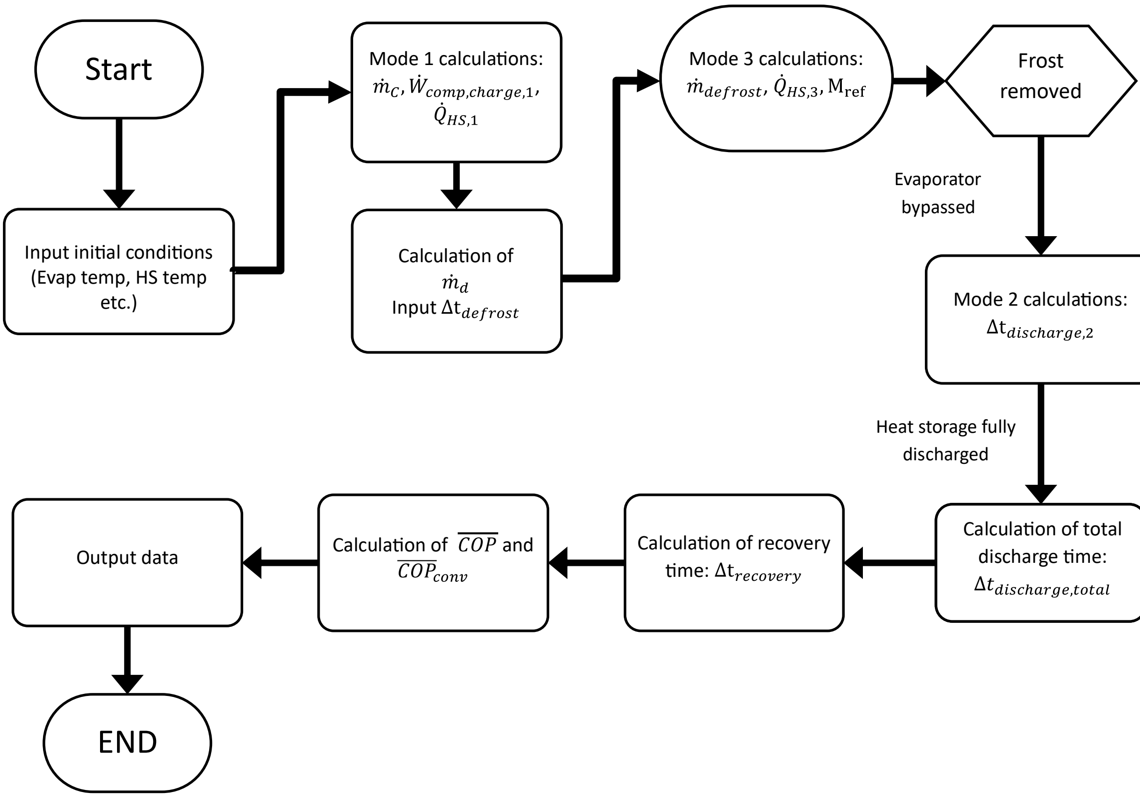

Fig. 4-1: Simulation flowchart of a run of the flexible heat pump

The steady-state model described in Chapter 3 is used for this simulation, incorporating latent heat storage with a fixed storage temperature throughout the process.

4.2.1 Assumptions adopted in this chapter

The aim of this chapter is to investigate the theoretical maximum improvement of the flexible heat pump defrosting method under ideal conditions by simplifying the mathematical model of the cycle. Therefore, additionally to the assumptions outlined in Chapter 3, the following specific assumptions are made in this chapter to simplify the proposed flexible heat pump concept. This allows for a focus on analysing the thermodynamic efficiency and comparing it to the traditional vapour compression cycle under ideal conditions:

1) Isothermal heat transfer: Heat transfer occurs under isothermal conditions in all heat exchangers and heat storage.

2) Ideal compression process: The compressor operates with 100 % isentropic efficiency.

3) Ideal storage process: Heat storage is assumed to have 100 % round-trip efficiency with negligible thermal losses between modes ($\%\Delta Q_{loss} = 0$). The same amount of energy charged in Mode 1 is available at the beginning of the discharging process.

4) <u>External loops are disregarded:</u> The following energy analysis does not require assumptions regarding the external loop, as only the maximum theoretical performance of the heat pumps is calculated using a similar fixed heating capacity under the same conditions for a fair performance comparison. According to the developed energy models, only assumptions about the suction and discharge pressures affect the COP. Therefore, reasonable condensing and evaporating temperatures are assumed for potential applications, and examples are provided.

4.2.2 Description of case study

In this case study, Mode 1 is operated for one hour. To address research question 1, it is necessary to estimate the ice mass on the evaporator after Mode 1, as previously explained. According to Eq. (3.32), approximately 1.25 kg of ice is expected to form on the evaporator after one hour of operation, based on the study by Reichl et al.[224] For consistency, the remaining input parameters for this study are also taken from their work and are summarised in Table 4-1. Although the condensing temperature of 35 °C is not typical for DHW heating in the UK, as discussed in Chapter 2, it can be used for underfloor heating applications or to heat buffer tanks for space heating, reaching sink water temperatures in the range of 30 °C – 35 °C[108,224,258,259]. This temperature is sufficient to assess the defrosting performance of the flexible heat pump compared to a conventional air-source heat pump.

Table 4-1: Input parameters

Parameters	**Value**
Condensing temperature [°C]	35
Evaporating temperature [°C]	-8
Heating capacity [kW]	3.6
Charging/Frosting time [h]	1
Mass of ice on evaporator [kg]	1.25
Compressor efficiency [%]	100

In this study, R410a is used as the primary refrigerant, following Reichl et al. research. Additionally, its low-GWP alternative, R32, is considered. Comparisons are also made with refrigerants R134a and R1234yf.

4.3 Results and discussions

4.3.1 Fixed defrost duration with varying storage temperature

Initially, the time parameters are fixed as the followings: $\Delta t_{charge} = 1\,\mathrm{h}$ constant; $\Delta t_{discharge,2}$ varies depending on the chosen storage temperature; $\Delta t_{defrost} = 5\,\mathrm{min}$ constant, as it was reported in the literature to be generally sufficient to melt the frost on the evaporator[260–262]. The melting temperature of the latent heat storage varies from 10 °C to 30 °C. The performance of the flexible heat pump when defrosting is operated has been analysed and the results are presented from Fig. 4-2 to Fig. 4-6.

Fig. 4-2 and Fig. 4-3 illustrate the average COP and COP improvement, respectively, of the flexible heat pump compared to a conventional heat pump using a reverse cycle defrost method depending on the heat storage temperature. The defrosting time for the baseline heat pump has been calculated using Eq. (3.46) as $\Delta t_{defrost,conv} \approx 2$ min. As seen in Fig. 4-2, the average COP of the flexible heat pump is always higher than the conventional heat pump using a reverse cycle defrosting method, for all refrigerants. The average COP of the conventional heat pump decreases when the storage temperature of the flexible heat pump increases. This is not because the conventional heat pump is impacted by the storage temperature, but because both heat pumps are run for the same duration to compare them as defined in Eqs. (3.43) and (3.48). The storage temperature is linked to the running time of the flexible heat pump by Eqs. (3.5), (3.15) and (3.30). This running time is then applied to the conventional heat pump.

The average COP of R134a is higher than the one of R410a for all tested storage temperatures. However, in Fig. 4-3, their improvement in COP varies from 11 % at $T_{HS} = 10$ °C to 11.2 % at $T_{HS} = 13.1$ °C for R410a and from 10.6 % at $T_{HS} = 10$ °C to 10.8 % at $T_{HS} = 12.6$ °C for R134a. Therefore, a storage temperature for maximum improvement can be found for both refrigerants in this configuration. They are $T_{max,\alpha} = 13.1$ °C for R410a and $T_{max,\alpha} = 12.6$ °C for R134a. The storage temperature corresponding to the highest improvement is slightly below the midpoint between the refrigerant temperature at the heat storage inlet, which is the condensing temperature here, and the evaporating temperature, for both refrigerants.

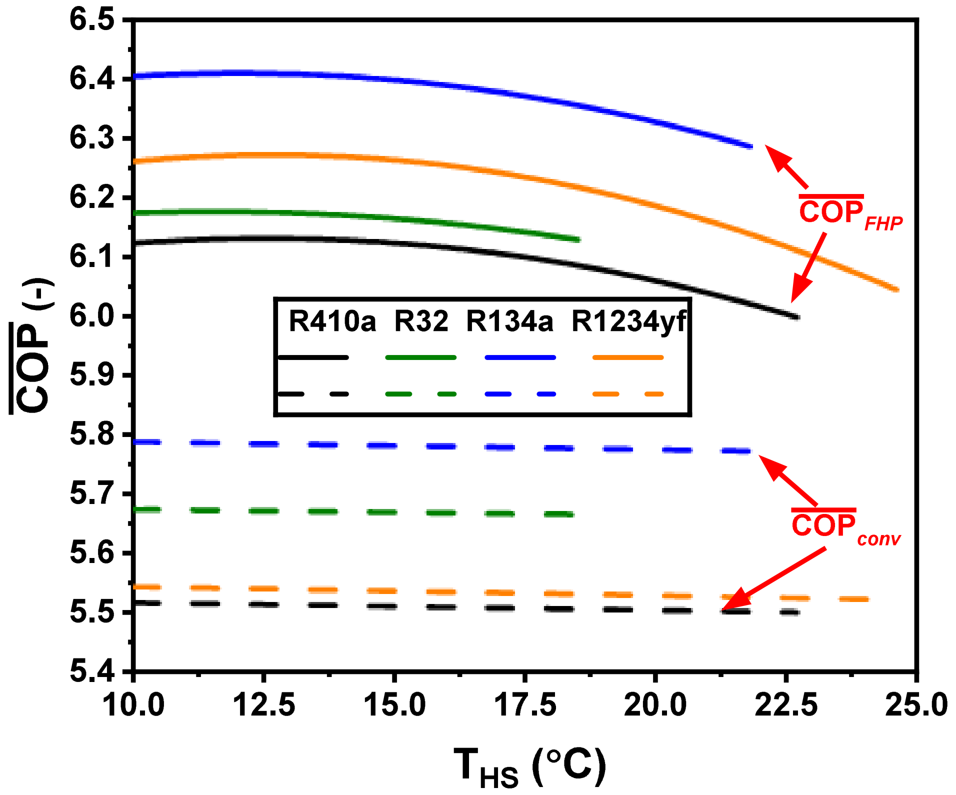

Fig. 4-2: Theoretical average COP depending on heat storage temperature for R134a and R410a and their potential low GWP replacements

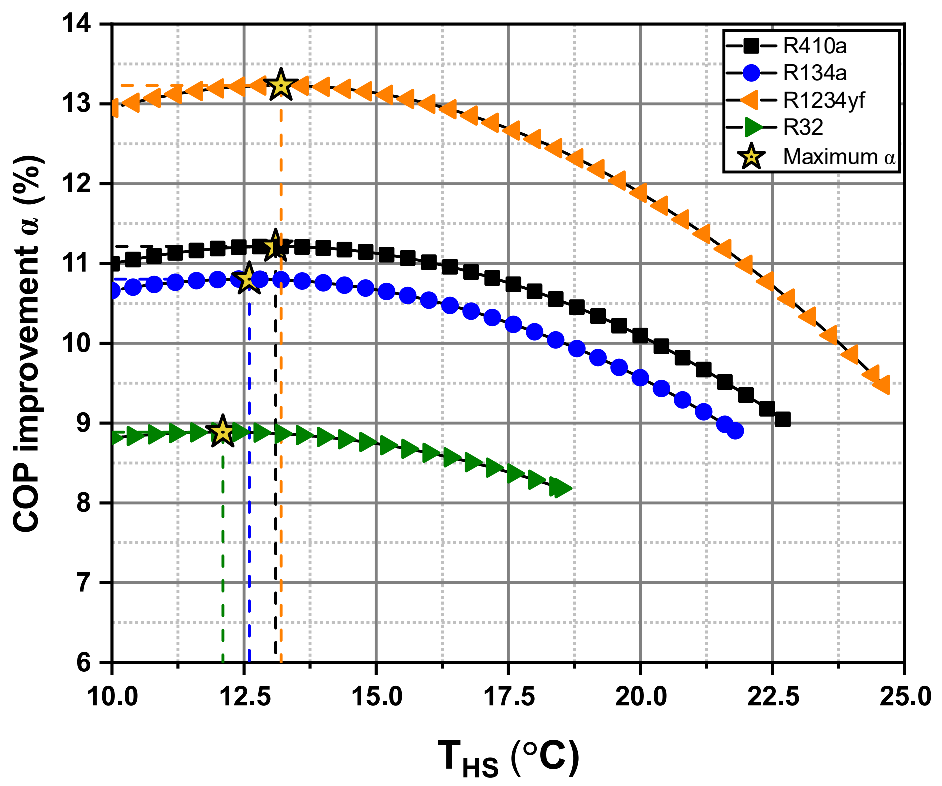

Fig. 4-3: Theoretical COP improvement depending on heat storage temperature for R134a and R410a and their potential low GWP replacements

The performance gap grows between the two refrigerants when T_{HS} increases, with R410a showing a slightly better improvement compared to a conventional heat pump than R134a. This implies that the flexible heat pump is more beneficial to R410a systems than to R134a systems, despite the performance difference remaining relatively close. This can be attributed to their enthalpy of vaporisation at 35 °C and the liquid specific heat capacity as reported in Table 3-6, as well as their isentropic lines shape seen in the P-H diagrams in Fig. 4-4.

The enthalpy of vaporisation is nearly identical for both refrigerants, resulting in a similar mass flow rate in the system, which should lead to comparable heat recovery in the thermal storage. However, the specific heat capacity of R410a is higher than that of R134a, compensating for its slightly lower mass flow rate and allowing for better heat recovery in the heat storage. This results in more energy being stored and a moderately longer discharge time, leading to improved performance. At the storage temperature for maximum improvement, the R410a system's total discharging time is longer ($\Delta t_{discharge,total} = 10.6$ min) than the one of R134a ($\Delta t_{discharge,total} = 10.1$ min), saving compressor power for a slightly extended period. Moreover, when calculating the COP improvement, compressor work in discharge is a crucial parameter to consider. Some refrigerants benefit more than others from an increase in evaporating temperature. While power consumption is reduced in all cases, the extent of improvement depends on the shape of their isentropic lines. Refrigerants with isentropic lines that deviate significantly from their saturation curve typically require more compressor work. As a result, the maximum improvement and related storage temperature depend on a balance of these properties, which can vary significantly depending on the refrigerant.

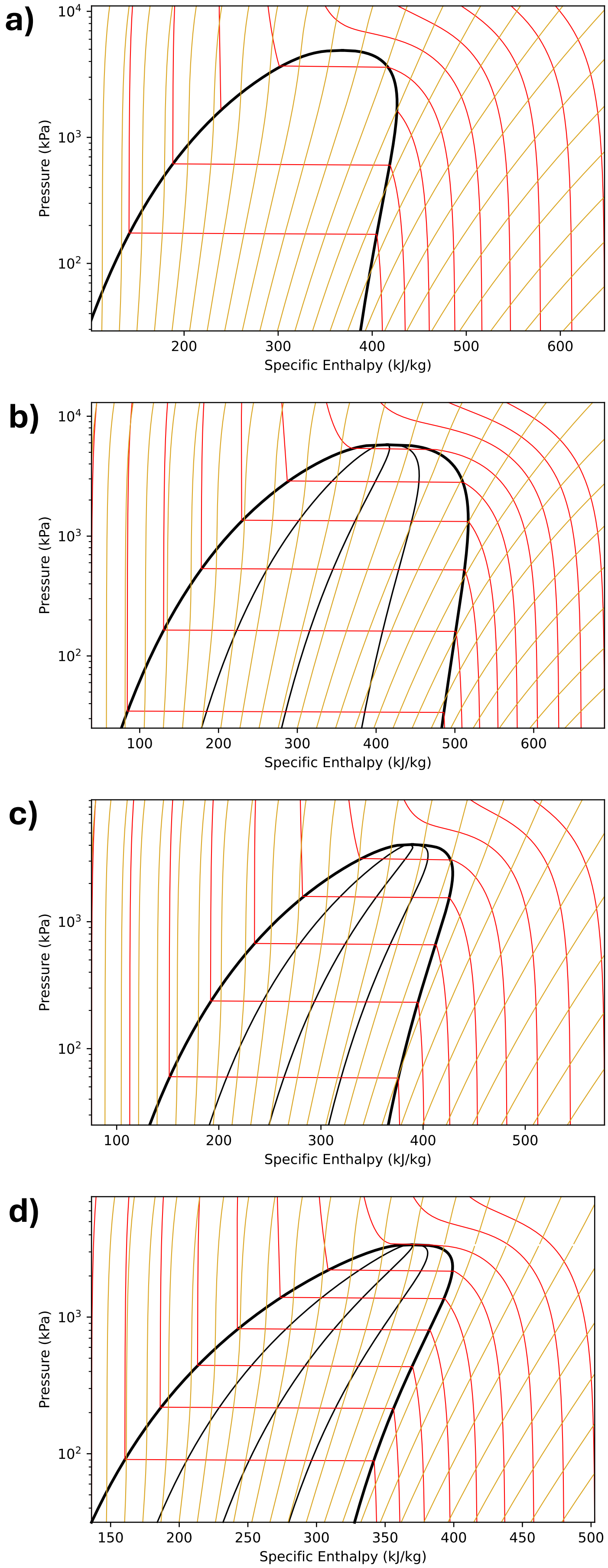

Fig. 4-4: P-H diagrams with isotherms (red) and isentropic (yellow) lines for (a) R410a; (b) R32; (c) R134a; (d) R1234yf

This analysis applies to other tested refrigerants as well. The system has been studied with potential low-GWP alternatives for R134a and R410a, namely R1234yf and R32. A storage temperature for the best efficiency can also be found for both and are $T_{HS} = 13.2$ °C for R1234yf and $T_{HS} = 12.1$ °C for R32. Although R1234yf has a lower average COP than R134a with this system, its improvement is greater and can go up to 13.2 %. R1234yf performs the best with this system due to its lowest enthalpy of vaporisation at 35 °C, resulting in the best heat recovery, as well as the favourable profile of its isentropic lines. On the other hand, R32 has a higher average COP than R410a but shows the least improvement, with the highest one being 8.9 %. Consequently, R32 lags in heat recovery because of its high enthalpy of vaporisation at 35 °C resulting in the lowest mass flow rate in Mode 1 among all tested refrigerants. Additionally, despite its low mass flow rate, R32 exhibits the highest compressor power during discharging, due to the significant deviation of its isentropic lines from its saturation curve. Consequently, its overall improvement in Mode 3 is relatively small compared to other refrigerants. Therefore, the enthalpy of vaporisation and the specific heat capacity at the heat storage inlet temperature, as well as the shape of the isentropic lines of the refrigerants are crucial parameters to consider when evaluating the performance of refrigerants with the flexible heat pump system.

Fig. 4-2 and Fig. 4-3 also show that even though storage temperatures up to 30 °C have been tested with this system, R410a and R134a can only perform with storage temperatures up to 22.7 °C and 21.8 °C, respectively. This is because when storage temperatures are too high, not enough heat can be recovered to ensure a full defrosting cycle. An upper limit can therefore be found for both refrigerants and their low-GWP alternatives.

Finally, it should be noted that the recovery phase described in section 3.2.3 does not have a significant impact on the performance of the flexible heat pump. At the storage temperatures where the system performs best for both R410a and R134a, the recovery time has been calculated as 1.8 minutes, accounting for approximately 2.8 % and 2.7 % of the total compressor work during the operation, respectively. For R32, the recovery time is 2 minutes, which represents about 3 % of the total compressor work. For R1234yf, the recovery time is 1.7 minutes, accounting for 2.5 %, which is the lowest among all refrigerants considered.

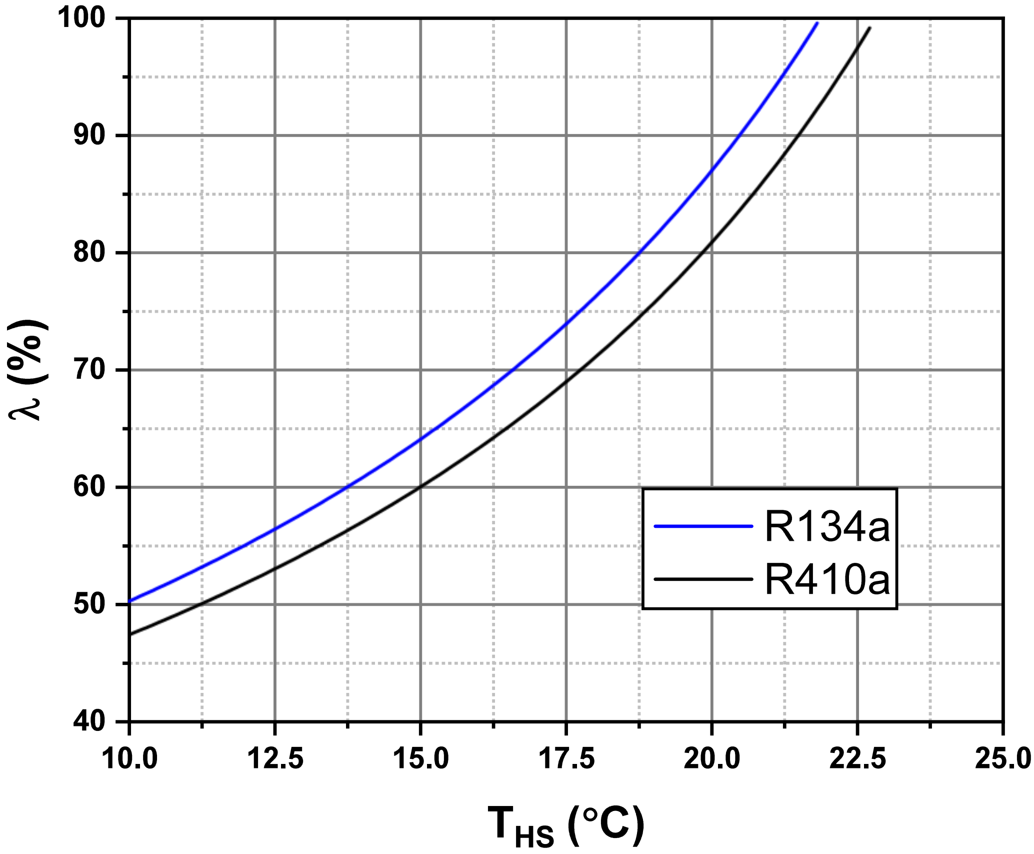

Fig. 4-5: Percentage of stored energy in the heat storage used to defrost for R134a and R410a

Fig. 4-5 presents the percentage of the recovered energy during Mode 1 that is used to defrost in Mode 3 depending on the storage temperature. At the topmost achievable storage temperatures, for R410a and R134a, almost 100 % of the heat stored is used to defrost the evaporator. As explained previously, an upper limit storage temperature is found, meaning that not enough heat can be recovered to ensure a complete defrosting beyond this point. This occurs because, at high storage temperatures, less heat is recovered from subcooling the refrigerant as the temperature difference between the storage and the condensing temperatures. Consequently, because the defrosting mode requires a higher discharging rate from the heat storage, a larger portion of the stored energy is used for that purpose. At lower storage temperatures, the portion used to defrost is significantly reduced. This rate is below 50 % for temperatures inferior to 11.3 °C for R410a. At the maximum improvement storage temperature found previously, the part of the energy used to defrost is 54 % for R410a and 56 % for R134a.

Because a 100 % efficiency roundtrip of the storage and fixed storage temperature have been assumed, the storage energy balance in Eq. (3.41) can be modified as,

$$\dot{Q}_{HS,3}\Delta t_{defrost} = \dot{Q}_{HS,1}\Delta t_{charge,defrost} \tag{4.1}$$

Therefore, $\Delta t_{charge,defrost}$, the required charging time to store enough heat for solely ensuring a complete defrosting, can be calculated. At maximum improvement, this time is 33 minutes for R410a and 34 minutes for R134a.

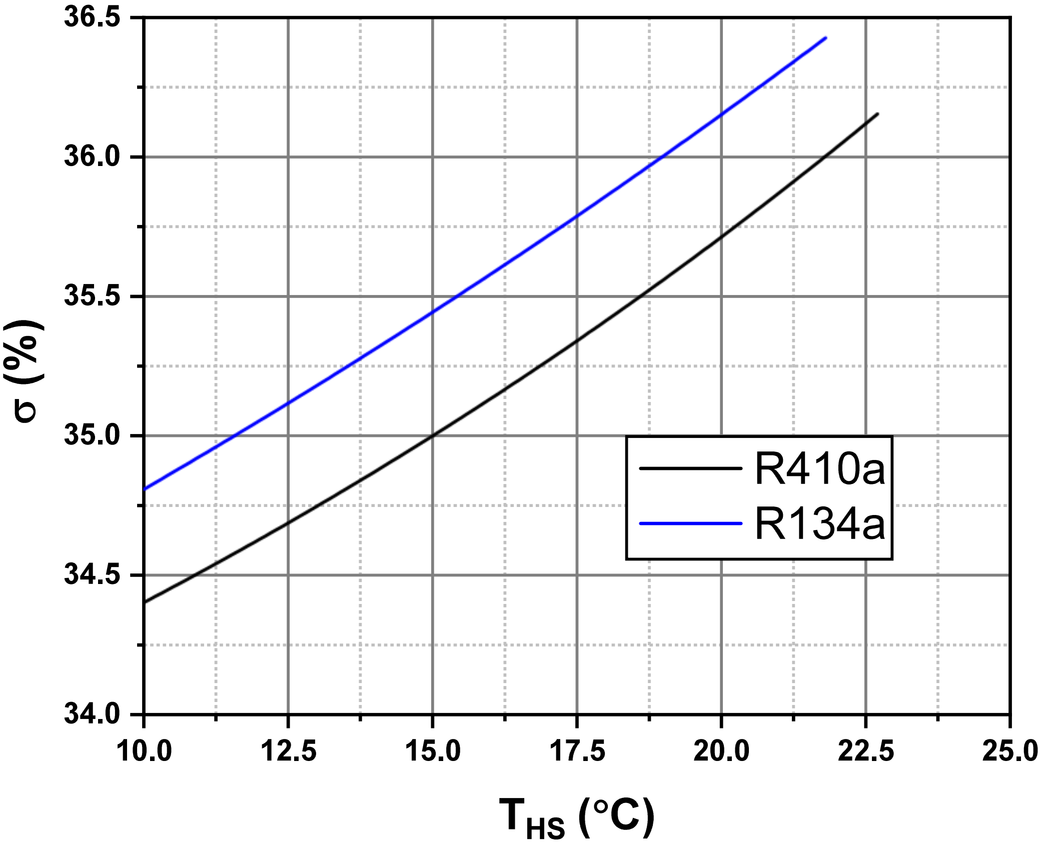

Fig. 4-6: Part of the mass flow rate used to defrost the evaporator ($\dot{m}_{defrost}$) as a ratio of the discharging mass flow rate ($\dot{m}_d$) for R134a and R410a

Fig. 4-6 shows the defrosting mass flow rate $\dot{m}_{defrost}$, expressed as a percentage of $\dot{m}_d$, influenced by the storage temperature. The increase of the σ ratio with the storage temperature indicates a higher mass flow rate used for defrosting. This results in a higher discharging rate of the heat storage during Mode 3. In fact, as shown in Eq. (3.31), when all parameters are fixed, a steady defrosting heat rate is set at $\dot{Q}_{defrost} = 1.4$ kW. Therefore, according to the definition in Eq. (3.34), the mass flow rate must increase to ensure the same defrosting rate in the evaporator at higher evaporating temperatures. A higher σ also means that a higher part of the mass flow rate will have to be compensated by the refrigerant storage. At the highest efficiency, the ratio σ is 34.8 % for R410a and 35.1 % for R134a.

4.3.2 Fixed storage temperature with varying defrost duration

In the following results, only R410a is used. The storage temperature has been set to the value corresponding to the previously determined maximum improvement, $T_{max,\alpha} =$ 13.1 °C. Mode 1 was operated for $\Delta t_{charge} = 1$ h, while the defrosting time was varied from 2 to 10 minutes. The storage temperature was kept constant, resulting in a fixed vaporisation enthalpy $(h_6 - h_{10})$ in Eq. (3.33). The impact of the defrosting time on the model is presented from Fig. 4-7 to Fig. 4-9.

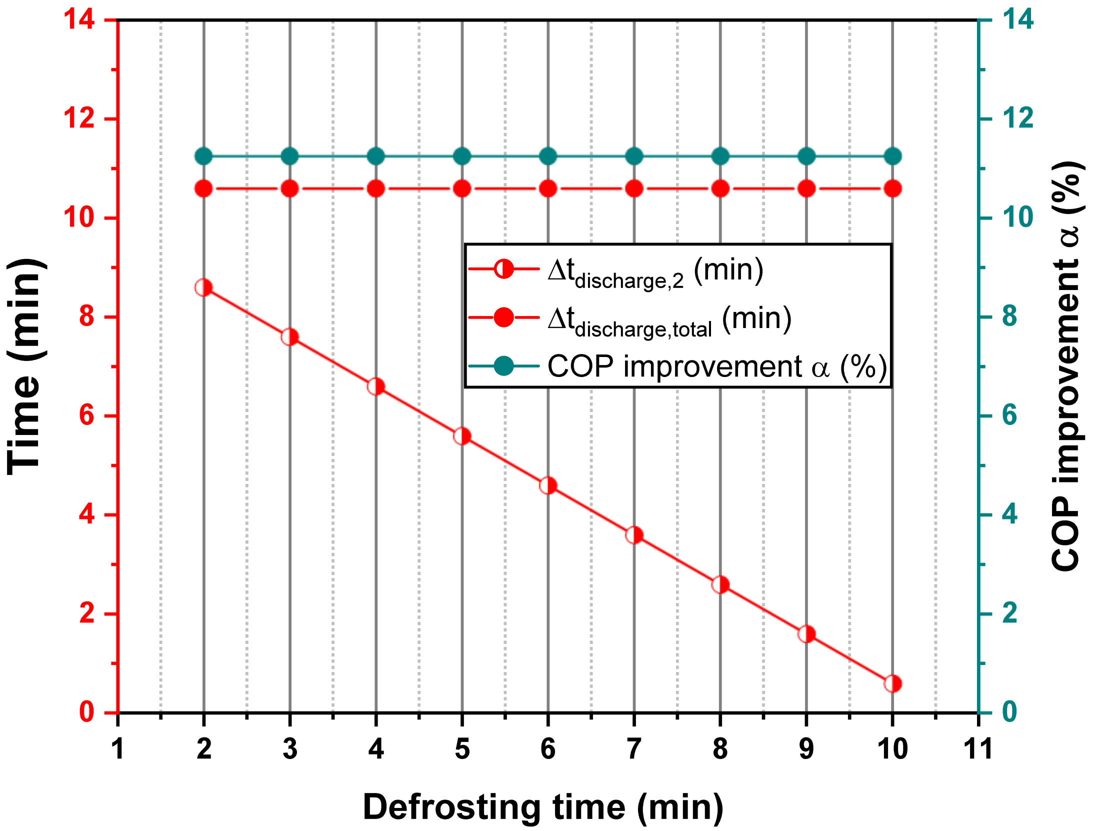

Fig. 4-7: Impact of the chosen defrosting time on COP improvement, storage discharging time after defrosting (Mode 2) and total discharging time

Fig. 4-7 presents the evolution of the storage discharging time after defrosting (Mode 2), the total discharging time, and the COP improvement when the defrosting duration varies. In this model, the COP improvement is not impacted by the variation of the defrosting time because the total discharging time remains constant, resulting in compressor power being saved over the same duration. Fig. 4-7 shows that despite $\Delta t_{discharge,total}$ staying constant, $\Delta t_{discharge,2}$ decreases when $\Delta t_{defrost}$ increases, as described in Eq. (3.40) and Eq. (3.41). Eq. (3.41) is the energy balance of the heat storage through a full charge/discharge. The charging part of the equation remains unchanged, as well as $\dot{Q}_{HS,2}$. Consequently, when

$\Delta t_{defrost}$ is increased, $\Delta t_{discharge,2}$ and $\dot{Q}_{HS,3}$ must decrease to conserve balance. This figure highlights that $\Delta t_{discharge,2}$ varies from 8.6 minutes to 0.6 minutes when $\Delta t_{defrost}$ varies from 2 to 10 minutes. Therefore, Fig. 4-7 shows that any assumption of the defrosting time between 2 to 10 minutes is mathematically valid to ensure energy balance.

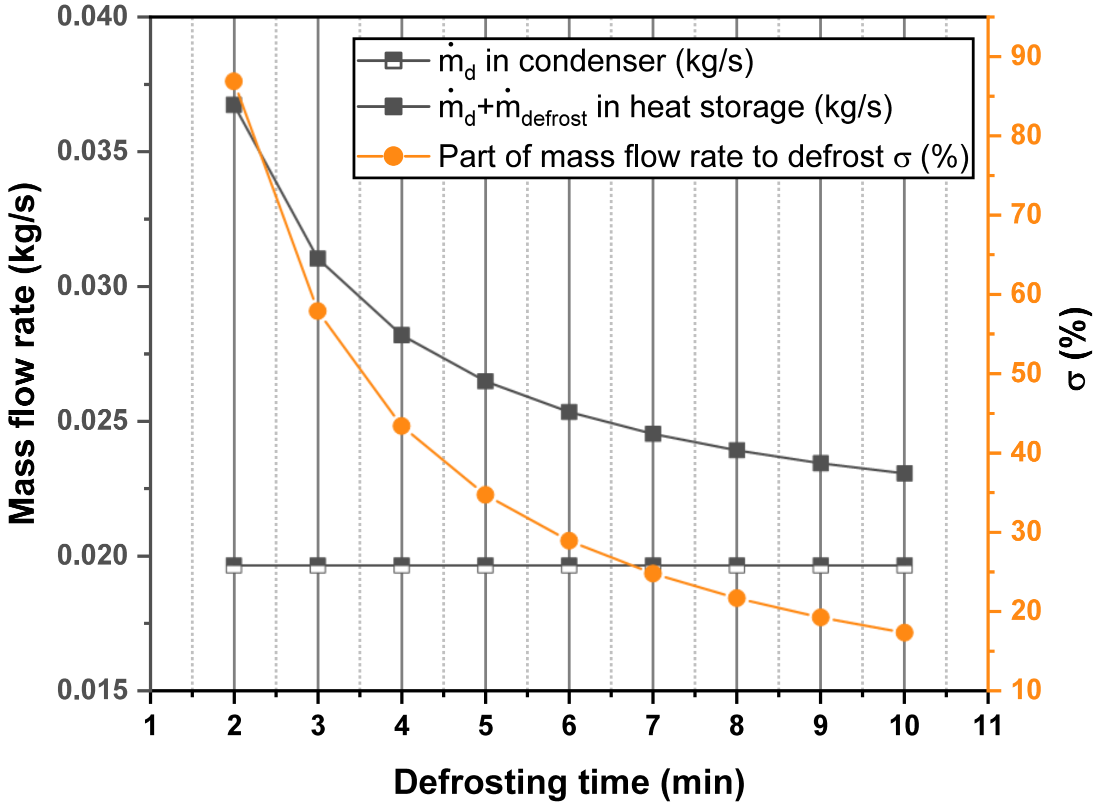

Fig. 4-8: Evolution of $\dot{m}_d$, $\dot{m}_d + \dot{m}_{defrost}$ and σ with defrosting time

Fig. 4-8 presents the variation of the discharging mass flow rate in the condenser ($\dot{m}_d$), the total discharging mass flow rate in heat storage during defrosting ($\dot{m}_d + \dot{m}_{defrost}$), and the part of the mass flow rate used for defrosting (σ) depending on defrosting time. The discharging mass flow rate in the condenser $\dot{m}_d$ remains constant and is not affected by the variation of the defrosting time, but only by the heating capacity and the value of $h_{7,r}$ in Eq. (3.12). In this model, this value is solely influenced by the evaporating temperature and compressor efficiency. Since the storage temperature and compressor efficiency are fixed, the discharging mass flow rate value is constant. This explains the constant value of $\dot{Q}_{HS,2}$ mentioned in the previous paragraph. It is also shown that $\dot{m}_d + \dot{m}_{defrost}$ and σ are decreasing when $\Delta t_{defrost}$ increases. This is because $\dot{m}_d$ is fixed and $\dot{m}_{defrost}$ decreases according to σ as defined by Eq. (3.35). The decrease of $\dot{m}_{defrost}$ is explicated by equations (3.31) and (3.34). The vaporisation enthalpy, the mass of ice, and the latent heat of fusion of ice are fixed, forcing the defrosting mass flow rate to decrease when $\Delta t_{defrost}$ increases to keep balance. At a defrosting time of 2 minutes, the percentage of mass flow rate used to defrost is 87 % of $\dot{m}_d$. It decreases sharply under 50 % at 4 minutes and continues to decrease up to 17 % for 10 minutes. It demonstrates the direct impact of the bypassed mass flow rate on the duration of the defrosting process.

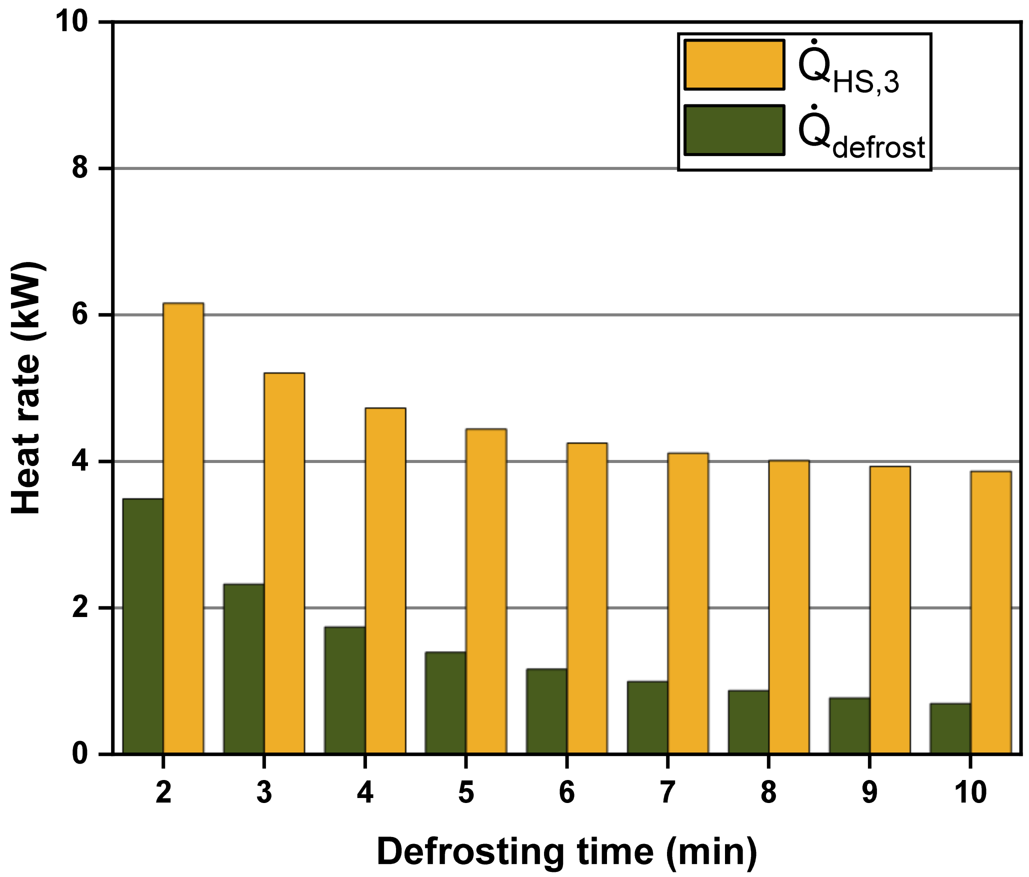

Fig. 4-9: Defrosting heat rate in the evaporator and discharging rate of the heat storage during defrosting

Fig. 4-9 illustrates the defrosting heat rate in the evaporator ($\dot{Q}_{defrost}$) and the discharging rate of the heat storage ($\dot{Q}_{HS,3}$) depending on the chosen defrosting time. Both parameters decrease when $\Delta t_{defrost}$ increases to maintain balance, with $\dot{Q}_{HS,3}$ also decreasing due to the reduction in $\dot{m}_{defrost}$, as explained in the previous paragraph. Because 87 % of $\dot{m}_d$ is required to defrost in 2 minutes, both $\dot{Q}_{defrost} = 3.5$ kW and $\dot{Q}_{HS,3} = 6.2$ kW are high for this chosen parameter. They decrease following the same trend to 0.7 kW for $\dot{Q}_{defrost}$ and 3.9 kW for $\dot{Q}_{HS,3}$ for 10 minutes of defrosting. From $\Delta t_{defrost} = 6$ min, the discharging rate of the heat storage is around 4 kW where the added mass flow rate to defrost is less than 30 % of $\dot{m}_d$. From $\Delta t_{defrost} = 7$ min, the heat rate in the evaporator is less than 1 kW.

Therefore, the defrosting mass flow rate can be adjusted to control the duration of the defrosting process and to regulate the amount of energy used for defrosting according to specific needs.

4.4 Summary

This chapter reports a thermodynamic analysis of the defrosting operation of the multi-valve flexible heat pump integrating a latent heat storage. It can provide an efficient defrosting cycle by condensing refrigerant inside the evaporator while extracting heat stored in a heat storage during the charging cycle. In consequence, the evaporating temperature is increased resulting in more compressor power saving and increased COP. The impact of the defrosting operation on the discharge cycle of the heat storage has been investigated, and the following conclusions are found:

- Depending on the storage temperature, a COP improvement varying from 11 % to 11.2 % for R410a and from 10.6 % to 10.8 % for R134a, compared to a conventional heat pump using a reverse cycle defrosting method, has been observed. Their low-GWP alternatives R1234yf and R32 have also been studied, and R1234yf has been concluded to be the best performing refrigerant with this system with an improvement up to 13.2 %.

- The storage temperatures for the best improvement are found to be $T_{max,\alpha} = 13.1$ °C for R410a and $T_{max,\alpha} = 12.6$ °C for R134a. For R1234yf this temperature is $T_{max,\alpha} = 13.2$ °C and $T_{max,\alpha} = 12.1$ °C for R32.

- An upper limit of the storage temperature is found for all refrigerants beyond which not enough heat can be recovered to ensure a full defrosting process.

- The recovery phase doesn't significantly affect the heat pump performance and is calculated to last 1.8 minutes for R134a and R410a at their top performing storage temperature. This value is 2 minutes for R32 and 1.7 minutes for R1234yf. It accounts for a range of 2.5 % – 3 % of the total compressor work throughout the operation, depending on the refrigerant.

- The defrosting operation only consumes a part of the stored energy during the running of Mode 1. This portion increases along with the chosen storage temperature. It is 54 % for R410a and 56 % for R134a at their storage temperature for maximum improvement.

- At higher storage temperatures, a greater part of the mass flow rate is redirected to defrost the evaporator which means more compensation is required from the refrigerant storage.
- A defrosting time of 5 minutes has initially been assumed, but it has been found that any assumption of the defrosting time between 2 to 10 minutes is mathematically valid to maintain energy balance in the system.
- The defrosting mass flow rate can be adjusted to control both the defrosting duration and the amount of energy directed to defrost the evaporator within the system.

Chapter 5 Exergy analysis of defrosting with latent heat storage

This chapter presents an exergy analysis of the multi-valve flexible heat pump system with integrated latent heat storage during both heating/charging and defrosting/discharging modes, with the aim of addressing research question 1. It is a follow up analysis of the previous Chapter 4, with a focus on identifying primary sources of losses when varying parameters such as the storage temperature, the compressor efficiency, and the storage-refrigerant temperature differential. R1234yf is the primary working fluid considered, with comparisons drawn to other refrigerants namely: R134a, R1234ze(E), propane, and R410a. Sections of this chapter are included in a published paper[263].

5.1 Introduction

In Chapter 4, an ideal model was used to calculate the performance of the flexible heat pump when defrosting is operated, and the results were compared with those of a conventional heat pump employing a reverse cycle method. The storage temperature was varied, and it was concluded that a storage temperature for maximising improvement could be found for R134a, R410a, R1234yf and R32. The analysis helped highlight the best theoretical improvement for this flexible heat pump and provided insights into its internal thermodynamic processes. While the energy performance of the heat pump during defrosting was studied, further investigation into the potential exergy losses within system is required.

To assess heat pump systems' efficiency, the standard metric often employed is energy efficiency known as the COP. Nonetheless, when aiming to determine opportunities for thermodynamic enhancement, exergy analysis is needed[234]. It is a useful tool to evaluate the variations in energy quality during a process and characterise the irreversibilities within the system while accounting for the environment's properties around it. The exergy refers to the maximum theoretical work extractable from a system relative to a reference state, named dead state, where exergy is zero. It can offer insights into the causes of irreversibility, or exergy destruction, such as heat transfer, fluid friction, chemical reactions etc. These irreversibilities result from the entropy generation through the process, transforming a reversible process into an irreversible one. As system performance deteriorates due to irreversibilities, exergy analysis emerges as a powerful tool for designing, optimising, and evaluating energy systems, with well-established principles[234,264–266]. It aims to maximise system performance while highlighting areas of exergy destruction, at component or system level. Hence, it has been widely applied to various fields such as cogeneration plant, energy storage, heat pumps, refrigeration etc.[225,231,267–271]. As highlighted in the literature review, the compressor and indoor heat exchanger are the components where most thermodynamic improvements within the cycle are focused, since optimising energy exchange in these components directly leads to an improvement in COP for heating applications. However, these components are not the only ones affecting the efficiency of the system. As shown in previous discussions, the evaporator, particularly due to frosting issues, can directly impact performance. The expansion valve, although it does not directly affect the COP, is also a significant source of energy losses.

In this chapter, Modes 1 and 3 of the flexible heat pump integrating a latent heat storage are characterised through an exergy analysis at component and system level. This analysis has been conducted on these modes to provide a comprehensive overview of the exergy losses in most operating modes of the flexible heat pump. In fact, Mode 3 (defrosting mode) is similar to Mode 2, except for the addition of the defrosting operation, and Mode 1 typically operates before any discharging process (unless Mode 4 is operated instead). Although Mode 4 is not directly studied in this analysis, the investigation of losses in the condensing process and the heat storage is applicable to it as well.

The chapter first outlines the methodology used and the assumptions made, followed by a presentation of the case study. The exergy destruction for both the entire system and its individual components is then calculated, along with their relative irreversibility under ideal and non-ideal conditions for both modes. The model from the previous chapter has been updated by considering both ideal and non-ideal operating conditions. A parametric investigation is carried out by varying key parameters including: the storage temperature, the compressor isentropic efficiency and the storage-refrigerant temperature differential. Finally, the potential for performance improvement is explored, and the key findings of the exergy analysis are presented for R1234yf and later for R134a, R1234ze(E), propane and R410a.

In summary, this comprehensive analysis aims to advance the understanding of thermodynamic losses in the operating modes of the multi-valve flexible heat pump, and to inform optimal design for minimising these losses.

5.2 Methodology

In Chapters 3 and 4, Modes 1 and 3, corresponding to the heating/charging and defrosting/discharging modes respectively, were introduced. In this chapter, an exergy analysis is conducted, on these two modes separately, rather than sequentially as done in Chapter 4. Mode 2 is not considered in this analysis. During the simulation, no specific duration is assigned to Mode 1 or Mode 3, as it is not required for the exergy analysis. However, for Mode 3, calculating the discharging rate of the latent heat storage as well as the defrosting rate in the evaporator is required, as indicated by Eqs. (3.76) and (3.74). Therefore, assumptions of the mass of ice m_{ice}, and the defrosting time $\Delta t_{defrost}$ are required to solve Eqs. (3.29), (3.31) and (3.34). The same values as in Chapter 4 are used here: m_{ice} is assumed to be 1.25 kg, as when Mode 1 was executed for one hour. Concerning $\Delta t_{defrost}$, it was demonstrated in Chapter 4 that any duration between 2 and 10 minutes is thermodynamically valid and does not impact the performance of the flexible heat pump. Therefore, the duration here has been fixed to 5 minutes, as in the previous chapter. These parameters are chosen solely to determine the mass flow rate in the frosted evaporator, the defrosting rate and the overall heat transfer in the heat storage during the defrosting operation; however, the process itself remains independent of time.

To proceed with the exergy analysis, assumptions regarding the components and external loops are required.

5.2.1 Assumptions adopted in this chapter

Differently than the previous chapter, exergy analysis requires accounting for the external loops in the heat pump system. Here, an air-source heat pump water heater is considered, with the external loops consisting of the water-loop in the condenser during Modes 1 and 3, and the air-loop in the evaporator during Mode 1, as shown in Fig. 3-8. Building on the model used in Chapter 4 for energy analysis, the exergy analysis investigates losses, requiring the consideration of non-ideal conditions. As a result, the following additional assumptions are made for the exergy analysis, along with those specified in Chapter 3:

1) <u>100% round-trip efficiency of the heat storage:</u> The heat storage is assumed to have negligible thermal losses between modes, meaning that heat losses to the environment are neglected. The same amount of energy charged in Mode 1 is available at the beginning of Mode 3 ($\%\Delta Q_{loss} = 0$).

2) Steady storage-refrigerant temperature differential: To simplify the analysis, the temperature difference between the heat storage and the refrigerant is assumed to be constant and equal during both the charging and discharging processes.

3) Fixed temperature difference in external loops: For this analysis, assumptions about the external loops are required to calculate the exergy destruction in both heat exchangers. However, since the impact of the external loops on heat pump operation is not the main focus of this study and was already discussed in the section *Pinch minimisation* in Chapter 2, a temperature difference of 10 K is assumed between the water inlet and outlet on the condenser side, and between the air inlet and outlet on the evaporator side. This is a common assumption in heat pump models[272,273].

5.2.2 Description of case study

R1234yf was initially chosen for this study, as it was the best performing refrigerant in the previous chapter. Later it is compared with R134a, R1234ze(E), propane and R410a. As in the previous chapter, the heating capacity is maintained at 3.6 kW, and data for the defrosting model is taken from the study by Reichl et al.[224]. The same condensing and evaporating temperatures are considered. Table 5-1 provides the relevant specifications for this case.

Table 5-1: Input parameters

Parameters	**Value**
Condensing temperature [°C]	35
Water inlet temperature [°C]	20
Water outlet temperature [°C]	30
Evaporating temperature [°C]	-8
Inlet air temperature [°C]	9.5
Outlet air temperature [°C]	-0.5
Heating capacity [kW]	3.6

The outlet water temperature is fixed to be 5 K below the condensing temperature:

$$T_{2w} = T_{cond} - 5 \tag{5.1}$$

This assumption is based on the supply water temperatures for low-temperature underfloor heating, with typical supply temperatures in the range of 30 – 35 °C as discussed in Chapter 4, and return temperatures in the range of 20 – 25 °C[259].

The inlet air temperature is set as the ambient temperature $T_{1a} = 9.5$ ℃, which corresponds to a lower average annual temperature observed in the UK over the past five years[274]. The dead state is defined as the ambient environment, with the reference temperature $T_0 =$ 9.5 ℃, as it is commonly done for heating application in heat pumps[236,275].

In this analysis, to account for heat exchange losses in the storage during the charging and discharging processes, the parameter ΔT_{HS} is introduced, representing the storage-refrigerant temperature differential, as follows

$$\Delta T_{HS} = \left|T_{ref} - T_{HS}\right| \tag{5.2}$$

When considering a latent heat storage, PCM is the primary storage type, which is also being considered here. In this case, T_{HS} is the storage/melting temperature of the PCM, and T_{ref} is the refrigerant temperature at the outlet of the PCM in Mode 1, and at the inlet of the PCM in Mode 3.

Considering assumption (2) of this chapter, ΔT_{HS} is constant and remains the same for both Modes 1 and 3. It should be noted that when $\Delta T_{HS} = 0$ K, in heating/charging mode, the refrigerant outlet temperature is equal to the PCM melting temperature. In defrosting/discharging mode, $\Delta T_{HS} = 0$ K implies that the refrigerant's evaporating temperature is equal to the PCM melting/solidification temperature.

Initially, the compressor isentropic efficiency is set at $\eta_{comp} = 75$ %, based on the findings of Olympios et al. for scroll compressors operating at pressure ratios below 5.5[276]. This efficiency is later varied in the study.

5.3 Results and discussion

Interpreting the exergy results helps identify and target sources of exergy waste within the system. In heat exchangers, exergy destruction is mainly due to heat transfer and circulating fluid friction. In the compressor, this is caused by deviations from ideal isentropic operation as well as mechanical and electrical losses. For the expansion valve, exergy losses occur due to the entropy generation caused by the refrigerant's temperature drop and fluid friction.

Here, the impact of storage temperature, compressor efficiency and storage-refrigerant temperature differential ΔT_{HS} on exergy losses at both the component and system levels are studied using the methodology outlined in the previous section. In this system, the integration of heat storage is evaluated in terms of its potential exergy losses and its impact on overall system performance. Moreover, as highlighted in Chapter 2, the literature demonstrates how crucial compressor efficiency is to the performance of the heat pump.

5.3.1 Impact of storage integration on exergy destruction

In this section, the effect of adding heat storage on both component-level and overall system exergy is examined. In particular, the influence of the storage-refrigerant temperature differential, as well as the storage temperature, is evaluated in terms of exergy destruction and relative irreversibilities.

The storage temperature selected corresponds to the value that provides maximum improvement, as determined by the methodology in Chapter 4. R1234yf is chosen as the refrigerant for this study. For R1234yf, at $T_{cond} = 35\ °C$ and $T_{evap} = -8\ °C$, this temperature was found to be $T_{max,\alpha}\ = 13.2\ °C$.

5.3.1.1 Impact of storage-refrigerant temperature differential

Fig. 5-1 shows the impact of storage-refrigerant temperature differential ΔT_{HS} on the relative irreversibilities of heat storage and evaporator in Modes 1 and 3. The storage temperature chosen here is associated with the maximum COP improvement for R1234yf, as stated previously.

The PCM tank relative irreversibility is increasing from 0 to 18 % in defrosting mode with the increase of ΔT_{HS} from 0 to 5 K, resulting in the PCM accounting for almost 1/5 of the overall system exergy destruction when $\Delta T_{HS} = 5$ K. This is because, as ΔT_{HS} increases, here defined as the temperature difference between the refrigerant's evaporating temperature and the PCM melting temperature, the mismatch between the two temperatures increases, leading to increased exergy destruction. In fact, the exergy destruction is multiplied by 10 and increases from 0.007 kW to 0.07 kW as ΔT_{HS} varies from 0.5 to 5 K. Consequently, when ΔT_{HS} is superior to 0 K, the process is irreversible.

The impact of ΔT_{HS} on the heat storage share of total exergy loss is higher in defrosting mode than it is in heating/charging mode. This is because an increase in ΔT_{HS} in Mode 3 results in a decrease in both the refrigerant temperature and pressure, as well as an increased temperature differential that remains throughout the heat transfer process. The refrigerant evaporating temperature remains constant and only latent heat is exchanged, unlike in the charging mode. Moreover, during the defrosting operation the mass flow rate through the storage and the expansion valve is higher than in the rest of the system, because of the addition of the defrosting mass flow rate $\dot{m}_{defrost}$. This results in increased heat transfer, which has a greater impact on the exergy flow.

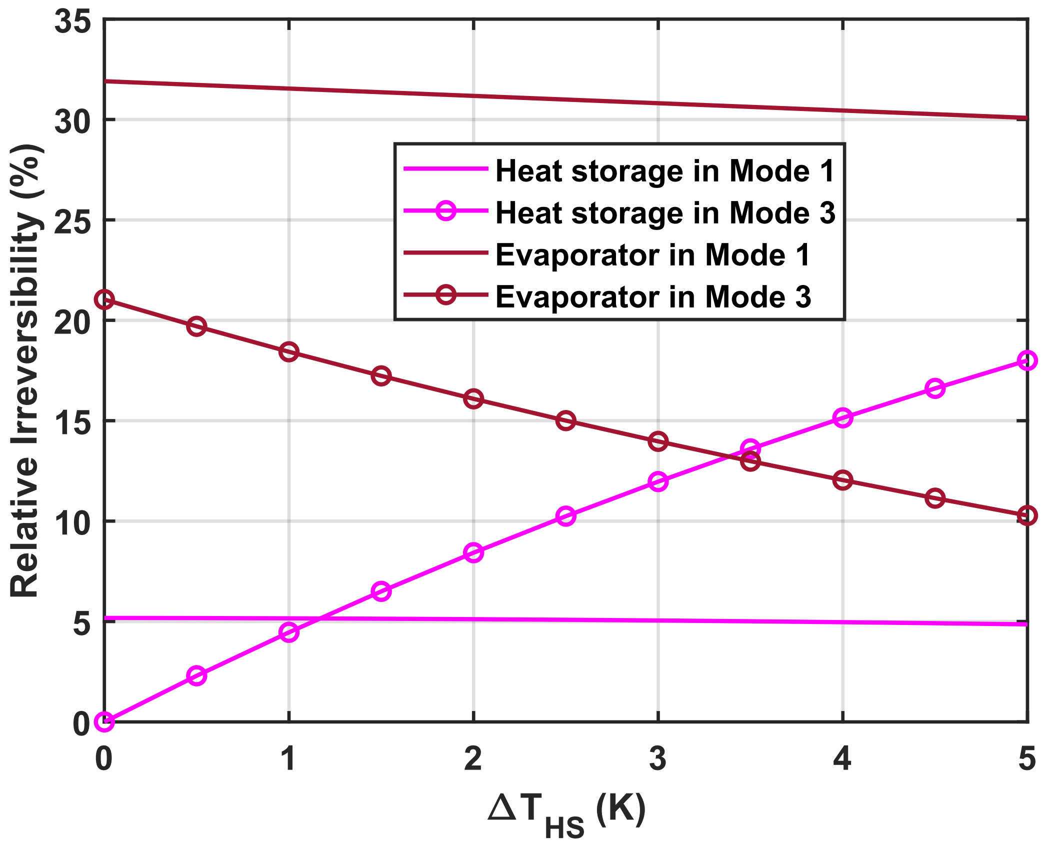

Fig. 5-1: Relative irreversibilities of heat storage and evaporator when storage-refrigerant temperature differential varies in Modes 1 and 3

As the heat storage relative irreversibility increases, there is a corresponding decrease in the evaporator's exergy loss ratio during defrosting mode, dropping significantly from around 21 % to 10.3 %, a reduction of 51 %. This is firstly due to the significant rise in the heat storage relative irreversibility, which in turn lessens the relative impact of the evaporator's defrosting process on the system's total exergy destruction. Secondly, this is also explained by the decrease in the evaporator's exergy destruction itself. Specifically, when ΔT_{HS} increases in defrosting mode, the refrigerant's evaporating temperature decreases, thereby reducing the temperature difference between the frosted evaporator and the refrigerant entering it, which results in lower exergy destruction.

In Mode 1, the heat storage share of total exergy destruction slightly decreases from 5.2 % to 4.9 %. The decrease is explained by the lower temperature variation inside the storage tank, reducing the heat transfer and the heating recovery process. As a result, the evaporator's relative irreversibility decreases as well because the refrigerant at the inlet of the evaporator is less subcooled, resulting in less heat transfer inside the evaporator. The overall impact of the increase of ΔT_{HS} is slightly higher for the evaporator with its exergy loss fraction decreasing from 32 % to 30 %. The difference in the impact of these two components on the total system exergy destruction in Mode 1 is significant, with the evaporator contributing 84 % more than the heat storage. This is primarily due to the considerably greater heat transfer occurring within the evaporator compared to the heat storage.

Since the PCM melting temperature is fixed to ensure maximum energy performance, minimising the temperature difference between the storage and the refrigerant's evaporating temperature during defrosting is essential to reduce exergy losses in the storage tank. This conclusion is also valid from an energy perspective, as a lower ΔT_{HS} results in higher refrigerant evaporating temperature during defrosting, which reduces power consumption and increases energy efficiency. Additionally, while a higher ΔT_{HS} in Mode 1 results in slightly lower exergy destruction, it negatively affects heat transfer in the storage tank in charging, which in turn limits the heat recovery process and reduces the overall efficiency of the flexible heat pump.

Therefore, it can be concluded that achieving the lowest possible ΔT_{HS} in both charging and defrosting modes is essential for maximum performance. This finding is supported by Rahimi et al.[277], who observed that the largest temperature differences occurred at the heat storage inlets during both charging and discharging, resulting in the highest entropy generation. In this study, the temperature difference at the inlet during defrosting corresponds to the ΔT_{HS} analysed, which further supports the need to reduce this value. This temperature difference can be controlled through the expansion valve and compressor setting and is, therefore, adjustable by the heat pump manufacturer. However, during charging, this temperature difference is determined by the condenser outlet temperature, and subcooling inside the condenser could be applied to reduce it. However, such subcooling would affect heat recovery in the heat storage. Moreover, as shown in the results, the impact of exergy destruction in the heat storage during charging on the overall system is relatively low and does not require critical adjustment of this value.

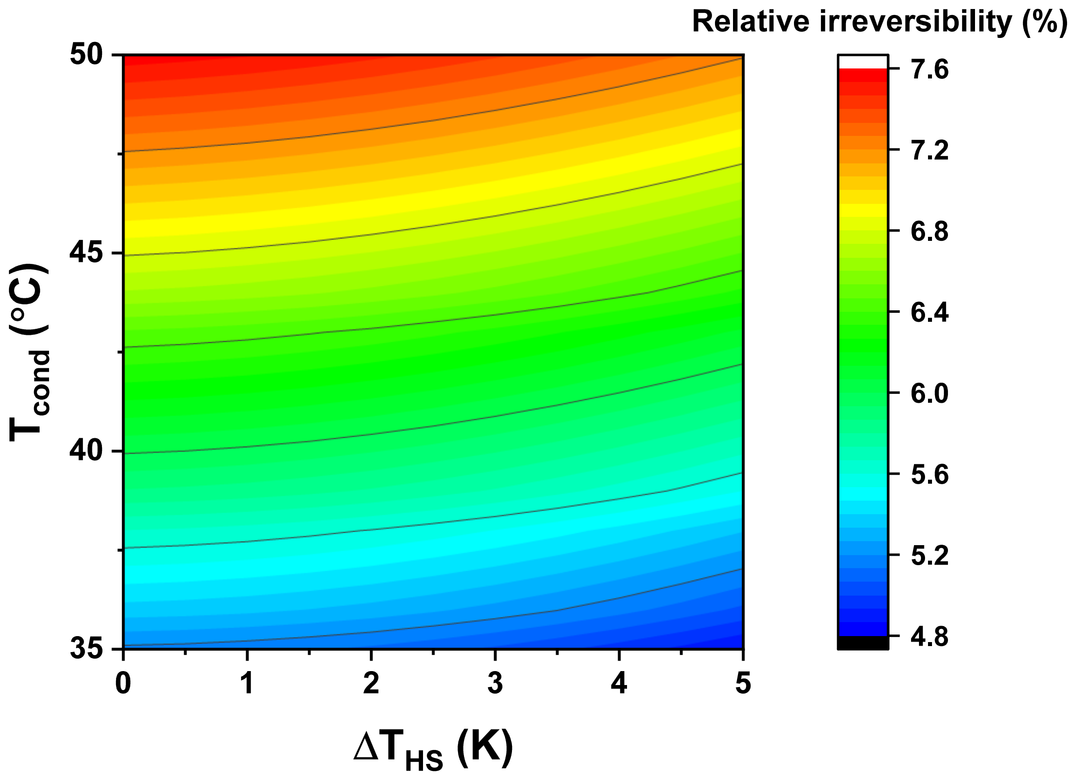

Fig. 5-2: Relative irreversibility of the heat storage depending on storage-refrigerant temperature differential and condensing temperature in Mode 1

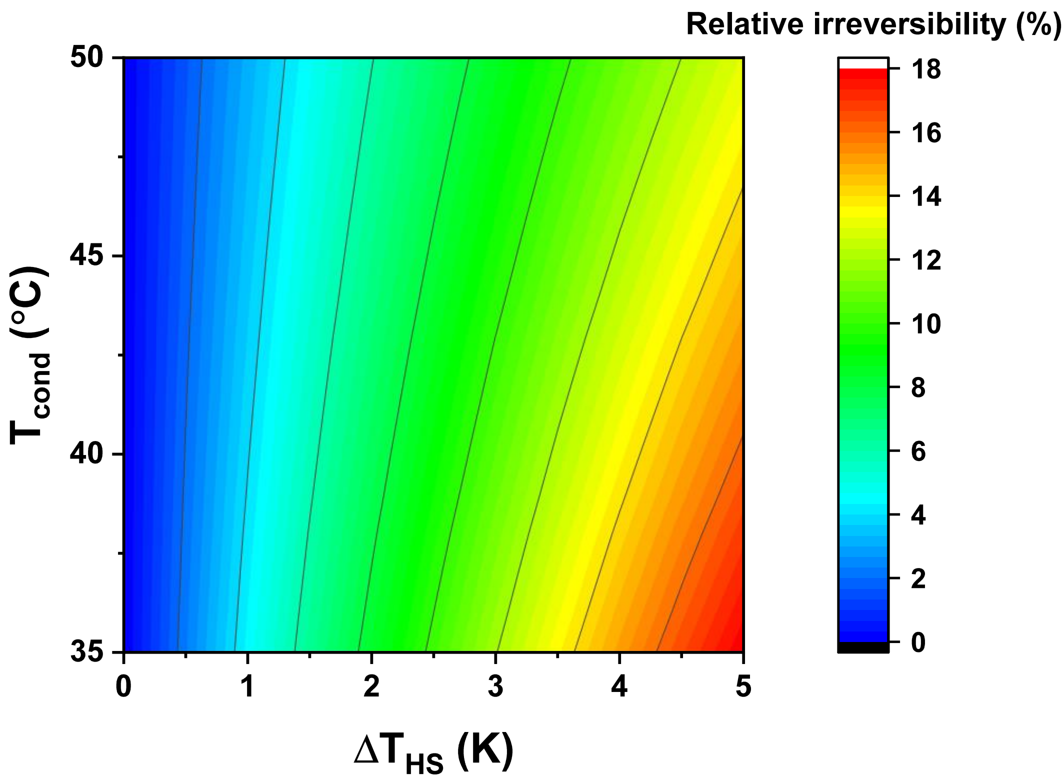

Fig. 5-3: Relative irreversibility of the heat storage depending on storage-refrigerant temperature differential and condensing temperature in Mode 3

Fig. 5-2 and Fig. 5-3 present the relative irreversibility of the heat storage at its top performing storage temperature for different condensing temperatures and ΔT_{HS} values, in both heating/charging and defrosting/discharging modes.

In Fig. 5-2, the results for Mode 1 are shown. In this mode, the condensing temperature is the inlet temperature to the storage, as previously highlighted. As shown in Chapter 4, the maximum improvement storage temperature for the flexible heat pump, for defrosting operation, is slightly below the midpoint between the condensing and evaporating temperatures. In Mode 1, higher condensing temperatures result in increased relative irreversibility. This occurs because, although the top performing storage temperature also rises, the temperature differential at the inlet between the refrigerant and the heat storage tank increases significantly. For example, at a condensing temperature of 35 °C and $T_{max,\alpha} = 13.2$ °C, the temperature differential at the inlet is 21.8 K. At a condensing temperature of 50 °C and $T_{max,\alpha} = 21.9$ °C, this differential is 28.1 K. This leads to a higher charging rate, increased entropy generation, and greater losses due to heat transfer. However, as shown in Fig. 5-2, this increase remains limited, and the impact of heat storage on overall system exergy destruction during charging is still relatively low, remaining below 8 % even at the highest levels of irreversibility. At the same condensing temperature, the relative irreversibility decreases as ΔT_{HS} increases, following the same trend across all condensing temperatures. For instance, at 50 °C, the relative irreversibility decreases from 7.6 % at $\Delta T_{HS} = 0$ K to 7.2 % at $\Delta T_{HS} = 5$ K, while at 35 °C, it drops from 5.2 % to 4.9 %. Although the decrease in relative irreversibility, and thus exergy destruction, suggests improved exergy performance, the increase in ΔT_{HS} also indicates a reduced charging rate, as noted previously. Given the small reductions in share of exergy destruction with increasing ΔT_{HS}, it is recommended to minimise this value to ensure maximum heat recovery and energy efficiency across all condensing temperatures.

In Fig. 5-3, the trend is different for Mode 3. Here, the main factor affecting exergy destruction is not the condensing temperature but ΔT_{HS}, as observed earlier in Fig. 5-1. The increase in ΔT_{HS} plays a more significant role in raising the relative irreversibility because variations in this parameter affect both the refrigerant temperature and pressure. Furthermore, this temperature differential remains constant throughout the latent heat exchange process. Moreover, heat transfer in the storage tank during discharging/defrosting is significantly higher than during charging. When $\Delta T_{HS} = 0$ K, the evaporating process inside the heat storage is reversible, resulting in a relative irreversibility of 0 % for all condensing temperatures. As ΔT_{HS} increases, the share of exergy loss rises, with a slightly higher rate of increase observed at lower condensing temperatures. For instance, at $\Delta T_{HS} = 5$ K, the relative irreversibility reaches 13 % for $T_{cond} = 50$ °C and 18 % for $T_{cond} = 35$ °C.

5.3.1.2 Impact of varying storage temperature

The impact of the selected storage temperature on exergy destruction for each system component, during both Modes 1 and 3, is illustrated in Fig. 5-4 and Fig. 5-5.

Notably, the expansion valve and the heat storage show the lowest irreversibility in the system for both modes, although the storage temperature affects these components differently. In heating/charging mode, exergy destruction in the expansion valve increases with storage temperature while it decreases in the heat storage. During charging, the maximum irreversibility for the expansion valve is 0.11 kW at $T_{HS} = 30$ °C. As storage temperature rises, the inlet temperature of the expansion valve also increases. Given the assumption of an isenthalpic throttling process, with a constant evaporating temperature (the outlet temperature of the valve), exergy destruction increases due to the greater temperature gradient across the valve, resulting in higher throttling losses. Therefore, greater subcooling of the refrigerant in the storage leads to a reduction in throttling losses.

Inversely, exergy destruction in the heat storage decreases as the storage temperature rises. During charging, exergy destruction in the heat storage is mainly driven by the temperature difference between the refrigerant and the latent heat storage at its inlet. As a result, a smaller temperature gradient in the tank at higher storage temperatures reduces exergy destruction. For example, at $T_{HS} = 30$ °C with $\Delta T_{HS} = 2.5$ K, the temperature gradient in the tank is only of 2.5 K, resulting in minimal heat transfer, low heat recovery, and exergy destruction of just 0.001 kW.

During Mode 1, in Fig. 5-4, the compressor shows the highest exergy destruction across all storage temperatures, although its value remains constant because the compressor efficiency ($\eta_{comp} = 75$ %) and power are fixed. Therefore, storage temperature does not affect exergy flow through the compressor. The evaporator has the second-highest exergy destruction for all tested temperatures, peaking at 0.17 kW at $T_{HS} = 10$ °C. It then decreases as storage temperature rises because less subcooling of the refrigerant reduces heat transfer in the evaporator. The condenser exergy destruction remains unaffected by changes in storage temperature, with a constant value of 0.11 kW, as the heating capacity is kept constant throughout the process.

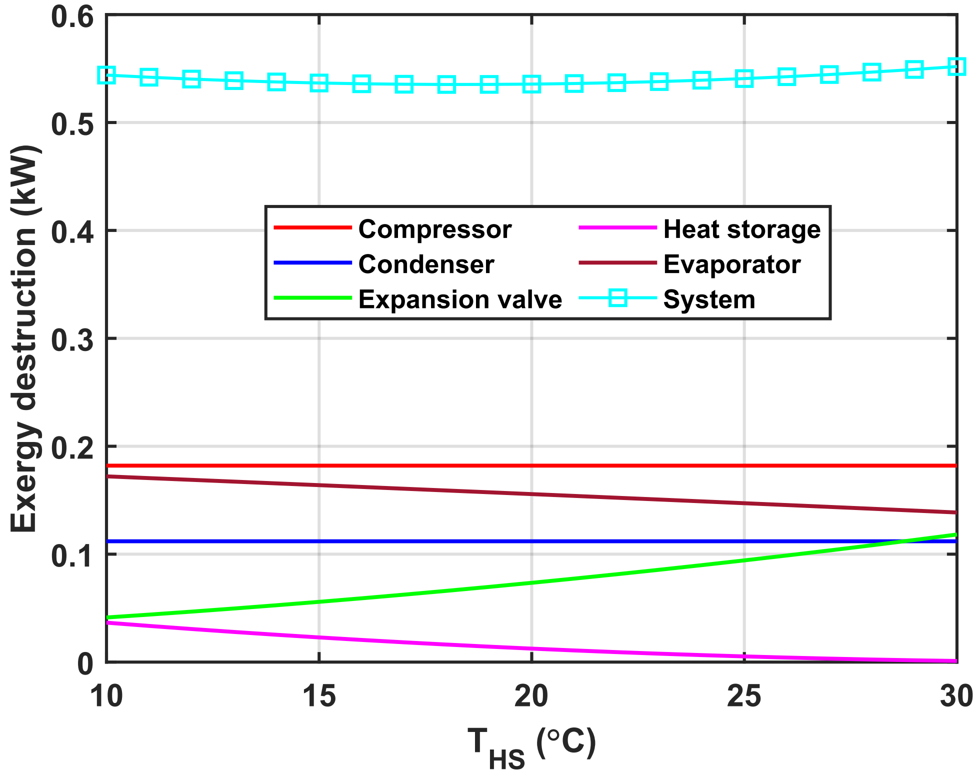

Fig. 5-4: Exergy destruction when storage temperature varies in Mode 1 ($\Delta T_{HS} = 2.5$ K)

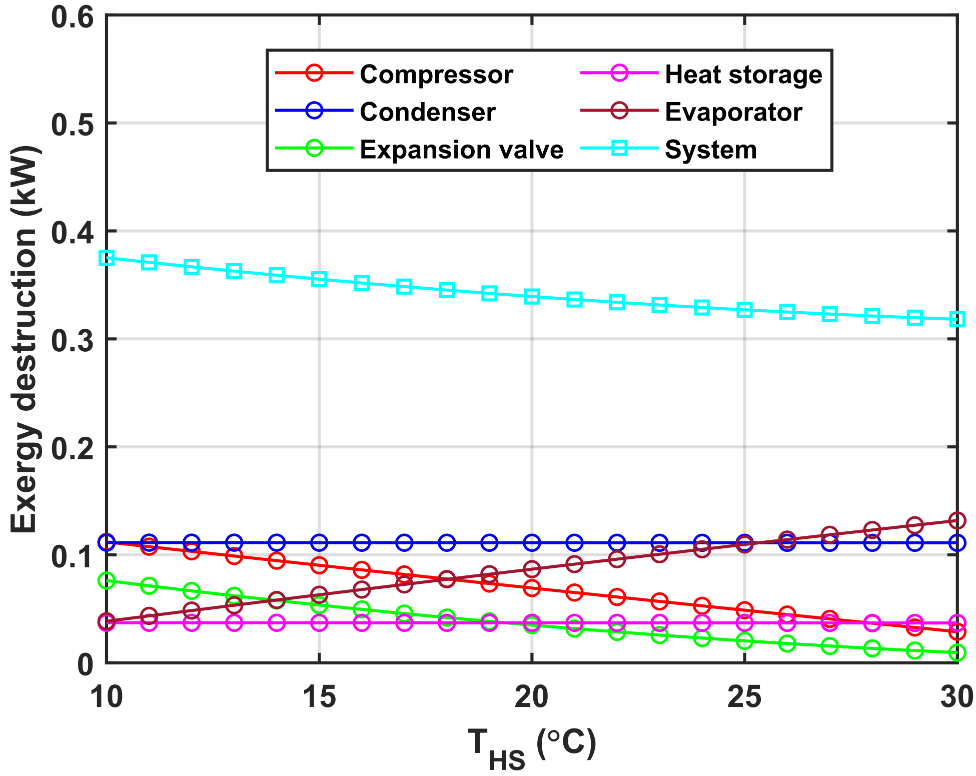

Fig. 5-5: Exergy destruction when storage temperature varies in Mode 3 ($\Delta T_{HS} = 2.5$ K)

In Fig. 5-5, during Mode 3, the evaporator exergy destruction increases linearly with storage temperature, rising from the lowest to the highest among all components, from 0.038 kW to 0.13 kW, representing an increase by a factor of 3.5. As explained in Fig. 5-1, this is because higher storage temperatures raise the refrigerant's evaporating temperatures, increasing the temperature gradient inside the frosted evaporator (held at $T_{ice} = 0$ °C) leading to higher exergy destruction. The condenser's exergy destruction remains similar to that in charging mode, at approximately 0.11 kW, due to constant heating capacity, although negligible variations occur with changes in storage temperature because of slight reductions in the discharge temperature.

During defrosting, the expansion valve shows a reverse trend compared to that in charging mode, with its exergy destruction decreasing as storage temperature rises. This occurs because the temperature difference across the valve decreases as the PCM melting temperature (and thus the refrigerant's evaporating temperature) increases, reducing throttling losses. Exergy destruction in the heat storage remains nearly constant at around 0.037 kW. As it was seen in Fig. 5-1 and Fig. 5-3, the primary cause of exergy destruction in the storage tank during defrosting is the storage-refrigerant temperature differential ΔT_{HS}. Since this parameter is fixed, the exergy destruction of the storage remains constant. It is also seen that, between the storage temperature $T_{HS} = 10$ °C and $T_{HS} = 20$ °C, the storage exergy destruction is the lowest compared to all other components, which coincides with the maximum improvement storage temperature range found in Chapter 4. The compressor exergy destruction in defrosting mode is significantly influenced by the storage temperature, showing a linear decrease as storage temperature rises. This is because higher storage temperatures increase the refrigerant's evaporating temperature, lower compression ratio and, thus, reduce entropy generation. The compressor exergy destruction is decreasing from 0.11 kW at $T_{HS} = 10$ °C to 0.03 kW at $T_{HS} = 30$ °C, a 73 % decrease.

An analysis of the system exergy destruction shows that, during Mode 1, the storage temperature for the lowest exergy destruction is $T_{min,ex} = 18$ °C, corresponding to an exergy destruction of 0.53 kW. This temperature is somewhat higher than $T_{max,\alpha} = 13.2$ °C found for achieving the best energy efficiency in Chapter 4. In Mode 3, the lowest system exergy destruction occurs at $T_{min,ex} = 30$ °C, with a value of 0.32 kW. This is because, during charging, the system exergy destruction is mainly influenced by losses in the evaporator, expansion valve, and storage tank, and a balance needs to be found between them. During defrosting mode, however, the reduction in system losses is primarily driven by the decrease in exergy destruction from the compressor and expansion valve, which are linked to the increase in evaporating temperature as the storage temperature rises. Additionally, during defrosting, system exergy destruction is between 30 % to 40 % lower than in charging, depending on the selected storage temperature. This reduction is due to the lower compression ratio required during defrosting, as previously stated. As a result, exergy destruction decreases in both the compressor and the overall system

Consequently, when the storage temperature varies, system losses are primarily influenced by the evaporator, expansion valve, and heat storage during heating/charging mode, and by the compressor and expansion valve during defrosting/discharging mode. Although storage temperatures minimising exergy destruction are found in both modes, they differ greatly from each other, and based on the analysis from Chapter 4, cannot guarantee the highest energy efficiency.

5.3.2 Influence of compressor efficiency

Fig. 5-6 and Fig. 5-7 present the impact of the compressor isentropic efficiency on exergy destruction, for individual components and the overall system in both Modes 1 and 3, assuming a medium ΔT_{HS} of 2.5 K for the heat storage.

In Fig. 5-6, during charging, the compressor isentropic efficiency, directly linked to compressor exergy destruction, has a significant influence on the overall system exergy destruction. The compressor exergy destruction decreases from 0.34 kW to 0 kW with the increase of compressor efficiency from 60 % to 100 %. Consequently, the system exergy destruction is reduced by almost half, implying a strong impact of the compressor isentropic efficiency. The condenser exergy destruction also decreases slightly with improved compressor efficiency due to the reduction in discharge temperature. Meanwhile, other components experience a slight increase in exergy destruction as higher compressor efficiency leads to increased mass flow rate and heat transfer in those components. However, these small increases do not change the overall downward trend in system exergy destruction. Therefore, during Mode 1, the compressor isentropic efficiency plays a key role in lowering the overall system exergy destruction.

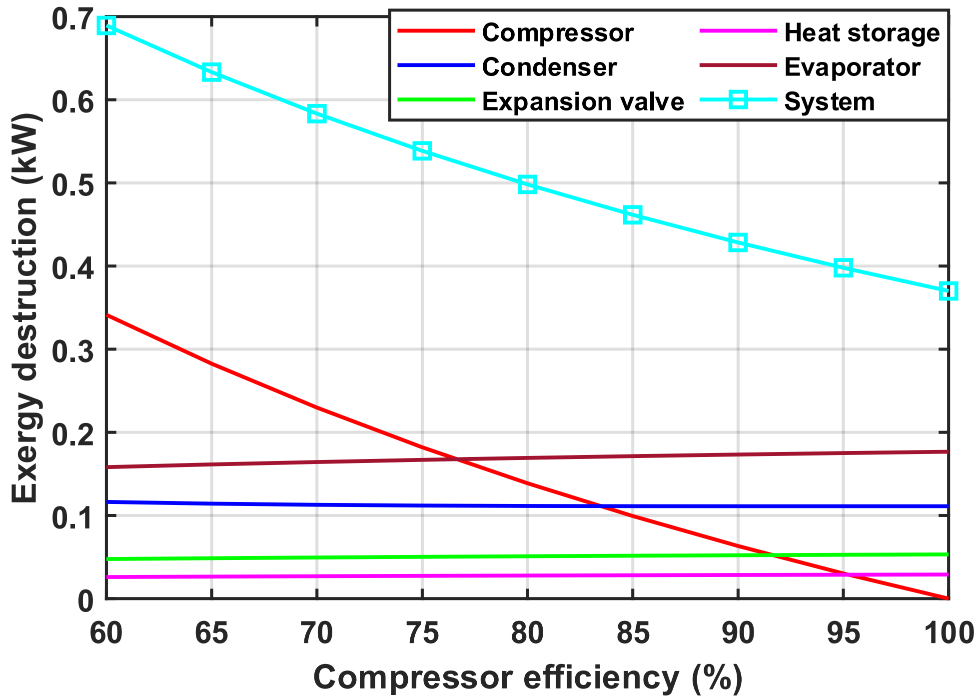

Fig. 5-6: Exergy destruction when compressor efficiency varies in Mode 1 ($\Delta T_{HS} = 2.5$ K)

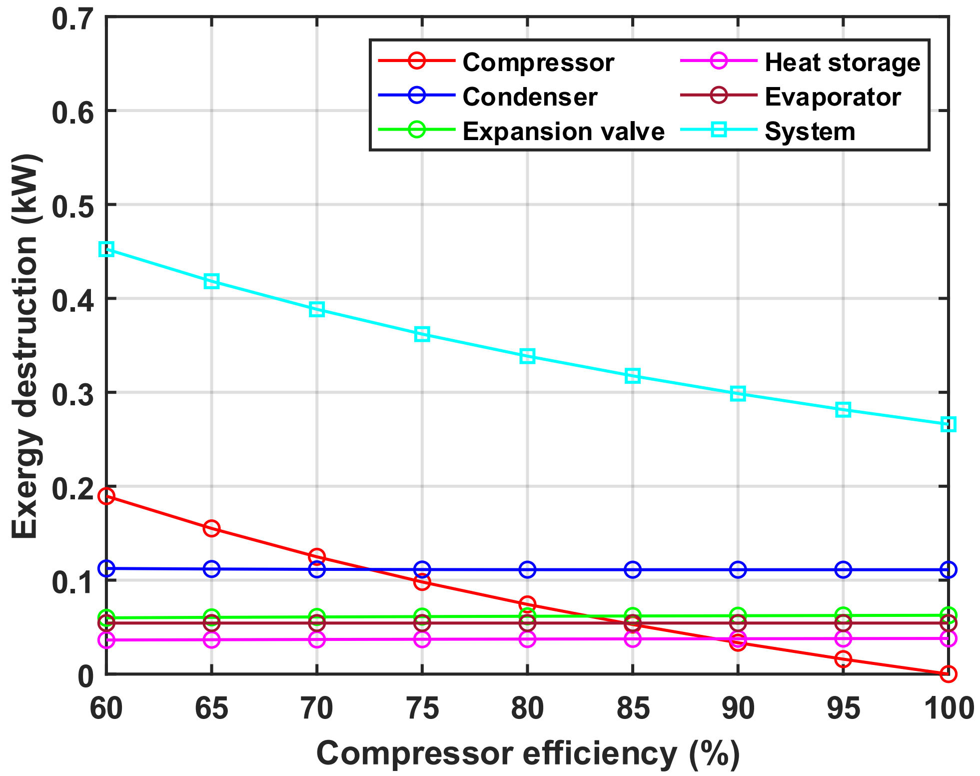

Fig. 5-7: Exergy destruction when compressor efficiency varies in Mode 3 ($\Delta T_{HS} = 2.5$ K)

In Fig. 5-7, during defrosting, the compressor and system exergy destruction follow a similar trend as during charging, with system exergy destruction also decreasing by almost half. The other components also behave similarly than in Mode 1. Since $\Delta T_{HS} = 2.5$ K is fixed for all tested compressor efficiencies, the exergy destruction in the storage tank is lower than that of the compressor, until the compressor efficiency reaches 90 %, at which point the compressor's exergy destruction becomes lower than that of the storage. Additionally, in Mode 3, system exergy destruction is about 30 % lower than in Mode 1, regardless of compressor efficiency. This is because, as explained in Chapter 4, the compression ratio is reduced during defrosting due to the increase in the refrigerant's evaporating temperature enabled by the heat storage. This in turns lowers exergy destruction in both the compressor and the system.

In conclusion, Fig. 5-6 and Fig. 5-7 illustrate that the compression ratio and isentropic efficiency have a major impact on the system's overall losses. This highlights the importance of careful equipment selection, as low-quality compressors can significantly reduce the overall system performance.

5.3.3 Combined effect of compressor efficiency and storage-refrigerant temperature differential

This section examines the combined impact of the storage-refrigerant temperature differential and compressor isentropic efficiency on exergy destruction for individual components and the whole system across different cases. The storage temperature is set to the value for maximum COP improvement in this configuration, which is $T_{max,\alpha} = 13.2$ °C.

Fig. 5-8 to Fig. 5-13 show the exergy destruction for each component and the entire system across six different scenarios.

Under ideal conditions, in Fig. 5-8 ($\Delta T_{HS} = 0$ K and $\eta_{comp} = 100$ %), which serves as a benchmark, the system exergy destruction is at its lowest: 0.37 kW in Mode 1 and 0.23 kW in Mode 3. As previously noted, exergy destruction during defrosting/discharging is over 30 % lower than in heating/charging mode due to reduced compression ratio. It is seen that, in this ideal case, the evaporator has the highest exergy destruction during charging, while the condenser has the highest exergy destruction during defrosting. In this scenario, most irreversibilities are driven by the temperature differentials between the two heat-exchanging fluids.

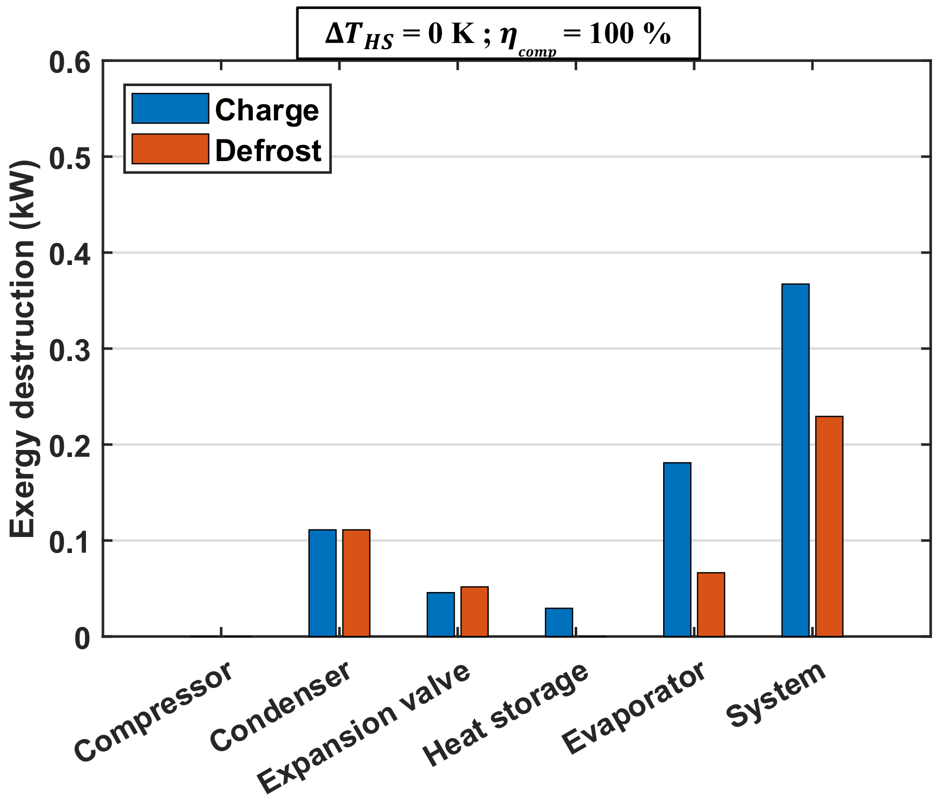

Fig. 5-8: Exergy destruction per component and system in Modes 1 and 3, at $\Delta T_{HS} = 0$ K, $\eta_{comp} = 100$ %

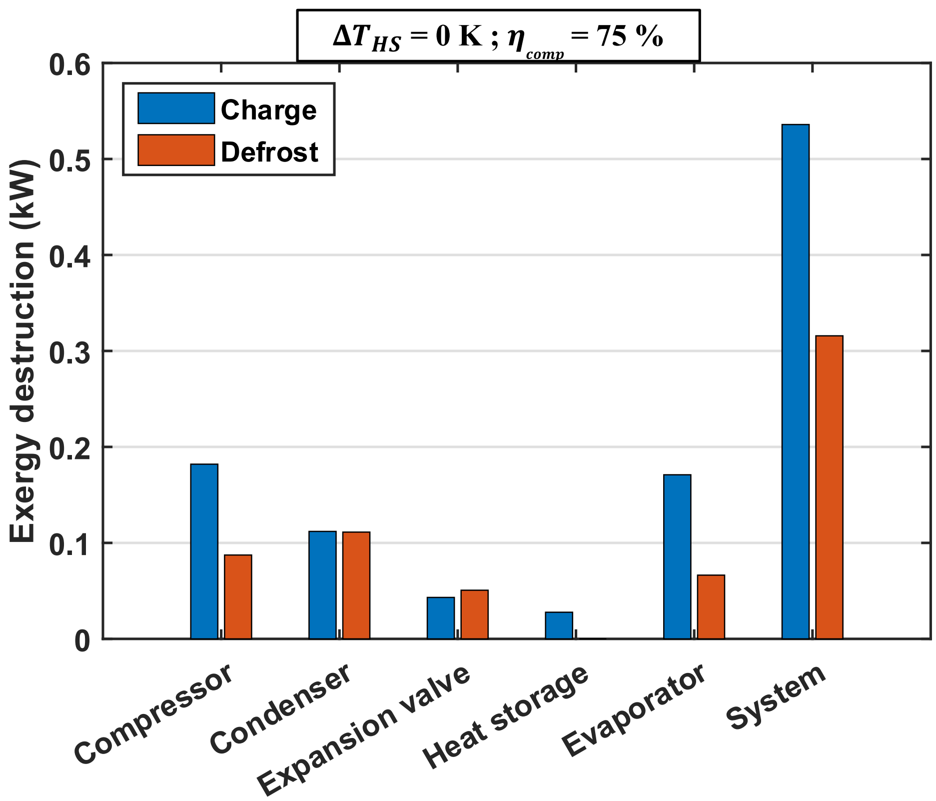

Fig. 5-9: Exergy destruction per component and system in both modes, at $\Delta T_{HS} = 0$ K, $\eta_{comp} = 75$ %

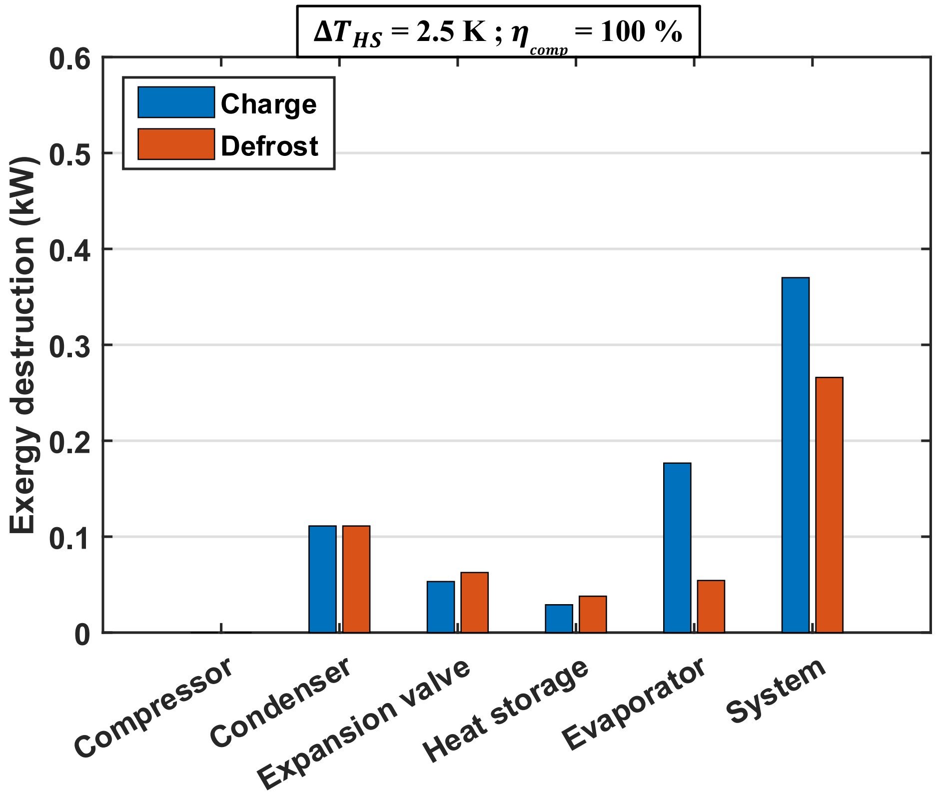

Fig. 5-10: Exergy destruction per component and system in both modes, at $\Delta T_{HS} =$ 2.5 K, $\eta_{comp} = 100$ %

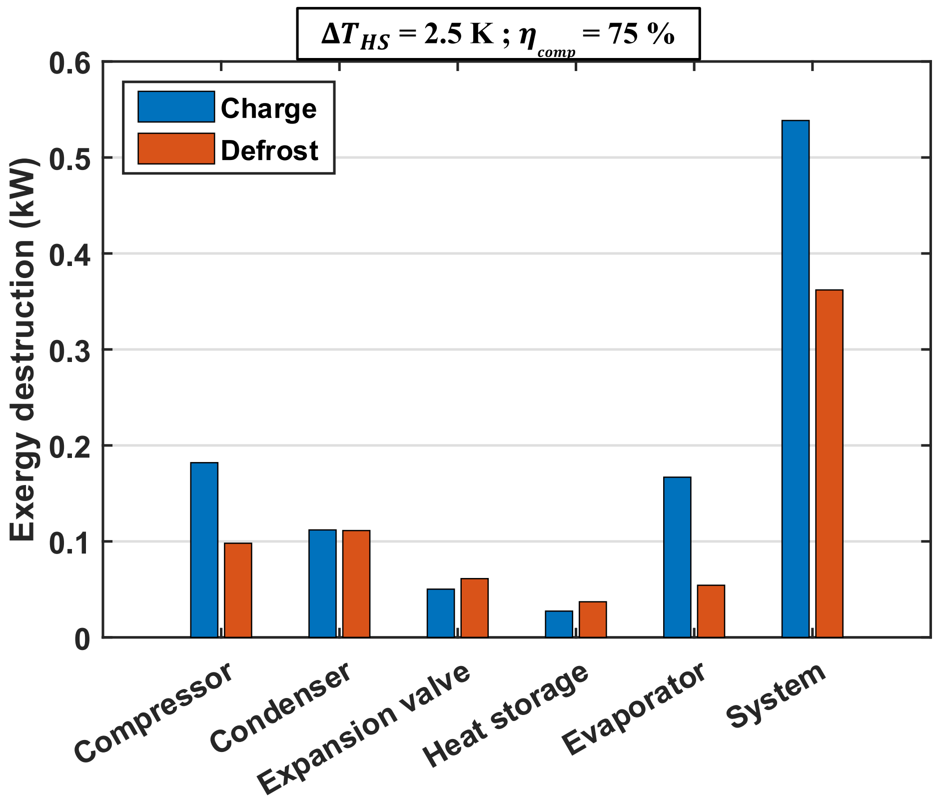

Fig. 5-11: Exergy destruction per component and system in both modes, at $\Delta T_{HS} =$ 2.5 K, $\eta_{comp} = 75$ %

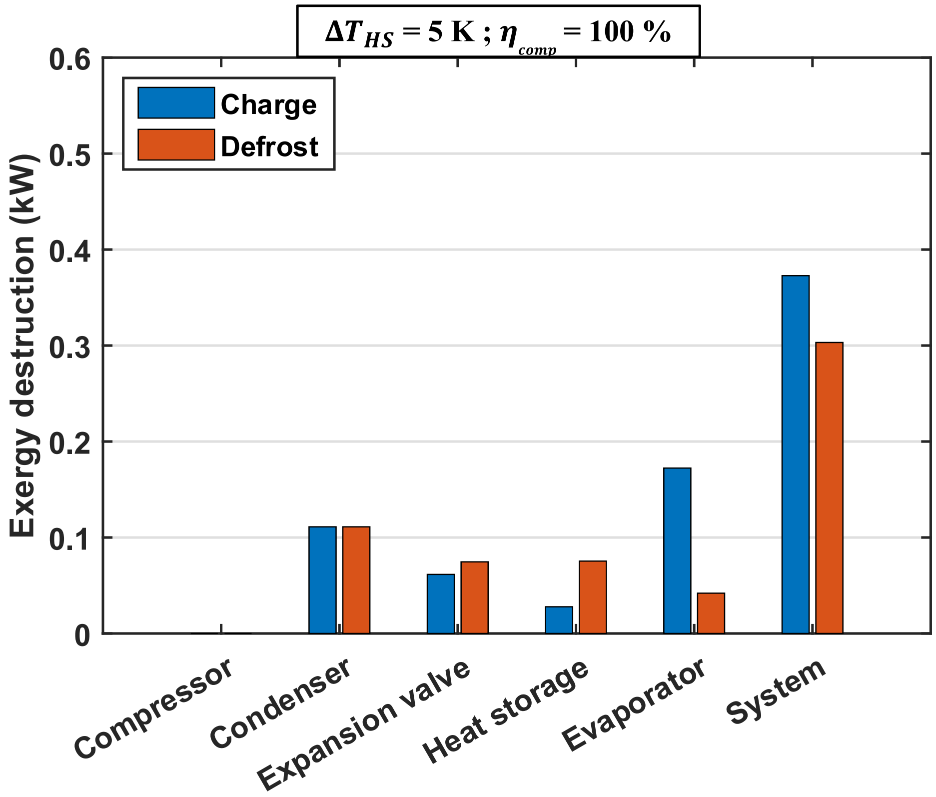

Fig. 5-12: Exergy destruction per component and system in both modes, at $\Delta T_{HS} = 5$ K, $\eta_{comp} = 100$ %

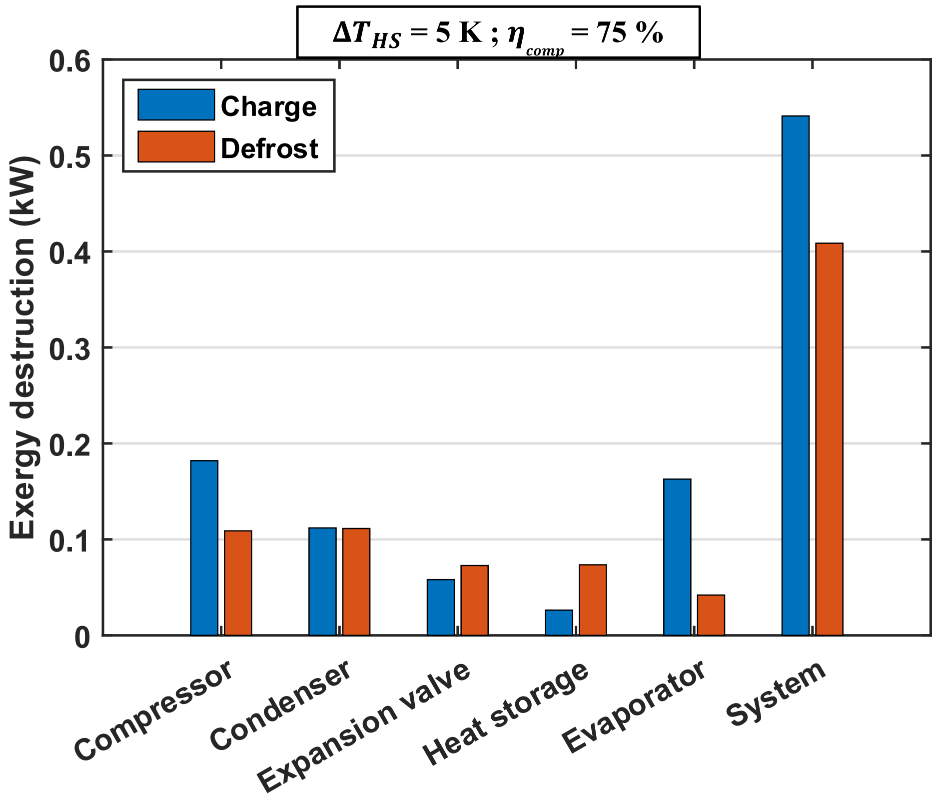

Fig. 5-13: Exergy destruction per component and system in both modes, at $\Delta T_{HS} = 5$ K, $\eta_{comp} = 75$ %

In Fig. 5-9, when $\Delta T_{HS} = 0$ K and $\eta_{comp} = 75$ %, the exergy destruction due to the compressor decreased efficiency, significantly increases the overall system exergy destruction, reaching 0.53 kW during Mode 1 and 0.31 kW during Mode 3, a 43 % and 35 % increase, respectively. Although exergy destruction in other components decreases slightly due to reduced mass flow rate, these changes do not significantly impact the overall system trend.

Fig. 5-10 shows the effect of increasing ΔT_{HS} from 0 to 2.5 K, primarily influencing the heat storage exergy destruction during Mode 3 which rises from 0 to 0.038 kW when $\eta_{comp} = 100$ %. The system exergy destruction during Mode 1 remains relatively unaffected, staying around 0.37 kW. However, in defrosting mode, the system exergy destruction increases to 0.27 kW. It is clear that even a small temperature difference between the refrigerant and the PCM melting temperature affects the system exergy destruction in Mode 3, though this effect is less significant than that of compressor isentropic efficiency.

In Fig. 5-11, both the compressor efficiency is reduced to 75 % and ΔT_{HS} is increased to 2.5 K. No component is in an ideal state, resulting in higher system exergy destruction: 0.54 kW during Mode 1 and 0.36 kW during Mode 3. The exergy destruction during charging is slightly higher than in Fig. 5-9 due to the increased contribution of the expansion valve. However, this increase is only 0.01 kW, underscoring the greater influence of compressor isentropic efficiency compared to ΔT_{HS} during Mode 1. In Mode 3, the combined effect of both ΔT_{HS} and the compressor isentropic efficiency is visible, yet the latter is more prominent on the system, with only a 16 % increase in the system exergy destruction, as compared to the case illustrated in Fig. 5-9, with the addition of the irreversible discharging process.

This conclusion is corroborated by Fig. 5-12 and Fig. 5-13, where ΔT_{HS} is increased to 5 K in both cases. In Fig. 5-12, the compression process is isentropic, while in Fig. 5-13 the compressor efficiency is 75 %. In Fig. 5-12, during Mode 1, the increase in ΔT_{HS} has no significant impact on system exergy destruction, which remains the same as in the ideal case. However, during Mode 3, exergy destruction rises to 0.3 kW, a 30% increase from the ideal case. In Fig. 5-13, the system exergy destruction during both modes are 0.54 kW and 0.41 kW, respectively. During charging, exergy destruction is similar to that in Fig. 5-11, emphasising the dominant role of the compressor. During defrosting, exergy destruction is the highest of all cases, representing a 32 % increase from Fig. 5-9, highlighting the need to minimise ΔT_{HS} in this operating mode.

In conclusion, the drop in compressor isentropic efficiency has a more substantial impact on the overall system exergy destruction, particularly during Mode 1. While ΔT_{HS} has a stronger impact on the system during Mode 3, especially at higher values, its influence remains less significant than that of the compressor isentropic efficiency. This highlights the importance of selecting high-quality components, as low-efficiency compressors can greatly reduce system performance. This result is consistent with findings in the literature for conventional heat pumps, such as those reported by Yataganbaba et al.[229]. Therefore, the addition of heat storage as an extra component does not outweigh the exergy losses caused by the compressor when the refrigerant-storage temperature differential is kept within 5 K.

5.3.4 Exergy analysis at 2.5 K storage-refrigerant temperature differential and 75 % compressor efficiency

Following the analysis of the impact of storage temperature, compressor efficiency, and storage-refrigerant temperature differential individually, the effect of non-ideal conditions is evaluated on relative irreversibilities, system exergy destruction and efficiency, for various refrigerants. Based on the previous findings, the parameters for the chosen case study are the storage temperature for maximum improvement $T_{max,\alpha}$, compressor efficiency of 75 % and storage-refrigerant temperature differential of $\Delta T_{HS} = 2.5$ K.

5.3.4.1 Relative irreversibility analysis in both modes for R1234yf

Fig. 5-14 and Fig. 5-15 present the relative irreversibility per component at $\Delta T_{HS} = 2.5$ K and $\eta_{comp} = 75$ % in Modes 1 and 3.

In both modes, the heat storage has the lowest relative irreversibility among all components, with 5 % during heating/charging and 10.2 % during defrosting/discharging. This is because, during charging, the exergy destruction in the tank is solely influenced by the finite temperature difference between the refrigerant and the storage temperature. In defrosting mode, while latent heat exchange process and increased mass flow rate also contribute, they do not outweigh the heat transfer losses in the condenser, the throttling losses through the expansion valve, or the exergy destruction in the frosted evaporator. As shown in Fig. 5-4 and Fig. 5-5, for a storage temperature of $T_{max,\alpha} = 13.2$ °C and a $\Delta T_{HS} = 2.5$ K, the exergy destruction in the heat storage remains the lowest of all components.

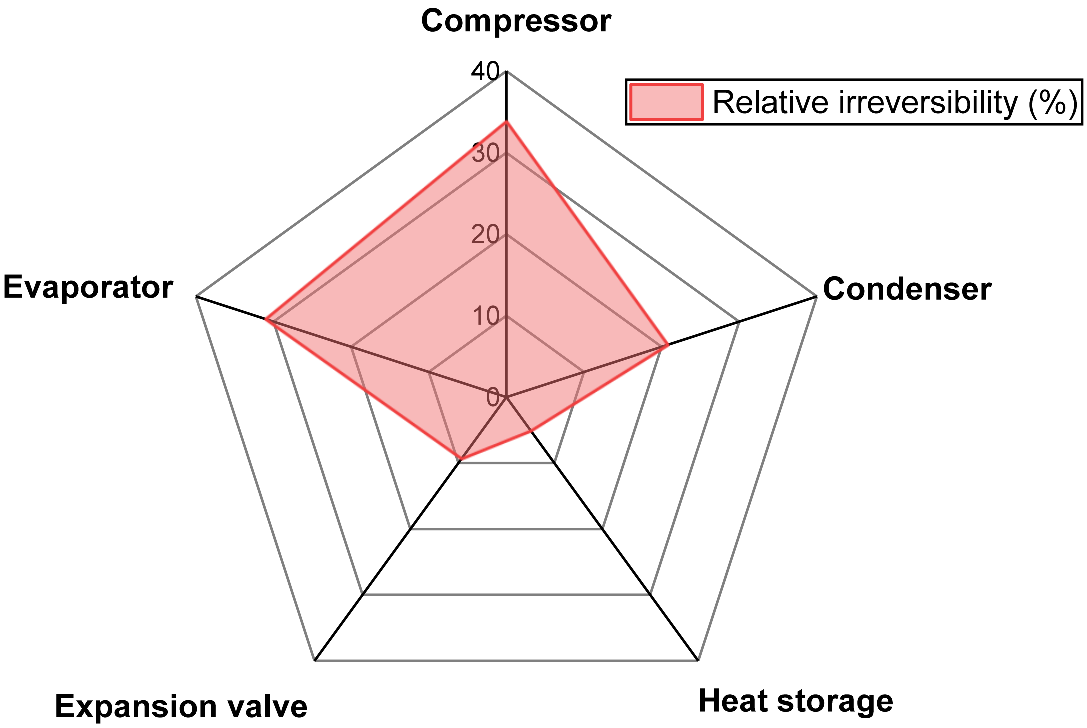

Fig. 5-14: Relative irreversibility per component in Mode 1

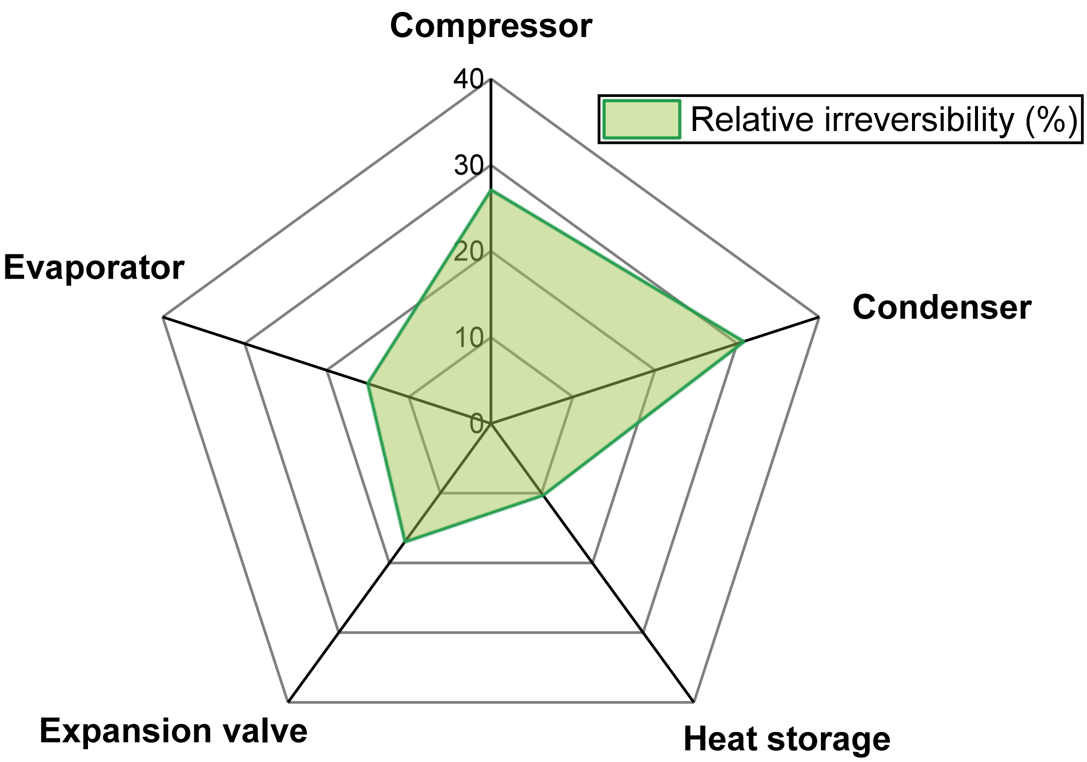

Fig. 5-15: Relative irreversibility per component in Mode 3

During Mode 1, as seen in Fig. 5-14, the highest relative irreversibility is observed in the compressor, at 34 %, followed by the evaporator at 31 % and the condenser at 21 %. The compressor's irreversibility, as discussed earlier, is due to its deviation from isentropic work, which becomes more pronounced with higher compression ratios. Since this deviation is larger during charging, compressor losses are higher in this mode. They are followed by losses in the heat exchangers: condenser and evaporator. These exergy destructions are mainly driven by the temperature differentials between the hot and cold fluids in the components. Moreover, during the charging process, the evaporator operates at a higher load than usual because of the presence of additional heat storage, which recovers subcooling heat. Therefore, more latent heat is required to complete evaporation and increases irreversibility in the evaporator. Lastly, the expansion valve is responsible for 9.3 % of the total losses, which is not negligible. This is mainly due to the significant pressure drop across the valve without any work recovery, and it is affected by the high temperature and pressure differences between the inlet and outlet.

In Mode 3, as shown in Fig. 5-15, the condenser has the highest relative irreversibility at 31 %, despite its exergy destruction remaining constant in both modes, as observed earlier. This increase is due to the reduced compression ratio and inactive evaporator, which raises the condenser's share of total irreversibility. The compressor's contribution to the system's irreversibility drops from 34 % during Mode 1 to 27 % during Mode 3, as compression ratio is reduced. The expansion valve plays a significantly greater role in defrosting mode, with its irreversibility rising to 17 %, although pressure differential is reduced. This can be explained by several factors: a reduction in the shares of exergy destruction by the compressor and the evaporator, the absence of temperature reduction through subcooling before expansion, and an increased mass flow rate through the valve in this mode. There is a substantial change in exergy flow in the expansion valve due to the pressure drop, despite the enthalpy at the inlet and outlet remaining equal. Careful consideration should therefore be given to selecting an expansion device that minimises entropy generation during the throttling process. Lastly, the frosted evaporator is responsible for 15 % of the total exergy losses, which is lower than during Mode 1 due to its inactivity. This loss is mainly influenced by the temperature differential between the incoming hot gas refrigerant and the iced coils. Although a large temperature difference promotes high heat transfer, it also increases exergy destruction and the risk of temperature shock. Therefore, a balance should be achieved to optimise defrosting efficiency.

5.3.4.2 System exergy destruction and efficiency for various refrigerants

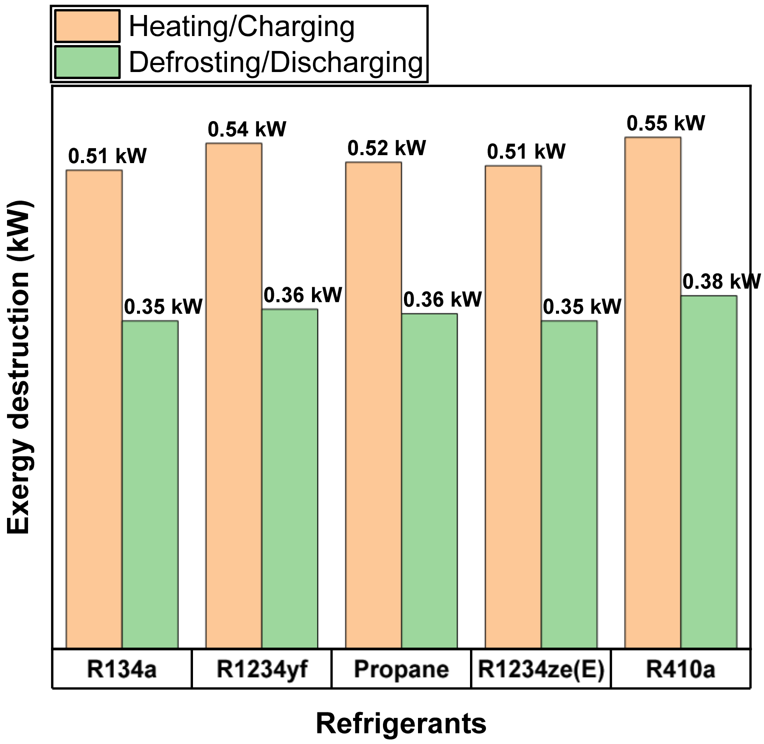

Fig. 5-16: System exergy destruction in Modes 1 and 3, for various refrigerants ($\Delta T_{HS} =$ 2.5 K and η_{comp} = 75 %)

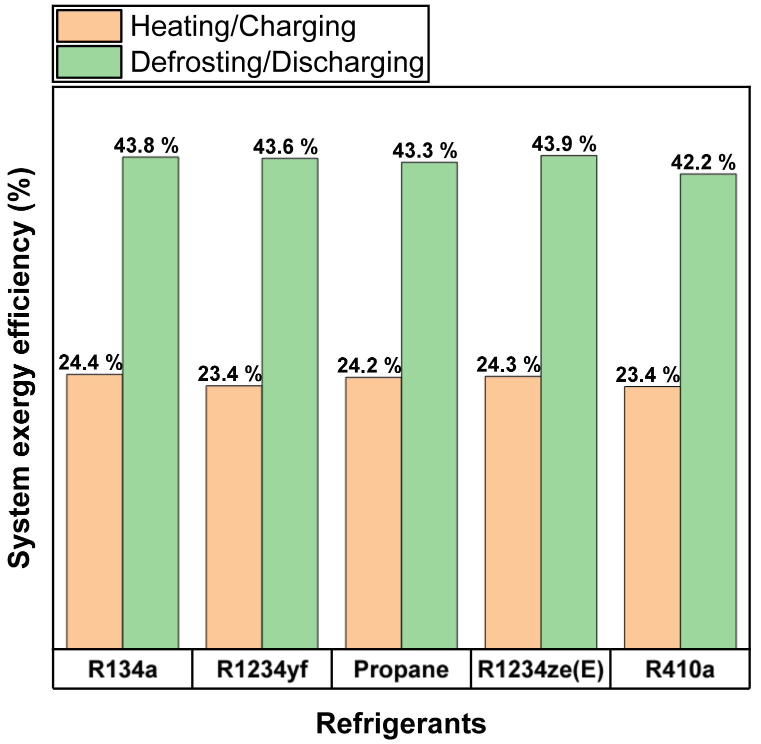

Fig. 5-17: Exergy efficiency in Modes 1 and 3, for various refrigerants (ΔT_{HS} = 2.5 K and η_{comp} = 75 %)

Fig. 5-16 and Fig. 5-17 illustrate the total exergy destruction and exergy efficiency of the system in Modes 1 and 3 for different refrigerants.

In Fig. 5-16, the results show that R134a and R1234ze(E) have the lowest exergy destruction during both modes, each with 0.51 kW in Mode 1 and 0.35 kW in Mode 3. R1234yf, R1234ze(E), and propane, as low-GWP alternatives to R134a, exhibit similar properties and, consequently, similar results. However, propane shows slightly higher exergy destruction during both modes compared to R134a and R1234ze(E), while R1234yf has higher exergy destruction during charging and is comparable to propane in defrosting mode. The refrigerant with the highest exergy destruction is R410a, with 0.55 kW in Mode 1 and 0.38 kW in Mode 3.

These findings align with the exergy efficiency results in Fig. 5-17, where R410a has the lowest efficiency in both modes, at 23.4 % in Mode 1 and 42.2 % in Mode 3. The R1234ze(E) system demonstrates the highest exergy efficiency in defrosting mode at 43.9 %, indicating that it effectively minimises both condenser and compressor losses in this mode. During charging, R134a achieves the highest efficiency at 24.4 %, also corresponding to the lowest exergy destruction in this mode.

Although Fig. 5-16 and Fig. 5-17 show slight variations among the refrigerants in both heating/charging and defrosting/discharging modes, they all fall within a similar efficiency range, around 24 % in Mode 1 and 43 % in Mode 3. The trend is consistent, with nearly double the efficiency during defrosting/discharging compared to heating/charging, largely due to the reduction in compression ratio. It can be concluded that all these refrigerants can be used with this system without significant differences in exergy performance.

5.3.5 Design implications based on exergy results

As demonstrated throughout this study, several key design considerations must be addressed to minimise the overall exergy destruction of the flexible heat pump during these two operating modes:

- <u>Compressor:</u> The compressor, as in conventional heat pump systems, was found to be the most influential component affecting overall exergy destruction. High compressor isentropic efficiency is therefore essential, and selecting efficient compressors should be a design priority to limit system-level irreversibilities.
- <u>Condenser:</u> Both heat exchangers significantly contribute to exergy losses, primarily due to the temperature difference between the working and secondary fluids. Our previous study shows that these losses are mainly influenced by the

water loop temperatures[263]. Minimising the temperature difference at the pinch point is critical for reducing irreversibilities. However, achieving this requires a larger heat exchanger surface area (especially since heat pumps operate more efficiently with a small temperature differential in the external loops[278]) which increases both cost and overall system volume. A combined exergy and economic analysis is recommended to determine the optimal condenser size for given operating conditions.

- Evaporator: The evaporator is also a major source of exergy losses, especially during the charging mode, where it becomes the second-largest contributor. Because the additional heat storage recovers subcooled heat from the refrigerant, the evaporator load and its irreversibility both increase. Proper design of the evaporator, tailored to outdoor conditions, is essential. As with the condenser, an exergy-economic approach can help identify an optimal design. During defrosting, the evaporator is inactive, and its exergy destruction is determined by the temperature difference between the iced coils and the hot gas refrigerant. To avoid excessive exergy destruction, losses, and potential temperature shock at the start of defrosting, it is important to balance this temperature difference in order to optimise defrosting efficiency.
- Heat storage: The heat storage contributes the least to total system exergy destruction in both modes. However, during defrosting, its influence becomes more significant. In this mode, the temperature difference between the refrigerant and the heat storage is critical and should be minimised to reduce its irreversibility.
- Expansion Valve: Losses in the expansion valve are non-negligible. In fact, under most of the tested storage temperatures, the exergy destruction in the expansion valve exceeds that in the heat storage. This suggests that exploring advanced or improved expansion technologies could further enhance system efficiency

5.4 Summary

In this chapter, an exergy analysis of the multi-valve flexible heat pump system, integrated with latent heat storage, has been conducted during its heating/charging and defrosting/discharging modes. The investigation aimed to identify the primary sources of exergy losses in various components and key parameters, including storage temperature, compressor isentropic efficiency, and ΔT_{HS}. Their impact on the different components and on the whole system has been evaluated, for R1234yf and other refrigerants and the following conclusions have been made:

- During defrosting, the temperature difference between the evaporating refrigerant and the heat storage medium strongly affects exergy destruction in both the heat storage and the system. An increase from 0 to 5 K results in a 30 % rise in the system exergy destruction. Minimising this temperature difference during discharging/defrosting is essential for improving the performance of the heat storage and can be adjusted by the manufacturer. In contrast, during charging, a higher storage-refrigerant temperature differential tends to reduce storage exergy destruction but lowers the charging rate, suggesting the need for an optimal balance between the two.

- Compressor isentropic efficiency was identified as the most critical factor influencing overall system exergy losses. Specifically, the drop in compressor isentropic efficiency has a stronger impact on the system than the variation of the ΔT_{HS} parameter within 5 K, in both modes. A reduction in efficiency from 100 % to 75 % increases total exergy destruction by 43 % during charging, and 35 % during defrosting. This highlights the need to select high-efficiency compressors.

- Variations in storage temperature primarily affect system losses through the evaporator, expansion valve, and heat storage during Mode 1. While in Mode 3, the compressor and expansion valve have the greatest influence, when the storage-refrigerant temperature differential is fixed.

- Finite temperature differences in the evaporator and condenser contribute significantly to exergy destruction. Under ideal compression, these two components dominate system losses in charging mode notably due to temperature differences with the external fluids, and increased load in the evaporator during charging. This highlights the need for optimised heat exchanger design, especially in the evaporator where charging imposes a high thermal load. However, the need for larger heat exchanger surfaces must be balanced against cost and size constraints. An exergy-economic analysis is recommended to guide optimal sizing under different conditions.

- During defrosting, exergy destruction in the inactive evaporator is mainly determined by the temperature difference between the iced coils and the incoming hot gas refrigerant. This can result in high exergy destruction, and the literature on hot gas bypass defrosting has shown that such conditions may cause temperature shock at the beginning of defrosting. Therefore, it is important to achieve a balance in this temperature difference to optimise defrosting efficiency.

- Exergy losses in the expansion valve are substantial and, in many cases, exceed those of the heat storage. This reinforces the potential value of integrating more efficient expansion processes to improve system performance.

- The flexible heat pump achieved nearly twice the exergy efficiency in discharging/defrosting mode compared to heating/charging. This improvement is primarily due to the lower compression ratio enabled by the higher evaporating temperature during defrosting, and inactive evaporator. It demonstrates the effectiveness of using stored thermal energy to support this process.

- The system has been tested with R1234yf, R134a, R1234ze(E), propane and R410a, and it has been concluded that their exergy efficiency falls within the same range in both modes.

Chapter 6 Energy, economic and environmental analysis of power-saving mode

This chapter presents an analysis of the energy, economic, and environmental performance of the multi-valve flexible heat pump system with integrated latent heat storage for power-saving applications. Building upon the model used in Chapter 4 for Modes 1 and 2, this analysis evaluates various parameters and their effects on system performance. The system's energy performance is investigated using refrigerant R1234yf and comparison are made with refrigerants R134a, R1234ze(E), propane, R32, and R410a. Furthermore, an economic and environmental assessment is provided, comparing its performance to that of a conventional air-source heat pump water heater (ASHPWH) and a new A-rated gas boiler, specifically for UK applications. The aim of this chapter is to address research question 2.

6.1 Introduction

In Chapters 4 and 5, a thermodynamic and exergy analysis of the flexible heat pump during the defrosting operation was conducted. In Chapter 4, an ideal model was first developed to evaluate the performance and internal thermodynamic processes of the flexible heat pump, operating sequentially in Modes 1, 3, and 2, and the results were compared to a conventional air-source heat pump using the reverse cycle defrosting method. In Chapter 5, an exergy analysis was performed to identify the primary sources of losses in Modes 1 and 3. The model was improved to assess the impact of various parameters, such as storage temperature, compressor efficiency, and ΔT_{HS}. Various refrigerants, including R134a, R410a, R1234yf, R1234ze(E), propane, and R32, were studied in the system. R1234yf, which showed the best performance in Chapter 4, was selected as the principal refrigerant for further study in Chapter 5 and this chapter.

In this chapter, the power-saving application of the flexible heat pump is investigated using latent heat storage. When defrosting is not required, Modes 1 and 2 can operate in sequence, allowing for an increase in the evaporating temperature in Mode 2, thus saving compressor power. Using the model equations from Chapter 3, this analysis takes into account non-ideal conditions to evaluate the thermodynamic performance of the flexible heat pump compared to a conventional heat pump, followed by an economic and environmental analysis. First, the methodology is detailed, then the system's performance is evaluated by varying several parameters, including condensing and evaporating temperatures, storage temperature, ΔT_{HS}, and superheating and subcooling degrees. Finally, an economic and environmental analysis is conducted to compare the economic and environmental attractiveness of the flexible heat pump in its power-saving mode with those of a conventional ASHPWH and a gas boiler, specifically for applications in the UK. The aim of this chapter is to assess the thermodynamic performance of the flexible heat pump's power-saving mode under non-ideal conditions and to evaluate its economic and environmental viability compared to a conventional heat pump in various scenarios, in order to address research question 2.

6.2 Methodology

In Chapter 3, Modes 1 and 2 were introduced and their working principles were explained. Using a similar approach as in Chapter 4, this chapter examines the operation of the flexible heat pump over a full charge/discharge cycle of the heat storage and evaluates the potential COP improvement. However, its calculation process differs from Chapter 4, as it was outlined in Chapter 3.

The simulation starts with Mode 1 lasting for a fixed Δt_{charge}. At the end of Mode 1, Mode 2 starts and continues until the heat storage is emptied, which lasts for $\Delta t_{discharge,2}$. The heating capacity remains constant throughout the process. It should be noted that, although Δt_{charge} is fixed, its value does not affect the overall performance of the flexible heat pump in this case. Unlike Chapter 4, there is no assumption of ice formation, which was the only parameter influenced by the heating/charging time in Mode 1. Here, as shown by Eq. (3.16) and Eq. (3.22), the charging time is proportional to the discharging time, so the COP improvement is not influenced by an increase or decrease in Δt_{charge}, as the time ratio would remain unchanged. The COP improvement is instead affected by parameters that influence the time ratio, such as storage temperature, ΔT_{HS}, etc.

After the energy assessment, an economic and environmental analysis is conducted on the flexible heat pump, based on the calculated energy performance. This is compared to that of a conventional ASHPWH and a gas boiler to evaluate the potential cost savings and environmental impact of using the flexible heat pump’s power-saving mode in an average UK household.

6.2.1 Assumptions adopted in this chapter

The model used to compute the heat pump performance and thermodynamic processes in this chapter is based on the equations for Modes 1 and 2 provided in Chapter 3. As in

Chapter 5, compressor efficiency is considered non-ideal, and the storage-refrigerant temperature differential is also considered. Additionally, subcooling in the condenser and superheating in the evaporator are also included as parameters. A latent heat storage is considered in this analysis. Moreover, the economic and environmental assessment requires certain assumptions regarding the external loops and designs of the heat pumps. As a result, the general assumptions for this chapter are the following:

1) Fixed compressor isentropic efficiency: Based on results from Chapter 5 and the literature, the compressor isentropic efficiency is fixed at 75 %[276].

2) Steady storage-refrigerant temperature differential: To simplify the analysis, the temperature difference between the heat storage and the refrigerant is assumed to be constant and equal during both the charging and discharging processes.

3) 100% round-trip efficiency of the heat storage: The heat storage is assumed to have negligible thermal losses between modes, meaning that heat losses to the environment are neglected. The same amount of energy charged in Mode 1 is available at the beginning of Mode 2 ($\%\Delta Q_{loss} = 0$).

4) Frosting/Defrosting is not considered: Since this chapter focuses on the power-saving application of the flexible heat pump, the impact of defrosting, which has already been discussed in Chapters 4 and 5, is not considered here.

5) Constant heat transfer coefficient in both heat exchangers: To evaluate the cost of the heat pumps, an estimation of heat exchangers' areas is required. For this purpose, a constant heat transfer coefficient is assumed for both heat exchangers based on literature. However, this assumption has no impact on the energy analysis, as the detailed geometry of the heat exchangers is not considered there.

6.2.2 Description of case study

Like the previous chapter, the study is mainly conducted with R1234yf, which was the best performing refrigerant in the system, as demonstrated in Chapter 4. Other refrigerants are also tested (R134a, R410a, R1234ze(E), propane, and R32), and their thermal properties have been listed in Chapter 3 (Table 3-6). For the energy and performance analysis, Mode 1 is initially set to $\Delta t_{charge} = 1$ h, after which Mode 2 is initiated for $\Delta t_{discharge,2}$, until the heat storage is emptied.

The condensing temperature is set at 65 °C, the evaporating temperature at 0 °C, and the heating capacity at 8.5 kW. These parameters are selected because no defrosting operation is considered in this analysis, so there is no need to account for ice formation as in previous chapters. As a result, the chosen parameters are not derived from earlier research but are instead set to reflect typical UK applications where no improved insulation or modifications have been made to the household heating system. This approach is intended to address research question 2.

As mentioned in Chapter 2, hot water in the UK is heated to high temperatures, leading to frequently oversized heating systems[32]. DHW is typically heated to 60 °C to prevent Legionella bacteria growth, and radiators in UK households are often designed to receive hot water at 50 °C[31]. Therefore, the condensing temperature is set at 65 °C, and the evaporating temperature is maintained at 0 °C to minimise the source-sink temperature difference, taking into account the assumed annual average ambient temperature in the UK of 9.5 °C[274]. This source-sink temperature difference is already significant for a domestic air-source heat pump, making this type of heat pump potentially highly energy-consuming[52]. The heating capacity is set at 8.5 kW, which has been found to be the optimal size for an air-source heat pump covering both DHW and space heating demand in Edinburgh[130,279]. The parameters used throughout this chapter are listed in Table 6-1.

Table 6-1: Chapter main parameters

Parameters	**Value**
Refrigerant	R1234yf
Condensing temperature [°C]	65
Evaporating temperature [°C]	0
Heating capacity [kW]	8.5
Compressor efficiency [%][276]	75

Following the energy analysis of the flexible heat pump, an economic and environmental analysis is conducted with R1234yf, and compared to a conventional ASHPWH and gas boiler for use in Edinburgh. The annual average heating demand for both DHW and space heating is taken from a study by Wang and He, which estimates it at 17,304 kWh for Edinburgh, based on the spatial and temporal ambient temperature variations[279]. In this chapter, the variation in ambient temperature's effect on both ASHPWH and flexible heat pump performance is not considered, as this study is steady-state, and the ambient air temperature is fixed at the annual average of 9.5 °C. Consequently, both heat pumps are assumed to provide a constant heating capacity of 8.5 kW. For simplification in the economic analysis, the average conditions are chosen. However, as mentioned previously, air-source heat pumps' performances are affected by ambient temperature variations, particularly due to frosting issues.

The return water temperature is set to 50 °C in a steady-state configuration with a 10 K temperature difference between the inlet and outlet, based on UK field trial data from Kelly et al.[31,36]. For the economic and environmental analysis, the combined charging and discharging times are set to one hour, as shown in Eq. (6.1)

$$\Delta t_{charge} + \Delta t_{discharge,2} = 1\ \mathrm{h} \tag{6.1}$$

This setting does not affect the performance calculation, as discussed previously and shown in Eqs. (3.16) and (3.22); the assumption about running time has no impact on performance as long as it does not change the time ratio, which is the case here. Furthermore, this choice simplifies the calculation of energy consumption costs. The average standard electricity and gas prices are based on September 2024 energy cap data from Ofgem for southern Scotland[280]. The CO_2e emission factors are sourced from official data provided by the UK Department for Energy Security and Net Zero[281]. The parameters used in this study are given in Table 6-2.

Table 6-2: Economic and environmental analysis parameters

Parameters	Value
Water inlet temperature [°C]	50
Water outlet temperature [°C]	60
Air inlet temperature [°C][274]	9.5
Air outlet temperature [°C]	4.5
Overall heat transfer coefficient of condenser [W/m^2 K][282]	200
Overall heat transfer coefficient of evaporator [W/m^2 K][282]	80
PCM mass [kg]	53
Average annual heating demand for both DWH and space heating in Edinburgh [kWh/year][279]	17,304
Gas price in Southern Scotland [£/kWh][280]	0.054
Daily standing charge for gas [£/day][280]	0.3166
Electricity price in Southern Scotland [£/kWh][280]	0.2183
Natural gas CO_2e emission factor [kg/kWh][281]	0.2026
Electricity production CO_2e emission factor [kg/kWh][281]	0.207
CO_2 penalty price [£/kg][283]	0.065
A-rated gas boiler efficiency [%][284]	92
Gas boiler lifetime [years][279]	15
Heat pump lifetime [years][279]	20
Interest rate [%][279]	8
Maintenance factor [-][244]	1.06
Leakage rate per year [%][248]	15
Recycling factor [%][248]	90

To evaluate the cost of adding a PCM tank, the material selected is RT35HC, manufactured by Rubitherm Technologies GmbH. This material was chosen due to its melting temperature, which aligns with the calculated range, and its important heat storage capacity. Its properties are listed in Table 6-3 and are obtained from Rubitherm Technologies' datasheet[285].

Table 6-3: PCM properties

Parameters	**Value**[285]
Melting temperature [°C]	34-36
Cooling temperature [°C]	36-34
Heat storage capacity ± 7.5% [kJ/kg]	240
Specific heat capacity [kJ/kg K]	2
Solid density at 25°C [kg/m^3]	880
Liquid density at 40°C [kg/ m^3]	770
Maximum operating temperature [°C]	70

In the following results, the energy performance of the flexible heat pump is evaluated across various condensing and evaporating temperatures, storage temperatures, ΔT_{HS}, as well as superheating and subcooling degrees. Additionally, an economic and environmental analysis is conducted, comparing the flexible heat pump to a conventional ASHPWH and a gas boiler, specifically for an application in Edinburgh.

6.3 Results and discussion

6.3.1 Energy and performance analysis

In this first section an energy analysis is performed, and various parameters impact are considered on the energy performance of the flexible heat pump.

6.3.1.1 Maximum improvement storage temperature under various condensing and evaporating temperatures

To begin the study, it is examined whether a maximum improvement temperature ($T_{max,\alpha}$) can be achieved for various combinations of condensing (T_{cond}) and evaporating temperatures (T_{evap}), along with their impact on $T_{max,\alpha}$. Each combination is tested, and

$T_{max,\alpha}$ is determined accordingly. It is important to note that, in Mode 2 (discharging/power-saving mode), the evaporating temperature corresponds to the storage temperature (T_{HS}) when $\Delta T_{HS} = 0$ K. Therefore, in the following sections, references to the evaporating temperature T_{evap} refer specifically to the evaporating temperature during Mode 1, not to the storage temperature T_{HS}. Additionally, the condensing temperature represents the inlet temperature of the storage in Mode 1, assuming no subcooling in the condenser. Initially, ΔT_{HS}, as well as the subcooling and superheating degrees (T_{sb} and T_{sh}, respectively), are assumed to be 0.

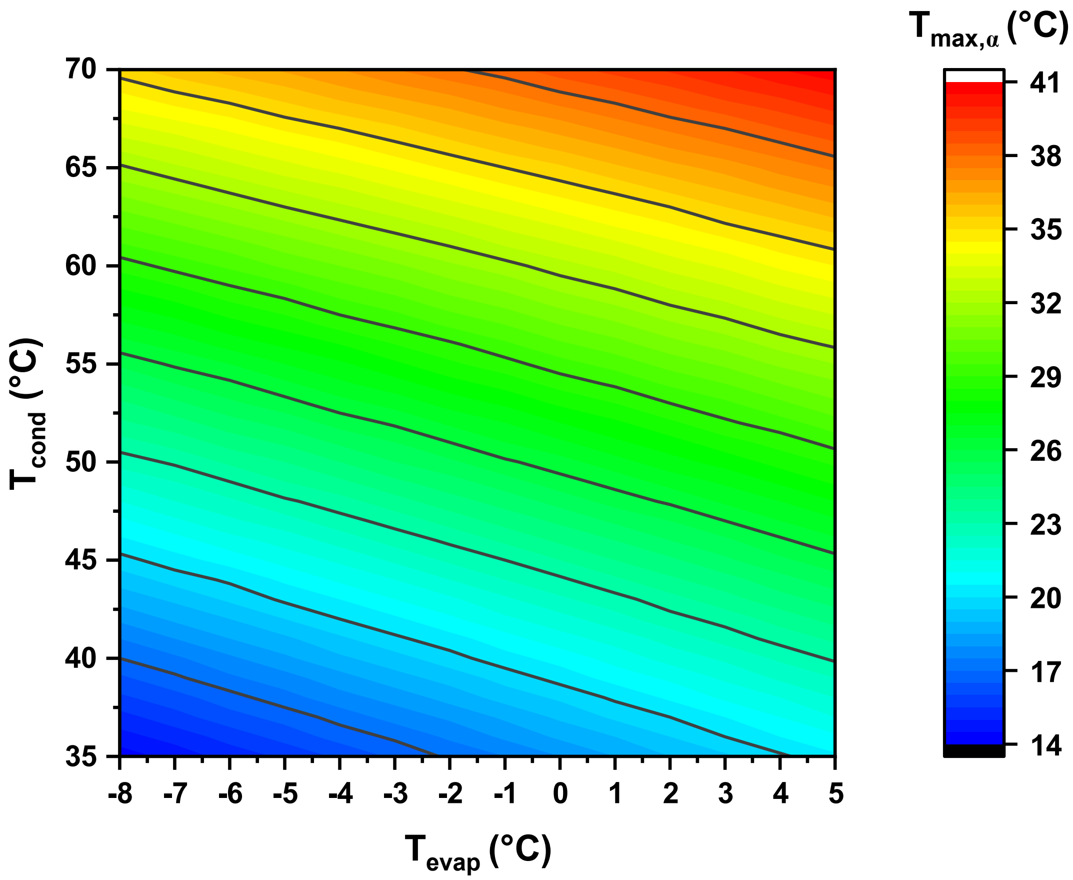

Fig. 6-1: Maximum improvement storage temperature as a function of condensing and evaporating temperatures ($\Delta T_{HS} = 0$; $T_{sb} = 0$; $T_{sh} = 0$)

Fig. 6-1 shows how the top performing storage temperature $T_{max,\alpha}$ varies as a function of the condensing and evaporating temperatures when Modes 1 and 2 are operated. For a given condensing temperature, $T_{max,\alpha}$ increases as the evaporating temperature rises. The highest values of $T_{max,\alpha}$ are observed when both the condensing and evaporating temperatures are at their highest, and the lowest values occur when both temperatures are at their lowest. Similarly, for a fixed evaporating temperature, $T_{max,\alpha}$ increases with higher condensing temperatures. For instance, when ΔT_{HS}, T_{sb} and T_{sh} are set to zero, with $T_{cond} = 35$ °C and

$T_{evap} = -8$ °C, $T_{max,\alpha}$ is 14.1 °C. When $T_{cond} = 70$ °C and $T_{evap} = 5$ °C, $T_{max,\alpha}$ reaches 40.9 °C. This occurs because, at higher condensing and evaporating temperatures, a balance must be found between maximising storage capacity, which depends on a larger temperature gradient in Mode 1 and thus a lower storage temperature, and maximising power-saving capacity in Mode 2, which requires a higher storage temperature. Therefore, the value of $T_{max,\alpha}$ found here differs from that in Chapter 4 due to the addition of the defrosting process, which shifts the balance. During defrosting, more heat is discharged from the heat storage to support the defrosting operation, requiring more stored heat, and resulting in less compressor power being saved. This reduces the potential maximum improvement and requires a different balance.

Considering this, it is also visible in Fig. 6-1 that the $T_{max,\alpha}$ value is consistently close to, but slightly higher than, the midpoint between the refrigerant temperature at the inlet of the heat storage (the condensing temperature here) and the evaporating temperature. This contrasts with the findings from Chapter 4 regarding the defrosting mode, where $T_{max,\alpha}$ was also near the midpoint between T_{cond} and T_{evap} but was slightly lower due to the defrosting process's influence. This scenario confirms that the maximum improvement storage temperature is influenced by both the energy stored in Mode 1 and the power consumption in Mode 2, which vary based on the selected storage temperature.

Thus, when selecting a storage material for a flexible heat pump to achieve the best energy efficiency, it is crucial to thoroughly evaluate the specific application parameters. For heat pumps operating under highly variable conditions, it may be preferable to opt for a sensible heat storage system, such as a water tank, as their storage temperature range is more flexible compared to a PCM storage tank, which has a fixed melting temperature.

6.3.1.2 Impact of varying storage temperature

In the following results, the impact of storage temperature on the system is analysed. The condensing temperature is fixed at 65 °C and the evaporating temperature at 0 °C. Additionally, ΔT_{HS} is assumed to be 0, with no subcooling in the condenser and no superheating at the evaporator outlet.

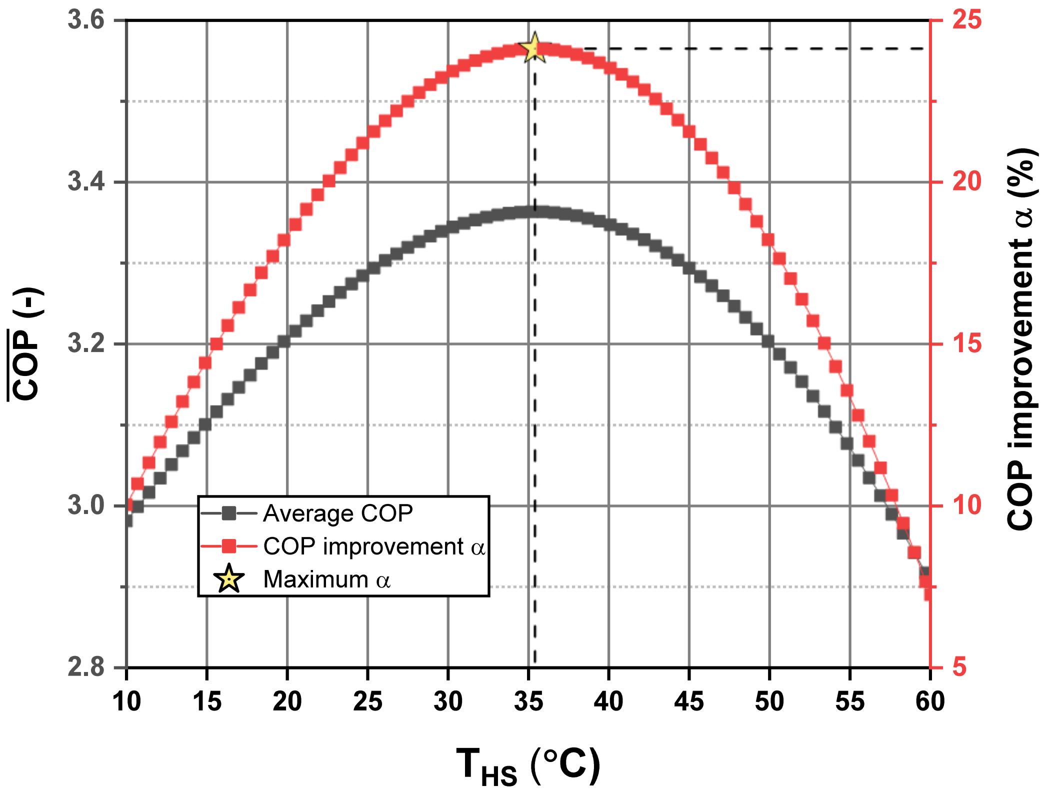

Fig. 6-2: Average COP and improvement depending on storage temperature ($\Delta T_{HS} = 0$; $T_{sb} = 0$; $T_{sh} = 0$)

Fig. 6-2 presents the average COP and improvement of the system as a function of the storage temperature for R1234yf. As illustrated, a storage temperature is identified for achieving the best system performance. In this case, for R1234yf, this storage temperature is 35.4 °C, corresponding to an average COP of 3.36 and a 24.1 % improvement from the COP of a conventional heat pump operating under same conditions. As observed previously, the $T_{max,\alpha}$ found here is slightly higher than the midpoint between the condensing and evaporating temperatures.

As previously discussed, the maximum improvement over the conventional heat pump depends on the storage temperature. For fixed condensing and evaporating temperatures, this value represents a balance between the heat recovery potential in charging mode and the compressor power saving in discharging mode. The improvement found here is greater than in Chapter 4, as both the condensing and evaporating temperatures are higher, and defrosting is not being operated.

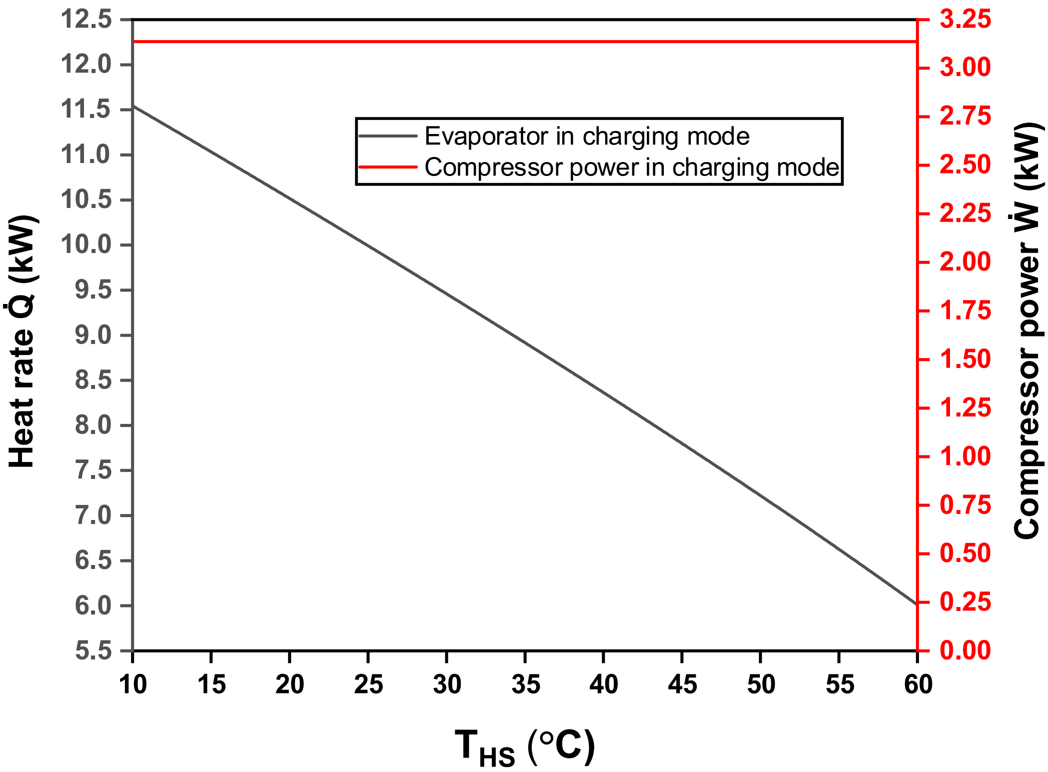

Fig. 6-3: Impact of the storage temperature on: heat rate in the evaporator and compressor power in Mode 1 ($\Delta T_{HS} = 0$; $T_{sb} = 0$; $T_{sh} = 0$)

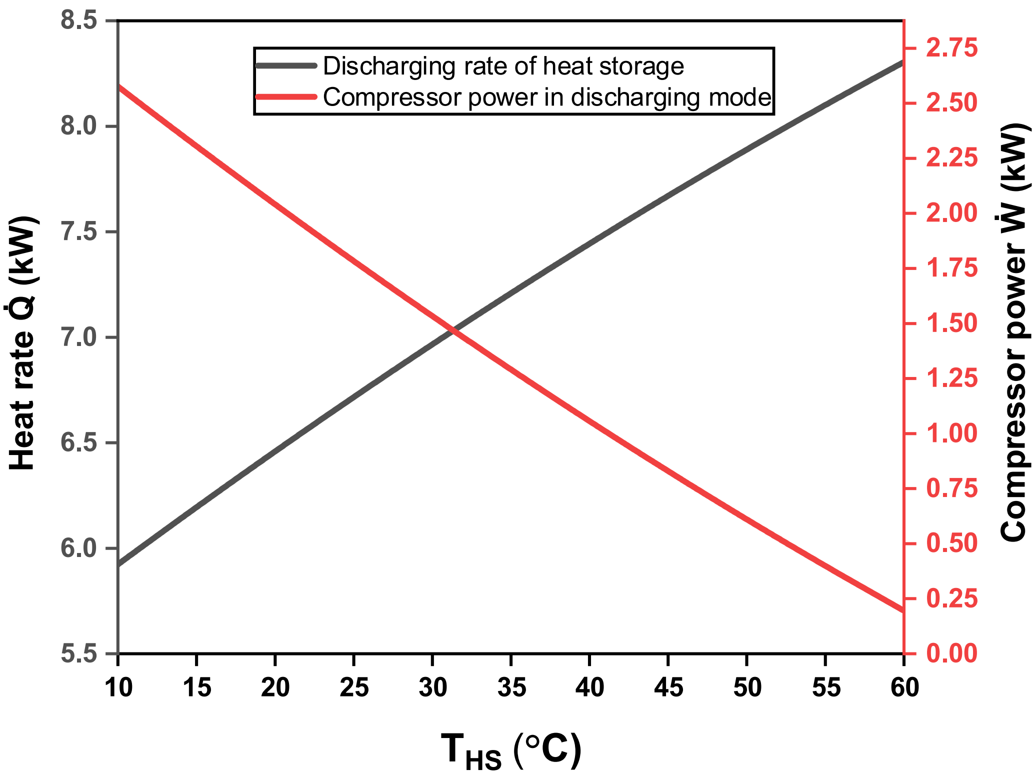

Fig. 6-4: Impact of the storage temperature on: discharging rate of the heat storage and compressor power in Mode 2 ($\Delta T_{HS} = 0$; $T_{sb} = 0$; $T_{sh} = 0$)

Fig. 6-3 and Fig. 6-4 show the variation in compressor power during both charging and discharging modes, along with the heat transfer rate in the evaporator and the discharge rate from the heat storage, as a function of storage temperature. Starting with the heat transfer rate in the evaporator during charging in Fig. 6-3, it is evident that it decreases significantly as the storage temperature increases. This is due to the fact that, as the storage temperature rises, the reduced temperature difference decreases heat transfer in the storage, requiring less heat to be absorbed from ambient air, based on the energy balance equation. With ΔT_{HS} set to 0, the refrigerant is subcooled to precisely match the storage temperature. As a result, the enthalpy at the outlet of the expansion valve is higher at higher storage temperatures, meaning less heat is required to fully evaporate the refrigerant in the evaporator. The heat transfer rate decreases from 11.5 kW at $T_{HS} = 10$ °C to 6 kW at $T_{HS} = 60$ °C, reducing in half. At the top performing storage temperature, the heat transfer rate in the evaporator is 8.9 kW, slightly higher than the condensing heat rate due to the added subcooling. Therefore, when designing the flexible heat pump, it is essential to consider strategies for increasing the heat transfer rate in the evaporator (such as using different types of heat exchangers, increasing air mass flow rate, or enlarging the surface area). For a conventional heat pump in this configuration, the heat rate in the evaporator calculated is 5.36 kW.

Conversely, in Fig. 6-4 the discharge heat rate in the heat storage increases with rising storage temperature, going from 5.9 kW at $T_{HS} = 10$ °C to 8.3 kW at $T_{HS} = 60$ °C. At the maximum improvement storage temperature, the discharge rate is 7.2 kW. There are two reasons for this: firstly, the discharge mass flow rate increases as the storage temperature rises. This occurs because an increase in the evaporating temperature reduces the discharge temperature at the compressor outlet due to the lower compression ratio, leading to a smaller enthalpy difference in the condenser. As the condensing rate is fixed, the mass flow rate increases from 0.077 kg/s to 0.081 kg/s across the tested temperature range. Secondly, the saturated vapour enthalpy of R1234yf increases with temperature. Since the enthalpy at the expansion valve outlet remains constant, the enthalpy difference increases, requiring more energy to evaporate the refrigerant. Optimising heat transfer in the heat storage is crucial to prevent discharging energy too quickly, ensuring power is saved for the longest possible duration.

Fig. 6-3 and Fig. 6-4 also show the evolution of compressor power in both charging and discharging modes. During charging, compressor power remains constant at 3.14 kW, as both the evaporating and condensing temperatures are fixed. In this model, the subcooling in the heat storage does not affect either the compressor power or the mass flow rate during charging, as it is determined by the fixed condensing rate. Subcooling in the storage, however, increases the required amount of heat to be absorbed from ambient air, and therefore the evaporator heat transfer, as previously explained. In discharging mode, compressor power decreases significantly with increasing storage temperature. This is because a higher storage temperature raises the refrigerant's evaporating temperature, reducing the compression ratio. Compressor power drops from 2.6 kW at $T_{HS} = 10$ °C to 0.2 kW at $T_{HS} = 60$ °C, while at the top performing storage temperature $T_{max,\alpha}$, compressor power is 1.3 kW, representing a reduction of nearly 60 % from Mode 1. As previously mentioned, although compressor power decreases at higher storage temperatures, this alone is not sufficient to achieve maximum performance. At higher storage temperatures, the heat recovery potential is limited due to the smaller temperature differential in the storage tank, meaning that while compressor power is saved, it is for a shorter duration.

6.3.1.3 Impact of varying storage-refrigerant temperature differential, superheating and subcooling degrees

In the following results, the maximum improvement storage temperature and system performance are evaluated for different values of ΔT_{HS}, as well as for varying degrees of superheating and subcooling. This approach, which has not been previously explored, allows for assessment of their impact on the overall system.

Fig. 6-5 illustrates the impact of the storage-refrigerant temperature differential ΔT_{HS} on the average COP, improvement, and $T_{max,\alpha}$ for R1234yf. The superheating and subcooling degrees are fixed to zero in order to isolate the effect of ΔT_{HS}. As ΔT_{HS} increases in Mode 1, the heat recovery process is reduced due to the smaller temperature difference in the heat storage. The refrigerant outlet temperature from the heat storage becomes $T_{ref,out} = T_{HS} + \Delta T_{HS}$. In the ideal case, where $\Delta T_{HS} = 0$ K, the refrigerant outlet temperature matches the PCM melting temperature, resulting in 100 % heat transfer efficiency. In Mode 1, ΔT_{HS} only affects heat transfer within the heat storage and the evaporator and has no impact on other components. In Mode 2, however, as ΔT_{HS} increases, the temperature difference between the PCM melting temperature and the refrigerant increases, which in turn modifies the refrigerant's evaporating pressure. Since the refrigerant's evaporating temperature is lower than the heat storage temperature during discharging to allow for evaporation, this increases the pressure ratio between the evaporating and condensing pressures, affecting compressor power. Additionally, heat transfer within the heat storage is impacted, as lower refrigerant's evaporating temperatures reduce the heat transfer rate, as shown in Fig. 6-4.

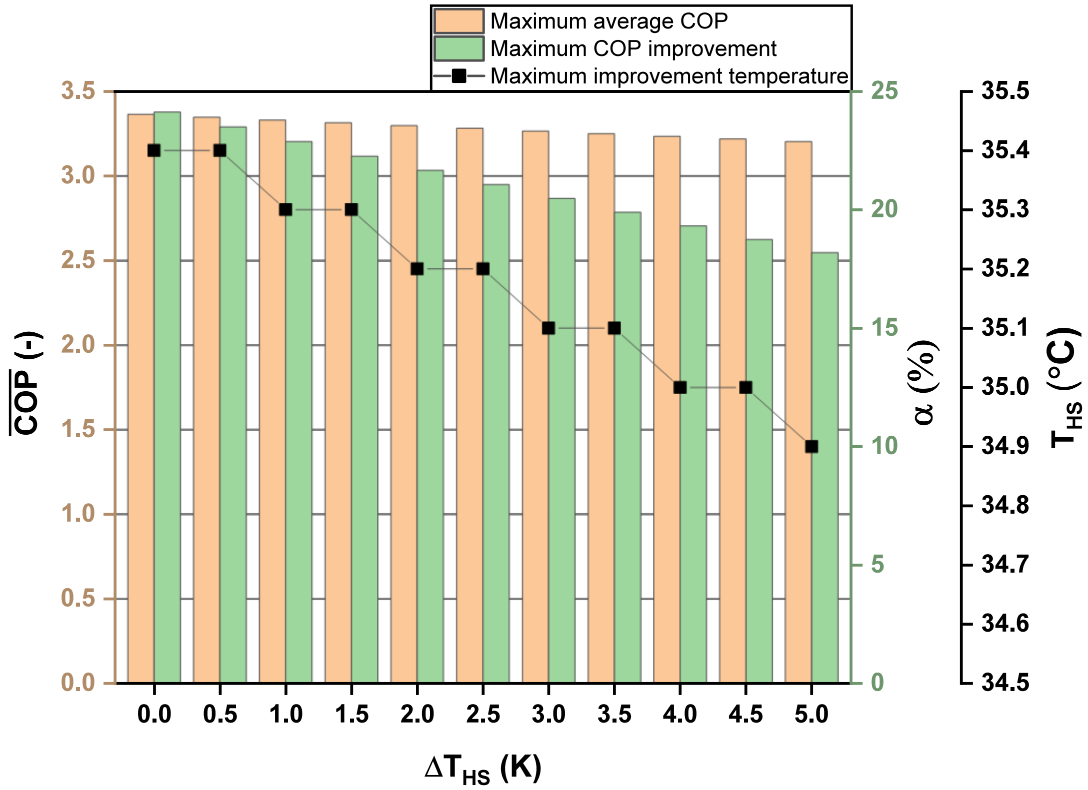

Fig. 6-5: $T_{max,\alpha}$ and corresponding average COP and improvement depending on ΔT_{HS}

Fig. 6-5 firstly shows the decrease of both the average COP and improvement with ΔT_{HS}. In the ideal case, the flexible heat pump has an average COP of 3.36, with a 24.1 % improvement compared to a conventional heat pump. When ΔT_{HS} increases to 5 K, these values decrease to 3.2 and 18.2 %, respectively. The average COP reduction is slight (~5 %) from $\Delta T_{HS} = 0$ K to $\Delta T_{HS} = 5$ K, but the impact on system improvement is more significant, with a 24 % decrease. This is because ΔT_{HS} does not affect the performance of the conventional heat pump, and as a result, any reduction in the flexible heat pump's average COP directly reduces its improvement. This highlights the difference between the absolute COP reduction and the relative decrease in system's improvement. The primary driver of this impact is Mode 2, where increasing ΔT_{HS} raises compressor power. However, the heat recovery process in Mode 1 is also affected by ΔT_{HS}. To achieve the best improvement compared to a conventional heat pump, ΔT_{HS} should be minimised, although the average COP of the flexible heat pump is only slightly affected by this parameter. These findings are consistent with Chapter 5, which emphasised that minimising ΔT_{HS} reduces the heat storage exergy losses in Mode 3.

Regarding the effect of ΔT_{HS} on $T_{max,\alpha}$, it can be seen that $T_{max,\alpha}$ decreases slightly as ΔT_{HS} increases, from 35.4 °C at $\Delta T_{HS} = 0$ K to 34.9 °C at $\Delta T_{HS} = 5$ K. As discussed in Fig. 6-1, the temperature for maximum COP improvement is linked to the condensing and evaporating temperatures during charging, and is slightly higher than their midpoint. This rule holds here, but $T_{max,\alpha}$ decreases slightly as ΔT_{HS} increases. This is because the maximum improvement storage temperature represents a balance between maximising heat recovery in Mode 1 and minimising compressor power in Mode 2. Since both processes are impacted by increases in ΔT_{HS}, this balance shifts slightly due to changes in refrigerant properties, particularly in Mode 2. As ΔT_{HS} increases, the evaporating temperature and pressure decrease, affecting the enthalpy of vaporisation, mass flow rate, and compressor power, deviating from the ideal conditions found at $\Delta T_{HS} = 0$ K. Consequently, $T_{max,\alpha}$ adjusts slightly, though the decrease is only around 1.5 %. Notably, Fig. 6-5 shows that the decrease is stepwise, occurring in 1 K intervals, as changes in refrigerant properties become noticeable only at these intervals for R1234yf.

In conclusion, minimising ΔT_{HS} is advisable to maximise system improvement and minimise exergy losses. However, while an increase of up to 5 K significantly impacts the potential achievable improvement, it has limited effects on the average COP and top performing storage temperature with R1234yf, and thus does not greatly influence the choice of a PCM tank.

Fig. 6-6 presents the average COP and improvement, and $T_{max,\alpha}$ as a function of the superheating degree T_{sh}. ΔT_{HS} and subcooling degree T_{sb} are set to zero in order to isolate the effect of superheat. A superheating degree of up to 10 K is considered and applied to both the flexible and conventional heat pumps. The results show that the average COP increases with increasing superheat. This is due to the reduction of entropic losses in the compressor, as the higher compressor's inlet temperature for the same pressure reduces the power required to reach the outlet pressure. The average COP rises from 3.36 to 3.43, a 2 % increase. However, the system improvement decreases from 25.1 % to 21.9 %, a 13 % drop. This is because the same superheating degree is applied to the conventional heat pump, increasing its COP and narrowing the performance gap between the two. This is more noticeable for the conventional heat pump, as the benefits of superheating are more pronounced for higher compression ratio. Nevertheless, even at a superheating degree of 10 K, the flexible heat pump still achieves an improvement of over 20 %.

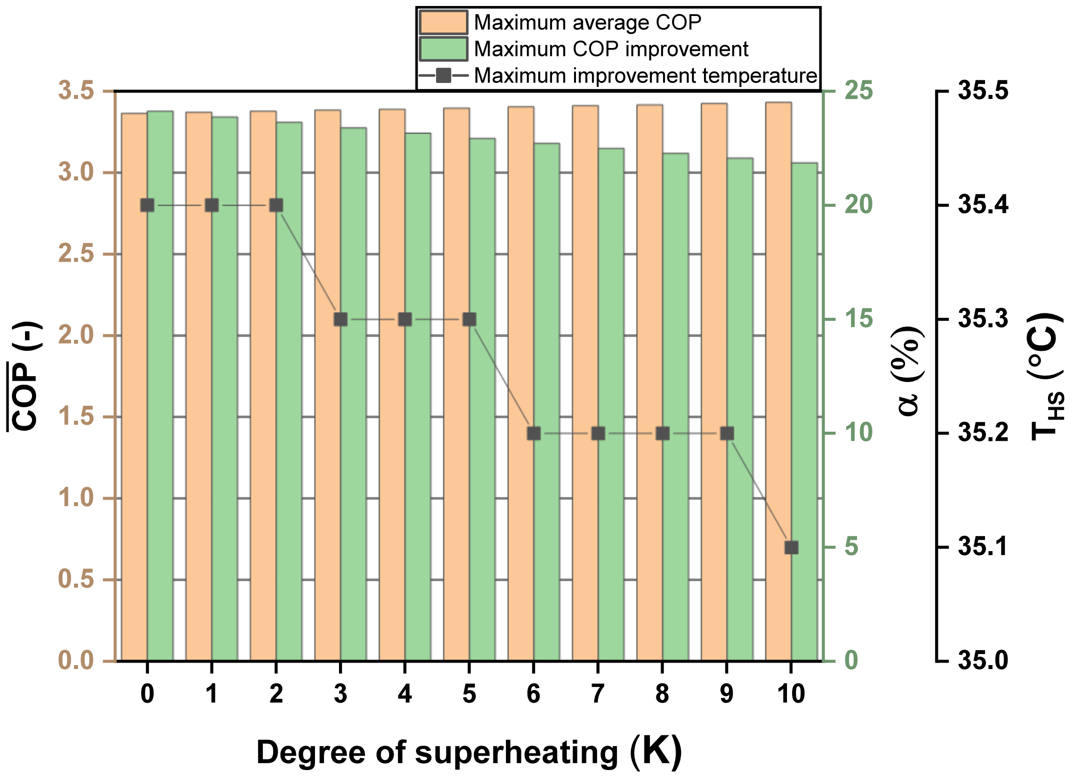

Fig. 6-6: $T_{max,\alpha}$ and corresponding average COP and improvement depending on the superheating degree T_{sh}

Fig. 6-6 also shows a slight decrease in the maximum improvement storage temperature with increasing superheat, dropping from 35.4 °C to 35.1 °C, a relatively small change. The decrease follows a step-like pattern, with small drops occurring every 3 K of superheating degree up to 6 K, followed by a drop after 4 K. The decrease of $T_{max,\alpha}$ can be attributed to a slight reduction in the mass flow rate due to the addition of superheat in both modes, which slightly reduces the heat recovery rate. Additionally, the increase in latent heat required to evaporate the refrigerant during discharging raises the heat rate in the heat storage during Mode 2, resulting in this minor adjustment in the best balance. However, the change is minimal and would have no significant impact on the choice of a PCM tank.

In conclusion, the superheating degree has an overall positive impact on the average COP and performance of the flexible heat pump, despite a slight effect on the top performing storage temperature and a modest drop in COP improvement. However, since the superheating degree benefits more higher compression ratios, it should be kept within a medium range to avoid negatively impacting the evaporator's heat transfer rate during charging, which would require further adjustments to increase it.

Fig. 6-7 presents the average COP and improvement, and best performing storage temperature as a function of the subcooling degree in the condenser. ΔT_{HS} and superheating degree T_{sh} are kept at zero to isolate the impact of subcooling. As previously mentioned, the subcooling degree examined here refers to the subcooling occurring in the condenser, before the refrigerant flows into the heat storage, and differs from subcooling within the heat storage itself.

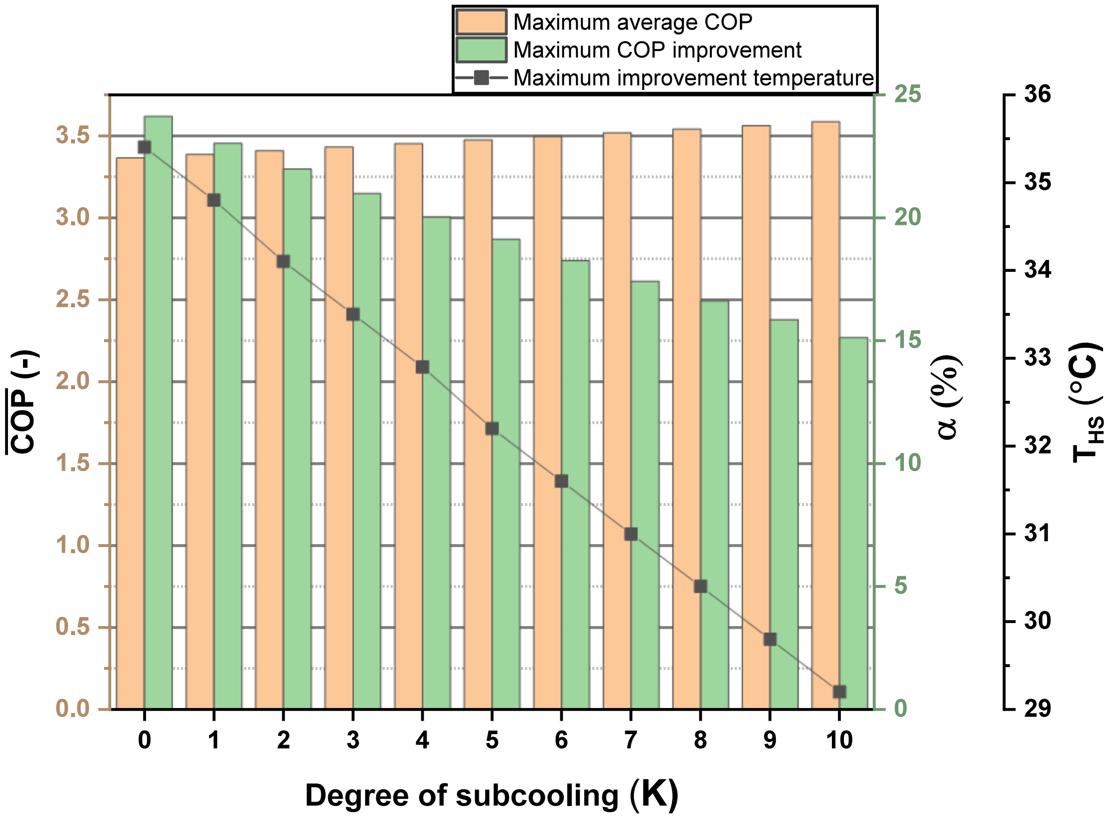

Fig. 6-7: $T_{max,\alpha}$ and corresponding average COP and improvement depending on the subcooling degree T_{sb}

The effect of increasing subcooling on the average COP is more pronounced than with superheating, rising from 3.36 to 3.6, a 7 % increase. This improvement is due to a reduction in the mass flow rate, as the heating capacity is assumed constant in this model. The increase in temperature difference within the condenser leads to a decrease in the calculated mass flow rate. However, as with superheating, the COP improvement decreases, here significantly, with increasing subcooling, dropping from 24.1 % to 15.1 %. This reduction occurs because the flexible heat pump's primary improvement comes from compressor power saving in Mode 2, leaving limited room for further gains compared to a conventional heat pump. A conventional heat pump, on the other hand, benefits greatly from a reduced mass flow rate and lower compressor power, especially in high-compression conditions. For example, the base COP of a conventional heat pump in this configuration is 2.7 with a compressor power of 1.48 kW. When subcooling is increased to 10 K, the COP improves by

15 %, rising to 3.11, while compressor power decreases significantly to 1.28 kW. For the flexible heat pump in Mode 2, while subcooling reduces compressor power for a same storage temperature, this benefit is offset by a reduction in that storage temperature as subcooling increases. As a result, at $T_{max,\alpha}$, compressor power increases from 0.59 kW to 0.64 kW as subcooling rises from 0 to 10 K. Moreover, increasing subcooling in the condenser during Mode 2 would accelerate the discharging rate of the heat storage, reduce the discharging time and limit potential performance improvement.

The top performing storage temperature is significantly affected by subcooling in the condenser, decreasing linearly from 35.4 ° C to 29.2 °C across the tested subcooling range, a difference of almost 6 K. This drop occurs due to the lower refrigerant's temperature at the inlet of the heat storage. As discussed in Fig. 6-1, the maximum improvement storage temperature is roughly midway between the refrigerant temperature at the storage inlet (which equals the condensing temperature when $T_{sb} = 0$ K) and the evaporating temperature in Mode 1. With increased subcooling at the condenser outlet, the inlet temperature of the storage decreases, lowering the best performing storage temperature found for the best heat recovery. As the storage temperature decreases, compressor power in Mode 2 increases accordingly. Although the average COP improves due to reduced power in Mode 1, the benefit in Mode 2 is diminished, leading to a reduction in overall improvement compared to a conventional heat pump.

Thus, subcooling in the condenser has a significant impact on the flexible heat pump's performance and on the choice of the PCM melting temperature. The subcooling degree should be controlled to maximise performance. Additionally, efforts should be made to ensure that the refrigerant inlet temperature to the heat storage remains as close as possible to the condenser outlet temperature by properly insulating the pipes between the components to prevent heat loss. Otherwise, the performance of the flexible heat pump could be substantially affected.

6.3.1.4 Impact of various operating scenarios on system

Building on the previous results, this section analyses the impact of different operating scenarios on components and performance of the flexible heat pump, considering variations in ΔT_{HS}, superheating and subcooling degrees, for R1234yf and other refrigerants. The scenarios are outlined in Table 6-4. Scenario 1 represents the ideal case and serves as a benchmark to assess the effects of varying parameters on the system. Different values for these parameters are selected, ranging from zero to a specified maximum based on prior results. The first three scenarios examine the impact of superheating and subcooling, while the subsequent scenarios combine these factors with ΔT_{HS} to assess their overall combined effect.

The condensing and evaporating temperatures, as well as compressor efficiency remain consistent with the previous analysis. All results are presented at the maximum improvement storage temperature for each scenario.

Table 6-4: Scenarios

Scenario	ΔT_{HS} **[K]**	**Superheating degree [K]**	**Subcooling degree [K]**
1	0	0	0
2	0	2	5
3	0	5	2
4	2.5	2	5
5	2.5	5	2
6	5	0	0
7	5	2	5
8	5	5	2

Fig. 6-8 to Fig. 6-10 demonstrate the effects of various scenarios on heat transfer rate in the evaporator and the heat storage, compressor power and the performance of the flexible heat pump. The first scenario, representing the ideal case, shows the greatest improvement in COP, as seen in Fig. 6-10, with a value of 24.1 % and a maximum improvement storage temperature of 35.4 °C, the highest among all the scenarios. This scenario also has the lowest compressor power during discharging in Fig. 6-9, at 1.27 kW, close to Scenario 3, which is at 1.28 kW. This makes Scenario 1 the best in terms of overall performance compared to a conventional heat pump. While the average COP for this scenario is 3.36, it is not the highest, Scenarios 2, 3, and 4 achieve higher COP values of 3.48, 3.43, and 3.41, respectively. The compressor power in Scenario 1 during charging is also the highest, at 3.14 kW, which is comparable to Scenario 6. This similarity is due to both scenarios having no superheat or subcooling in the condenser. Moreover, the heat transfer in the evaporator in Mode 1 is the highest at 8.9 kW, and the discharging heat rate in the heat storage is 7.2 kW, as seen in Fig. 6-8. This is because, at higher storage temperatures and without superheating or subcooling degrees, the heat transfer rates are at the highest.

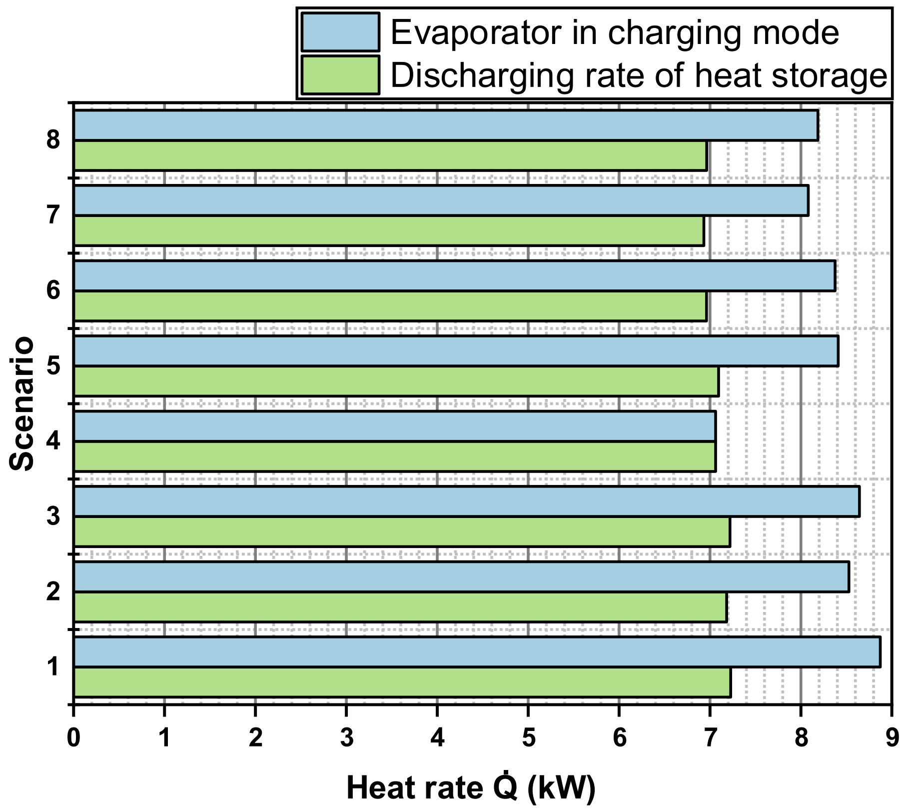

Fig. 6-8: Impact of different scenarios on evaporating rate in Mode 1 and discharging rate of heat storage in Mode 2

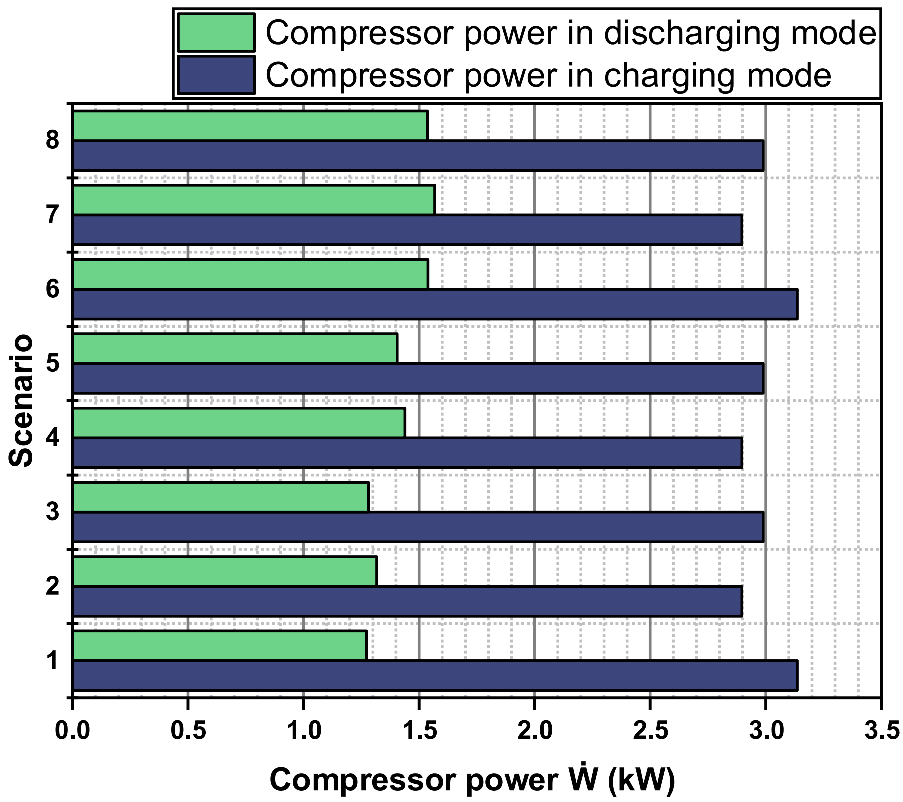

Fig. 6-9: Impact of different scenarios on compressor power in Modes 1 and 2

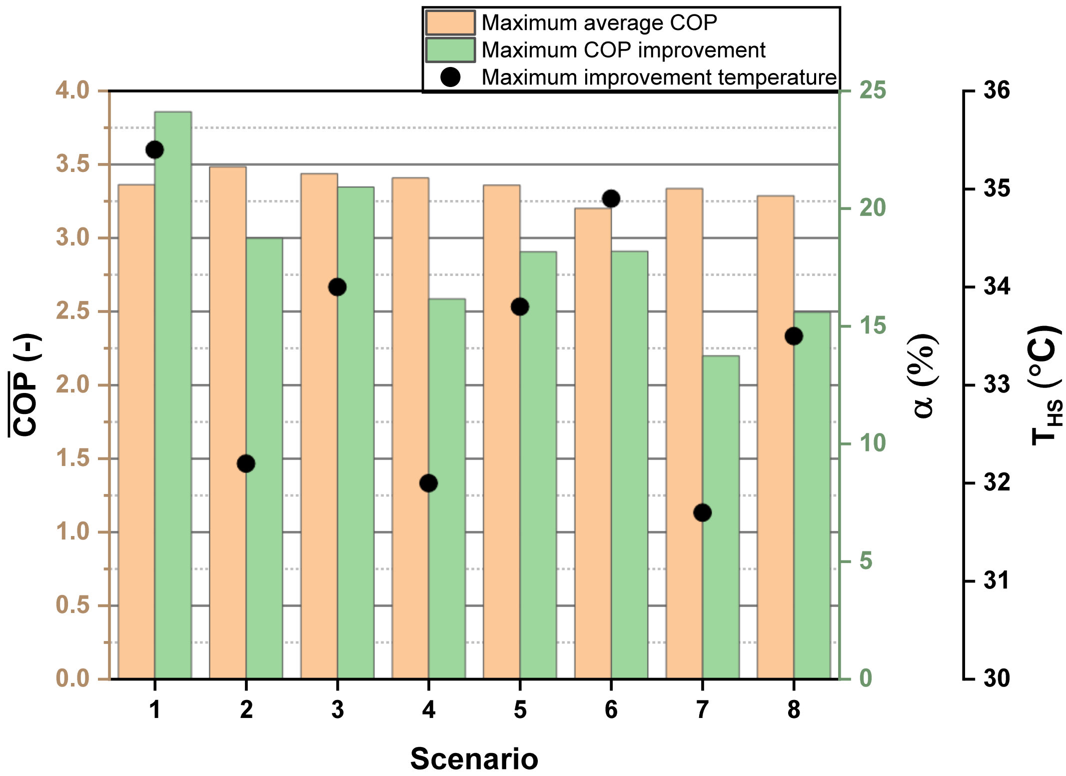

Fig. 6-10: Impact of different scenarios on average COP and improvement, and $T_{max,\alpha}$

For the other scenarios, an increase in ΔT_{HS}, superheating and subcooling degrees generally reduces the mass flow rate, the maximum improvement storage temperature, and the overall improvement. In Fig. 6-10, Scenarios 7 and 8 show the least improvement, with 13.7 % and 15.6 %, respectively. Scenario 7, in particular, faces a 43 % drop in efficiency compared to Scenario 1. Their top performing storage temperatures are 31.7 °C and 33.5 °C, with Scenario 7 having the lowest temperature. Both scenarios also have the highest ΔT_{HS} value tested ($\Delta T_{HS} = 5$ K), combined with non-zero degrees of superheating and subcooling. This results in a lower heat recovery efficiency in Mode 1. As seen in Fig. 6-9, they also have the highest compressor power values observed in Mode 2 with 1.57 kW and 1.54 kW, respectively. The lower storage temperature during discharging further contributes to higher compressor power. In Fig. 6-8, their heat transfer rates in the evaporator are around 8 kW and 8.2 kW, respectively, and 7 kW in the heat storage during discharging for both. This is due to the reduced mass flow rate in both modes, the lower temperature difference in the storage during Mode 1, and the lower storage temperature, which reduces the latent heat of vaporisation in Mode 2.

Scenario 6 also has a ΔT_{HS} of 5 K but no superheating or subcooling degrees, which results in a higher COP improvement of 18.2 % and a maximum improvement temperature of 34.9 °C. While the average COP is the lowest, at 3.2, the improvement remains significant.

This is because the modelled conventional heat pump does not benefit from power reductions with the absence of subcooling and superheating. In this scenario, the heat recovery is reduced, and the compressor power increases due to the high ΔT_{HS}, the lack of mass flow rate reduction (which would normally be caused by non-zero subcooling or superheating degrees) keeps compressor power high in both charging (3.1 kW) and discharging (1.5 kW). The heat transfer in the evaporator, 8.4 kW, and discharging heat rate, 7 kW, are moderate due to the high ΔT_{HS}, though they remain slightly higher than other scenarios due to the absence of mass flow rate reduction.

Scenarios 2 and 3 both achieve higher average COP than the ideal scenario, with improvements of 18.7 % and 21 %, respectively. These higher average COP are due to lower compressor power during charging compared to the ideal scenario, driven by reductions in the mass flow rate. Scenario 2 achieves a slightly better average COP, as subcooling in the condenser has a greater impact on compressor power reduction during charging than the increase in superheating degree. However, Scenario 3 shows greater overall improvement because its top performing storage temperature (34 °C) is higher than in Scenario 2 (32.2 °C), leading to less compressor power during discharging. Although both scenarios perform well, they assume that heat transfer in the storage is 100 % efficient, which is not realistic.

A more realistic case is represented by Scenario 5, which achieves an 18.2 % improvement and an average COP of 3.36, the same as the ideal scenario. In this case, there is a good balance in compressor power consumption, with 3 kW in Mode 1 and 1.4 kW in Mode 2. The ΔT_{HS} is moderate, and the subcooling in the condenser is kept at a minimal 2 K to allow for maximum heat recovery. The top performing storage temperature is 33.8 °C, close to the ideal scenario, with only a 4.5 % reduction. This ensures that the melting temperature of the chosen PCM remains within the same range. The heat transfer in the evaporator is 8.4 kW, and the discharging rate in the heat storage is 7.1 kW. Both are moderate compared to other scenarios, yet still relatively high.

Scenario 4 is also a realistic case demonstrating good performance. Although it has the third-lowest improvement at 16.2 %, its average COP of 3.41 is higher than that of the ideal scenario. Its maximum improvement storage temperature is 32 °C, the second lowest, due to significant subcooling in the condenser of 5 K. Its discharging compressor power is 1.4 kW, higher than in the ideal case, but its charging compressor power is among the lowest, at 2.9 kW. This is because of the large subcooling, which reduces the mass flow rate, leading to a better COP. However, a conventional heat pump would benefit more from this reduction.

The discharging heat rate is among the lowest at 7 kW, largely due to the reduced mass flow rate. Similarly, the heat transfer rate in the evaporator during charging is the lowest observed, also at 7 kW.

In summary, the best-performing scenarios are those with minimal ΔT_{HS}, with this parameter having a greater impact in Mode 2. When combined with subcooling in the condenser, the impact is positive on the average COP but negative on the COP improvement. The superheating degree has less effect on both. Any scenario with parameters in the tested range will provide performance gains. However, it is important to adjust these parameters according to the heat pump's operating conditions. A balance must be found between subcooling's effect on compressor power, heat transfer in the evaporator, heat recovery in the storage, and overall improvement. While reductions in compressor power and heat transfer rate can have a positive or neutral effect, the decline in heat recovery can limit the overall improvement and benefits of the flexible heat pump's power-saving mode.

Fig. 6-11 to Fig. 6-15 illustrate the impact on performance of different scenarios applied to the flexible heat pump with various refrigerants. The scenarios presented are the same as those outlined in Table 6-4. As in the previous analysis with R1234yf in Fig. 6-8 to Fig. 6-10, Scenario 1 represents the ideal case and serves as the benchmark for all refrigerants. Similarly, Scenario 7 shows the least improvement, while Scenario 5 offers the best realistic improvement.

Fig. 6-11, shows the performance of propane. In the ideal case, the maximum improvement storage temperature is 35.3 °C, very close to that of R1234yf, with an average COP of 3.45 and an improvement of 18.2 %. This drops to 10.5 % in Scenario 7 and 13.9 % in Scenario 5, with a top performing storage temperature of 33.6 °C. For R32, in Fig. 6-12, the best improvement is 14.8 % with a best performing storage temperature of 36.6 °C, dropping to 8.3 % in Scenario 7 and 11.2 % in Scenario 5, where the maximum improvement storage temperature is 34.6 °C. For R134a, in Fig. 6-13, the maximum improvement is 17.5 % with a corresponding storage temperature of 34.7 °C, dropping to 10.2 % in Scenario 7 and 13.5 % in Scenario 5, with a storage temperature of 33.2 °C. For R410a, in Fig. 6-14, the ideal scenario shows a 22.4 % improvement with a corresponding storage temperature of 39 °C, dropping to 11.6 % in Scenario 7 and 16 % in Scenario 5, with a top performing storage temperature of 36 °C. Finally, for R1234ze(E), in Fig. 6-15, the best improvement is 18.9 % with a corresponding storage temperature of 34.4 °C, dropping to 11 % in Scenario 7 and 14.5 % in Scenario 5, with a storage temperature of 33 °C.

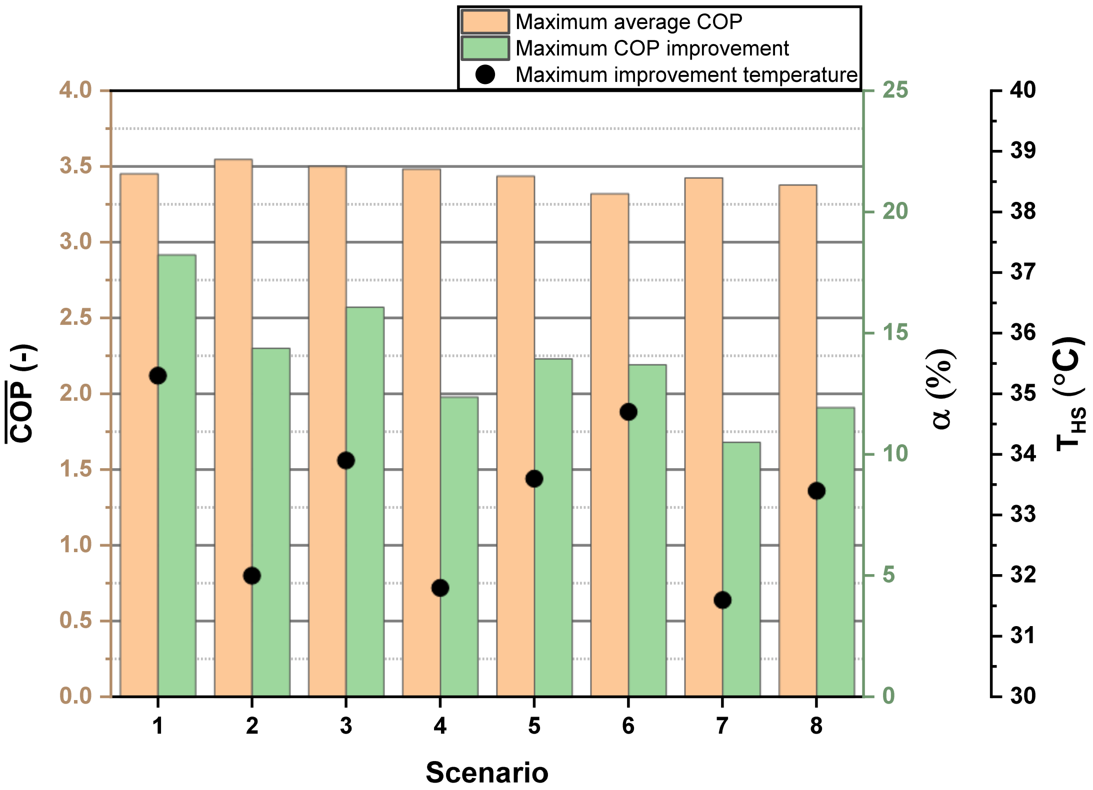

Fig. 6-11: Scenarios impact on average COP and improvement, and $T_{max,\alpha}$ for propane

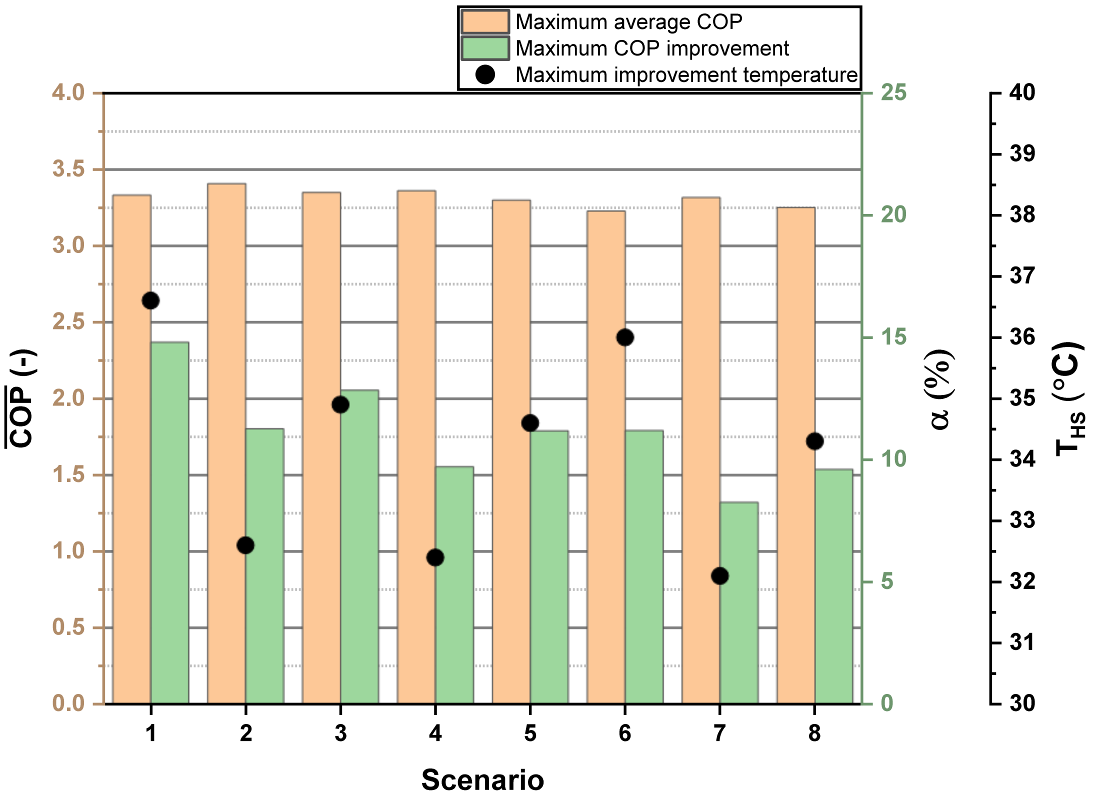

Fig. 6-12: Scenarios impact on the average COP and improvement, and $T_{max,\alpha}$ for R32

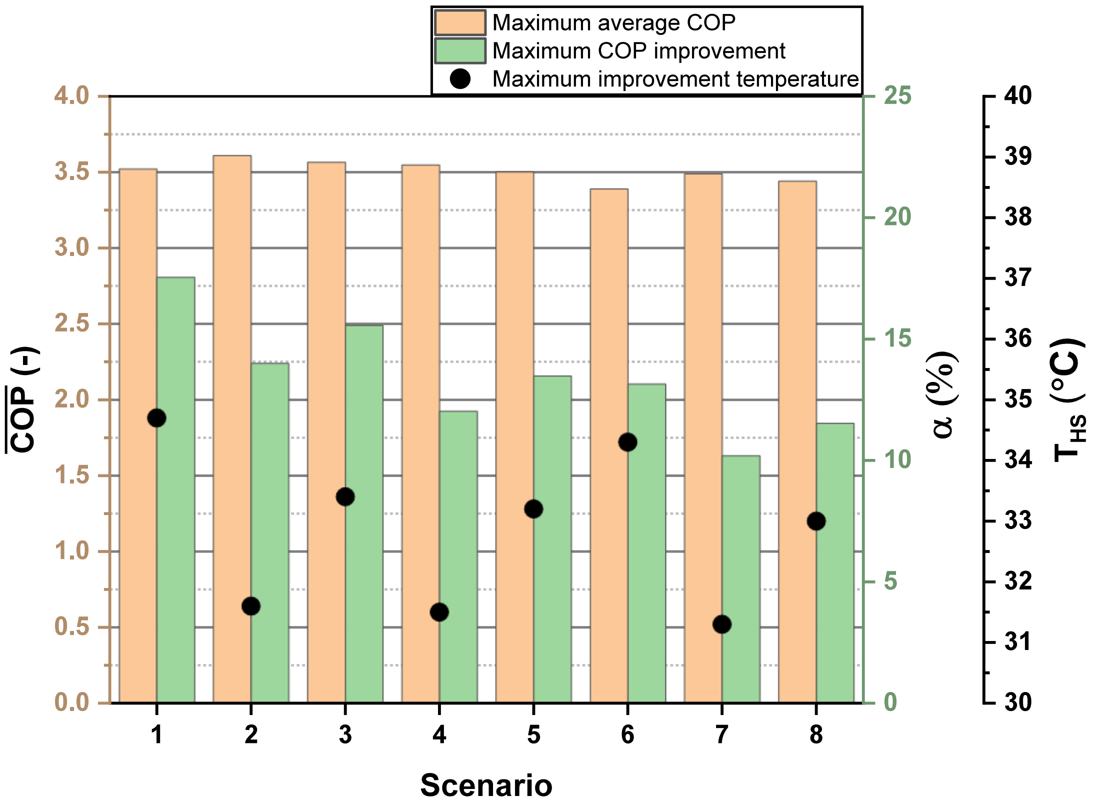

Fig. 6-13: Scenarios impact on average COP and improvement, and $T_{max,\alpha}$ for R134a

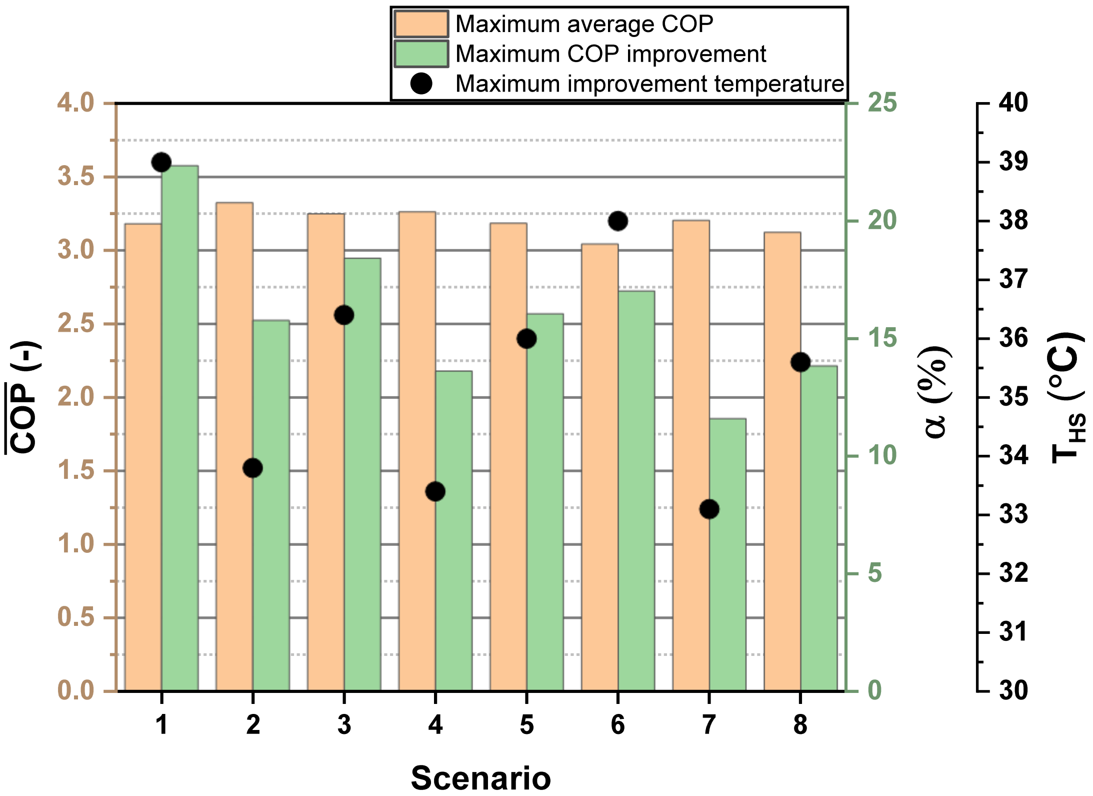

Fig. 6-14: Scenarios impact on average COP and improvement, and $T_{max,\alpha}$ for: R410a

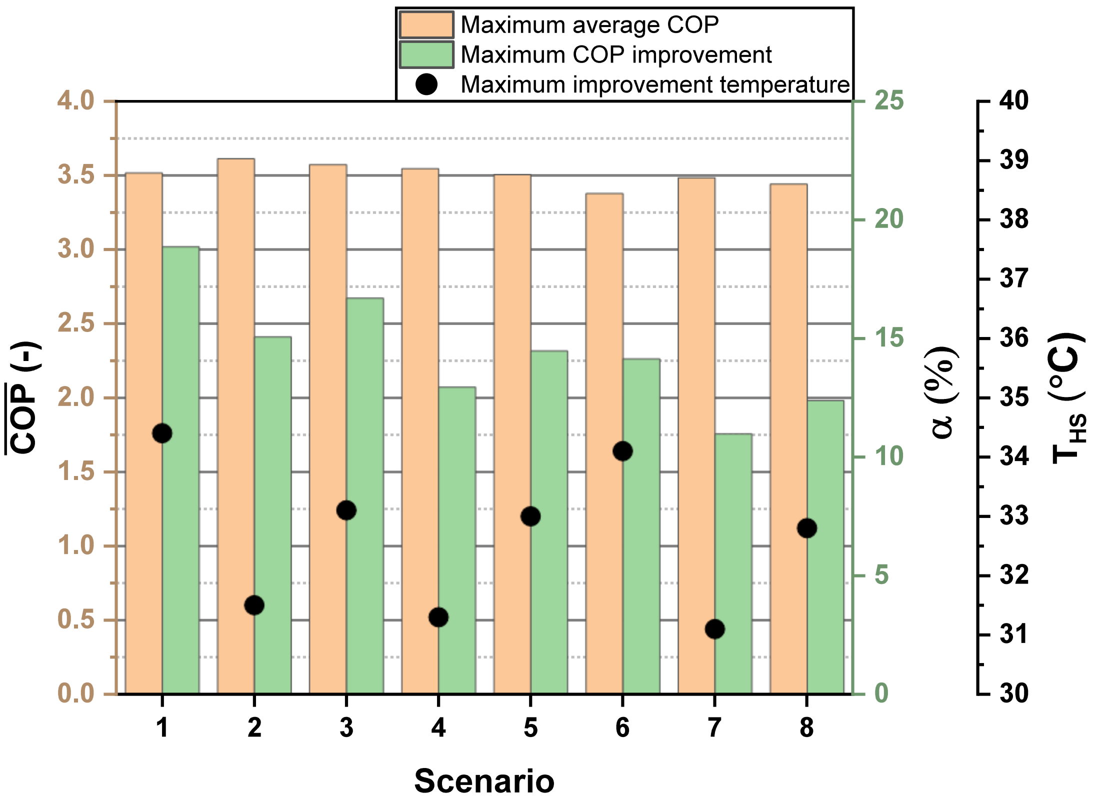

Fig. 6-15: Scenarios impact on average COP and improvement, and $T_{max,\alpha}$ for R1234ze(E)

It is noteworthy that R1234ze(E), a low-GWP substitute for R134a, has top performing storage temperatures very close to R134a, with the largest difference, across all scenarios, being just 0.3 °C, likely due to their similar properties as listed in Table 3-6.

While subcooling and superheating degrees, as well as ΔT_{HS}, have similar effects on each refrigerant, their overall performance with the flexible heat pump varies. As discussed in Chapter 4, R410a shows the greatest improvement after R1234yf, largely due to its strong heat recovery during charging. This is attributed to its significant specific heat capacity at the heat storage inlet, and its low latent heat of vaporisation at the condensing temperature, resulting in a high mass flow rate. R410a is followed by R1234ze(E), propane, R134a, and finally R32. The differences in performance among these refrigerants arise primarily from their properties, which affect heat recovery at the storage inlet and power consumption in Mode 2, especially through the shape of their isentropic lines. For example, in Chapter 4, R32 had a poor heat recovery process due to its high latent heat of vaporisation at 35 °C, combined with high power consumption during discharging due to the deviation of its isentropic lines. This resulted in the lowest improvement. At 65 °C, however, R32's enthalpy of vaporisation is not the highest of all tested refrigerant, and its specific heat capacity is the second highest, leading to decent heat recovery. Nonetheless, the deviation of its isentropic lines has a stronger impact on its overall improvement, lowering its performance compared to other refrigerants. Propane, for instance, has the highest enthalpy of vaporisation and a lower specific heat capacity than R32, yet it still outperforms R32 with an ideal improvement of 18.2 %, 23 % higher than that of R32. This is because the isentropic lines of propane deviate less from its saturation curves, allowing it to benefit more from an increase in evaporating temperature. The properties of all refrigerants mentioned are detailed in Table 3-6.

Regarding maximum improvement storage temperatures, the correlation identified in Fig. 6-1 is validated here, as the $T_{max,\alpha}$ of all refrigerants is close but superior to the midpoint between the refrigerant's inlet temperature at the storage and the evaporating temperature. R1234ze(E) has the lowest top performing storage temperature, closely followed by R134a. The differences in $T_{max,\alpha}$ between refrigerants are generally small, except for R410a, which shows a much higher maximum improvement storage temperature in the ideal case, at 39 °C in Scenario 1. This is due to R410a's high heat recovery efficiency at this condensing temperature, which allows it to recover significant amounts of heat with a smaller temperature difference. Therefore, the storage temperature for the maximum improvement is influenced by the refrigerant’s temperature at the heat storage inlet, its thermal properties at this temperature, and the evaporating temperature in Mode 1.

6.3.2 Economic and environmental analysis

In this section, an economic and environmental analysis is carried out for the flexible heat pump using R1234yf, compared to a conventional ASHPWH and a gas boiler in a UK application. The charging and discharging times are set according to Eq. (6.1) to simplify the calculation of energy consumption costs.

6.3.2.1 Economic analysis

Table 6-5 lists the main additional components required for the flexible heat pump compared to a conventional ASHPWH. To enhance heat transfer in the evaporator during Mode 1, the chosen strategy was to increase the heat transfer area, as discussed in Chapter 3, which subsequently affects the component cost. Table 6-6 provides the initial equipment cost (CapEx) and the annual capital and maintenance cost rate, which includes the CRF and maintenance factor, for each heating system.

In Table 6-6, the boiler price is based on a 24 kW combi boiler, which provides both DHW and space heating. This is the smallest capacity available on the market for this type of boiler[286]. However, the high heating capacity does not impact the gas boiler's operating cost, which is solely linked to the average household energy consumption and boiler efficiency, as shown in Eq. (3.96). The heating capacity primarily affects the CapEx, annual capital cost and maintenance cost rate, but it remains the lowest and most affordable option available in the UK for combi gas boilers.

Table 6-5: Additional components of the flexible heat pump

Components	**Classic ASHPWH**	**Flexible heat pump**	**Variations**
Compressor	X	X	-
Condenser	X	X	-
Heat storage tank	-	X	+Additional heat storage tank
Expansion valve	X	X	-
Evaporator	X	X	+ Increased heat transfer area

Table 6-6: CapEx and annual capital and maintenance cost rate for a gas boiler, a conventional ASHPWH and the flexible heat pump

Heating system	**CapEx [£]**	**Capital and maintenance cost rate [£/year]**
Gas boiler	720	89.2
Conventional ASHPWH	2163.2	233.6
Flexible heat pump	3228.4	348.5

The equipment cost of the flexible heat pump is based on the ideal case (Scenario 1 in Table 6-7), including the sizes of the heat storage tank, evaporator, and condenser. Installation costs have not been considered, as they vary greatly depending on the company and specific conditions. However, heat pump installation tends to be much more expensive than that of gas boilers, especially in the UK[240]. This is largely due to a smaller number of qualified technicians for heat pumps. Gas boilers remain the most commonly used heating system in the UK. Over the past decades, they have been mass-produced, making them a mature and cost-effective technology[287]. According to Renaldi et al.[240], the higher installation cost of air-source heat pumps is partly due to the fact that most installers are small local companies with limited competition. As more competitors and qualified technicians enter the market, heat pump installation costs may decrease, they said.

Table 6-6 shows that the CapEx and annual cost rate of a gas boiler are considerably lower than those of heat pumps. The annual cost rate for a gas boiler is approximately 62 % lower than that of a conventional ASHPWH and 74 % lower than that of the flexible heat pump. Moreover, the current electricity market in the UK poses a challenge for the deployment of heat pumps, as electricity prices are around four times higher than those of natural gas on a per kWh basis (as shown in Table 6-2). The UK government has introduced incentives, such as the BUS[288], which offers up to £7,500 off the cost of equipment and installation for air-source heat pumps and ground-source heat pumps. Additionally, as manufacturing capacity increases and more heat pumps are available on the market, the equipment costs may gradually decrease. Nonetheless, policymakers should recognise the economic disadvantage of heat pumps compared to gas boilers and implement policies that promote the widespread adoption of low-carbon heating technologies.

In Table 6-6, it is also shown that the CapEx and annual cost rate of the flexible heat pump are 49 % higher than those of a conventional ASHPWH. This increase is primarily due to the addition of the heat storage and the cost of 53 kg of the selected PCM tank, which alone accounts for about one-quarter of the total price of the flexible heat pump. Although this additional equipment is costly, there may be opportunities to replace the PCM with cheaper alternatives, or to use a water tank for storing sensible heat in the system instead.

The following sections evaluate the operational costs and environmental impacts for different scenarios involving the flexible heat pump and the conventional ASHPWH. The scenarios considered are outlined in Table 6-7.

Table 6-7: Economic and environmental analysis scenarios

Scenario	ΔT_{HS} [K]	Superheat degree [K]	Subcool degree [K]
1	0	0	0
2	0	2	2
3	2.5	2	2
4	5	2	2

Based on the analysis from Section 6.3.1.4 and Table 6-7, the most realistic scenario with the best improvement is Scenario 3, where ΔT_{HS}, subcooling and superheating degrees are kept to a minimum, providing the greatest improvement compared to a conventional heat pump. The other scenarios are included for comparison to assess their impact on operating costs, total expenses, and emissions, with Scenario 1 representing the ideal case.

In Fig. 6-16 and Fig. 6-17, the impact of the various scenarios from Table 6-7 on annual operating costs and energy consumption is shown for both heat pump systems and compared with a gas boiler. The operating costs have been calculated with and without the penalty price for CO_2e emissions.

In Fig. 6-16, in the first case (without CO_2e penalties), the gas boiler is consistently cheaper than the conventional ASHPWH in all scenarios, with an average operating cost of £1,131/year, £263 less than the conventional ASHPWH in Scenario 1. As subcooling and superheating degrees increase in the following scenarios, the conventional ASHPWH has an operating cost of £1,343, still £212 higher than the gas boiler. In comparison, the flexible heat pump performs much closer to the gas boiler and is even cheaper in the first two scenarios thanks to its power-saving mode, which helps reduce electricity costs. In Scenario 2, with only subcooling and superheating degrees increased, the operating cost decreases to £1,105/year, £26 cheaper than the gas boiler. In Scenario 3, accounting for ΔT_{HS}, it rises slightly to £1,131/year, matching the gas boiler and staying £212 lower than the conventional ASHPWH. Even in the worst-case Scenario 4, the flexible heat pump's operating cost is £1,157/year, still lower than that of the conventional ASHPWH and only £26 more than the gas boiler.

Despite its lower operating cost, the gas boiler has significantly higher annual energy consumption compared to both heat pumps in all scenarios, as shown in Fig. 6-17. The gas boiler consumes roughly 18,809 kWh/year, while the best-case consumption for the conventional ASHPWH is 6,151 kWh/year, and for the flexible heat pump in Scenario 3, it is 5,181 kWh/year. This gap is primarily due to the much lower price of natural gas compared to electricity in the UK. As a result, higher consumption has a less significant impact on the operating cost for gas systems compared to electric heat pumps. Electricity prices and energy performances play a crucial role in determining the economic appeal of heat pumps, even though their energy consumption is lower. The flexible heat pump's power-saving mode reduces energy consumption by an average of 17 % per year compared to the conventional ASHPWH, which is directly reflected in the reduced operating cost.

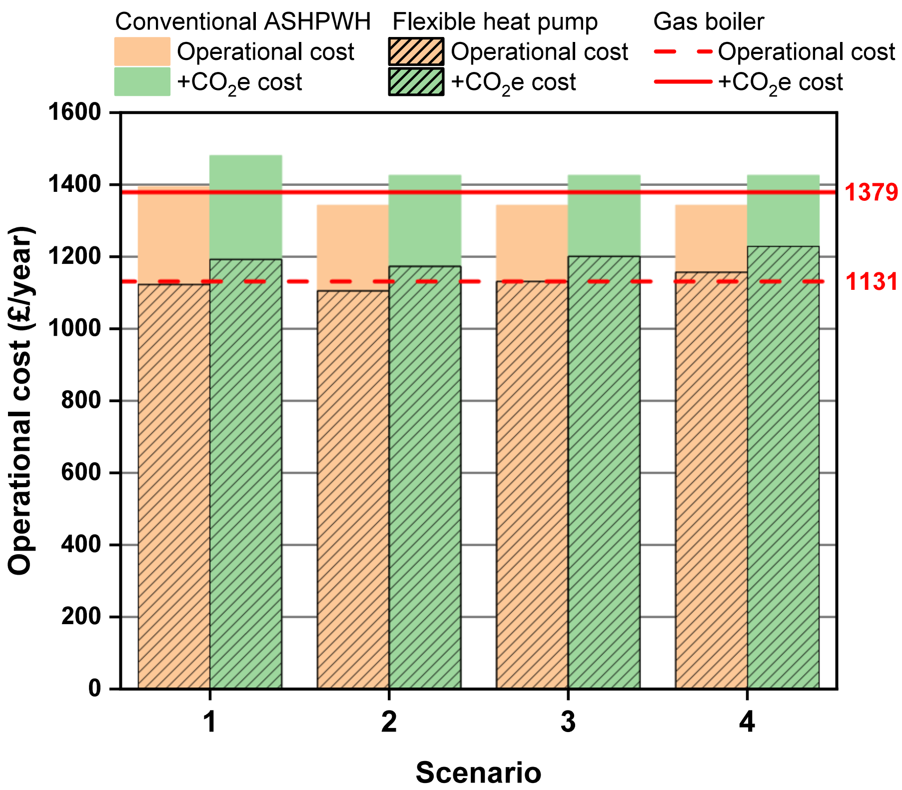

Fig. 6-16: Operational cost per year of a gas boiler, conventional ASHPWH and flexible heat pump with and without CO_2e cost

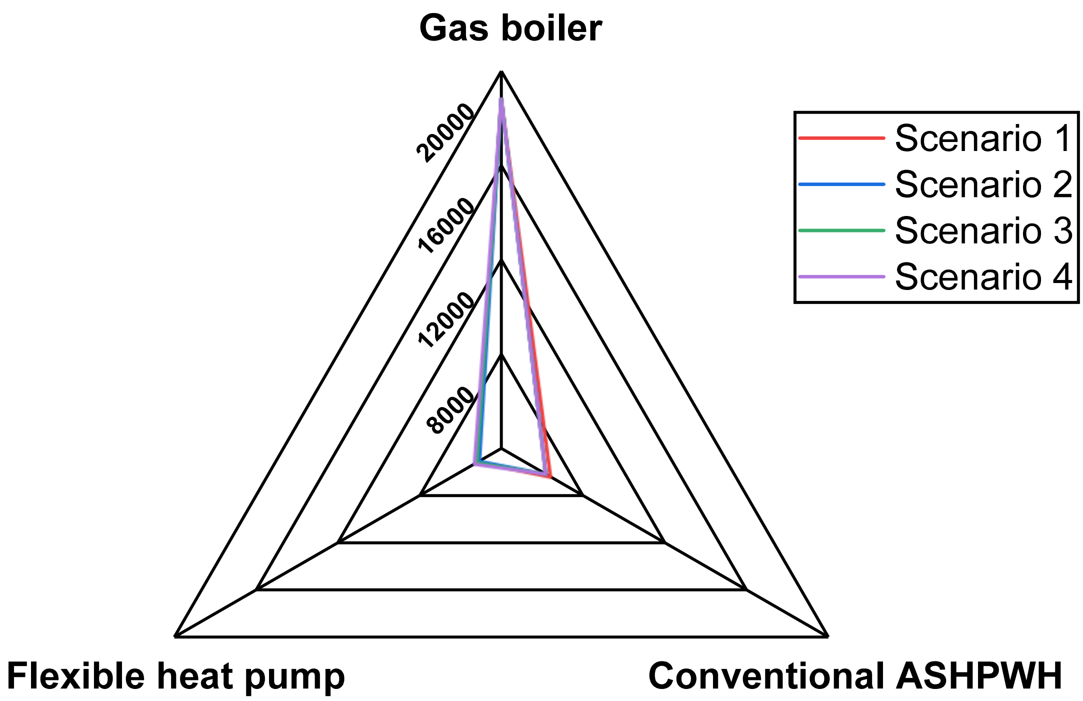

Fig. 6-17: Scenarios impact on annual energy consumption in kWh/year

However, with a focus on transitioning to low-emission technologies, environmental impact must be considered when comparing heating systems. The social cost of CO_2e emissions is an important factor and has been added to the operating costs in Fig. 6-16. When accounting for CO_2e penalties, the gas boiler's operating cost rises by approximately 22 % to £1,379/year due to its high energy consumption. While this is still lower than the conventional ASHPWH, which has an operating cost of £1,425/year in the best scenarios, it is more expensive than the flexible heat pump in all cases. For instance, in Scenario 3, the flexible heat pump's operating cost is £1,200/year, £179 less than the gas boiler. This reduction is achieved through the power-saving mode of the flexible heat pump.

Finally, the difference in operating costs across scenarios is relatively small, with a range of just £55 between the best (Scenario 2) and worst (Scenario 4) cases for the flexible heat pump, indicating that scenario variation has a limited impact on operating costs. The flexible heat pump’s power-saving mode shows promise in reducing operating costs, and when combined with government grants and potential future reductions in electricity prices, it could significantly enhance the economic attractiveness of heat pumps compared to gas boilers.

In Table 6-8 and Table 6-9, the total annual expenses for both heat pumps and the payback period for the flexible heat pump, compared to a conventional ASHPWH, are presented across different scenarios. The payback period is calculated based on the CapEx and annual cost savings. As shown, despite the higher initial cost of the flexible heat pump, the payback period remains within a reasonable range, varying from 3.7 to 4.4 years depending on the scenario, with an average of 4 years. The payback period increases as the difference in total annual cost rates between the two heat pumps decreases. Notably, the ideal Scenario 1 negatively affects the conventional ASHPWH’s cost efficiency, as it does not lead to a reduction in energy consumption. In the other scenarios, the annual cost for the conventional ASHPWH decreases to £1,664.1/year.

For the flexible heat pump, Scenario 1 offers the shortest payback period of 3.7 years, though it is not the minimised in terms of annual cost rate with £1,540.8/year. Scenario 2 is the best scenario with the lowest annual cost rate of £1,520.4/year, largely due to significant energy savings from subcooling, superheating, and an ideal heat storage tank. However, this is not a realistic scenario. Scenario 3, which is more practical, shows an annual cost of £1,540.5/year, slightly lower than Scenario 1. The difference between the best and worst scenarios is minimal, only £19/year, and in all cases, the flexible heat pump’s annual cost rate remains lower than that of the conventional ASHPWH. Thus, the variation between scenarios, in that range, has a limited impact on both the annual cost and the payback period.

Table 6-8: Total annual cost rate for the conventional ASHPWH and flexible heat pump across various scenarios

Scenario	Total annual cost rate [£/year]	
	Conventional ASHPWH	Flexible heat pump
1	1713.6	1540.8
2	1664.1	1520.4
3	1664.1	1540.5
4	1664.1	1559.7

Table 6-9: Payback period based on a conventional ASHPWH depending on scenario

Scenario	Payback period [years]
1	3.7
2	4
3	4.2
4	4.4

In conclusion, even when considering a pessimistic scenario with the highest equipment cost for the flexible heat pump, including the relatively expensive PCM tank and the increased evaporator heat transfer area, it consistently achieves a lower annual cost rate than the conventional ASHPWH because of its operating cost saving. An average payback period of 4 years demonstrates the economic viability of the power-saving mode of the flexible heat pump compared to a conventional ASHPWH, confirming its potential attractiveness.

6.3.2.2 Environmental analysis

This section evaluates the environmental impact of the flexible heat pump in comparison to a conventional ASHPWH and a gas boiler.

Fig. 6-18 illustrates the annual CO_2e emissions for these systems across different scenarios, based on the emission factors of natural gas and electricity. For the heat pumps, CO_2e emissions arise from the indirect emissions associated with electricity production, linked to their power consumption. In contrast, the gas boiler's emissions are based on the direct combustion of natural gas and its energy consumption.

Firstly, the gas boiler's emissions are significantly higher than both the conventional ASHPWH and the flexible heat pump, regardless of the scenario. The gas boiler emits around 3.8 tons of CO_2e per year for DHW and space heating, in Edinburgh. In comparison, under the worst-case scenarios, Scenario 1 for the conventional ASHPWH and Scenario 4 for the flexible heat pump, emissions are approximately 1.3 tons and 1.1 tons per year, respectively, both below 1.5 tons/year. Despite the high carbon emission factor of electricity production in the UK, which is slightly higher than that of natural gas, the lower energy consumption of the heat pumps results in their annual emissions being nearly three times lower than those of the gas boiler.

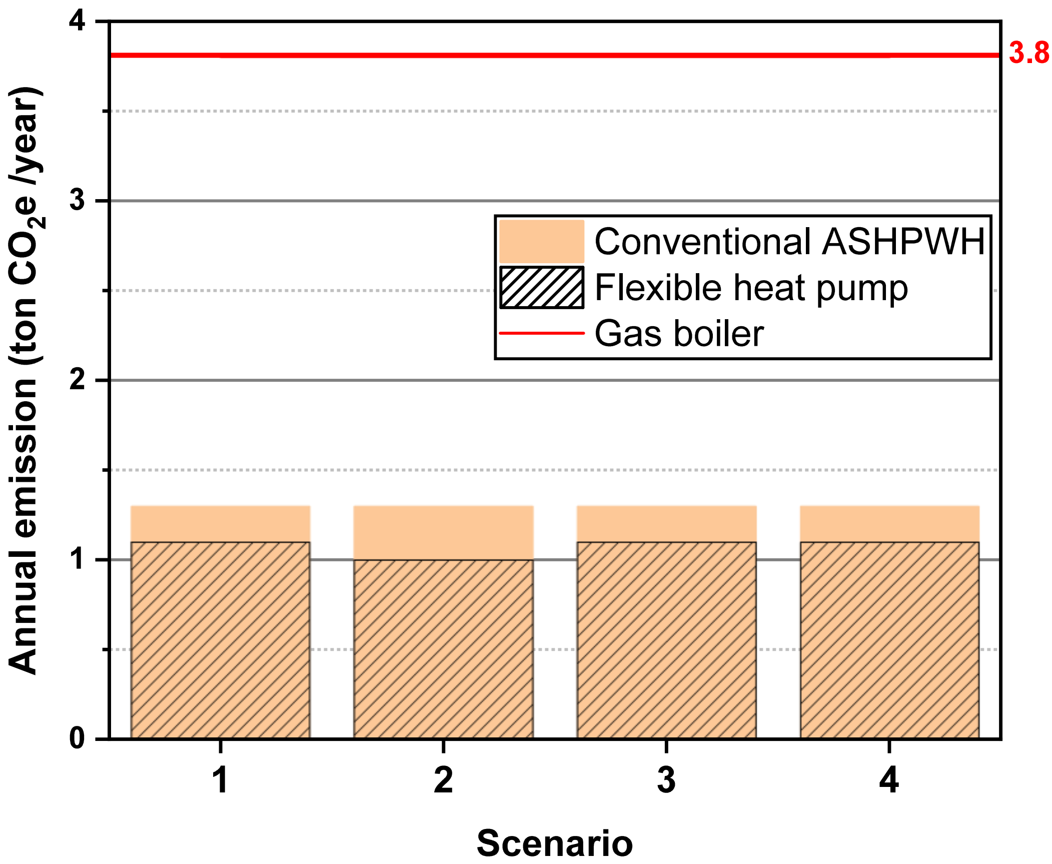

Fig. 6-18: Annual CO_2e emissions of gas boiler, conventional ASHPWH and flexible heat pump across different scenarios

When comparing the conventional ASHPWH with the flexible heat pump, it is clear that the flexible heat pump consistently leads to less CO_2e emissions in all scenarios. This reduction is especially pronounced in Scenario 2, where the conventional ASHPWH is responsible for 1.3 tons/year, while the flexible heat pump causes about 1 ton/year, 23 % lower. In Scenario 3, the emission reduction is around 15 %, with 1.3 tons/year for the conventional ASHPWH and 1.1 tons/year for the flexible heat pump. The substantial decrease in emissions is directly due to the flexible heat pump's reduced power consumption, which is particularly beneficial in the UK, where the carbon emission factor for electricity production is relatively high. As a result, any reduction in annual energy consumption directly leads to a significant reduction in annual CO_2e emissions.

In conclusion, the flexible heat pump demonstrates a considerable potential to reduce CO_2e emissions compared to a conventional ASHPWH, particularly in countries where electricity production has a high carbon footprint.

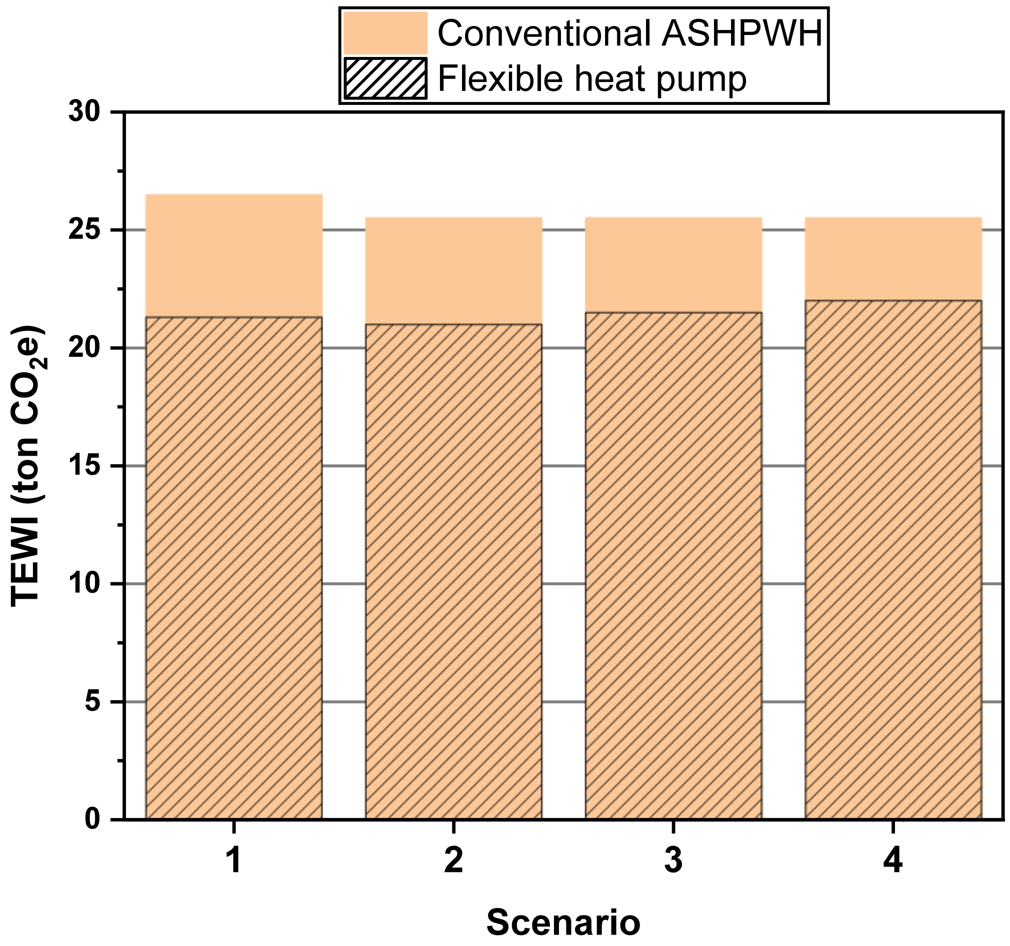

Fig. 6-19: TEWI of a conventional ASHPWH and flexible heat pump across different scenarios

Fig. 6-19 illustrates the TEWI of a conventional ASHPWH and the flexible heat pump across different scenarios. TEWI accounts for both direct and indirect CO_2e emissions over the entire operating life of a system, providing a more comprehensive measure of the environmental impact of heat pumps. The goal is to achieve the lowest possible TEWI value.

Direct emissions are caused by refrigerant leakage and represent the CO_2e emissions released into the atmosphere due to refrigerant losses during operation and recycling.

Indirect emissions are generated by the electricity production required to power the system, which depends on its energy consumption. Since the same refrigerant is used in both systems and Mode 1 of the flexible heat pump is comparable to the running mode of the conventional ASHPWH, both systems are charged with the same amount of refrigerant, due to their equal heating capacities. As a result, the direct emissions from refrigerant leakage are identical for both heat pumps, amounting to 42.2 kg of CO_2e over their lifetimes, which is relatively low. This small value is due to the heat pumps' small heating capacity, low refrigerant's GWP and low refrigerant charge, as well as high recycling efficiency. These direct emissions account for only 1.7 % of the TEWI for the conventional ASHPWH and 2 % for the flexible heat pump in Scenario 1. Therefore, their contribution is minimal and primarily influenced by the choice of refrigerant. In this case, the main impact on TEWI comes from indirect emissions.

The key difference lies in the indirect emissions, which are directly related to the energy consumption of the heat pumps and shown in Fig. 6-18. As illustrated in Fig. 6-19, the TEWI of the flexible heat pump is consistently lower than that of the conventional ASHPWH across all scenarios, thanks to its reduced energy consumption from its power-saving mode. In Scenario 1, the ideal case for the flexible heat pump, its TEWI is 21.3 tons of CO2e, while the TEWI of the conventional ASHPWH is 26.5 tons, a 20 % reduction for the flexible heat pump. In the more realistic Scenario 3, the TEWI for the conventional ASHPWH is 25.5 tons, compared to 21.5 tons for the flexible heat pump, resulting in a 16 % reduction.

In conclusion, the reduction in power consumption by the flexible heat pump has a significant positive impact on the environmental footprint of the heat pump, leading to important emissions reductions both annually and over the system's lifetime. Thus, the reduction in power consumption from heat pumps, such as the flexible heat pump, combined with a potential decrease in the electricity production's emission factor, could further minimised the environmental impact of heat pumps.

Therefore, the flexible heat pump's power-saving mode shows great potential to enhance both the economic and environmental appeal of heat pumps for future applications in the UK.

6.4 Summary

In this chapter, the power-saving application of the flexible heat pump operating in Modes 1 and 2 with latent heat storage was thoroughly evaluated. The primary objective was to investigate its thermodynamic performance and compare it to that of a conventional heat pump. The evaluation was conducted under both ideal conditions and by varying parameters, including condensing and evaporating temperatures, storage temperature, ΔT_{HS}, and the degrees of superheating in the evaporator and subcooling in the condenser. The refrigerants tested included R1234yf, R134a, R410a, R1234ze(E), propane, and R32. To address research question 2, an economic and environmental analysis was also performed to assess the attractiveness of the flexible heat pump in its power-saving mode compared to a conventional ASHPWH and a new A-rated gas boiler, for an application in Edinburgh. The following conclusions were made:

- The storage temperature for the maximum improvement ($T_{max,\alpha}$) of the flexible heat pump increases with higher condensing and evaporating temperatures. $T_{max,\alpha}$ was consistently close to, but slightly above, the midpoint between the refrigerant temperature at the storage inlet and the evaporating temperature in Mode 1, for all refrigerants tested. The results confirmed that $T_{max,\alpha}$ is influenced by both the heat recovery process in Mode 1 and the power consumption in Mode 2, depending on the properties of the refrigerant. Among the refrigerants tested, R1234yf outperformed the others, followed by R410a, R1234ze(E), propane, R134a, and R32.

- When considering variations in ΔT_{HS}, as well as the degrees of superheating in the evaporator and subcooling in the condenser, the best-performing scenarios were those with minimal ΔT_{HS}. Subcooling in the condenser positively influenced the average COP but negatively impacted overall COP improvement. The superheating degree had a lesser effect on both average COP and improvement. These effects were verified across all tested refrigerants.

- Despite selecting a maximum initial equipment cost scenario, the flexible heat pump consistently achieved a lower total annual cost rate compared to the conventional ASHPWH, primarily due to its operating cost saving. The average payback period was approximately 4 years, confirming the system's economic viability. This could be further enhanced by: considering potential government incentives and potential reductions in electricity prices; cost savings from a more affordable PCM tank or alternative heat storage options; exploring different heat transfer enhancement strategies in the evaporator.

- The operating cost of the flexible heat pump was lower or equal to that of a gas boiler in the UK, across three of the four tested scenarios and only slightly higher in the fourth.

When the social cost of CO_2e emissions was accounted for, the flexible heat pump was more economical in all tested scenarios, further enhancing its financial attractiveness.

- The TEWI of the flexible heat pump was consistently lower than that of the conventional ASHPWH in all scenarios, primarily due to its reduced power consumption. If combined with potential reductions in the CO_2e emission factor of electricity production, the flexible heat pump could help further reduce the environmental impact of heat pumps.

Chapter 7 Energy analysis of storage charging at lower temperature during off-heating periods

This chapter presents the performance and thermodynamic insights of the multi-valve flexible heat pump system with integrated latent and sensible heat storage when it is charged at lower temperature in Mode 4. Building upon the analysis in Chapter 6, this chapter differentiates by focusing on the different charging process from Mode 4, also known as the lower temperature charging mode, which is an alternative to Mode 1 when heating is not required. The chapter provides a detailed examination of the system's performance and operational processes, analysing various internal parameters and their impacts. It also compares the performance of the refrigerant R1234yf with other refrigerants namely R134a, R1234ze(E), propane, R32, and R410a. The primary objective of this chapter is to assess the differences in operational performance when using Mode 4 for charging instead of Mode 1, further addressing research question 2.

7.1 Introduction

In Chapter 6, the sequential operation of the heating/charging (Mode 1) and discharging/power-saving modes (Mode 2) was analysed. A model was developed to study the performance of the flexible heat pump under both ideal and non-ideal conditions, and it was compared to a conventional heat pump operating under the same conditions. The study identified the maximum improvement storage temperature correlation based on the refrigerant's inlet temperature at the storage and the evaporating temperature in Mode 1 for R1234yf, and other refrigerants. Various parameters, including, the storage temperature, the storage-refrigerant temperature differential ΔT_{HS}, superheating and subcooling degrees and their impact on the system's energy efficiency, were considered. The system was tested with various refrigerants: R134a, R410a, R1234yf, R1234ze(E) propane, and R32. Finally, an economic and environmental analysis was conducted to evaluate the economic and environmental benefits of the flexible heat pump in power-saving mode compared to a conventional ASHPWH and an A-rated gas boiler, for an application in Edinburgh.

In this chapter, an energy analysis of the flexible heat pump is performed when Mode 4 is used instead of Mode 1 for the charging process. As mentioned in Chapter 3, an alternative charging process, Mode 4, is available for the multi-valve flexible heat pump. Mode 4 is solely a charging mode used when heating is not required, involving charging at a lower temperature below the condensing temperature for heat supply. In this mode, charging occurs by condensing the refrigerant inside the heat storage. The chapter begins by introducing the methodology, followed by an analysis of the system's performance and operation, focusing on the impact of parameters such as ΔT_{HS}, compressor efficiency, and heat storage losses between modes. The performances of the system using different refrigerants with latent heat storage, including R1234yf, R134a, R1234ze(E), propane, and R410a, are compared. Later, the performance of R1234yf with a sensible heat storage system is considered. This work aims to characterise the operation of the flexible heat pump when Mode 4 is used instead of Mode 1, specifically to determine whether charging the heat storage at a lower temperature when heating is not needed offers any advantages, and whether improvements can be made compared to a conventional heat pump.

7.2 Methodology

In Chapter 3, Mode 4 was introduced as a mode that allows heat to be stored in the heat storage when heating is not necessary. Mode 4 serves as an alternative to Mode 1, enabling charging of the heat storage at a lower refrigerant temperature and pressure, which in turn reduces compressor power consumption. The model used in this chapter, detailed in Chapter 3, differs from that in Chapter 6 due to the variation in the charging process.

During Mode 4, the condensing temperature of the refrigerant is the storage temperature when $\Delta T_{HS} = 0$ K. The simulation follows the same procedure as in Chapter 6, with Mode 4 operating for a duration of Δt_{charge}. The condensing heat rate is assumed to be constant and equal to the heating capacity during discharging. Both the condensing heat rate in Mode 4 and the duration of Δt_{charge} do not impact the average COP of the flexible heat pump. This is because the charging time is proportional to the discharging time, and the condensing rate in the heat storage is proportional to the compressor power. Following the charging in Mode 4, the discharging/power-saving mode (Mode 2) is initiated and runs for a duration of $\Delta t_{discharge,2}$, until all the stored heat in the system is fully utilised.

Since no heat is provided during Mode 4, only the discharging time is counted for the total heat provided by the flexible heat pump when calculating the COP improvement. However, both charging and discharging times are considered for the total work consumed, as power is still required during Mode 4. Therefore, the objective is to determine whether the power consumption reduction throughout the process is beneficial, considering that compressor power is consumed during the charging process without providing heat.

7.2.1 Assumptions adopted in this chapter

The model used in this chapter is based on the equations for Modes 4 and 2 described in Chapter 3. The modelling process of Mode 2 is similar to the one used in Chapter 6. The model considers realistic efficiency values, including compressor efficiency, ΔT_{HS}, and heat storage's losses to the environment. Both latent and sensible thermal storage are considered. As this is solely an energy analysis, no assumptions are made regarding the external loops in evaporator and condenser. Therefore, the assumptions for this chapter are as follows:

1) Fixed compressor isentropic efficiency: Based on results from Chapter 5 and the literature, the compressor isentropic efficiency is initially fixed at 75 %[276].

2) Steady storage-refrigerant temperature differential: To simplify the analysis, the temperature difference between the heat storage and the refrigerant is assumed to be constant and equal during both the charging and discharging processes.

3) Frosting/Defrosting is not considered: As this chapter focuses on the performance of the system during the sequential operation of Modes 4 and 2, the effects of frosting and defrosting are excluded from the analysis.

4) Charging heat rate is equal to the heating capacity: Since the charging heat rate during Mode 4 is proportional to the compressor power and does not affect the performance calculation, it is assumed to be equal to the heating capacity during Mode 2 and remains constant.

7.2.2 Description of case study

The performance of the flexible heat pump is evaluated over a full charge/discharge cycle of the heat storage and compared to a conventional heat pump. The analysis examines the impact of various parameters on system operation. As in the previous chapter, the initial analysis uses R1234yf as the working fluid, with additional consideration given to refrigerants R134a, R1234ze(E), propane, R410a, and R32. The charging time is set at $\Delta t_{charge} = 1$ h, after which Mode 2 is initiated for $\Delta t_{discharge,2}$ until the heat storage is fully discharged.

The main case parameters used here are consistent with those in Chapter 6, representing an average UK application, and are listed in Table 7-1. Various parameters, including compressor efficiency, ΔT_{HS}, and thermal storage losses have been considered. Their impact on system operation and performance is examined and analysed.

It should be noted that, in the following sections, the evaporating temperature T_{evap} refers to the evaporating temperature when exchanging with the ambient during Mode 4, while the condensing temperature T_{cond} refers to the condensing temperature during Mode 2 for heat supply. These are independent of the storage temperature. The condensing temperature of the refrigerant during charging in Mode 4 will be referred to as the "charging temperature," and the evaporating temperature of the refrigerant during discharging in Mode 2 will be referred to as the "discharging temperature."

Table 7-1: Chapter main parameters

Parameters	Value
Refrigerant	R1234yf
Condensing temperature T_{cond} [°C]	65
Evaporating temperature T_{evap} [°C]	0
Heating capacity/Charging rate [kW]	8.5
Compressor efficiency [%][276]	75

7.3 Results and discussion

7.3.1 Results for latent heat storage system

Firstly, the operation is conducted with latent heat storage at a fixed temperature, similar to the previous chapter. The impact of storage temperature, ΔT_{HS}, compressor efficiency and storage's thermal losses, is evaluated.

7.3.1.1 Impact of storage-refrigerant temperature differential

In the following results, the impact of the parameter ΔT_{HS} is analysed.

Fig. 7-1 shows the average COP as a function of storage temperature and ΔT_{HS} for R1234yf. Overall, the average COP is slightly lower than when running Modes 1 and 2. For example, at the top performing storage temperature in this configuration, $T_{max,\alpha} = 35.4$ ℃ and $\Delta T_{HS} = 0$ K, the average COP is 3.31, while it was 3.36 in Chapter 6. This is because heating is not provided during the charging process, but some power is still consumed, though less than in Mode 1, as previously explained. As expected from the results in Chapter 5 and 6, the average COP is always higher when $\Delta T_{HS} = 0$ K. This implies that there is no difference between the refrigerant temperature and the PCM melting temperature, as they are equal, making it the ideal case.

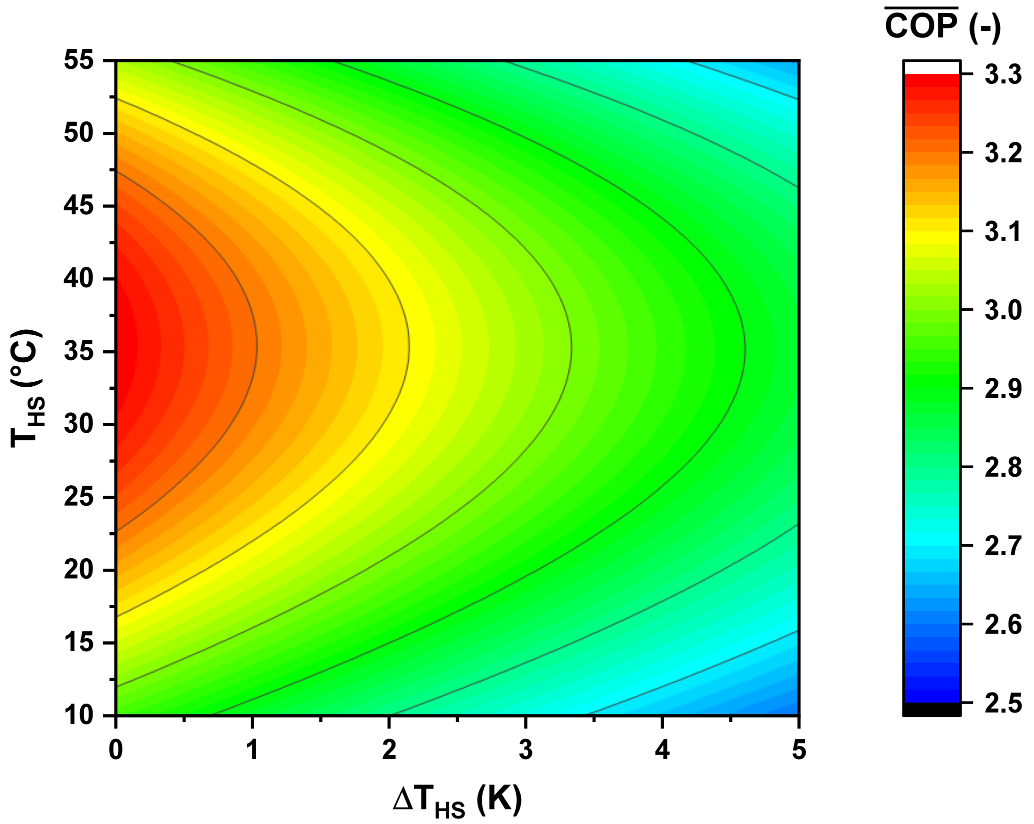

Fig. 7-1: Average COP depending on T_{HS} and ΔT_{HS}

The impact of the ΔT_{HS} variation in Mode 2 has been explained in previous chapters. In Mode 4, a similar pressure difference occurs during the charging process. When $\Delta T_{HS} =$ 0 K, the refrigerant's condensing pressure corresponds to its saturated temperature at the PCM melting point. However, as ΔT_{HS} increases, the refrigerant pressure also rises because the condensing temperature of the refrigerant needs to be higher than the PCM melting temperature. This leads to higher discharge pressure and increased power consumption. Therefore, the ΔT_{HS} parameter influences power consumption in both Modes 4 and 2, unlike in Mode 1, where ΔT_{HS} has no effect on compressor power during charging.

The lowest average COP values are observed at the highest ΔT_{HS} and the most extreme T_{HS} values. At the highest T_{HS}, compressor power is high due to the greater pressure ratio during charging, leading to a drop in the average COP. Conversely, at the lower T_{HS}, compressor power is lower during charging but increases during discharging because the storage temperature is linked to the refrigerant evaporating temperature, resulting in higher compressor power and a reduction in the average COP.

Using the same methodology as with the other modes, Fig. 7-1 clearly shows that a storage temperature for maximum improvement, $T_{max,\alpha}$, can also be identified in this scenario, located around the median value between the evaporating temperature (for heat exchange with the ambient) and condensing temperature (for heat supply). Like when running Modes 1 and 2, its value is close to, but slightly higher than, the midpoint between these temperatures.

The impact of ΔT_{HS} on the average COP is slightly more pronounced at $T_{max,\alpha}$ than at the extreme temperatures, $T_{HS} = 10$ °C and $T_{HS} = 55$ °C. At $T_{max,\alpha}$, the COP decreases from 3.31 to 2.88 across the range of tested ΔT_{HS}, representing a 13 % reduction. This reduction is approximately 12 % for both $T_{HS} = 10$ °C and $T_{HS} = 55$ °C. At $\Delta T_{HS} = 0$ K, $T_{max,\alpha}$ is 35.4 °C with an average COP of 3.31, indicating a 22.3 % improvement compared to a conventional heat pump. This is slightly lower than the 24.1 % improvement from running Modes 1 and 2. When ΔT_{HS} increases to 5 K, $T_{max,\alpha}$ slightly decreases to 35.1 °C, and the average COP drops significantly to 2.88, reducing the improvement to 6.1 %. Notably, the reduction in average COP is more closely linked to the increase in ΔT_{HS} than to the minor shift in $T_{max,\alpha}$ from 35.4 °C to 35.1 °C. Here, the impact on the average COP and improvement is more substantial than in the previous chapter. This impact is thoroughly studied in the following results. At $\Delta T_{HS} = 5$ K, whether T_{HS} is 35.4 °C or 35.1 °C, the average COP remains consistent at around 2.88. The influence of ΔT_{HS} on $T_{max,\alpha}$ for different refrigerants is illustrated in Fig. 7-2.

Fig. 7-2 shows that the temperature $T_{max,\alpha}$ varies depending on the value of ΔT_{HS}. Although it was previously demonstrated, and is also evident in Fig. 7-2, that the impact of ΔT_{HS} on the maximum improvement storage temperature for R1234yf is minimal, this is not the case for all refrigerants. R134a, which has properties similar to R1234yf, is also largely unaffected by changes of ΔT_{HS}, with its $T_{max,\alpha}$ varying only from 35 °C at $\Delta T_{HS} = 0$ K to 35.1 °C at $\Delta T_{HS} = 0.5$ K, and remaining at this value for the rest of the tested ΔT_{HS} range. Theoretically, $T_{max,\alpha}$ should not vary significantly with ΔT_{HS}, as it is primarily linked to T_{cond} and T_{evap}, and the properties of the refrigerants at these temperatures, as previously discussed. However, in the case of R32 and R410a (R410a is an equal mixture of R32 and R125), the effect of ΔT_{HS} is more pronounced. For R410a, $T_{max,\alpha}$ decreases from 38.8 °C at $\Delta T_{HS} = 0$ K to 36.9 °C at $\Delta T_{HS} = 5$ K. For R32, it decreases from 36.8 °C to 35.7 °C. This is explained by the refrigerants' properties, specifically the latent heat of vaporisation at $T_{HS} \pm \Delta T_{HS}$.

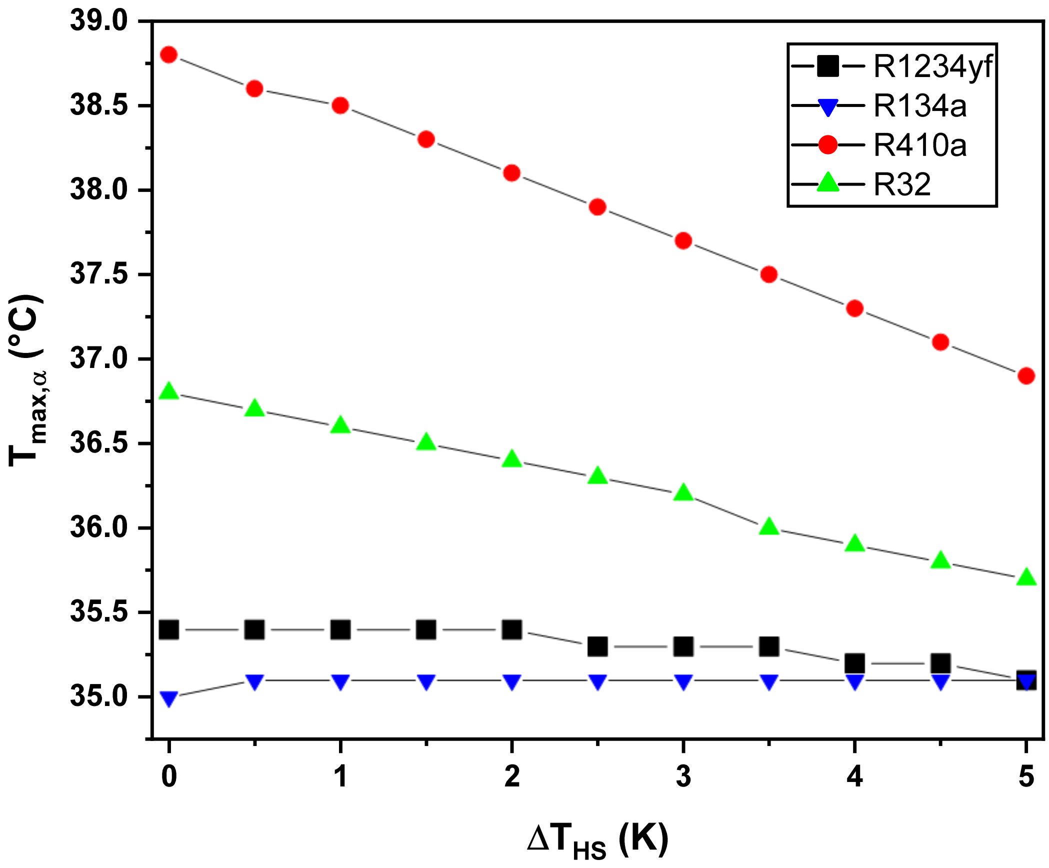

Fig. 7-2: Variation of $T_{max,\alpha}$ with ΔT_{HS} for R1234yf, R134a, R410a and R32

Differently that in the previous chapters, here, the storage temperature is linked to the refrigerant condensing temperature/pressure in charging mode (Mode 4) and to its evaporating temperature/pressure in discharging mode (Mode 2). Therefore, the maximum improvement storage temperature at a ΔT_{HS} value represents the best balance between both heat recovery and compressor power consumption during charging, as well as compressor power consumption during discharging, thereby ensuring maximum operational efficiency. When ΔT_{HS} increases, the charging temperature and the discharging temperature deviate from these best conditions. As a result, if the refrigerant properties change significantly with temperature, the top performing storage temperature must be adjusted to re-establish balance. This adjustment is particularly important because of parameters such as the latent heat of vaporisation at the charging temperature (Mode 4) and at the discharging temperature (Mode 2), as these affect other factors like mass flow rate, compressor power, and discharging time, all critical for achieving maximum performance.

Notably, in this case, the charging process relies on the latent heat of vaporisation at the charging temperature in Mode 4, rather than sensible heat transfer from subcooled refrigerant. As such, the latent heat of vaporisation directly influences heat recovery in the storage. In Mode 2, as previously discussed, the latent heat of vaporisation at the discharging temperature directly impacts the discharging rate of the storage. For refrigerants such as R134a and R1234yf, this parameter only shows slight variation. However, for R32, the variation is more significant, and for R410a, as a mixture of R32 and R125, the changes are even more substantial. The variation in the enthalpy of vaporisation with respect to ΔT_{HS}, as well as the corresponding maximum improvement storage temperatures for R1234yf, R134a, R410a, and R32, are detailed in Table 7-2.

Table 7-2: Refrigerants enthalpy of vaporisation and $T_{max,\alpha}$ depending on ΔT_{HS}

ΔT_{HS}	$T_{max,\alpha}$ (°C)				Enthalpy of vaporisation (kJ/kg)							
					R1234yf		R134a		R410a		R32	
	R1234yf	R134a	R410a	R32	$+\Delta T_{HS}$	$-\Delta T_{HS}$	$+\Delta T_{HS}$	$-\Delta T_{HS}$	$+\Delta T_{HS}$	$-\Delta T_{HS}$	$+\Delta T_{HS}$	$-\Delta T_{HS}$
0	35.4	35	38.8	36.8	136.7	136.7	168.3	168.3	161.9	161.9	245.3	245.3
1	35.4	35.1	38.5	36.6	135.8	137.5	167.2	169.2	162.5	164.5	243.4	248.1
2	35.4	35.1	38.1	36.4	134.8	138.4	166.2	170.2	159.2	167.2	241.4	251.7
3	35.3	35.1	37.7	36.2	134	139.4	165.2	171.2	158	170	239.5	253.7
4	35.2	35.1	37.3	35.9	133.2	140.3	164.1	172.2	156.7	172.4	237.7	256.7
5	35.1	35.1	36.9	35.7	132.3	141.3	163.1	173.1	155.4	175	235.7	259.2

In the following figures, the storage temperature is fixed at $T_{max,\alpha}$, and R1234yf is used as the refrigerant unless otherwise specified.

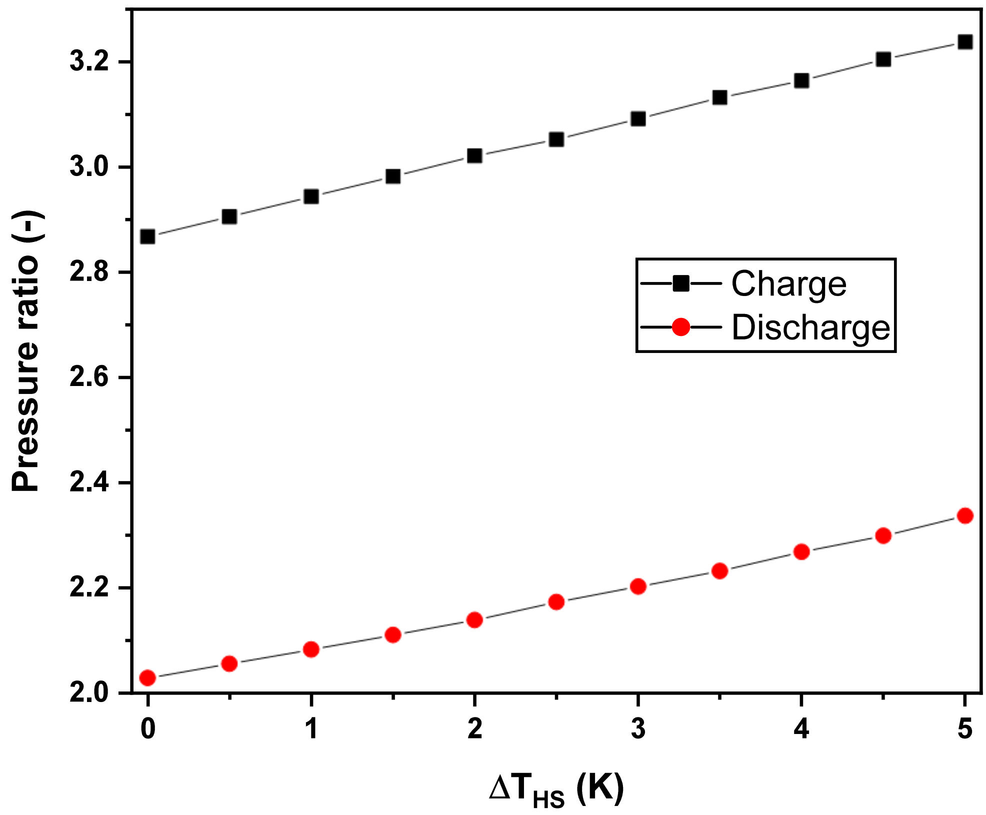

Fig. 7-3: Variation with ΔT_{HS} in both modes of pressure ratio

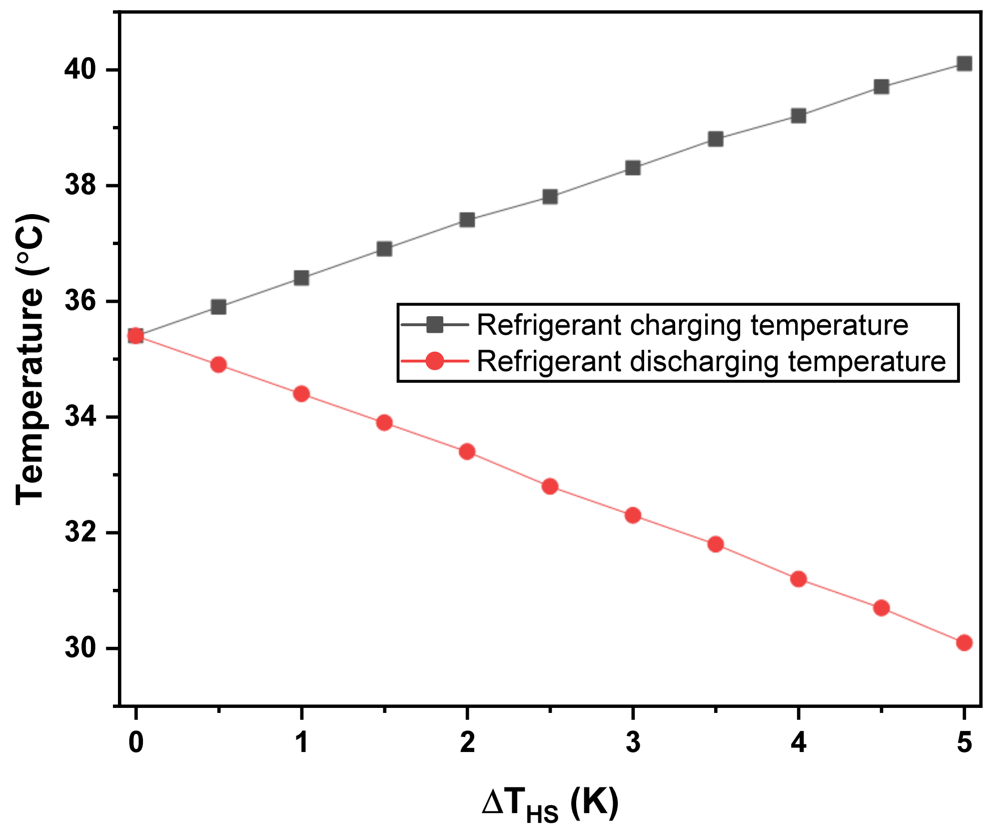

Fig. 7-4: Variation with ΔT_{HS} in both modes of refrigerant charging and discharging temperatures

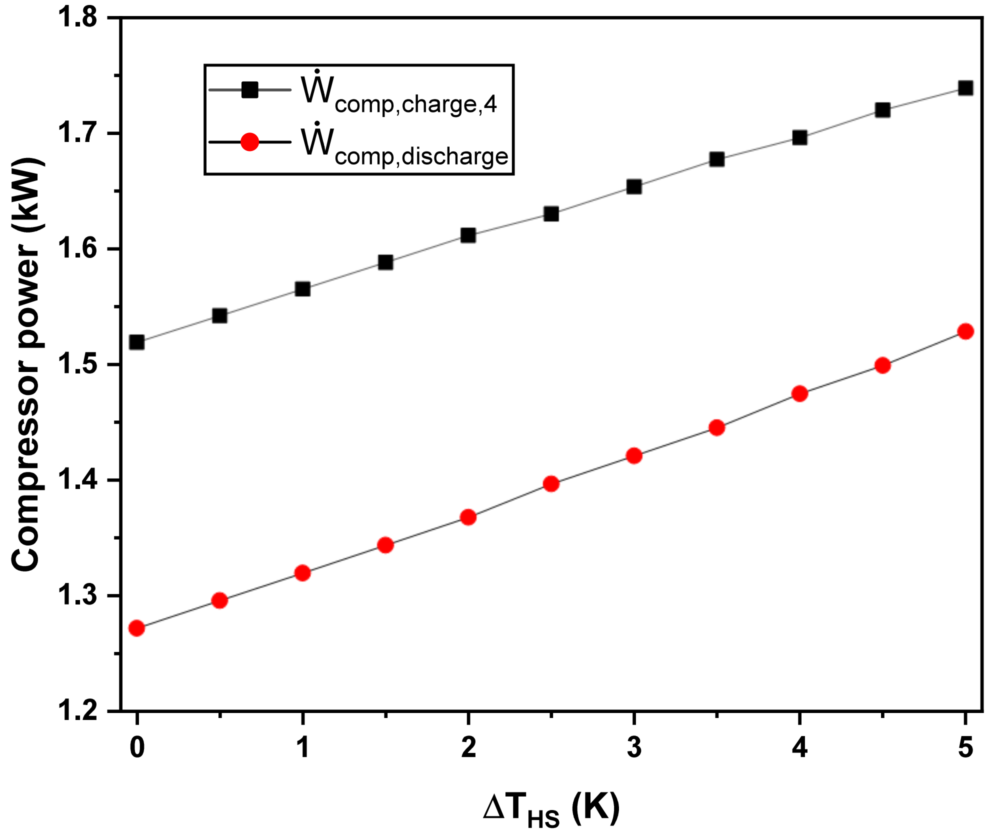

Fig. 7-5: Variation with ΔT_{HS} in both modes of compressor power

Fig. 7-3 to Fig. 7-5 illustrate the impact of the storage-refrigerant temperature differential ΔT_{HS} on the pressure ratio, refrigerant charging temperature (refrigerant condensing temperature in Mode 4), discharging temperature (refrigerant evaporating temperature in Mode 2), and compressor power in both Modes 4 and 2.

In Fig. 7-3, the impact of ΔT_{HS} on the pressure ratio during charging and discharging is shown. As ΔT_{HS} increases, the pressure ratio in both modes (ratio between condensing and evaporating pressures of the refrigerant during the mode) rises in a similar pattern. At $\Delta T_{HS} =$ 0 K, the refrigerant's charging temperature matches the PCM melting temperature. When ΔT_{HS} increases, the refrigerants' charging temperature increases, creating a higher temperature differential between the hot refrigerant and the storage temperature, as illustrated in Fig. 7-4, where the rise in refrigerant charging temperature is represented by black squares. The charging temperature is considered between 35.4 °C and 40.1 °C, according to the increase in the ΔT_{HS} from 0 to 5 K, and the corresponding variation in $T_{max,\alpha}$.

A similar trend is observed during discharging, where the pressure ratio also increases. As, ΔT_{HS} rises, the refrigerant's discharging temperature decreases, allowing heat transfer from the storage tank to the refrigerant. This is depicted in Fig. 7-4, where the drop in refrigerant discharging temperature, represented by red circles, is shown as ΔT_{HS} increases. The discharging temperature drops from 35.4 °C to 30.1 °C, as ΔT_{HS} increases. This behaviour is similar to what was discussed in Chapter 6 when operating Mode 2. The pressure ratio during discharging is consistently lower than during the charging process, due to the smaller source-sink temperature differential in discharging.

Both temperature and pressure ratio variations directly affect compressor power, as shown in Fig. 7-5. During both charging and discharging, compressor power increases in response to the rise in pressure ratio as ΔT_{HS} increases. Compressor power rises from 1.52 kW to 1.74 kW during charging and from 1.27 kW to 1.53 kW during discharging. Compressor power in discharging remains steadily lower than in charging, which corresponds to the lower pressure ratio during discharging, as shown in Fig. 7-3. The ratio between compressor power during charging and discharging remains constant as ΔT_{HS} increases, because the pressure ratio increases linearly in both cases.

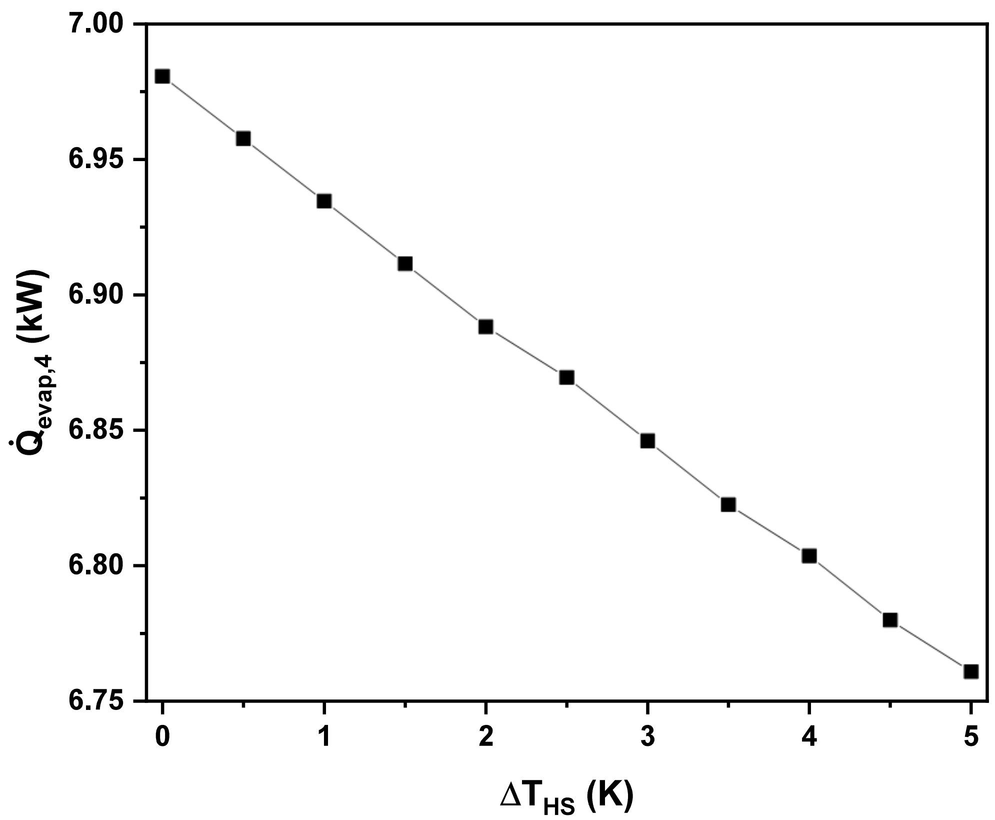

Fig. 7-6: Variation with ΔT_{HS} of evaporator heat transfer rate in Mode 4

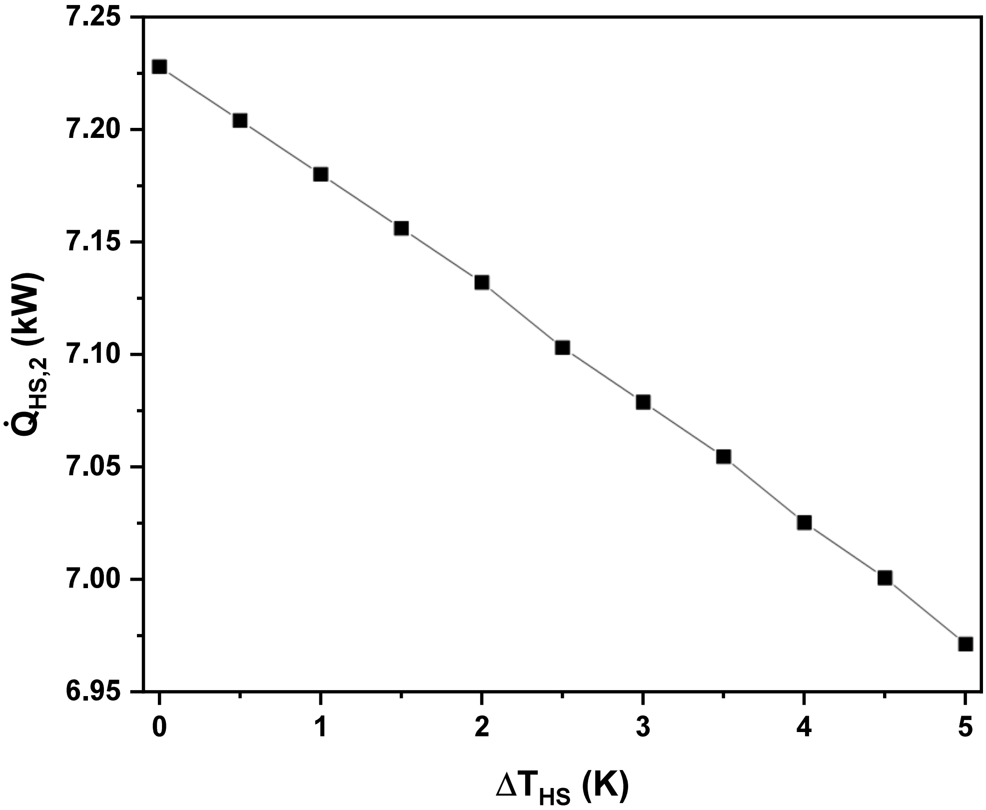

Fig. 7-7: Variation with ΔT_{HS} of discharging rate of storage in Mode 2

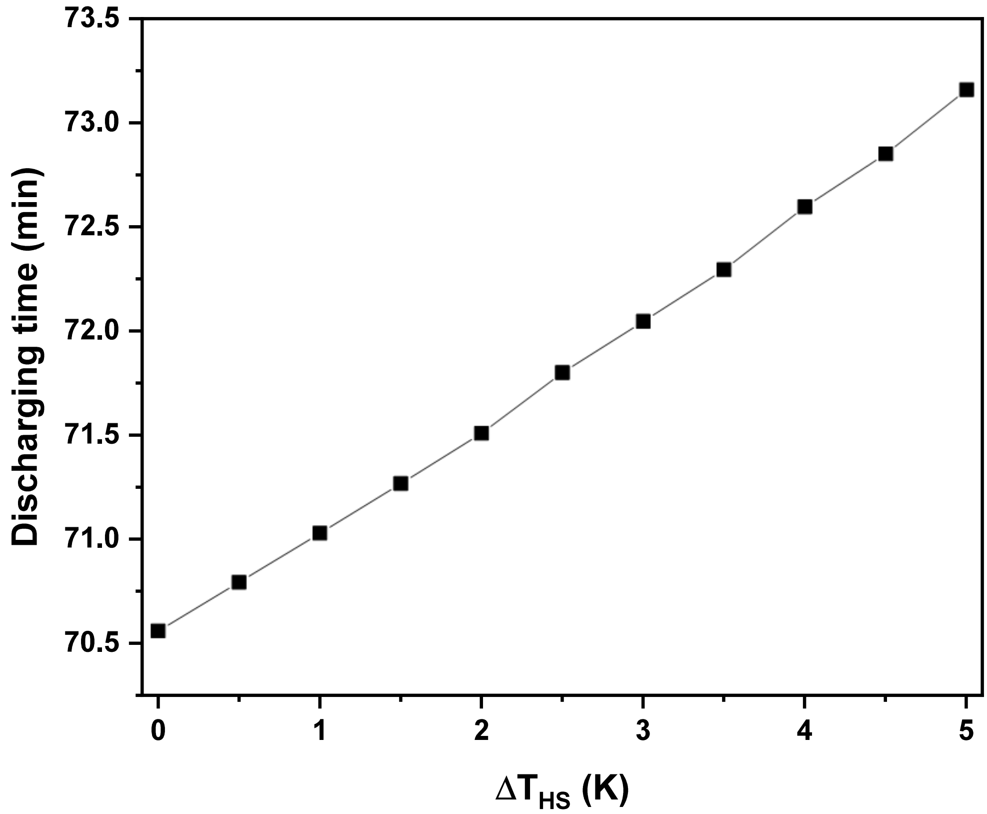

Fig. 7-8: Variation with ΔT_{HS} of discharging time in Mode 2

Fig. 7-6 to Fig. 7-8 present the heat rate in the evaporator during charging (Mode 4), the discharging heat rate in the storage tank, and discharging time in Mode 2, all as functions of ΔT_{HS}.

As shown in Fig. 7-6 and Fig. 7-7, the evaporator heat transfer rate in Mode 4, and discharging rate of the storage in Mode 2 decrease linearly as ΔT_{HS} increases. The decrease in the evaporator heat rate is due to the rising charging pressure and temperature with increasing ΔT_{HS}, as observed in Fig. 7-3 and Fig. 7-4. At higher charging temperatures, the saturated liquid enthalpy of R1234yf increases, from 248 kJ/kg at $\Delta T_{HS} = 0$ K to 254.8 kJ/kg at $\Delta T_{HS} = 5$ K. With the higher saturated liquid enthalpy and a constant evaporating temperature, the refrigerant's vapor quality increases after throttling at the evaporator inlet, requiring less heat for evaporation. As a result, the heat rate in the evaporator drops slightly from about 6.98 kW to 6.76 kW.

In Fig. 7-7, the discharging heat rate in the heat storage also decreases. This is caused by the decrease in discharging pressure and temperature, leading to a lower saturated vapor enthalpy, from 384.7 kJ/kg at $\Delta T_{HS} = 0$ K to 381.7 kJ/kg at $\Delta T_{HS} = 5$ K. Since the condensing temperature T_{cond} during discharging is fixed at 65 °C and the vapor quality at the storage inlet remains constant, less heat is required to reach the saturated vapor state as ΔT_{HS} increases. This is causing the discharging rate in the heat storage to drop from 7.23 kW to 6.97 kW. The heat rate during discharging is slightly higher than the evaporating rate during charging, despite the fixed charging heat rate of 8.5 kW. This is because the refrigerant charging temperature in Mode 4 is around 35 °C, while during discharging, the condensing temperature is fixed at $T_{cond} = 65$ °C. As shown in Table 3-6, for R1234yf at 65 °C, the enthalpy of vaporisation is lower than at 35 °C. Therefore, the discharging mass flow rate is higher than the charging one, which increases the discharging heat rate. However, this effect is mitigated by the lower latent heat required to evaporate the refrigerant at the discharging temperature in Mode 2.

Finally, Fig. 7-8 shows the discharging time as a function of ΔT_{HS}, increasing linearly from 70.6 to 73.2 minutes. The discharging time exceeds the charging time because the discharging rate is lower than the fixed charging rate of 8.5 kW, and according to Eq. (3.23), the discharging time must be longer to maintain balance. As explained earlier, the discharging heat rate decreases with increasing ΔT_{HS}, and since both the charging rate and time are fixed, the discharging time increases to maintain balance. This means that the time ratio $\delta_{4,2}$ is greater than 1, allowing for longer discharging times compared to when charging with Mode 1. While the increase in discharging time due to the rise in ΔT_{HS} does not improve performance in this case given the increased compressor power at higher ΔT_{HS} for both modes, it does suggest that reducing the discharging rate could extend the discharging time.

7.3.1.2 Impact of various parameters and refrigerants on average COP and improvement

This section analyses the influence of ΔT_{HS}, compressor efficiency, condensing temperature T_{cond}, thermal losses from the heat storage to the environment, and refrigerant selection on the average COP and improvement. In the following analysis, when ΔT_{HS} is fixed, its value is set at $\Delta T_{HS} = 2.5$ K.

Fig. 7-9 to Fig. 7-11 illustrate the impact of ΔT_{HS}, storage thermal losses, and compressor efficiency on the average COP and improvement.

In Fig. 7-9, both the average COP and improvement decrease as ΔT_{HS} increases. As previously demonstrated, an increase in ΔT_{HS} leads to a higher compression ratio and greater power consumption in both modes, which results in a drop in average COP. This is because the total heat supplied to the water loop during Mode 2 increases only slightly (as shown in Fig. 7-8), while power consumption rises more significantly in both modes. Specifically, the average COP and improvement decrease from 3.31 and 22.3 % at $\Delta T_{HS} = 0$ K to 2.88 and 6.15 % at $\Delta T_{HS} = 5$ K, at $T_{max,\alpha}$. This represents a 13 % decrease in average COP and a 72 % decrease in COP improvement, the latter being the most affected by this parameter. This significant drop occurs because, as discussed in Chapter 6, ΔT_{HS} does not affect the COP of the conventional heat pump. Therefore, while the flexible heat pump average COP decreases, the conventional heat pump COP remains constant, leading to a great decline in the improvement. As in the previous chapter, the conventional heat pump COP is 2.7.

Thus, an increase of the ΔT_{HS} parameter up to 5 K, significantly impacts the performance of the flexible heat pump in Modes 4 and 2, especially compared to Modes 1 and 2. When charging the heat storage tank in Mode 4, this parameter should be carefully considered and minimised to enhance efficiency.

In Fig. 7-10 and Fig. 7-11, ΔT_{HS} is fixed at 2.5 K, providing a reasonable average COP value of 3.1 and a 13.7 % improvement under non-ideal conditions.

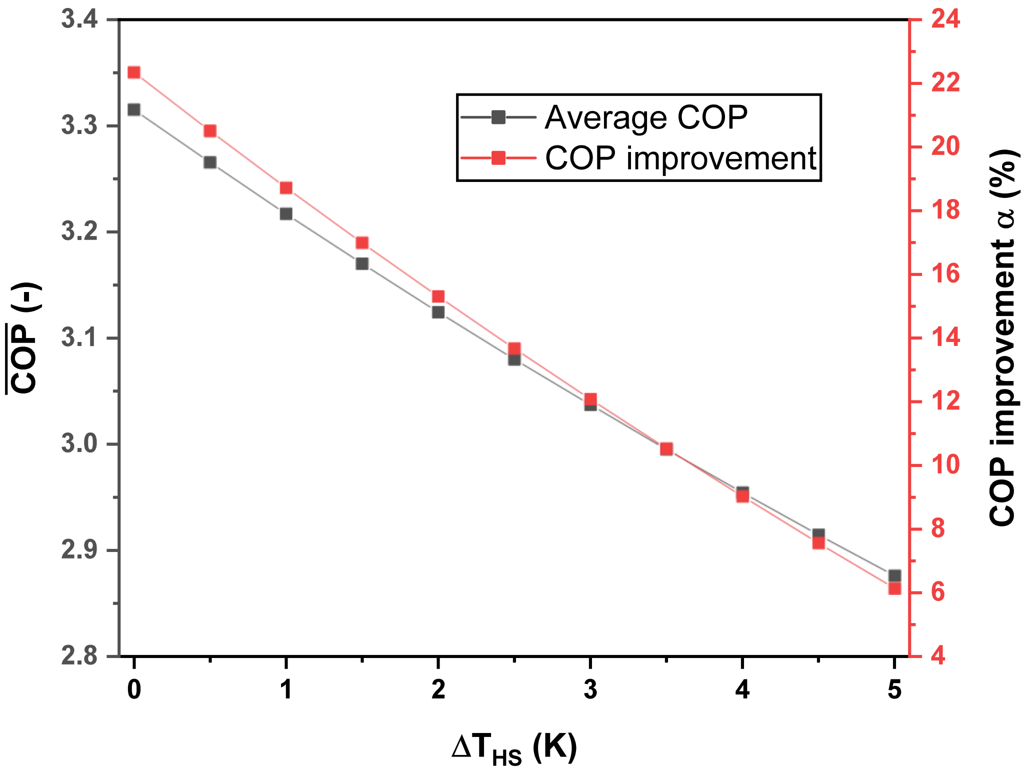

Fig. 7-9: Variation of the average COP and improvement depending on storage-refrigerant temperature differential

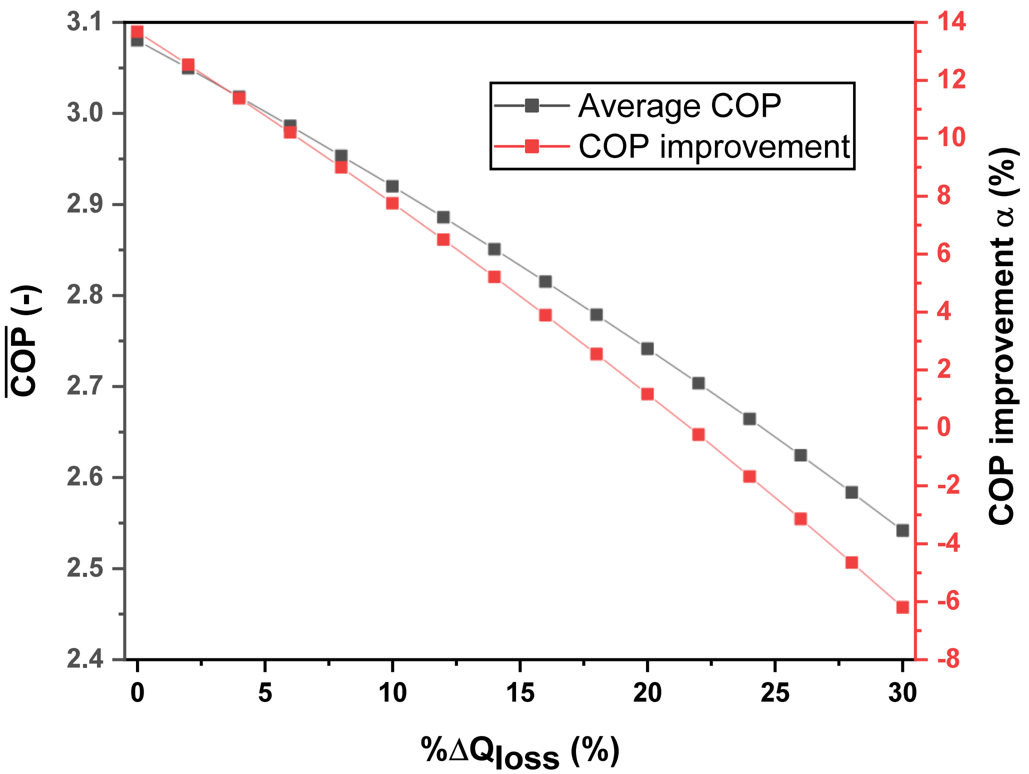

Fig. 7-10: Variation of the average COP and improvement depending on thermal storage losses

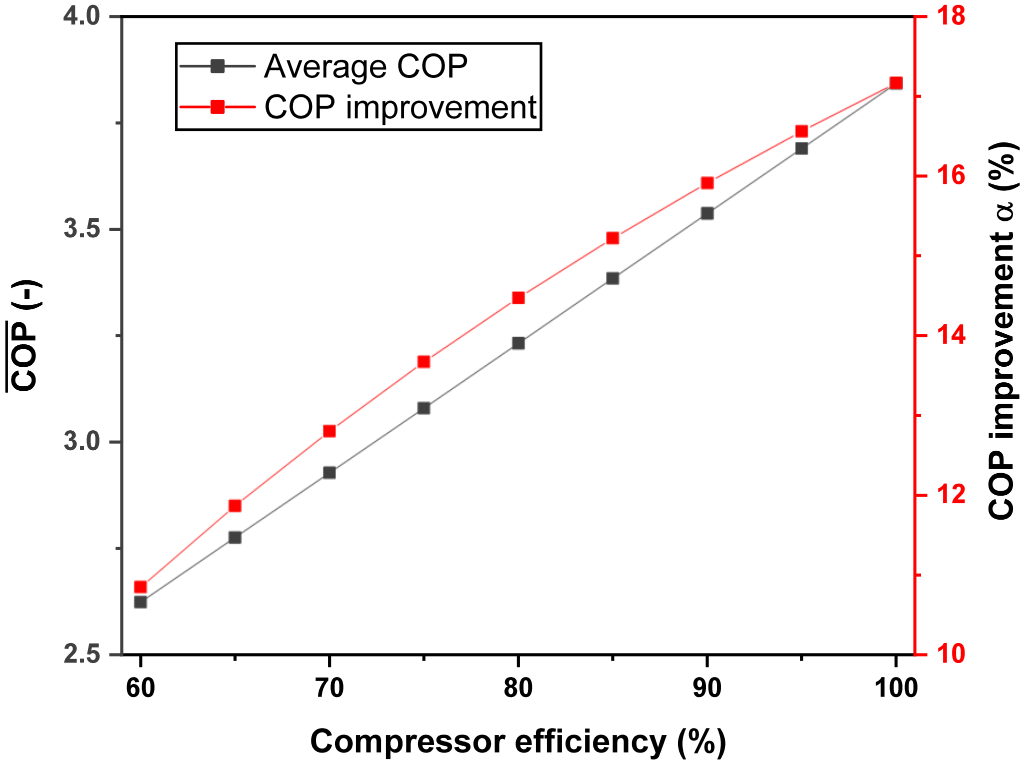

Fig. 7-11: Variation of the average COP and improvement depending on compressor efficiency

In Fig. 7-10, both the average COP and improvement decrease as the percentage of thermal losses to the environment ($\%\Delta Q_{loss}$) increases. These losses represent the portion of energy stored during charging that is lost to the environment, reducing the amount of heat available during discharging. Consequently, higher thermal losses shorten the discharging time and degrade the overall performance of the flexible heat pump, even though its power consumption during charging remains constant. Both the average COP and improvement follow the same downward trend, with the improvement dropping from 13.7 % at $\%\Delta Q_{loss} = 0$ % to 1.2 % at $\%\Delta Q_{loss} = 20$ %, a 91 % decrease. Beyond 22 % losses, the improvement becomes negative, falling from -0.2 % at $\%\Delta Q_{loss} = 22$ % to -6.2 % at $\%\Delta Q_{loss} = 30$ %. This demonstrates the importance of minimising storage losses through effective insulation, especially if heat has to be stored for a long time. Otherwise, the flexible heat pump becomes less efficient than a conventional heat pump, when running Modes 4 and 2.

Lastly, Fig. 7-11 shows the average COP and improvement as a function of compressor efficiency. Both increase with compressor efficiency, with the average COP following a linear trend and the improvement curve showing a slight arc. As discussed in Chapter 5, higher compressor efficiency reduces power consumption by decreasing exergy destruction, resulting in a higher average COP and improvement. The improvement rises from 10.9 % at η_{comp} = 60 % to 17.2 % at η_{comp} = 100 %, a 58 % increase. Thus, compressor efficiency is another important parameter for improving the performance of the flexible heat pump in Modes 4 and 2, though in that case, it is less critical compared to ΔT_{HS} and thermal losses to the environment.

Fig. 7-12 shows the COP improvement at the storage temperature $T_{max,\alpha}$, as a function of the condensing temperature for heat supply T_{cond} in Mode 2 and ΔT_{HS}. The highest COP improvement occurs at $\Delta T_{HS} = 0$ K and the maximum tested condensing temperature of 70 °C. As explained earlier, the improvement decreases with increasing ΔT_{HS}, with greater improvements observed at higher condensing temperatures due to the reduced compressor power required for heating compared to a conventional heat pump.

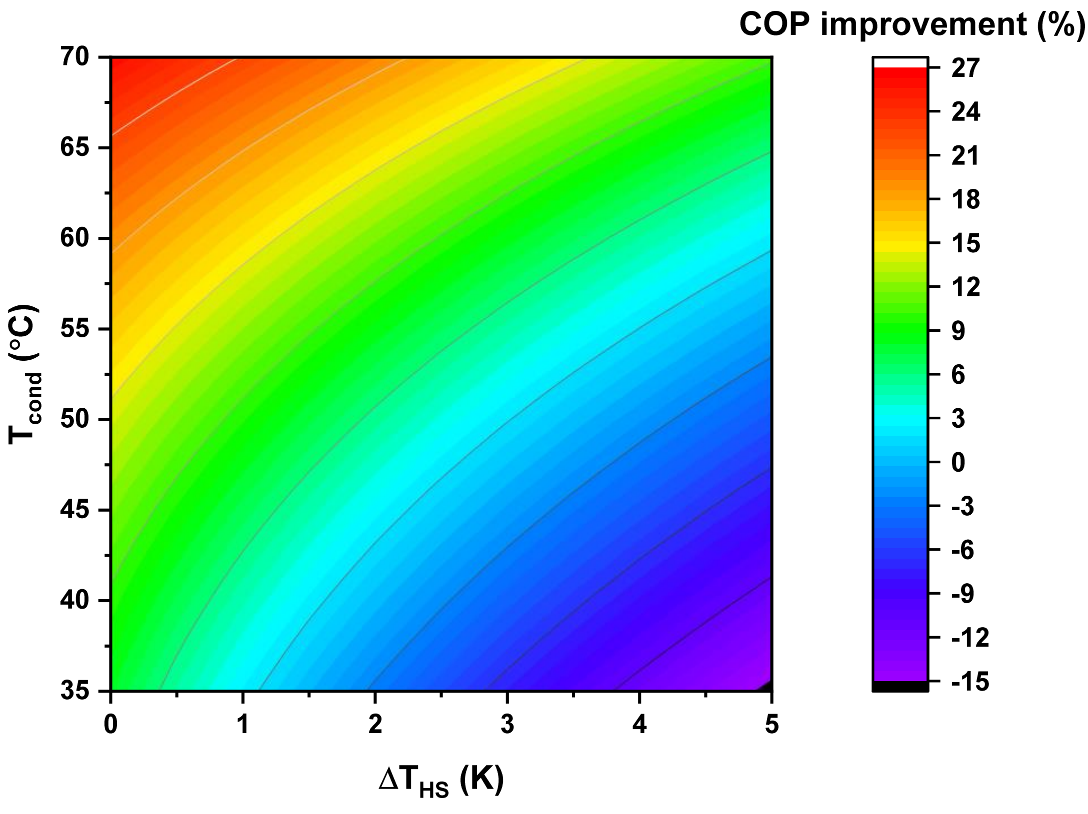

Fig. 7-12: COP improvement depending on T_{cond} and ΔT_{HS} at $T_{max,\alpha}$

As seen in Fig. 7-12, there is a contour line starting at $\Delta T_{HS} = 1.5$ K and $T_{cond} = 35$ °C, where the COP improvement becomes negative, reaching -0.2 % at these values. This negative trend worsens as ΔT_{HS} increases at the same condensing temperature, reaching a maximum decline of -15.5 % at $\Delta T_{HS} = 5$ K. The contour line extends up to a condensing temperature of 56 °C, where the improvement is -0.6 % for $\Delta T_{HS} = 5$ K. This occurs because, as ΔT_{HS} increases, the compressor power consumption during both charging and discharging rises, while the compressor power of the compared conventional heat pump remains constant, given its fixed condensing and evaporating temperatures. Moreover, since no heat is supplied during the charging phase, the overall heat provided only increases slightly due to the modest increase in discharging time (as shown in Fig. 7-8), while the compressor consumption grows substantially. As a result, the performance of the flexible heat pump diminishes to the point where its average COP becomes lower than that of a conventional heat pump.

This effect is more pronounced at lower condensing temperatures, as the improvement margin from a conventional heat pump is already minimal with a smaller temperature differential between the sink and source. Even a slight increase in the compression ratio for the flexible heat pump (which requires compressor power during charging, unlike the conventional heat pump), significantly affects the improvement. For higher condensing temperatures, this impact is less severe because the improvement margin from the conventional heat pump is greater, and the slight increase in temperature differential from ΔT_{HS} has a limited effect when the source-sink temperature differential is already large.

Therefore, there are scenarios where using Mode 4 to charge the storage for later discharge is less efficient than simply operating the heat pump in conventional mode, as Mode 4 consumes power without providing heat. Therefore, the use of this mode should be carefully considered based on the operating conditions and the chosen ΔT_{HS} value. To achieve the best improvement and maximise power saving, particularly at lower pressure ratios between condensing and evaporating pressures, ΔT_{HS} should be kept to a minimum. This parameter has a critical impact on overall performance when operating Modes 4 and 2.

Fig. 7-13 illustrates the average COP and improvement for various refrigerants at $\Delta T_{HS} =$ 2.5 K. R1234yf shows the highest improvement, with 13.7 % and a corresponding average COP of 3.1. Although it does not have the highest COP, it provides the greatest improvement relative to the conventional heat pump COP, as observed in other modes. R410a ranks second, with a 10.8 % improvement and an average COP of 2.9. While it performs well in terms of improvement compared to the baseline, its COP is the lowest among the tested refrigerants due to its high power consumption. This is attributed to the shape of its isentropic lines and its relatively high mass flow rate. R1234ze(E), propane, and R134a come in third, fourth, and fifth, respectively, with improvements of 9.1 %, 8.2 %, and 7.7 %, all achieving an average COP of 3.2. Lastly, R32 is the least effective in this configuration, as seen in other modes, with a 5.8 % improvement and an average COP of 3.1, similar to R1234yf.

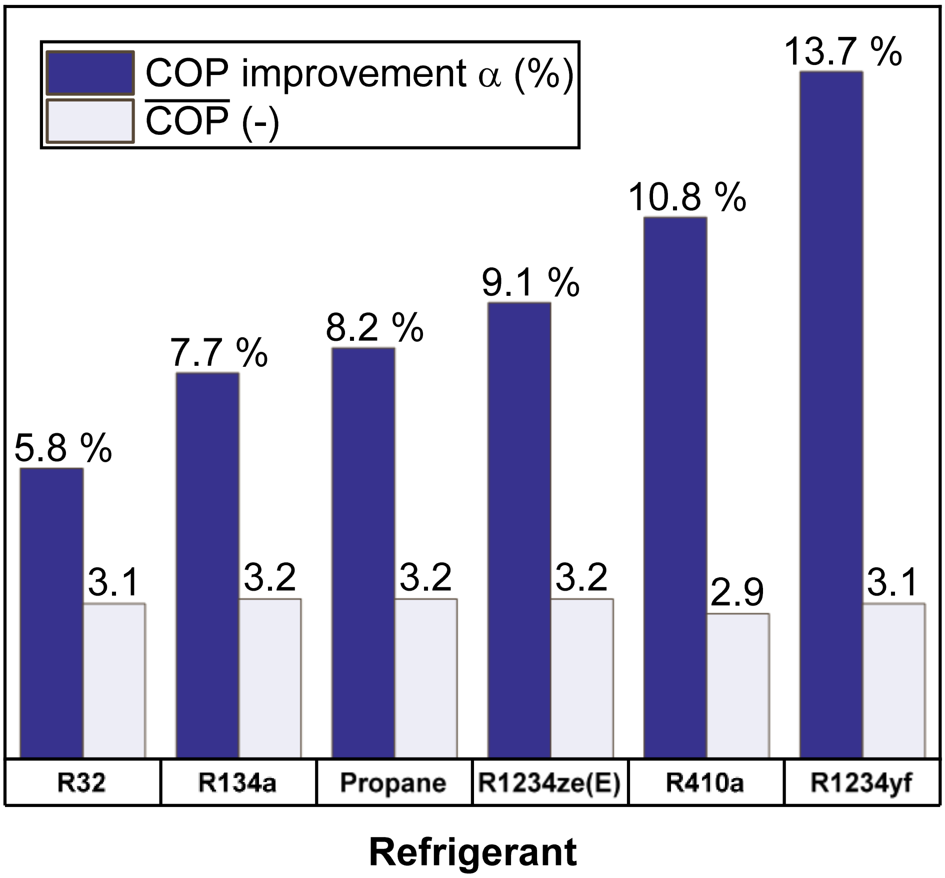

Fig. 7-13: Average COP and improvement for various refrigerants at $\Delta T_{HS} = 2.5$ K

The ranking of refrigerants, as well as their performance relative to the conventional heat pump, remains consistent with the previous chapters. These results are influenced by factors such as the discharging time, which is linked to their discharging mass flow rate and enthalpy of vaporisation at the discharging temperature; and power consumption, which is tied to their mass flow rates and isentropic lines. Since the charging rate and time are fixed, the amount of heat charged is the same for all refrigerants in Mode 4, but their mass flow rate differs depending on their enthalpy of vaporisation at the charging temperature and isentropic lines shape. This in turn impacts the power consumption during Mode 4.

The improvement is primarily associated with the potential benefit for refrigerants of increasing their evaporating temperature under these operating conditions, as explained in the previous chapters. Here, the benefit is linked to several parameters, such as the charging and discharging mass flow rates, which impact the discharging rate in the heat storage. Additional parameters impacting performance include the power consumption during the charging process in Mode 4, where no heat is provided, thereby reducing the overall COP. Refrigerants with higher power consumption during charging will experience lower overall improvements, mainly due to the shape of their isentropic lines. Their power consumption during discharging is also critical in evaluating the benefit of increasing the evaporating temperature and is primarily linked to their isentropic lines. All these factors contribute to determining which refrigerants benefit the most from the reduction in the compression ratio under these operating conditions.

In conclusion, R1234yf exhibits the best improvement across all modes of the flexible heat pump, followed by R410a. However, the refrigerants with the highest average COP are R134a, R1234ze(E), and propane.

7.3.2 Results for sensible heat storage system

In this section, the operation is conducted with a sensible heat storage system to assess its impact and compare its performance with that of a latent heat storage system. For a fair comparison, both systems are evaluated under similar storage-refrigerant temperature differential ΔT_{HS}, as in previous sections. In the case of the sensible heat storage system, ΔT_{HS} is defined as the absolute difference between the refrigerant temperature (T_{ref}) and the temperature of the tank contents, which in this case is water (T_w), expressed as

$$\Delta T_{HS} = \left|T_{ref} - T_w\right| \qquad \text{Eq. (7.1)}$$

To maintain consistency with the conditions evaluated previously, ΔT_{HS} is set to 2.5 K.

For the sensible heat storage system, an additional parameter is considered: the deviation of the water temperature from the maximum improvement storage temperature found for the latent heat storage system, denoted as ΔT_w. It defines the temperature range of the water in the tank. Yu et al.[223] highlighted that the performance in power-saving mode (Modes 1 and 2) of a flexible heat pump using a sensible storage tank was maximised when this temperature differential was minimised. Consequently, the following results use a temperature range in the water storage tank that varies between

$$T_{w,1} = T_{max,\alpha} - \Delta T_w \qquad \text{Eq. (7.2)}$$

$$T_{w,2} = T_{max,\alpha} + \Delta T_w \qquad \text{Eq. (7.3)}$$

During charging, the temperature in the tank rises from $T_{w,1}$ to $T_{w,2}$, while during discharging it decreases from $T_{w,2}$ to $T_{w,1}$.

7.3.2.1 Impact of deviation from maximum improvement storage temperature

Fig. 7-14 and Fig. 7-15 show how the charging and discharging times, as well as the average COP and improvement, change as the deviation in water temperature from the maximum improvement storage temperature (ΔT_w) increases.

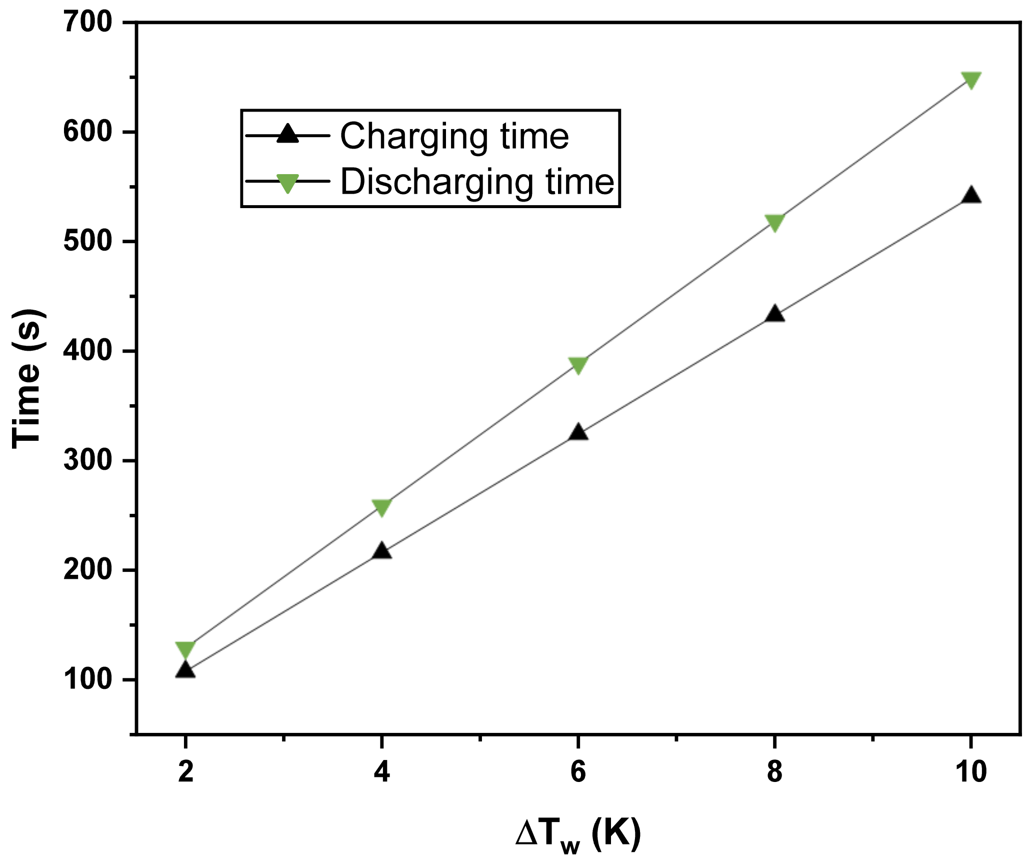

Fig. 7-14: Variation with ΔT_w of charging and discharging times

In Fig. 7-14, both charging and discharging times increase linearly as ΔT_w rises from 2 K to 10 K. Specifically, the charging time rises from 108.2 seconds to 541 seconds, while the discharging time increases from 129.5 seconds to 649 seconds. This occurs because a higher set temperature during charging necessitates more time to reach, and similarly, discharging takes longer as the temperature decreases during the reverse process.

Despite the extended discharging time, Fig. 7-15 shows that both the average COP and improvement decrease with an increasing ΔT_w. The improvement drops from 13.6 % to 12.9 % as ΔT_w rises from 2 K to 10 K. This decline is attributed to the increased pressure ratio caused by a larger temperature difference, which deviates from the best conditions during both the charging and discharging phases. Consequently, compressor power increases during both processes, reducing overall system improvement. However, this decline is relatively small, only 5.1 %, due to the graduate progression of the water temperature in the tank.

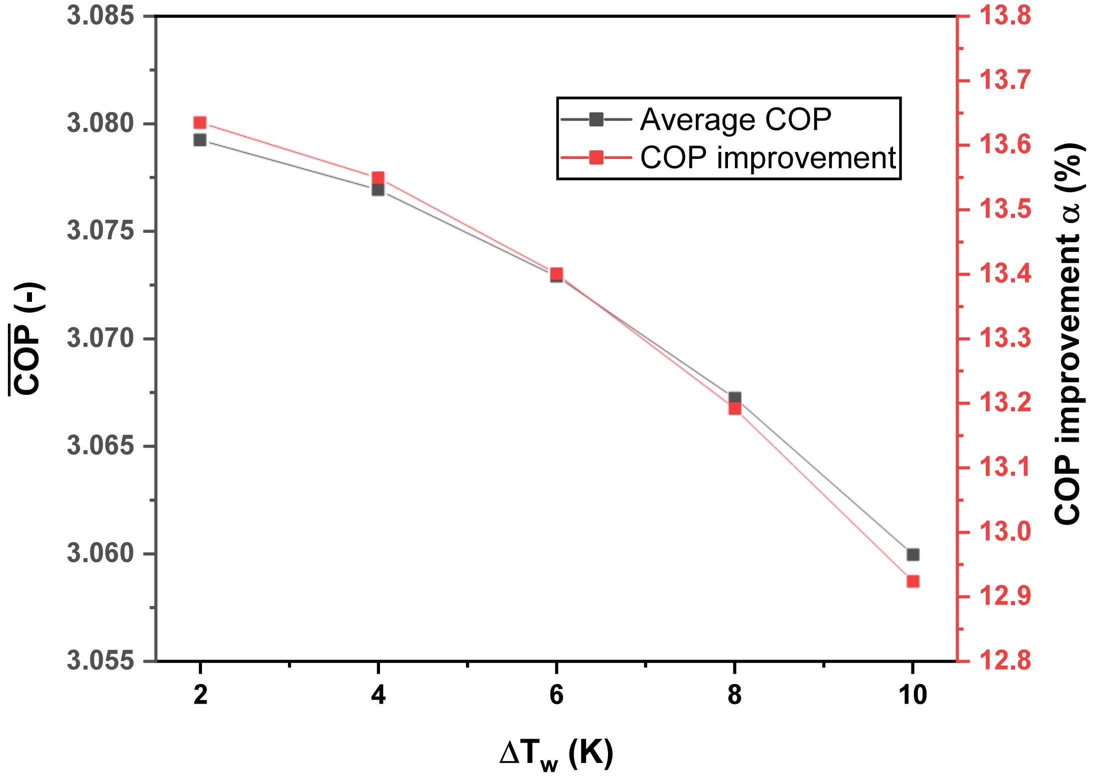

Fig. 7-15: Variation with ΔT_w of average COP and improvement

It is important to note that when the water temperature range deviates only slightly from the maximum improvement storage temperature $T_{max,\alpha}$, performance remains nearly identical to that of the latent heat storage system, with an improvement of 13.6 % at $\Delta T_w = 2$ K compared to 13.7 % for latent heat storage. Additionally, the average COP experiences only a slight decrease in absolute value, dropping from about 3.08 to 3.06, as ΔT_w rises from 2 K to 10 K. Therefore, this minimal variation has an insignificant impact within this range of ΔT_w. However, to ensure maximum performance, it is recommended to minimise the deviation of the water temperature from the top performing storage temperature as much as possible. That said, for smoother operation of the flexible heat pump, this value should be large enough to avoid excessive switching between charging and discharging, which could increase the negative effects of mechanical shock and compressor wear. Therefore, a balance must be found between minimising temperature deviation and ensuring stable system operation.

7.3.2.2 Impact of thermal storage losses to the environment

This section evaluates the impact of thermal storage losses to the environment on the performance of the system when using sensible heat storage.

Fig. 7-16 to Fig. 7-18 illustrate the variation in charging and discharging times, the time ratio, and the average COP and improvement in relation to thermal storage losses for the extreme water temperature differentials tested, $\Delta T_w = 2$ K and $\Delta T_w = 10$ K. The time ratio $\delta_{4,2}$ is defined as the ratio of discharging to charging time, as shown in Eq. (3.28).

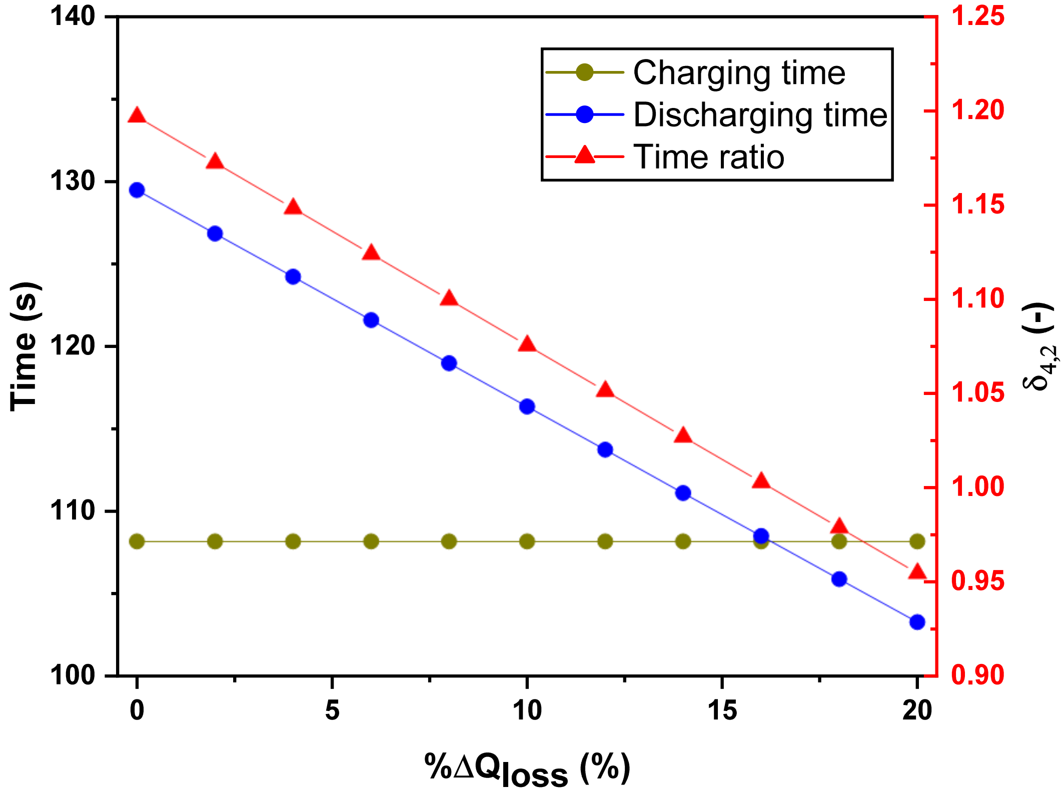

Fig. 7-16: Variation with thermal storage losses of charging and discharging times, and time ratio at $\Delta T_w = 2$ K

In Fig. 7-16 and Fig. 7-17, it can be observed that the charging time remains constant as the percentage of thermal storage losses increase, while both the discharging time and time ratio decrease. Specifically, the charging time is not impacted by heat storage losses to the environment happening after the charging phase. However, a significant reduction is observed in both the discharging time and the time ratio. The discharging time decreases from 129.5 seconds to 103.3 seconds, and the time ratio drops from 1.2 to 0.95 as losses increase from 0 % to 20 % for $\Delta T_w = 2$ K. For $\Delta T_w = 10$ K, the discharging time decreases from 648.8 seconds to 511.6 seconds, and the time ratio is similarly dropping from 1.2 to

0.95. While the absolute discharging times differ for each ΔT_w, the trend and proportionate decrease in the time ratio are consistent. When thermal storage losses exceed 18%, the time ratio drops below 1, indicating that the charging time becomes longer than the discharging time. In this case, the heat pump consumes power for a longer period to charge the heat storage tank than it does to provide heat during discharging.

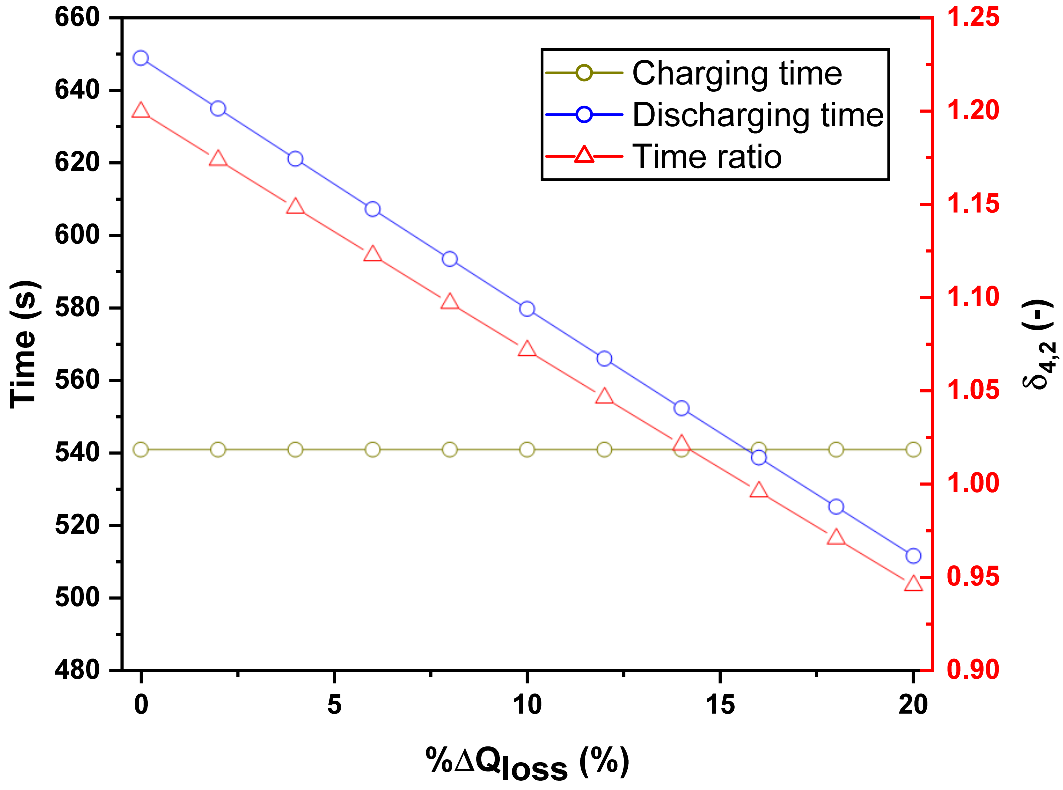

Fig. 7-17: Variation with thermal storage losses of charging and discharging times, and time ratio at $\Delta T_w = 10$ K

As discussed with latent heat storage in Fig. 7-10, thermal losses reduce the energy available during discharging. With less heat available, the water tank discharges more quickly. Since the charging time remains constant, the time ratio decreases, indicating less discharging time for the same charging duration. This reduction in discharging time leads to a decrease in both the average COP and improvement, as seen in Fig. 7-18. Because the charging time and compressor power consumption remain constant, the reduction in discharging time results in lower heat provided, diminishing the overall efficiency of the flexible heat pump. For 0 % losses, the COP improvement reaches a maximum of 13.6 % for $\Delta T_w = 2$ K and 12.9 % for $\Delta T_w = 10$ K. However, it drops to 1.6 % and 3 %, respectively, for 20 % losses representing an 88 % decrease in the first case and a 76 % decrease in the second case.

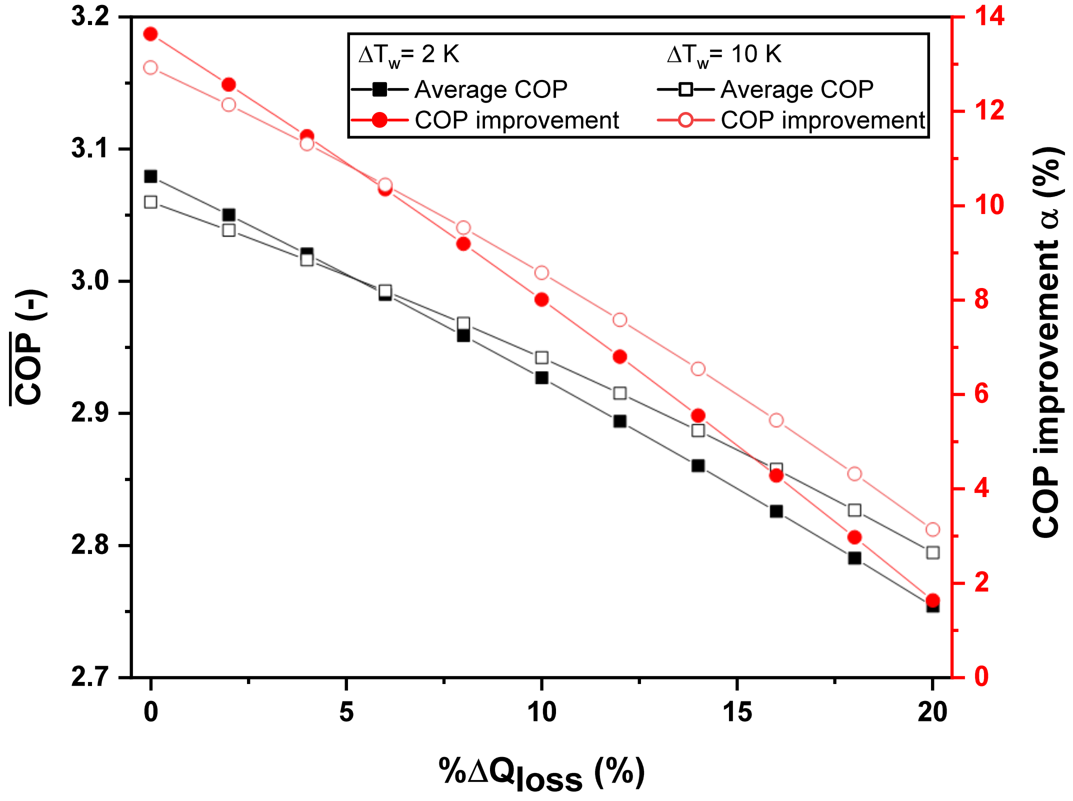

Fig. 7-18: Variation with thermal storage losses of average COP and improvement

From Fig. 7-18, it is also seen that beyond 6 % losses, the average COP and improvement are greater for $\Delta T_w = 10$ K. This is because the average COP is influenced by both the time ratio between discharging and charging times and the power consumption during these processes. Since the temperature range is narrower for $\Delta T_w = 2$ K, the reduction in discharging time due to losses has a more significant impact on the balance compared to $\Delta T_w = 10$ K.

Therefore, as with latent heat storage, it is essential to minimise thermal storage losses to the environment and appropriately adjust the water temperature differential to ensure maximum performance and improvement of the flexible heat pump.

7.4 Summary

In this chapter, the performance and energy analysis of the flexible heat pump system when using Mode 4 to charge the heat storage at a lower temperature, when heating is not required, has been made. Both latent and sensible heat storage systems have been considered. The impact on performance of various parameters, including, ΔT_{HS}, compressor efficiency, heat storage losses, condensing temperature for heat supply, and ΔT_w, has been evaluated. The effect of different refrigerants, including R1234yf, R134a, R1234ze(E), propane, R32, and R410a, has also been studied. The results have demonstrated that Mode 4, as a charging process, still shows improvements compared to a conventional heat pump, although it affects system performance differently than Mode 1, where the heat pump provides both heating and charging. The key findings are the following:

- Increasing ΔT_{HS} when running Modes 4 and 2 significantly reduces the average COP and improvement due to higher pressure ratios and increased power consumption during both charging and discharging modes. This effect is more pronounced than when running Modes 1 and 2. The maximum improvement storage temperature shifts depending on the refrigerant as ΔT_{HS} increases, particularly for refrigerants like R32 and R410a, which show more significant deviations in properties, even over short temperature ranges. Therefore, ΔT_{HS} should be carefully considered and minimised when running these modes, to ensure maximum performance, especially at lower pressure ratios.

- The average COP and improvement are lower when using Mode 4 as a charging mode compared to Mode 1, primarily due to the absence of heating during charging.

- R1234yf consistently shows the best improvement in every operating mode, with a 13.7 % improvement and an average COP of 3.1 in this configuration at $\Delta T_{HS} = 2.5$ K. The performance of other refrigerants aligns with previous findings, with R410a and R1234ze(E) following R1234yf in terms of improvement, while R32 performs the worst.

- Thermal losses to the environment have been considered for both sensible and latent heat storage systems. These losses reduce discharging times and negatively affect the overall performance of the flexible heat pump. Notably, for latent heat storage systems with losses exceeding 20 %, the flexible heat pump becomes less efficient than a conventional heat pump, highlighting the importance of proper insulation to prevent heat loss between modes.

- When using sensible heat storage, such as a water tank, attention should be given to the temperature differential inside the tank, specifically the parameter ΔT_w, which reflects deviations from the top performing storage temperature found. To ensure maximum performance, it is recommended to minimise this parameter; however, it should still be large enough to avoid excessive switching between charging and discharging modes, as frequent switching could negatively affect the system's smooth operation. Minimising unnecessary switching can also help improve the average COP, particularly in the presence of thermal losses between modes.

Looking ahead, this mode could be especially valuable in off-peak or peak shaving scenarios, as it allows the heat storage to be charged when heating is not required, taking advantage of lower electricity prices. For this reason, further economic studies could be conducted using a more detailed model of daily heating demand during a peak winter heating day.

Chapter 8 Conclusions and outlook

In the transition efforts to low-emission technologies like in the heating sector, heat pump adoption has been increasing but still currently meet only a small fraction of heating demand. In the UK, air-source heat pumps present a promising alternative for individual dwellings. However, the literature indicates that air-source heat pumps would face operational challenges in the UK context, where both flexibility and low operating costs are required, yet high temperature lifts are needed during peak winter days. This combination reduces efficiency and increases operating costs. This issue is enhanced in winter, when cold and humid conditions cause frosting on the evaporator, further reducing performance and making air-source heat pumps less competitive with gas boilers.

This raises the following research question: How can air-source heat pumps be improved cost-effectively to overcome these challenges in a UK setting?

In response, this thesis introduces a multi-valve flexible heat pump concept that integrates heat storage, aimed at addressing these UK-specific challenges. The primary goal was to establish a benchmark numerical study of this innovative heat pump design and assess its potential to address the two major hurdles for air-source heat pumps in the UK, therefore paving the way for future designs considerations and in-depth analysis.

8.1 Summary of thesis findings

The defrosting cycle of the multi-valve flexible heat pump was evaluated against a conventional reverse cycle defrosting approach, specifically addressing lack of heat availability in the cycle and the challenge of maintaining continuous heating during defrosting without complex designs. An idealised model with latent heat storage was developed to compare the thermodynamic behaviour and performance of both cycles, facilitating simpler comparison with conventional reverse cycle defrosting. This preliminary study under idealised conditions highlighted the influence of key parameters, including storage temperature, refrigerant type, and defrost duration, on system efficiency. Results show that the flexible heat pump can achieve efficient defrosting by condensing refrigerant in the frosted evaporator after being evaporated in the heat storage. A storage temperature was identified for maximum COP improvement, depending on refrigerant properties. R1234yf demonstrated the highest COP improvement (13.2 %), with R134a showing the highest average COP; the lowest COP improvement was seen with R32 (8.9 %) and the lowest average COP with R410a. Various defrosting durations were tested, showing no theoretical impact on COP improvement, with times from 2 to 10 minutes being mathematically valid to respect energy balance.

Following the energy analysis of the defrosting operation, an exergy analysis was conducted on Modes 1 and 3, using latent heat storage, to identify key sources of exergy losses and assess system efficiency across the primary operating modes of the flexible heat pump. The thermodynamic model from Chapter 4 was adjusted to account for primary sources of irreversibility, including storage temperature, condensing temperature, compressor efficiency, and the storage-refrigerant temperature differential ΔT_{HS}. The largest temperature differential occurred at heat storage inlet points during both charging and discharging. In charging, this differential is influenced by the condenser outlet temperature, while in discharging, it is controlled by ΔT_{HS}[226]. Results indicate that increasing ΔT_{HS} significantly raises exergy losses in defrosting/discharging mode. In heating/charging mode, it leads to minor reduction in storage losses. Therefore, this parameter should be minimised during discharging, while a balance should be found during charging between the required charging rate and exergy destruction. Compressor isentropic efficiency is the most influential factor in reducing exergy losses of the system. Finite temperature differences in the evaporator and condenser are major sources of exergy destruction, particularly during charging. This highlights the importance of optimising heat exchanger design while balancing cost and size constraints. During defrosting, exergy losses in the inactive evaporator mainly result from temperature difference between the iced coils and the hot gas, so managing this difference is crucial to prevent temperature shock and improve defrosting efficiency. System exergy efficiency in defrosting/discharging mode was found to be twice that in heating/charging mode across all tested refrigerants, with the highest exergy efficiency beings 24.4 % in Mode 1 for R134a, and 43.9 % in Mode 3 for R1234ze(E). This improvement is largely attributed to reduced entropy generation during compression due to a lower compression ratio.

Afterwards, the power-saving application of the flexible heat pump was examined. This operation addresses the inefficiency and high operating cost of air-source heat pumps when operating at high temperature lifts. It was evaluated with a latent heat storage and key parameters such as condensing and evaporating temperatures, superheating and subcooling degrees were incorporated into the thermodynamic model to investigate their impact on the system's thermodynamic behaviour. Results showed that the power-saving mode could effectively increase the COP of the flexible heat pump compared to a conventional heat pump cycle. Specifically, it was found that the maximum improvement storage temperature, highlighted in Chapter 4, increased with higher evaporating and condensing temperatures and was always slightly above the midpoint between the heat storage inlet and evaporating temperatures across all tested refrigerants. Consistent with findings in Chapter 4, R1234yf demonstrated the highest improvement at 24.1 % (in ideal conditions) followed by R410a, R1234ze(E), propane, R134a, and R32. Among the tested parameters, ΔT_{HS} has the greatest impact on reducing the flexible heat pump's average COP, while T_{sb} has the greatest impact on reducing its improvement. The economic and environmental analysis was then conducted to compare the operation of the flexible heat pump over a year of space heating and DHW production in Edinburgh, with a conventional ASHPWH and an A-rated gas boiler. The supplied temperature of the heat pumps was 65 °C, matching the average UK dwelling heating system. It was found that, the flexible heat pump had a lower total annual cost rate than a conventional ASHPWH, thanks to its power-saving mode. Furthermore, the average payback period was four years and could be further reduced if the PCM storage was replaced by a cheaper alternative. Additionally, while the operating costs of the ASHPWH were consistently higher than those of the A-rated gas boiler, the flexible heat pump was cheaper or comparable in three of the four scenarios tested, and only marginally higher by £26 in the least favourable case. When accounting for CO_2e social cost, the flexible heat pump became even more economical across all scenarios. This reduction in operating costs is further supported by CO_2e emission savings, with the flexible heat pump leading to nearly 3.5 times lower emissions than a gas boiler. Finally, in the environmental analysis, both heat pumps' TEWI were evaluated, and the flexible heat pump consistently demonstrated lower TEWI than a conventional ASHPWH across all scenarios. This was largely due to reductions in indirect emissions from decreased electricity consumption. These findings underscore the potential efficiency, economic viability, and environmental benefits of the flexible heat pump compared to both a conventional ASHPWH and a gas boiler, in a UK application.

Finally, the last operating mode of the flexible heat pump was investigated: charging the heat storage at a lower temperature when heating is not required. Both latent and sensible heat storage options were assessed. Performance was evaluated against a conventional heat pump cycle to determine whether storing heat in the absence of heating demand could provide benefits for later use. Extended parameters such as: ΔT_{HS}, compressor efficiency, heat storage losses, condensing temperature for heat supply, and the deviation in water temperature from the maximum improvement storage temperature (ΔT_w) were assessed to understand their effects on performance. Results showed that running Mode 4 instead of Mode 1 still showed improvement over the conventional cycle. However, the average COP and overall improvement were slightly lower than when running Mode 1, as Mode 4 consumes power and doesn't provide heating. For instance, in ideal conditions with R1234yf and a latent heat storage, the COP improvement reached 22.3 % with Mode 4, compared to 24.1 % with Mode 1. The ranking of refrigerants observed across other operating modes was confirmed here, with R1234yf performing best, followed by R410a, R1234ze(E), propane, R134a, and R32. This analysis confirms a correlation between refrigerant properties and the operating principles of the flexible heat pump. Specifically, the shape of the refrigerants' isentropic lines, heat recovery potential, and mass flow rates under operating conditions, influence their potential benefit from increasing their evaporating temperature, which in turn affects the overall performance improvement with the flexible heat pump. The influence of ΔT_{HS} on performance was most pronounced when running Modes 4 and 2, indicating that minimising this parameter is essential for maximum efficiency. When using a sensible heat storage, such as a water tank, ΔT_w became an important factor; it should be low enough to maintain tank temperature close to the maximum value observed with latent heat storage, yet high enough to prevent excessive switching between charging and discharging and to avoid potential heat losses. Increasing ΔT_w up to 10 K was found to have minimal impact on performance. Finally, thermal losses from the storage between modes were evaluated for both storage types, showing that high thermal losses significantly reduce discharging time and performance. This underscores the importance of careful insulation of the storage tanks to maintain the highest performance, especially when heat needs to be stored for long periods of time.

The models and analyses in this thesis addressed the challenges identified in the literature review and the main research questions. The multi-valve flexible heat pump with integrated heat storage demonstrated a novel defrosting method with higher efficiency than conventional reverse cycle defrosting, and enabling continuous heating while defrosting. Moreover, the power-saving mode showed significant potential for improving performance and reducing costs when supplying hot water up to 60 °C. Thus, this thesis establishes the flexible heat pump's potential for efficient operation in UK applications, providing a theoretical foundation for further research and development.

8.2 Directions for future research

Further research is recommended to advance this concept toward practical applications.

<u>A dynamic modelling approach</u> could provide significant insights into the flexible heat pump's real performance. While this thesis used a steady-state model for foundational

analysis, a dynamic model could better capture the complex processes involved and allow for a broader range of parameter evaluations. For instance, the frosting model in Chapter 4 was simplified to approximate ice buildup on the evaporator and estimate the energy needed for defrosting. However, frost formation and melting involve complex physics and factors such as evaporator heat transfer rates, outdoor dew point, and evaporator design, which play a significant role in the process. A dynamic air-source heat pump model could more accurately represent the frosting and defrosting processes, which would help optimise the required refrigerant charge and prevent issues such as excessive pressure shock or liquid slugging in the compressor, as reported in dynamic simulations of hot gas bypass defrosting[289]. Such modelling could also be valuable for evaluating the dynamic impact of frosting on heating capacity and power consumption when additional heat storage is present[290]. Additionally, as highlighted in Chapter 3, the heat storage model used focused on latent heat exchange at a constant temperature on the refrigerant side. In reality, PCM phase change process is non-uniform and involves sensible heat transfer. A comprehensive PCM model could evaluate precise charging and discharging rates, ideal coil placement, and ways to achieve homogeneous heat exchange. Notably, a dynamic approach allows us to see how quickly the heat pump and the storage can respond to load demand and to evaluate their dynamic performance depending on it[291].

<u>Control strategies</u> for switching between modes should also be investigated. As discussed in Chapter 3, mode-switching in the flexible heat pump should be automated through an effective control strategy. The examples in Chapters 2 and 3 provide a starting point, but a more detailed investigation into control strategies, especially using a dynamic model, could improve performance by optimising the timing and conditions for switching between modes.

<u>Refrigerant selection</u> is a critical factor in improving the heat pump performance. This thesis provides a roadmap in refrigerant selection, but further research could extend to refrigerant blends. For instance, while the economic analysis in Chapter 6 used R1234yf due to its improvement, R134a offered the highest COP, suggesting that using R134a might lower operating costs further. Therefore, blends involving R134a might offer performance benefits while reducing its environmental impact, providing a balance between efficiency and regulatory compliance.

<u>Improved heating demand model and economic analysis</u> would also enhance the results accuracy. The heating demand used in Chapter 6 was an annual average based on spatial and temporal temperature variations in Edinburgh. However, heating demand fluctuates seasonally and daily, depending on household occupancy and usage patterns. As such, the

heat pump would likely operate most times in part-load conditions below the assumed 8.5 kW average when heating demand is lower. A dynamic model combined with a refined heat demand model could show more accurate operating cost projections. Additionally, Chapter 7 demonstrated the benefits of Mode 4, but further investigation could quantify cost savings when operating it during off-peak electricity tariffs, in the night for instance.

Finally, an improved experimental rig could provide more precise validation of the flexible heat pump concept. The experimental setup mentioned in Chapter 3 demonstrated the feasibility of a flexible heat pump layout using off-the-shelf parts. A more precise rig would allow for more rigorous testing and investigate practical application issues, supporting the transition of this concept from theory to real world use.

References

1. United Nations. *No more hot air ... please ! - Emissions Gap Report 2024*. (2024).

2. United Nations. The Paris Agreement. https://www.un.org/en/climatechange/paris-agreement.

3. International Energy Agency. Heating. https://www.iea.org/energy-system/buildings/heating#tracking (2023).

4. International Energy Agency. *The future of Heat Pumps*. http://www.sulpu.fi/documents/184029/189661/The future of Heat Pumps.pdf (2022).

5. Rosenow, J., Gibb, D., Nowak, T. & Lowes, R. Heating up the global heat pump market. *Nature Energy* vol. 7 901–904 (2022).

6. Department for Business Energy & Industrial Strategy. *Domestic Heat Distribution Systems: Evidence Gathering*. (2021).

7. UK Parliament. Constituency data: Central heating. *House of Commons Library* https://commonslibrary.parliament.uk/constituency-data-central-heating-2021-census/ (2024).

8. UK Department for Energy Security and Net Zero. Final UK greenhouse gas emissions national statistics: 1990 to 2022. *Accredited official statistics* https://www.gov.uk/government/statistics/final-uk-greenhouse-gas-emissions-national-statistics-1990-to-2022 (2024).

9. UK Government. Climate Change Act 2008. https://www.legislation.gov.uk/ukpga/2008/27/contents (2008).

10. Climate Change Committee. *Progress in reducing emissions: 2021 Report to Parliament*. (2021).

11. Chandrashekar, M. HEAT PUMPS. in *Solar Energy Conversion II* 447–468 (Elsevier, 1981).

12. Gaur, A. S., Fitiwi, D. Z. & Curtis, J. Heat pumps and our low-carbon future: A comprehensive review. *Energy Res. Soc. Sci.* **71**, 101764 (2021).

13. Nishimura, T. ‘Heat pumps - Status and trends’ in Asia and the Pacific. *Int. J. Refrig.* **25**, 405–413 (2002).

14. Çengel, Y. A. & Boles, M. A. *Thermodyamics: An engineering approach*. (McGraw-Hill, 2006).

15. Ansermet, J.-P. & Bréchet, S. *Thermodynamique*. (EPFL PRESS, 2020).

16. Pitarch, M., Hervas-Blasco, E., Navarro-Peris, E., Gonzálvez-Maciá, J. & Corberán, J. M. Evaluation of optimal subcooling in subcritical heat pump systems. *Int. J. Refrig.* **78**, 18–31 (2017).

17. Zehnder, M. Efficient air-water heat pumps for high temperature lift residential heating, including oil mitigation aspects. (2004).

18. Reinholdt, L. *et al.* Heat pump COP, part 1: Generalized method for screening of system integration potentials. in *Proceedings of the13th IIR-Gustav Lorentzen Conference on Natural Refrigerants* vol. 2 1380 (2018).

19. Chua, K. J., Chou, S. K. & Yang, W. M. Advances in heat pump systems : A review. *Appl. Energy* **87**, 3611–3624 (2010).

20. Secretary of State for Business Energy and Industrial Strategy. *Heat and Buildings Strategy*. (2021).

21. Lamb, N. & Elmes, D. Increasing heat pump adoption: analysing multiple perspectives on preparing homes for heat pumps in the UK. *Carbon Neutrality* **3**, (2024).

22. Sohail, A. Motivations and Barriers Associated with Adopting Domestic Heat Pumps in the UK. (2023).

23. Patil, G. J. Evaluating the Economic and Environmental Feasibility of Domestic Hot Water and Heating through a Hybrid Photovoltaic Integrated Heat Pump System in UK Homes. (2024).

24. Rosenow, J. *Analysis: Running costs of heat pumps versus gas boilers*. (2022).

25. Rehman, O. A. *et al.* Analysis on integration of heat pumps and thermal energy storage in current energy system: From research outputs to energy policies. *J. Energy Storage* **97**, 112795 (2024).

26. Jung, Y., Oh, J., Han, U. & Lee, H. A comprehensive review of thermal potential and heat utilization for water source heat pump systems. *Energy Build.* **266**, 112124 (2022).

27. Carroll, P., Chesser, M. & Lyons, P. Air Source Heat Pumps field studies: A systematic literature review. *Renew. Sustain. Energy Rev.* **134**, 110275 (2020).

28. Wang, Y., Wang, J. & He, W. Development of efficient, flexible and affordable heat pumps for supporting heat and power decarbonisation in the UK and beyond: Review and perspectives. *Renew. Sustain. Energy Rev.* **154**, (2022).

29. Energy Saving Trust. In-depth guide to heat pumps. https://energysavingtrust.org.uk/advice/in-depth-guide-to-heat-pumps/ (2024).

30. UK Department for Business Energy & Industrial Strategy. RHI monthly

deployment data: September 2022. https://www.gov.uk/government/statistics/rhi-monthly-deployment-data-september-2022-quarterly-edition (2022).

31. Kelly, N. J., Tuohy, P. G. & Hawkes, A. D. Performance assessment of tariff-based air source heat pump load shifting in a UK detached dwelling featuring phase change-enhanced buffering. *Appl. Therm. Eng.* **71**, 809–820 (2014).

32. Reguis, A., Tunzi, M., Vand, B., Tuohy, P. & Currie, J. Energy performance of Scottish public buildings and its impact on the ability to use low-temperature heat. *Energy Build.* **290**, 113064 (2023).

33. Reguis, A., Vand, B. & Currie, J. Challenges for the Transition to Low-Temperature Heat in the UK : A Review. *Energies* **14**, 1–26 (2021).

34. Millar, M. A., Burnside, N. & Yu, Z. An investigation into the limitations of low temperature district heating on traditional tenement buildings in Scotland. *Energies* **12**, 1–17 (2019).

35. Millar, M. A., Burnside, N. M. & Yu, Z. District heating challenges for the UK. *Energies* **12**, (2019).

36. Kelly, N. J. & Cockroft, J. Analysis of retrofit air source heat pump performance: Results from detailed simulations and comparison to field trial data. *Energy Build.* **43**, 239–245 (2011).

37. Jenkins, D., Tucker, R., Ahadzi, M. & Rawlings, R. The performance of air-source heat pumps in current and future offices. *Energy Build.* **40**, 1901–1910 (2008).

38. Arpagaus, C., Bless, F., Uhlmann, M., Schiffmann, J. & Bertsch, S. High temperature heat pumps : Market overview , state of the art , research status , refrigerants , and application potentials. *Energy* **152**, 985–1010 (2018).

39. Hewitt, N. J., Huang, M. J., Anderson, M. & Quinn, M. Advanced air source heat pumps for UK and European domestic buildings. *Appl. Therm. Eng.* **31**, 3713–3719 (2011).

40. Leonzio, G., Fennell, P. S. & Shah, N. Air-source heat pumps for water heating at a high temperature: State of the art. *Sustain. Energy Technol. Assessments* **54**, 102866 (2022).

41. Sezen, K. & Gungor, A. Performance analysis of air source heat pump according to outside temperature and relative humidity with mathematical modeling. *Energy Convers. Manag.* **263**, 115702 (2022).

42. Saffari, M., Keogh, D., Rosa, M. De & Finn, D. P. Technical and economic assessment of a hybrid heat pump system as an energy retrofit measure in a residential building. *Energy Build.* **295**, 113256 (2023).

43. Guoyuan, M., Qinhu, C. & Yi, J. Experimental investigation of air-source heat

pump for cold regions. *Int. J. Refrig.* **26**, 12–18 (2003).

44. Bahman, A. M., Parikhani, T. & Ziviani, D. Multi-objective optimization of a cold-climate two-stage economized heat pump for residential heating applications. *J. Build. Eng.* **46**, 103799 (2022).

45. Liu, J., Zhou, L., Cheng, J., Lin, Z. & Zhang, X. A novel two-stage compression air-source heat pump cycle combining space heating , cooling , and domestic hot water production. *Energy Build.* **285**, 112863 (2023).

46. Zhang, L., Jiang, Y., Dong, J. & Yao, Y. Advances in vapor compression air source heat pump system in cold regions : A review. *Renew. Sustain. Energy Rev.* **81**, 353–365 (2018).

47. Bertsch, S. S. & Groll, E. A. Air Source Heat Pump for Northern Climates Part I : Simulation of Different Heat Pump Cycles. *Int. Refrig. Air Cond. Conf.* (2006).

48. Yu, Z. & Ouderji, Z. H. A unified approach for the thermodynamic comparison of heat pump cycles. *Commun. Eng.* (2023) doi:10.1038/s44172-023-00112-0.

49. Bertsch, S. S. & Groll, E. A. Two-stage air-source heat pump for residential heating and cooling applications in northern U.S. climates. *Int. J. Refrig.* **31**, 1282–1292 (2008).

50. Arpagaus, C., Bless, F., Uhlmann, M., Schiffmann, J. & Bertsch, S. S. High temperature heat pumps : Market overview , state of the art , research status , refrigerants , and application potentials. *Energy* **152**, (2018).

51. Mateu-royo, C., Navarro-esbrí, J., Mota-babiloni, A., Amat-albuixech, M. & Molés, F. Theoretical evaluation of different high-temperature heat pump configurations for low-grade waste heat recovery Évaluation théorique de différentes configurations de pompes à chaleur à haute température pour la récupération de chaleur résiduelle à basse t. *Int. J. Refrig.* **90**, 229–237 (2018).

52. UK Department for Business Energy & Industrial Strategy. *Evidence Gathering – Low Carbon Heating Technologies Domestic High Temperature Heat Pumps*. (2016).

53. Willem, H., Lin, Y. & Lekov, A. Review of energy efficiency and system performance of residential heat pump water heaters. *Energy Build.* **143**, 191–201 (2017).

54. Wang, X., Hwang, Y. & Radermacher, R. Two-stage heat pump system with vapor-injected scroll compressor using R410A as a refrigerant. *Int. J. Refrig.* **32**, 1442–1451 (2009).

55. Winandy, E. L. & Lebrun, J. Scroll compressors using gas and liquid injection : experimental analysis and modelling. *Int. J. Refrig.* **25**, 1143–1156 (2002).

56. Oquendo, F. M. T., Peris, E. N., Macia, J. G. & Corberán, J. M. Performance of a scroll compressor with vapor-injection and two-stage reciprocating compressor operating under extreme conditions. *Int. J. Refrig.* **63**, 144–156 (2016).

57. Wang, Y., Wang, J. & He, W. Development of efficient , flexible and affordable heat pumps for supporting heat and power decarbonisation in the UK and beyond : Review and perspectives. *Renew. Sustain. Energy Rev.* **154**, 111747 (2022).

58. Cuevas, C. & Lebrun, J. Testing and modelling of a variable speed scroll compressor. *Appl. Therm. Eng.* **29**, 469–478 (2009).

59. Wang, X., Hwang, Y. & Radermacher, R. Investigation of potential benefits of compressor cooling. *Appl. Therm. Eng.* **28**, 1791–1797 (2008).

60. Hervas-Blasco, E., Pitarch, M., Navarro-Peris, E. & Corberán, J. M. Study of different subcooling control strategies in order to enhance the performance of a heat pump. *Int. J. Refrig.* **88**, 324–336 (2018).

61. Jensen, J. K., Ommen, T., Reinholdt, L., Markussen, W. B. & Elmegaard, B. Heat pump COP , part 2 : Generalized COP estimation of heat pump processes. in *Proceedings of the13th IIR-Gustav Lorentzen Conference on Natural Refrigerants* (2018). doi:10.18462/iir.gl.2018.1386.

62. Ommen, T. *et al.* Generalized COP estimation of heat pump processes for operation off the design point of equipment. *Refrig. Sci. Technol.* **2019-Augus**, 998–1005 (2019).

63. Jin, Y., Gao, N. & Wang, T. Influence of heat exchanger pinch point on the control strategy of Organic Rankine cycle (ORC). *Energy* **207**, 118196 (2020).

64. Emadi, M. A. & Mahmoudimehr, J. Modeling and thermo-economic optimization of a new multi-generation system with geothermal heat source and LNG heat sink. *Energy Convers. Manag.* **189**, 153–166 (2019).

65. Pitarch, M., Navarro-Peris, E., Gonzálvez-Maciá, J. & Corberán, J. M. Experimental study of a heat pump with high subcooling in the condenser for sanitary hot water production. *Sci. Technol. Built Environ.* **24**, 105–114 (2018).

66. Obika, E., Heberle, F. & Brüggemann, D. Thermodynamic analysis of novel mixtures including siloxanes and cyclic hydrocarbons for high-temperature heat pumps. *Energy* **294**, 130858 (2024).

67. Venkatarathnam, G., Mokashi, G. & Murthy, S. S. Occurrence of pinch points in condensers and evaporators for zeotropic refrigerant mixtures. *Int. J. Refrig.* **19**, 361–368 (1996).

68. Liu, Z., Zhao, L., Zhao, X. & Li, H. The occurrence of pinch point and its effects on the performance of high temperature heat pump. *Appl. Energy* **97**, 869–875 (2012).

69. Gao, P. & Zhao, L. Theoretical and experimental investigation on components' proportion of zeotropic mixtures based on relation between temperature and enthalpy during phase change. *Energy Convers. Manag.* **49**, 1567–1573 (2008).

70. Fukuda, S., Kondou, C., Takata, N. & Koyama, S. Low GWP refrigerants R1234ze(E) and R1234ze(Z) for high temperature heat pumps. *Int. J. Refrig.* **40**, 161–173 (2013).

71. Kondou, C. & Koyama, S. Thermodynamic Assessment of High-Temperature Heat Pumps for Heat Recovery. in *International Refrigeration and Air Conditioning Conference* (2014).

72. Vering, C., Kroppa, H., Venzik, V., Streblow, R. & Müller, D. Towards an integral decision-making process applied to the refrigerant selection in heat pumps. *Renew. Energy* **192**, 815–827 (2022).

73. ASHRAE. *Update on New Refrigerants Designations and Safety Classifications*. (2022).

74. European Parliament & Council. *Regulation (EU) 2024/573 of the European Parliament and of the Council of 7 February 2024 on fluorinated greenhouse gases, amending Directive (EU) 2019/1937 and repealing Regulation (EU) No 517/2014*. *Official Journal of the European Union* vol. L https://eur-lex.europa.eu/legal-content/DE/TXT/?uri=CELEX:32024R0573 (2024).

75. Environment Agency & UK Department for Environment Food & Rural Affairs. Bans on F gas in new products and equipment: current and future. https://www.gov.uk/guidance/bans-on-f-gas-in-new-products-and-equipment-current-and-future#:~:text=All F gases 'Single split',systems%2C such as chillers or (2023).

76. climalife. *New A2L refrigerants : the balanced approach*.

77. Carrier. *New Refrigerants Impact Standards and Codes*. *Carrier Engineering Newsletter* vol. 3 (2015).

78. Sarbu, I. A review on substitution strategy of non-ecological refrigerants from vapour compression-based refrigeration , air-conditioning and heat pump systems. *Int. J. Refrig.* **46**, 123–141 (2014).

79. Sun, D., Wang, C., Liu, Z., Qin, J. & Liu, Z. Experimental and simulation study on R134a / RE170 / R152a mixture as R134a replacement in a moderately-high temperature heat pump. *Appl. Therm. Eng.* **236**, 121643 (2024).

80. Joon, H., Baek, C., Kang, H., Kim, D. & Kim, Y. Performance evaluation of a gas injection CO 2 heat pump according to operating parameters in extreme heating and cooling conditions. *Energy* **154**, 337–345 (2018).

81. Neksa, P. CO2 heat pump systems. *Int. J. Refrig.* **25**, 421–427 (2002).

82. Lorentzen, G. & Pettersen, J. A new, efficient and environmentally benign system for car air-conditioning. *Int. J. Refrig.* **16**, (1993).

83. Lorentzen, G. The use of natural refrigerants: a complete solution to the CFC/HCFC predicament. *Int. J. Refrig.* **18**, 190–197 (1995).

84. Lorentzen, G. Revival of carbon dioxide as a refrigerant. *Int. J. Refrig.* **17**, (1994).

85. Fernandez, N., Hwang, Y. & Radermacher, R. Comparison of CO2 heat pump water heater performance with baseline cycle and two high COP cycles. *Int. J. Refrig.* **33**, 635–644 (2025).

86. Hu, B., Li, Y., Cao, F. & Xing, Z. Extremum seeking control of COP optimization for air-source transcritical CO2 heat pump water heater system. *Appl. Energy* **147**, 361–372 (2015).

87. Cao, F., Song, Y. & Li, M. Review on development of air source transcritical CO 2 heat pump systems using direct-heated type and recirculating-heated type. *Int. J. Refrig.* **104**, 455–475 (2019).

88. Ituna-yudonago, J. F., Belman-flores, J. M., Elizalde-blancas, F. & García-valladares, O. Numerical investigation of CO 2 behavior in the internal heat exchanger under variable boundary conditions of the transcritical refrigeration system. *Appl. Therm. Eng.* **115**, 1063–1078 (2017).

89. Liu, F., Groll, E. A. & Ren, J. Comprehensive experimental performance analyses of an ejector expansion transcritical CO 2 system. *Appl. Therm. Eng.* **98**, 1061–1069 (2016).

90. Boewe, D. E., Bullard, C. W., Yin, J. M. & Hrnjak, P. S. Contribution of Internal Heat Exchanger to Transcritical R-744 Cycle Performance. *HVAC&R Res.* **7**, (2001).

91. Song, Y. & Cao, F. The evaluation of the optimal medium temperature in a space heating used transcritical air-source CO 2 heat pump with an R134a subcooling device. *Energy Convers. Manag.* **166**, 409–423 (2018).

92. Dai, B. *et al.* Life cycle energy , emissions and cost evaluation of CO2 air source heat pump system to replace traditional heating methods for residential heating in China: System configurations. *Energy Convers. Manag.* **218**, 112954 (2024).

93. Saikawa, M. & Koyama, S. Thermodynamic analysis of vapor compression heat pump cycle for tap water heating and development of CO 2 heat pump water heater for residential use. *Appl. Therm. Eng.* **106**, 1236–1243 (2016).

94. Hashimoto, K. *Technology and Market Development of Co2 heat pump water heaters (Eco cute) in Japan*. (2006).

95. Elbel, S. Historical and present developments of ejector refrigeration systems with

emphasis on transcritical carbon dioxide air-conditioning applications. *Int. J. Refrig.* **34**, 1545–1561 (2011).

96. Chen, X., Zhou, Y. & Yu, J. A theoretical study of an innovative ejector enhanced vapor compression heat pump cycle for water heating application. *Energy Build.* **43**, 3331–3336 (2011).

97. Yu, J., Song, X. & Ma, M. Theoretical study on a novel R32 refrigeration cycle with a two-stage suction ejector. *Int. J. Refrig.* **36**, 166–172 (2013).

98. Sarkar, J. Ejector enhanced vapor compression refrigeration and heat pump systems — A review. *Renew. Sustain. Energy Rev.* **16**, 6647–6659 (2012).

99. Yari, M. & Sirousazar, M. Performance analysis of the ejector-vapour. *J. Power Energy, Part A Proc. Inst. Mech. Eng.* **221**, 1089–1098 (2007).

100. Arpagaus, C., Bless, F., Schiffmann, J. & Bertsch, S. S. Multi-temperature heat pumps : A literature review. *Int. J. Refrig.* **69**, 437–465 (2016).

101. Xu, X., Hwang, Y. & Radermacher, R. Refrigerant injection for heat pumping / air conditioning systems : Literature review and challenges discussions. *Int. J. Refrig.* **34**, 402–415 (2010).

102. Liu, Z. & Soedel, W. A Mathematical Model for Simulating Liquid and Vapor Two-Phase Compression Processes and Investigating Slugging Problems in Compressors. *HVAC&R Res.* **1**, (2011).

103. Biao, X. *et al.* Experimental study of an improved air-source heat pump system with a novel three-cylinder two-stage variable volume ratio rotary compressor. *Int. J. Refrig.* **100**, 343–353 (2019).

104. Wang, W., Li, Y. & Cao, F. Extremum seeking control for efficient operation of an air-source heat pump water heater with internal heat exchanger cycle vapor injection. **99**, 153–165 (2019).

105. Baek, C., Heo, J., Jung, J., Cho, H. & Kim, Y. Performance characteristics of a two-stage CO 2 heat pump water heater adopting a sub-cooler vapor injection cycle at various operating conditions. *Energy* **77**, 570–578 (2014).

106. Minh, N. Q., Hewitt, N. J. & Eames, P. C. Improved Vapour Compression Refrigeration Cycles : Literature Review and Their Application to Heat Pumps. in *International Refrigeration and Air Conditioning Conference* (2006).

107. Okuma, T., Radermacher, R. & Hwang, Y. A novel application of thermoelectric modules in an HVAC system under cold climate operation. *J. Electron. Mater.* **41**, 1749–1758 (2012).

108. Wu, C. *et al.* Low-temperature air source heat pump system for heating in severely cold area: Long-term applicability evaluation. *Build. Environ.* **208**, 108594 (2022).

109. Ceylan, H. Review on the two-stage vapor injection heat pump with a flash tank. *Eng. Sci. Technol. an Int. J.* **48**, 101583 (2023).

110. Wei, W. *et al.* Technical, economic and environmental investigation on heating performance of quasi-two stage compression air source heat pump in severe cold region. *Energy Build.* **223**, 110152 (2020).

111. Sun, S., Guo, H. & Gong, M. Thermodynamic analysis of single-stage compression air-source heat pumps with different recuperation ways for large temperature lift. *Int. J. Refrig.* **108**, 91–102 (2019).

112. Sun, S., Guo, H., Lu, D., Bai, Y. & Gong, M. Performance of a single-stage recuperative high-temperature air source heat pump. *Appl. Therm. Eng.* **193**, 116969 (2021).

113. Osterman, E. & Stritih, U. Review on compression heat pump systems with thermal energy storage for heating and cooling of buildings. *J. Energy Storage* **39**, 102569 (2021).

114. Meng, X., Zhou, X. & Li, Z. Review of the Coupled System of Solar and Air Source Heat Pump. *energies* **17**, 6045 (2024).

115. Ren, C., Lin, J. & Guo, N. Performance and Optimization of Novel Solar-Assisted Heat Pump System with Hybrid Thermal Energy Storage. *energies* **17**, 5944 (2024).

116. Shi, G. H., Aye, L., Li, D. & Du, X. J. Recent advances in direct expansion solar assisted heat pump systems: A review. *Renew. Sustain. Energy Rev.* **109**, 349–366 (2019).

117. Sun, X., Dai, Y., Novakovic, V., Wu, J. & Wang, R. Performance Comparison of Direct Expansion Solar-assisted Heat Pump and Conventional Air Source Heat Pump for Domestic Hot Water. *Energy Procedia* **70**, 394–401 (2015).

118. Liu, Z. *et al.* Performance and feasibility study of solar-air source pump systems for low-energy residential buildings in Alpine regions. *J. Clean. Prod.* **256**, (2020).

119. Du, H. *et al.* Performance Analysis of Solar and Air Source Heat Pump Hybrid Heating Systems applied in Shandong Rural Area. *IOP Conf. Ser. Earth Environ. Sci.* **238**, (2019).

120. Wang, G. *et al.* Experimental study on a novel PV/T air dual-heat-source composite heat pump hot water system. *Energy Build.* **108**, 175–184 (2015).

121. Pei, G., Ji, J., Han, C. & Fan, W. Performance of solar assisted heat pump using PV evaporator under different compressor frequency. in *ISES Solar World Congress 2007, ISES 2007* vol. 2 935–939 (2007).

122. Cai, J., Ji, J., Wang, Y., Zhou, F. & Yu, B. A novel PV/T-air dual source heat pump water heater system: Dynamic simulation and performance characterization. *Energy*

Convers. Manag. **148**, 635–645 (2017).

123. Plytaria, M. T., Bellos, E., Tzivanidis, C. & Antonopoulos, K. A. Financial and energetic evaluation of solar-assisted heat pump underfloor heating systems with phase change materials. *Appl. Therm. Eng.* **149**, 548–564 (2019).

124. Yao, J., Xu, H., Dai, Y. & Huang, M. Performance analysis of solar assisted heat pump coupled with build-in PCM heat storage based on PV/T panel. *Sol. Energy* **197**, 279–291 (2020).

125. Wu, J., Xian, T. & Liu, X. All-weather characteristic studies of a direct expansion solar integrated air source heat pump system based on PCMs. *Sol. Energy* **191**, 34–45 (2019).

126. Highlights, T., Heat, I. & Conference, P. The next step in the green revolution : Heat Pumps with Thermal Storage. *IEA Heat Pumping Technologies MAGAZINE* vol. 40 (2021).

127. Hirschey, J., Li, Z., Gluesenkamp, K. R., LaClair, T. J. & Graham, S. Demand reduction and energy saving potential of thermal energy storage integrated heat pumps. *Int. J. Refrig.* **148**, 179–192 (2023).

128. Dincer, I. & Rosen, M. A. *Thermal energy storage: systems and applications*. *Wiley* (2011).

129. Hepbasli, A. & Kalinci, Y. A review of heat pump water heating systems. *Renew. Sustain. Energy Rev.* **13**, 1211–1229 (2009).

130. Renaldi, R., Kiprakis, A. & Friedrich, D. An optimisation framework for thermal energy storage integration in a residential heat pump heating system. *Appl. Energy* **186**, 520–529 (2017).

131. Zhou, C. *et al.* A Review of the Performance Improvement Methods of Phase Change Materials : Application for the Heat Pump Heating System. *energies* **16**, 2676 (2023).

132. Gu, H., Chen, Y., Yao, X., Huang, L. & Zou, D. Review on heat pump (HP) coupled with phase change material (PCM) for thermal energy storage. *Chem. Eng. J.* **455**, 140701 (2023).

133. Zou, D. *et al.* Experimental research of an air-source heat pump water heater using water-PCM for heat storage. *Appl. Energy* **206**, 784–792 (2017).

134. Gado, M. G. & Hassan, H. Energy-saving potential of compression heat pump using thermal energy storage of phase change materials for cooling and heating applications. *Energy* **263**, 126046 (2023).

135. Lin, Y., Fan, Y., Yu, M., Jiang, L. & Zhang, X. Performance investigation on an air source heat pump system with latent heat thermal energy storage. *Energy* **239**,

121898 (2022).

136. Koşan, M. & Aktaş, M. Experimental investigation of a novel thermal energy storage unit in the heat pump system. *J. Clean. Prod.* **311**, (2021).

137. Long, J. Y. & Zhu, D. S. Numerical and experimental study on heat pump water heater with PCM for thermal storage. *Energy Build.* **40**, 666–672 (2008).

138. Le, K. X. *et al.* High Temperature Air Source Heat Pump Coupled with Thermal Energy Storage : Comparative Performances and Retrofit Analysis. in *Energy Procedia* vol. 158 3878–3885 (Elsevier B.V., 2019).

139. Péan, T. Q., Salom, J. & Costa-Castelló, R. Review of control strategies for improving the energy flexibility provided by heat pump systems in buildings. *J. Process Control* **74**, 35–49 (2019).

140. Aguilera, J. J. *et al.* Operation optimization in large-scale heat pump systems: A scheduling framework integrating digital twin modelling, demand forecasting, and MILP. *Appl. Energy* **376**, 124259 (2024).

141. Mugnini, A., Evens, M. & Arteconi, A. Model predictive controls for residential buildings with heat pumps: Experimentally validated archetypes to simplify the large-scale application. *Energy Build.* **320**, 114632 (2024).

142. Wüllhorst, F., Reuter-Schniete, J., Maier, L. & Müller, D. Heat pump and thermal energy storage: Influences of photovoltaic, the control strategy, and price assumptions on the optimal design. *Renew. Energy* **236**, 121409 (2024).

143. Lee, K.-H., Joo, M.-C. & Baek, N.-C. Experimental Evaluation of Simple Thermal Storage Control Strategies in Low-Energy Solar Houses to Reduce Electricity Consumption during Grid On-Peak Periods. **8**, 9344–9364 (2015).

144. Dar, U. I., Sartori, I., Georges, L. & Novakovic, V. Advanced control of heat pumps for improved flexibility of Net-ZEB towards the grid. *Energy Build.* **69**, 74–84 (2014).

145. Schibuola, L., Scarpa, M. & Tambani, C. Demand response management by means of heat pumps controlled via real time pricing. *Energy Build.* **90**, 15–28 (2015).

146. Afram, A. & Janabi-Sharifi, F. Theory and applications of HVAC control systems – A review of model predictive control (MPC). *Build. Environ.* **72**, 343–355 (2014).

147. Aschidamini, G. L. *et al.* Comprehensive Review on the Control of Heat Pumps for Energy Flexibility in Distribution Networks. doi:10.1109/ACCESS.2025.3569761.

148. Kuboth, S., Weith, T., Heberle, F., Welzl, M. & Brüggemann, D. Experimental Long-Term Investigation of Model Predictive Heat Pump Control in Residential Buildings with Photovoltaic Power Generation. doi:10.3390/en13226016.

149. Tomás, L., Lämmle, M. & Pfafferott, J. Demonstration and Evaluation of Model Predictive Control (MPC) for a Real-World Heat Pump System in a Commercial Low-Energy Building for Cost Reduction and Enhanced Grid Support. (2025) doi:10.3390/en18061434.

150. Klepic, V., Wolf, M. & Pröll, T. Extension of a low-tech Model Predictive Control (MPC) algorithm for grid-supportive heat pump operation. *Energy Build.* **323**, 114733 (2024).

151. Carroll, P., Chesser, M. & Lyons, P. Air Source Heat Pumps field studies : A systematic literature review. *Renew. Sustain. Energy Rev.* **134**, 110275 (2020).

152. Wang, S. W. & Liu, Z. Y. A new method for preventing HP from frosting. *Renew. Energy* **30**, 753–761 (2005).

153. Tassou, S. A. & Marquand, C. J. Effects of evaporator frosting and defrosting on the performance of air-to-water heat pumps. *Appl. Energy* **28**, 19–33 (1987).

154. Yao, Y., Jiang, Y., Deng, S. & Ma, Z. A study on the performance of the airside heat exchanger under frosting in an air source heat pump water heater/chiller unit. *Int. J. Heat Mass Transf.* **47**, 3745–3756 (2004).

155. Huang, D., He, Z. L. & Yuan, X. L. Dynamic characteristics of an air-to-water heat pump under frosting/defrosting conditions. *Appl. Therm. Eng.* **27**, 1996–2002 (2007).

156. Rodriguez, A. G., Neal, D. O., Davis & Kondepudi, S. Effect of reduced evaporator airflow on the high temperature performance of air conditioners. *Energy Build.* **24**, 195–201 (1996).

157. Ma, L. *et al.* Advancements in anti-frosting and defrosting techniques for air source heat pumps: A comprehensive review of recent progress. *Appl. Energy* **377**, 124358 (2025).

158. Wang, W., Xiao, J., Guo, Q. C., Lu, W. P. & Feng, Y. C. Field test investigation of the characteristics for the air source heat pump under two typical mal-defrost phenomena. *Appl. Energy* **88**, 4470–4480 (2011).

159. Votsis, P. P., Tassou, S. A., Wilson, D. R. & Marquand, C. J. Investigation of the performance of a heat pump under frosting and defrosting conditions. *Heat Recover. Syst. CHP* **9**, 399–406 (1989).

160. Zhang, L., Hihara, E. & Saikawa, M. Combination of air-source heat pumps with liquid desiccant dehumidification of air. *Energy Convers. Manag.* **57**, 107–116 (2012).

161. Zhang, L., Dang, C. & Hihara, E. Performance analysis of a no-frost hybrid air conditioning system with integrated liquid desiccant dehumidification. *Int. J. Refrig.* **33**, 116–124 (2010).

162. Kwak, K. & Bai, C. A study on the performance enhancement of heat pump using electric heater under the frosting condition: Heat pump under frosting condition. *Appl. Therm. Eng.* **30**, 539–543 (2010).

163. Mader, G. & Thybo, C. A new method of defrosting evaporator coils. *Appl. Therm. Eng.* **39**, 78–85 (2012).

164. Mei, V. C. *et al.* A frost-less heat pump. *ASHRAE Trans.* **108**, 452–459 (2002).

165. Wang, D., Tao, T., Xu, G., Luo, A. & Kang, S. Experimental study on frosting suppression for a finned-tube evaporator using ultrasonic vibration. *Exp. Therm. Fluid Sci.* **36**, 1–11 (2012).

166. Adachi, K., Saiki, K., Sato, H. & Ito, T. Ultrasonic frost suppression. *Japanese J. Appl. Physics, Part 1 Regul. Pap. Short Notes Rev. Pap.* **42**, 682–685 (2003).

167. Tan, H. *et al.* Experimental study on defrosting mechanism of intermittent ultrasonic resonance for a finned-tube evaporator. *Exp. Therm. Fluid Sci.* **52**, 308–317 (2014).

168. Amer, M. & Wang, C. C. Review of defrosting methods. *Renew. Sustain. Energy Rev.* **73**, 53–74 (2017).

169. Byun, J. S., Lee, J. & Jeon, C. D. Frost retardation of an air-source heat pump by the hot gas bypass method. *Int. J. Refrig.* **31**, 328–334 (2008).

170. Ameen, F. R., Coney, J. E. R. & Sheppard, C. G. W. Experimental study of warm-air defrosting of heat-pump evaporators. *Int. J. Refrig.* **16**, 13–18 (1993).

171. Bansal, P., Fothergill, D. & Fernandes, R. Thermal analysis of the defrost cycle in a domestic freezer. *Int. J. Refrig.* **33**, 589–599 (2010).

172. Abdel-Wahed, R. M., Hifni, M. A. & Sherif, S. A. Hot water defrosting of a horizontal flat plate cooling surface. *Int. J. Refrig.* **6**, 152–154 (1983).

173. Hewitt, N. & Huang, M. J. Defrost cycle performance for a circular shape evaporator air source heat pump. *Int. J. Refrig.* **31**, 444–452 (2008).

174. Song, M., Xu, X., Mao, N., Deng, S. & Xu, Y. Energy transfer procession in an air source heat pump unit during defrosting. *Appl. Energy* **204**, 679–689 (2017).

175. Wellig, B., Imholz, M., Albert, M. & Hilfiker, K. Defrosting the fin tube evaporators of air/water heat pumps using ambient air. in *9th International IEA Heat Pump Conference* (2008).

176. Melo, C., Knabben, F. T. & Pereira, P. V. An experimental study on defrost heaters applied to frost-free household refrigerators. *Appl. Therm. Eng.* **51**, 239–245 (2013).

177. Huang, D., Li, Q. & Yuan, X. Comparison between hot-gas bypass defrosting and reverse-cycle defrosting methods on an air-to-water heat pump. *Appl. Energy* **86**,

1697–1703 (2009).

178. Parker Hannifin Corporation. *Hot Gas Defrost for Ammonia Evaporators*. http://www.parker.com/literature/Refrigerating Specialties Division/Brochures/Bulletin 90-11c.pdf (2012).

179. Hu, B., Wang, X., Cao, F., He, Z. & Xing, Z. Experimental analysis of an air-source transcritical CO2 heat pump water heater using the hot gas bypass defrosting method. *Appl. Therm. Eng.* **71**, 528–535 (2014).

180. Xi, Z. *et al.* Experimental studies on hot gas bypass defrosting control strategies for air source heat pumps. *J. Build. Eng.* **43**, 103165 (2021).

181. Choi, H., Kim, B., Kang, D. & Chun, K. Defrosting method adopting dual hot gas bypass for an air-to-air heat pump. *Appl. Energy* **88**, 4544–4555 (2011).

182. Rong, X. *et al.* Experimental study on a multi-evaporator mutual defrosting system for air source heat pumps. *Appl. Energy* **332**, 120528 (2023).

183. Niu, J., Ma, G. & Xu, S. Experimental research on hot liquid defrosting system with multiple evaporators. *Appl. Therm. Eng.* **179**, 115710 (2020).

184. Ma, G., Lu, T., Liu, F., Niu, J. & Xu, S. Experimental study on hot liquid subcooling defrosting of an air source heat pump with multi-connected outdoor units. *Energy Build.* **291**, 113104 (2023).

185. Minglu, Q., Liang, X., Shiming, D. & Yiqiang, J. A study of the reverse cycle defrosting performance on a multi-circuit outdoor coil unit in an air source heat pump – Part I : Experiments. *Appl. Energy* **91**, 122–129 (2012).

186. Dong, J., Deng, S., Jiang, Y., Xia, L. & Yao, Y. An experimental study on defrosting heat supplies and energy consumptions during a reverse cycle defrost operation for an air source heat pump. *Appl. Therm. Eng.* **37**, 380–387 (2012).

187. Ma, J., Kim, D., Braun, J. E. & Horton, W. T. Development and validation of a dynamic modeling framework for air-source heat pumps under cycling of frosting and reverse-cycle defrosting. *Energy* **272**, 127030 (2023).

188. Ma, L. *et al.* Experimental investigation on an air source heat pump system with coupled liquid-storage gas-liquid separator regarding heating and defrosting performance. *Int. J. Refrig.* **134**, 176–188 (2022).

189. Qu, M., Pan, D., Xia, L., Deng, S. & Jiang, Y. A study of the reverse cycle defrosting performance on a multi-circuit outdoor coil unit in an air source heat pump – Part II : Modeling analysis. *Appl. Energy* **91**, 274–280 (2012).

190. Mashhadian, A., Ismail, T., Bach, C. K. & Alexander, A. A Review Of The Effects And Mitigation Of Frost With Focus On Air-Source Heat Pump Applications. in *19th International Refrigeration and Air Conditioning Conference* (2022).

191. Shen, J., Qian, Z., Xing, Z., Yu, Y. & Ge, M. A review of the defrosting methods of air source heat pumps using heat exchanger with phase change material. *Energy Procedia* **160**, 491–498 (2019).

192. Song, M., Tian, Y., Zhang, L., Dang, C. & Hu, Y. Review on the optimization studies of reverse cycle defrosting for air source heat pump units with multi-circuit outdoor coils. *Int. J. Green Energy* **20**, 1401–1422 (2023).

193. O'Neal, D. L., Peterson, K. & Anand, N. K. Effect of short-tube orifice size on the performance of an air source heat pump during the reverse-cycle defrost. *Int. J. Refrig.* **14**, 52–57 (1991).

194. Ding, Y., Ma, G., Chai, Q. & Jiang, Y. Experiment investigation of reverse cycle defrosting methods on air source heat pump with TXV as the throttle regulator. *Int. J. Refrig.* **27**, 671–678 (2004).

195. Qu, M., Xia, L., Deng, S. & Jiang, Y. An experimental investigation on reverse-cycle defrosting performance for an air source heat pump using an electronic expansion valve. *Appl. Energy* **97**, 327–333 (2012).

196. Song, M., Deng, S., Mao, N. & Ye, X. An experimental study on defrosting performance for an air source heat pump unit with a horizontally installed multi-circuit outdoor coil. *Appl. Energy* **165**, 371–382 (2016).

197. Yu, S., Su, Y., Cai, W. & Qiu, G. Experimental investigation on an air source heat pump system with a novel anti-frosting evaporator. *Appl. Therm. Eng.* **221**, (2023).

198. Anand, N. K., Schliesing, J. S., O'Neal, D. L. & Peterson, K. T. Effects of Outdoor Coil Fan Pre-Start on Pressure Transients during the Reverse Cycle Defrost of a Heat Pump. *ASHRAE Trans.* (1989).

199. Huang, D., Yuan, X. & Zhang, X. Effects of fan-starting methods on the reverse-cycle defrost performance of an air-to-water heat pump. *Int. J. Refrig.* **27**, 869–875 (2004).

200. Wang, F., Liang, C. H., Yang, M. T. & Zhang, X. S. Preliminary study of a novel defrosting method for air source heat pumps based on superhydrophobic fin. *Appl. Therm. Eng.* **90**, 136–144 (2015).

201. Jhee, S., Lee, K. & Kim, W. Effect of surface treatments on the frosting / defrosting behavior of a fin-tube heat exchanger. *Int. J. Refrig.* **25**, 1047–1053 (2002).

202. Wang, W. *et al.* Performances of air source heat pump system for a kind of mal-defrost phenomenon appearing in moderate climate conditions. *Appl. Energy* **112**, 1138–1145 (2013).

203. Zheng, X., Shi, R., You, S., Han, Y. & Shi, K. Experimental study of defrosting control method based on image processing technology for air source heat pumps. *Sustain. Cities Soc.* **51**, 101667 (2019).

204. Bai, X., Liu, S., Deng, S., Zhang, L. & Wei, M. An optimal control strategy for ASHP units with a novel dual-fan outdoor coil for evener frosting along airflow direction based on GRNN modelling. *Energy Build.* **292**, 113136 (2023).

205. Wang, W. *et al.* A novel defrosting initiation strategy based on convolutional neural network for air-source heat pump. *Int. J. Refrig.* **128**, 95–103 (2021).

206. Lawrence, J. M. W. & Evans, J. A. Refrigerant flow instability as a means to predict the need for defrosting the evaporator in a retail display freezer cabinet. *Int. J. Refrig.* **31**, 107–112 (2008).

207. Paone, N. & Rosi, G. L. Fiber-optic ice sensors for refrigerators. in *Society of Photo-Optical Instrumentation Engineers* vol. 1511 129–139 (1991).

208. Wang, W., Xiao, J., Feng, Y., Guo, Q. & Wang, L. Characteristics of an air source heat pump with novel photoelectric sensors during periodic frost-defrost cycles. *Appl. Therm. Eng.* **50**, 177–186 (2013).

209. Jang, J. Y., Bae, H. H., Lee, S. J. & Ha, M. Y. Continuous heating of an air-source heat pump during defrosting and improvement of energy efficiency. *Appl. Energy* **110**, 9–16 (2013).

210. Wenju, H. *et al.* An experimental study on the operating performance of a novel reverse-cycle hot gas defrosting method for air source heat pumps. *Appl. Therm. Eng.* **31**, 363–369 (2011).

211. Qu, M., Deng, S. & Jiang, Y. An experimental Study on the Defrosting Performance of a Pcm-Based Reverse-Cycle Defrosting Method for Air Source Heat Pumps. *Int. J. Air-Conditioning Refrig.* **18**, 327–337 (2010).

212. Dong, J., Jiang, Y., Yao, Y. & Zhang, X. Operating performance of novel reverse-cycle defrosting method based on thermal energy storage for air source heat pump. *J. Cent. South Univ. Technol.* **18**, 2163–2169 (2011).

213. Minglu, Q., Liang, X., Deng, S. & Yiqiang, J. Improved indoor thermal comfort during defrost with a novel reverse-cycle defrosting method for air source heat pumps. *Build. Environ.* **45**, 2354–2361 (2010).

214. Dong, J., Zhang, L. & Jiang, Y. A comparative study on system performances of multi-split air source heat pump with different energy accumulators and storage methods. *Energy Build.* **231**, 110588 (2021).

215. Qu, M., Li, T., Deng, S., Fan, Y. & Li, Z. Improving defrosting performance of cascade air source heat pump using thermal energy storage based reverse cycle defrosting method. *Appl. Therm. Eng.* **121**, 728–736 (2017).

216. Qu, M., Tang, Y., Zhang, T., Li, Z. & Chen, J. Experimental investigation on the multi-mode heat discharge process of a PCM heat exchanger during TES based reverse cycle defrosting using in cascade air source heat pumps. *Appl. Therm. Eng.*

151, 154–162 (2019).

217. Long, Z., Jiankai, D., Yiqiang, J. & Yang, Y. A novel defrosting method using heat energy dissipated by the compressor of an air source heat pump. *Appl. Energy* **133**, 101–111 (2014).

218. Wang, Z. *et al.* Experimental analysis on a novel frost-free air-source heat pump water heater system. *Appl. Therm. Eng.* **70**, 808–816 (2014).

219. Wang, F. *et al.* Performance investigation of a novel frost-free air-source heat pump water heater combined with energy storage and dehumidification. *Appl. Energy* **139**, 212–219 (2015).

220. Wang, Z., Wang, F., Ma, Z., Song, M. & Fan, W. Experimental performance analysis and evaluation of a novel frost-free air source heat pump system. *Energy Build.* **175**, 69–77 (2018).

221. Wang, Z., Wang, F., Ma, Z., Li, C. & Xu, Y. Performance evaluation of a novel frost-free air-source heat pump integrated with phase change materials (PCMs) and dehumidification. *Energy Procedia* **121**, 134–141 (2017).

222. Wang, Z. *et al.* Dynamic character investigation and optimization of a novel air-source heat pump system. *Appl. Therm. Eng.* **111**, 122–133 (2017).

223. Yu, Z., Mckeown, A., Ouderji, Z. H. & Essadik, M. A flexible heat pump cycle for heat recovery. *Commun. Eng.* 17 (2022) doi:10.1038/s44172-022-00018-3.

224. Reichl, C. *et al.* Frosting in heat pump evaporators part A: Experimental investigation. *Appl. Therm. Eng.* **199**, (2021).

225. Zhang, N., Lu, Y., Kadam, S. & Yu, Z. A fuel cell range extender integrating with heat pump for cabin heat and power generation. *Appl. Energy* **348**, 121600 (2023).

226. Bouadila, S., Lazaar, M., Skouri, S., Kooli, S. & Farhat, A. Energy and exergy analysis of a new solar air heater with latent storage energy. *Int. J. Hydrogen Energy* **39**, 15266–15274 (2014).

227. Nami, H., Ranjbar, F., Yari, M. & Saeidi, S. Thermodynamic analysis of a modified oxy-fuel cycle, high steam content Graz cycle with a dual-pressure heat recovery steam generator. *Int. J. Exergy* **21**, 331 (2016).

228. Yari, M. Exergetic analysis of various types of geothermal power plants. *Renew. Energy* **35**, 112–121 (2010).

229. Yataganbaba, A., Kilicarslan, A. & Kurtbaş, I. Exergy analysis of R1234yf and R1234ze as R134a replacements in a two evaporator vapour compression refrigeration system. *Int. J. Refrig.* **60**, 26–37 (2015).

230. Dincer, I. & Rosen, M. A. *Exergy: Energy,Environment And Sustainable*

Development. Elsevier (Elsevier, 2007).

231. Jegadheeswaran, S., Pohekar, S. D. & Kousksou, T. Exergy based performance evaluation of latent heat thermal storage system: A review. *Renew. Sustain. Energy Rev.* **14**, 2580–2595 (2010).

232. Rahimi, M., Ardahaie, S. S., Hosseini, M. J. & Gorzin, M. Energy and exergy analysis of an experimentally examined latent heat thermal energy storage system. *Renew. Energy* **147**, 1845–1860 (2020).

233. Rezaei, M. *et al.* Performance and cost analysis of phase change materials with different melting temperatures in heating systems. *Energy* **53**, 173–178 (2013).

234. Dincer, I. & Rosen, M. A. *Exergy Analysis of Heating, Refrigerating, and Air Conditioning*. (Elsevier, 2015).

235. Byrne, P. Analyse exergétique du fonctionnement de thermofrigopompes. in *Rencontres Universitaires de Genie Civilversitaires de Genie Civil* (2015). doi:hal-01167578.

236. Byrne, P. & Ghoubali, R. Exergy analysis of heat pumps for simultaneous heating and cooling. *Appl. Therm. Eng.* **149**, 414–424 (2019).

237. Asbik, M. *et al.* Exergy analysis of solar desalination still combined with heat storage system using phase change material (PCM). *Desalination* **381**, 26–37 (2016).

238. Stephan, W. *et al. Design Handbook for Reversible Heat Pump Systems with and without Heat Recovery*. (2011).

239. Mancini, R., Zühlsdorf, B., Kjær Jensen, J., Brix Markussen, W. & Elmegaard, B. Deriving guidelines for the design of plate evaporators in heat pumps using zeotropic mixtures. *Energy* **156**, 492–508 (2018).

240. Renaldi, R., Hall, R., Jamasb, T. & Roskilly, A. P. Experience rates of low-carbon domestic heating technologies in the United Kingdom. *Energy Policy* **156**, 112387 (2021).

241. Sanaye, S. & Shirazi, A. Thermo-economic optimization of an ice thermal energy storage system for air-conditioning applications. *Energy Build. j* **60**, 100–109 (2013).

242. Pelella, F., Zsembinszki, G., Viscito, L., Mauro, A. & Cabeza, L. F. Thermo-economic optimization of a multi-source (air/sun/ground) residential heat pump with a water/PCM thermal storage. *Appl. Energy* **331**, 120398 (2023).

243. Rubitherm Technologies GmbH. RubiTherm Technologies. https://www.rubitherm.eu/en/productcategory/organische-pcm-rt.

244. Nikitin, A. *et al.* Comparative study of air source and ground source heat pumps in 10 coldest Russian cities based on energy-exergy-economic-environmental analysis. *J. Clean. Prod.* **321**, 128979 (2021).

245. Dincer, I., Rosen, M. A. & Ahmadi, P. *Optimization of energy systems*. *Optimization of Energy Systems* (2017). doi:10.1002/9781118894484.

246. Yang, L. W. *et al.* Analysis of operation performance of three indirect expansion solar assisted air source heat pumps for domestic heating. *Energy Convers. Manag.* **252**, 115061 (2022).

247. Zhang, N., Lu, Y., Kadam, S. & Yu, Z. A fuel cell range extender integrating with heat pump for cabin heat and power generation. *Appl. Energy* **348**, 121600 (2023).

248. Staubach, D., Michel, B. & Revellin, R. Refrigerant selection from an economic and TEWI analysis of cascade refrigeration systems in Europe based on annual weather data. *Appl. Therm. Eng.* **230**, 120747 (2023).

249. Ibrahim, O., Fardoun, F., Younes, R. & Louahlia-Gualous, H. Air source heat pump water heater: Dynamic modeling, optimal energy management and mini-tubes condensers. *Energy* **64**, 1102–1116 (2014).

250. Johnson, E. P. Air-source heat pump carbon footprints: HFC impacts and comparison to other heat sources. *Energy Policy* **39**, 1369–1381 (2011).

251. Sánchez, D. *et al.* Energy performance evaluation of R1234yf, R1234ze(E), R600a, R290 and R152a as low-GWP R134a alternatives. *Int. J. Refrig.* **74**, 267–280 (2017).

252. Sayyaadi, H., Amlashi, E. H. & Amidpour, M. Multi-objective optimization of a vertical ground source heat pump using evolutionary algorithm. *Energy Convers. Manag.* **50**, 2035–2046 (2009).

253. Duprez, M. E., Dumont, E. & Frère, M. Modelling of reciprocating and scroll compressors. *Int. J. Refrig.* **30**, 873–886 (2007).

254. Shuxue, X., Jianhui, N., Zengyan, C. & Guoyuan, M. Experimental research on vapor-injected heat pump using injection subcooling. *Appl. Therm. Eng.* **136**, 674–681 (2018).

255. Schulz, M. & Kourkoulas, D. *Regulation (EU) No 517/2014 of the European Parliament and of the Council of 16 April 2014 on fluorinated greenhouse gases and repealing Regulation (EC) No 842/2006. Official Journal of the European Union* http://eur-lex.europa.eu/eli/reg/2014/517/oj (2014).

256. REFPROP | NIST. https://www.nist.gov/srd/refprop.

257. Essadik, M., Hajabdollahi, Z., Mckeown, A., Lu, Y. & Yu, Z. A multi-valve flexible heat pump system with latent thermal energy storage for defrosting operation.

Energy Build. **321**, 114656 (2024).

258. Østergaard, D. S., Smith, K. M., Tunzi, M. & Svendsen, S. Low-temperature operation of heating systems to enable 4th generation district heating: A review. *Energy* **248**, 123529 (2022).

259. Wahi, P., Konstantinou, T., Tenpierik, M. J. & Visscher, H. Lower temperature heating integration in the residential building stock: A review of decision-making parameters for lower-temperature-ready energy renovations. *J. Build. Eng.* **65**, 105811 (2023).

260. Chung, Y., Na, S. I., Yoo, J. W. & Kim, M. S. A determination method of defrosting start time with frost accumulation amount tracking in air source heat pump systems. *Appl. Therm. Eng.* **184**, 116405 (2021).

261. Milev, G., Al-Habaibeh, A., Fanshawe, S. & Siena, F. L. Investigating the effect of the defrost cycles of air-source heat pumps on their electricity demand in residential buildings. *Energy Build.* **300**, 113656 (2023).

262. Ma, J., Kim, D. & Braun, J. E. Dynamic Modeling of Air Source Heat Pumps under Reverse-cycle Defrosting. in *International Refrigeration and Air Conditioning Conference* (2022).

263. Essadik, M., Ouderji, Z. H. & Yu, Z. Combined exergy-pinch point analysis of a multi-valve flexible heat pump with integrated latent thermal energy storage for defrosting operation. *Int. J. Refrig.* **176**, 254–267 (2025).

264. Bejan, A. Entropy generation minimization: The new thermodynamics of finite-size devices and finite-time processes. *J. Appl. Phys.* **79**, 1191–1218 (1996).

265. Bejan, A. & Kestin, J. Entropy Generation Through Heat and Fluid Flow. *J. Appl. Mech.* **50**, 475 (1983).

266. Dincer, I. & Cengel, Y. A. Energy, Entropy and Exergy Concepts and Their Roles in Thermal Engineering. *Entropy* **3**, 116–149 (2001).

267. Reyes, E. T., Nuñez, M. P. & Cervantes de G., J. Exergy analysis and optimization of a solar-assisted heat pump. *Energy* **23**, 337–344 (1998).

268. Kumar, A. & Kumar, R. Thermodynamic analysis of a novel compact power generation and waste heat operated absorption, ejector-jet pump refrigeration cycle. *J. Mech. Sci. Technol.* **28**, 3895–3902 (2014).

269. Wang, Z., Wang, F., Gao, X., Li, K. & Lou, Y. Exergy analysis of a frost-free air source heat pump system. *J. Mech. Sci. Technol.* **33**, 2439–2450 (2019).

270. Hajabdollahi, Z. & Fu, P. F. Multi-objective based configuration optimization of SOFC-GT cogeneration plant. *Appl. Therm. Eng.* **112**, 549–559 (2017).

271. Baldi, M. G. & Leoncini, L. Effect of reference state characteristics on the Thermal Exergy analysis of a building. *Energy Procedia* **83**, 177–186 (2015).

272. Dongellini, M., Naldi, C. & Morini, G. L. Influence of sizing strategy and control rules on the energy saving potential of heat pump hybrid systems in a residential building. *Energy Convers. Manag.* **235**, 114022 (2021).

273. Lawrence Berkeley National Laboratory. Buildings.Fluid.HeatPumps. *Modelica Library* https://simulationresearch.lbl.gov/modelica/releases/v9.1.0/help/Buildings_Fluid_HeatPumps.html#:~:text=TemperatureDifference dTEva_nominal,inlet %5BK.

274. MET Office. Climate summaries. https://www.metoffice.gov.uk/research/climate/maps-and-data/summaries/index.

275. Pons, M. On the reference state for exergy when ambient temperature fluctuates. *Int. J. Thermodyn.* **12**, 113–121 (2009).

276. Olympios, A. V, Song, J., Ziolkowski, A., Shanmugam, V. S. & Markides, C. N. Data-driven compressor performance maps and cost correlations for small-scale heat-pumping applications. *Energy* **291**, 130171 (2024).

277. Rahimi, M., Ardahaie, S. S., Hosseini, M. J. & Gorzin, M. Energy and exergy analysis of an experimentally examined latent heat thermal energy storage system. *Renew. Energy* **147**, 1845–1860 (2020).

278. Sustainable Energy Authority of Ireland. *Heat Pumps - Technology Guide*. https://www.seai.ie/publications/Heat-Pump-Technology-Guide.pdf (2020).

279. Wang, Y. & He, W. Temporospatial techno-economic analysis of heat pumps for decarbonising heating in Great Britain. *Energy Build.* **250**, 111198 (2021).

280. Ofgem. Get energy price cap standing charges and unit rates by region. https://www.ofgem.gov.uk/energy-advice-households/get-energy-price-cap-standing-charges-and-unit-rates-region.

281. UK Department for Energy Security & Net Zero. Greenhouse gas reporting: conversion factors 2024. https://www.gov.uk/government/publications/greenhouse-gas-reporting-conversion-factors-2024 (2024).

282. Khorasaninejad, E. & Hajabdollahi, H. Thermo-economic and environmental optimization of solar assisted heat pump by using multi-objective particle swam algorithm. *Energy* **72**, 680–690 (2014).

283. UK Department for Energy Security & Net Zero. UK ETS: Carbon prices for use in civil penalties, 2024. https://www.gov.uk/government/publications/determinations-of-the-uk-ets-carbon-price/uk-ets-carbon-prices-for-use-in-civil-penalties-2024 (2023).

284. UK Department for Business Energy & Industrial Strategy. *Heat in Buildings - Boiler Plus*. (2017).

285. Rubitherm Technologies GmbH. Technical Datasheet RT35HC. 2020 (2020).

286. Myers, M., Kourtza, E., Kane, D. & Harkin, S. The Cost of Installing Heating Measures in Domestic Properties. *Delta Energy Environ.* (2018).

287. UK Department for Levelling Up Housing & Communities. English Housing Survey 2021 to 2022: energy. https://www.gov.uk/government/statistics/english-housing-survey-2021-to-2022-energy/english-housing-survey-2021-to-2022-energy#heating-and-feeling-comfortable-in-the-home (2023).

288. UK Government. Boiler Upgrade Scheme.

289. Liu, Z., Tang, G. & Zhao, F. Dynamic simulation of air-source heat pump during hot-gas defrost. *Appl. Therm. Eng.* **23**, 675–685 (2003).

290. Tang, J., Hu, X., Herman, C. & Gong, G. Computational modeling and prediction of the performance of air source heat pumps under frost prevention and retardation conditions. *Energy Build.* **224**, 110264 (2020).

291. Violidakis *et al.* Dynamic modelling of an ultra high temperature PCM with combined heat and electricity production for application at residential buildings. *Energy Build.* **222**, 110067 (2020).